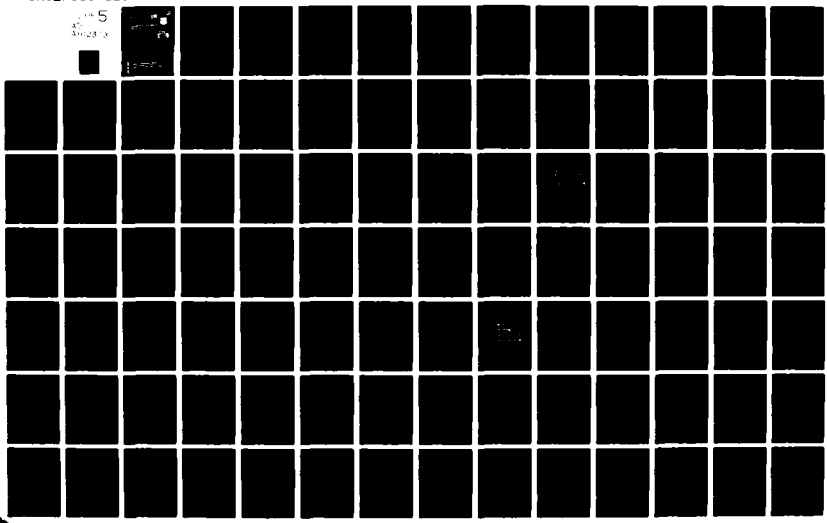


AD-A102 303

HARRIS CORP MELBOURNE FL GOVERNMENT COMMUNICATION SY--ETC F/G 17/2.1
MILLIMETER WAVE ALTERNATE ROUTE STUDY.(U)
APR 81 W C ADAMS, J J PAN, W C WHITEHEAD F30602-79-C-0055
RADC-TR-81-42 NL

UNCLASSIFIED

5
4023



RADC-TR-81-42
Final Technical Report
April 1981

LEVEL II

AD A102303

**MILLIMETER WAVE ALTERNATE
ROUTE STUDY**

Harris Corporation

W. C. Adams
J. J. Pan
W. C. Whitehead

E. T. Horton, Jr.
J. W. Reid
G. P. Martin

DTIC
ELECTE
AUG 3 1981
S D
E

APPROVED FOR PUBLIC RELEASE; DISTRIBUTION UNLIMITED

ROME AIR DEVELOPMENT CENTER
Air Force Systems Command
Griffiss Air Force Base, New York 13441

81 8

09 048

This report has been reviewed by the RADC Public Affairs Office (PAO) and is releasable to the National Technical Information Service (NTIS). As such, it will be releasable to the general public, including foreign nations.

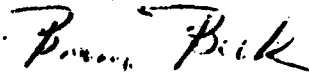
RADC-TR-81-42 has been reviewed and is approved for publication.

APPROVED:



FREDERICK SCHMANDT
Project Engineer

APPROVED:



BRUNO BEEK
Acting Technical Director
Communications and Control Division

FOR THE COMMANDER:



JOHN P. HUSS
Acting Chief, Plans Office

If your address has changed or if you wish to be removed from the RADC mailing list, or if the addressee is no longer employed by your organization, please notify RADC (DCCT) Griffiss AFB NY 13441. This will assist us in maintaining a current mailing list.

Do not return this copy. Retain or destroy.

UNCLASSIFIED

SECURITY CLASSIFICATION OF THIS PAGE (When Data Entered)

19 REPORT DOCUMENTATION PAGE		READ INSTRUCTIONS BEFORE COMPLETING FORM	
1. REPORT NUMBER RADC TR-81-42	2. GOVT ACCESSION NO. AD-A10303	3. RECIPIENT'S CATALOG NUMBER (9)	
4. TITLE (and Subtitle) MILLIMETER WAVE ALTERNATE ROUTE STUDY		5. TYPE OF REPORT, PERIOD COVERED Final Technical Report. Dec 78 - Feb 80	6. PERFORMING ORG. REPORT NUMBER N/A
7. AUTHOR W. C. Adams J. J. Pan W. C. Whitehead	E. T. Horton, Jr. J. W. Reid G. P. Martin	8. CONTRACT OR GRANT NUMBER(s) F30602-79-C-0055	
9. PERFORMING ORGANIZATION NAME AND ADDRESS Harris Corporation/Government Communications Systems Division P O Box 37, Melbourne FL 32901		10. PROGRAM ELEMENT, PROJECT, TASK AREA & WORK UNIT NUMBERS 62702F 4519122	
11. CONTROLLING OFFICE NAME AND ADDRESS Rome Air Development Center (DDCT) Griffiss AFB NY 13441		12. REPORT DATE Apr 1981	13. NUMBER OF PAGES 380
14. MONITORING AGENCY NAME & ADDRESS (if different from Controlling Office) Same		15. SECURITY CLASS. (of this report) UNCLASSIFIED	
16. DISTRIBUTION STATEMENT (of this Report) Approved for public release; distribution unlimited.		17. SECURITY CLASS. (of this report) UNCLASSIFIED	
17. DISTRIBUTION STATEMENT (of the abstract entered in Block 20, if different from Report) Same		18. DECLASSIFICATION/DOWNGRADING SCHEDULE N/A	
18. SUPPLEMENTARY NOTES RADC Project Engineer: Frederick Schmandt (DDCT)			
19. KEY WORDS (Continue on reverse side if necessary and identify by block number) Millimeter Communication Modulation Digital			
20. ABSTRACT (Continue on reverse side if necessary and identify by block number) The present state-of-the-art regarding millimeter wave applications and millimeter component technology was assessed for both tactical and strategic applications. Anti-jam techniques and multiple-path diversity for improving reliability were investigated. A detailed hardware and propagation analysis to determine the millimeter bands which can most effectively satisfy system requirements from a cost/implementation and system availability tradeoff point of view was conducted for various			

DD FORM 1473 JAN 73 EDITION OF 1 NOV 65 IS OBSOLETE

UNCLASSIFIED

SECURITY CLASSIFICATION OF THIS PAGE (When Data Entered)

411224 210

UNCLASSIFIED

SECURITY CLASSIFICATION OF THIS PAGE(When Data Entered)

potential applications.

UNCLASSIFIED

SECURITY CLASSIFICATION OF THIS PAGE(When Data Entered)

ACCESSION FOR	
NTIS GRA&I	<input checked="" type="checkbox"/>
DTIC TAB	<input type="checkbox"/>
Unannounced	<input type="checkbox"/>
Justification	
By _____	
Distribution/ _____	
Availability Codes	
Dist	Avail and/or Special
A	

TABLE OF CONTENTS

<u>Paragraph</u>	<u>Title</u>	<u>Availability Codes</u>		<u>Page</u>
		<u>Dist</u>	<u>Avail and/or Special</u>	
1.0	INTRODUCTION.....	A		1-1
1.1	Overview of the Nature of the Study.....			1-1
1.2	Description of the Study Approach.....			1-2
1.3	Organization of the Study Final Report.....			1-3
1.4	Study Summary.....			1-3
1.4.1	Transmission Frequency.....			1-4
1.4.2	Antijam Techniques.....			1-4
1.4.3	Path Diversity to Alleviate Rain Effects.....			1-5
1.4.4	Multiple Path Diversity to Alleviate Jamming Effects..			1-6
1.4.5	Investigations of Adaptive Phased Array Antenna Techniques.....			1-6
1.4.6	System Architectural Studies.....			1-7
1.4.7	Hardware Analysis.....			1-8
2.0	ANALYSIS OF RAIN EFFECTS.....			2-1
2.1	Atmospheric Effects on Millimeter Wave Propagation....			2-1
2.1.1	Cause Mechanisms.....			2-2
2.1.2	Utilization of Millimeter Wave Spectrum.....			2-4
2.1.3	Rain Type and Rain Effects.....			2-5
2.1.4	Attenuation Due to Clouds.....			2-8
2.1.5	Rain Effects Versus Communication Systems.....			2-10
2.2	Rain-Induced Attenuation and Rain Statistics.....			2-14
2.2.1	Rain Parameters.....			2-14
2.2.2	Rain Statistics.....			2-15
2.2.3	Rain Attenuation.....			2-17
2.3	Rain-Induced Polarization Degradation.....			2-20
2.3.1	Polarization Degradation Effects Frequency Reuse Communications Systems.....			2-20
2.3.2	Rain-Induced Cross Polarization.....			2-21
2.3.3	Rain-Induced Attenuation and Phase Shift.....			2-22
2.4	Millimeter Wave Propagation Over the Water.....			2-26
2.5	Link Availability and System Design.....			2-29
2.5.1	System Availability and Path Availability.....			2-29
2.5.2	System Budget Design Including Rain Effects.....			2-35
3.0	SURVEY OF ANTIJAM TECHNIQUES AND JAMMING EFFECTS.....			3-1
3.1	Introduction.....			3-1
3.2	Figure of Merit for Spread Spectrum Communication Systems.....			3-1
3.3	Chirp (Linear FM) Spread Spectrum Systems.....			3-5

TABLE OF CONTENTS (Continued)

<u>Paragraph</u>	<u>Title</u>	<u>Page</u>
3.4	Frequency Hopping Spread Spectrum Communication System.....	3-8
3.5	Direct Sequence Spread Spectrum Systems.....	3-17
3.6	Selection of Candidate Spread Spectrum AJ System.....	3-22
4.0	EVALUATION OF PATH DIVERSITY TO ALLEVIATE RAIN EFFECTS.....	4-1
4.1	Diversity Methods.....	4-3
4.1.1	Path Diversity.....	4-3
4.1.2	Adaptive Transmitter Power Diversity.....	4-10
4.1.3	Millimeter Wave/Microwave Frequency Diversity.....	4-11
4.1.4	Transmission Delay Diversity.....	4-12
4.2	Diversity Design Consideration.....	4-13
4.3	Adaptive Polarization Correction to Counteract Rain-Induced Cross Polarization.....	4-17
5.0	EVALUATION OF MULTIPLE PATH DIVERSITY TO ALLEVIATE JAMMING EFFECTS.....	5-1
5.1	Introduction.....	5-1
5.2	Communications Network Architecture.....	5-2
6.0	INVESTIGATIONS OF ADAPTIVE PHASED ARRAY ANTENNA TECHNIQUES.....	6-1
6.1	Introduction.....	6-1
6.2	Reflector Feed Adaptive Null Steering.....	6-3
6.2.1	Description of the Approach.....	6-3
6.2.2	Analytical Approach.....	6-7
6.2.3	Calculated Nulling Performance.....	6-10
6.2.4	Comparison With a Sidelobe Canceller.....	6-17
6.3	Millimeter Wave Adaptive Feed Design.....	6-20
6.4	Low Loss RF Weights.....	6-27
6.5	Conclusions.....	6-35
7.0	SYSTEM ARCHITECTURAL STUDIES.....	7-1
7.1	System Link Budget Considerations.....	7-1
7.2	Alternate Routing Technique for DCS.....	7-9
7.2.1	DCS.....	7-11
7.2.2	Millimeter Wave Alternate Routing to Counteract Rain Effects.....	7-17
7.2.3	Millimeter Wave Link Architectures.....	7-17

TABLE OF CONTENTS (Continued)

<u>Paragraph</u>	<u>Title</u>	<u>Page</u>
7.2.4	Selection of Millimeter Wave Architecture for DCS.....	7-25
7.3	AJ Improvements in Tactical Communications Systems Using Direct Sequence QPSK Spreading.....	7-26
7.4	Total Processing Gain Obtainable From Directive Antennas and Spectrum Spreading.....	7-33
7.5	Systems Considerations.....	7-35
7.5.1	Atmospheric Absorption.....	7-36
7.5.2	Rain Loss.....	7-36
7.5.3	Antenna Beamwidths.....	7-39
7.5.4	Coherence Bandwidth Considerations at MMW Frequencies.....	7-40
7.5.5	Acquisition and Tracking in Spread Spectrum Systems...	7-43
7.5.6	Spectrum Allocations at MMW Frequencies.....	7-44
7.5.7	The Effects of Bandlimiting and Aliasing Upon BPSK Signals.....	7-44
7.6	Summary and Conclusions.....	7-71
8.0	HARDWARE ANALYSIS.....	8-1
8.1	System Considerations.....	8-2
8.1.1	Modulation Method Consideration.....	8-2
8.1.2	Calculation of Error Probabilities.....	8-4
8.1.3	Frequency Selection.....	8-6
8.1.3.1	Introduction.....	8-6
8.1.3.2	System Bandwidth Consideration.....	8-7
8.1.3.3	Determination of Intermediate Frequencies (IF).....	8-7
8.1.3.3.1	1 GHz IF Bandwidth.....	8-7
8.1.3.3.2	2 GHz IF Bandwidth.....	8-8
8.1.3.3.3	Single or Dual Conversion.....	8-8
8.1.3.3.4	Inspection of Spurious-Free IF Bandpass Spectra.....	8-9
8.1.3.3.5	In-Band Spurs Calculation.....	8-11
8.1.3.4	Spurs Other Than IF In-Band's.....	8-17
8.1.3.4.1	Spurious Output Generation Mode.....	8-17
8.1.4	Repeater Spacing.....	8-18
8.2	Nodal Terminal.....	8-19
8.2.1	Transmitter/Receiver Components Consideration.....	8-19
8.2.2	Modem General Description.....	8-32
8.2.2.1	Modem Design Goals.....	8-32
8.2.2.2	Modem Code Generator Guidelines.....	8-34
8.2.2.3	Modem Circuit Design.....	8-36
8.2.2.4	Spread Spectrum Modulation Format.....	8-45
8.2.2.5	Detailed Circuit Design - Code Generator.....	8-45
8.2.3	Selection of Filters.....	8-48
8.2.4	Baseband Components.....	8-50

TABLE OF CONTENTS (Continued)

<u>Paragraph</u>	<u>Title</u>	<u>Page</u>
8.2.5	Fiber-Optic Interconnection.....	8-51
8.2.6	Hardware Package Concept.....	8-54
8.2.7	Nodal Terminal Antennas.....	8-56
8.2.8	Link Quality Measurement at Nodal Terminals.....	8-62
8.3	Repeater Terminals.....	8-68
8.3.1	Systems Considerations for Active and Passive Repeater Terminals.....	8-74
8.3.1.1	Introduction.....	8-74
8.3.1.2	Near Field Versus Far Field Passive Reflector Considerations.....	8-76
8.3.1.3	Two-Hop Passive Repeater Configurations.....	8-79
8.3.1.4	Three-Hop Passive Repeater Configurations.....	8-95
8.3.2	Passive Repeater.....	8-98
8.3.3	Repeater Modem.....	8-101
8.3.4	Receiver.....	8-101
8.3.5	Transmitter.....	8-104
8.4	Millimeter Wave Frequency - Channel Arrangements.....	8-106
9.0	RECOMMENDATIONS.....	9-1
9.1	Wideband Fiber-Optic Interface Electronics for Integrated Millimeter Wave Terminals.....	9-1
9.2	Millimeter Wave Adaptive Array Feed Design.....	9-4
9.3	Low Cost Wideband Millimeter Wave VCO Development.....	9-7
APPENDIX A	MILLIMETER WAVE ALTERNATE ROUTE LINK ENGINEERING AND ADAPTIVE ARRAY PROCESSING TO PROVIDE ANTIJAM PROTECTION.....	A-1

LIST OF ILLUSTRATIONS

<u>Figure</u>	<u>Title</u>	<u>Page</u>
1.4.1	Atmospheric Attenuation as Function of Frequency.....	1-5
2.1	Atmospheric Attenuation Due to Water Vapor and Oxygen Absorption.....	2-3
2.1.1	Dispersion and Attenuation of Dry Air in the Wings of O ₂ Resonance for Homogeneous Path at Horizon and 10 km (After J.H. Liebe and W.M. Welch).....	2-5
2.1.3	Transmission Through a Layer of Water at Various Common Carrier Frequencies (After Hogg and Chu).....	2-9
2.1.5	Geometrical Upper Bound on Multipath Delay Spread.....	2-13
2.2.3	Coefficients γ and ζ of Rain Attenuation (After CCIR).....	2-19
2.3.3-1	Rain-Induced Differential Attenuation Between Polarizations I and II for Various Rain Rates (After Hogg and Chu).....	2-23
2.3.3-2	Rain-Induced Differential Phase Shift Between Polarizations I and II for Various Rain Rates (After Hogg and Chu).....	2-24
2.3.3-3	Calculated Rain-Induced Cross Polarization of Horizontally and Vertically Polarized Waves (After Chu).....	2-27
2.3.3-4	Calculated Rain-Induced Cross Polarization of Circularly Polarized Waves (After Chu).....	2-28
2.5.1	Rain Outage Chart (After T.L. Osbourne).....	2-34
2.5.2-1	Cumulative Rainfall Distribution for Point Rates at Washington, D.C.....	2-40
2.5.2-2	38 and 44 GHz Path Availability Versus System Margin in Vicinity of Washington, D.C.....	2-41
3.3-1	Up/Down Chirp System Using SAW Devices.....	3-5
3.3-2	Up Chirp Orthogonal Code System Using SAW Devices.....	3-6
3.4	FH FSK Spread Spectrum System.....	3-8
3.5-1	BPSK Direct Sequence Spread Spectrum System.....	3-17
3.5-2	QPSK DS System.....	3-20
3.5-3	Interleaved One-Half Data Rate QPSK System.....	3-21
3.6	Comparison of Direct-Sequence and Frequency-Hop Techniques (Quadrature Phase Modulation and Replica Jamming Assumed).....	3-24
4.0-1	Long Distance Millimeter Wave Communication Using Satellite as a Repeater.....	4-2
4.0-2	Long Distance Millimeter Wave Communication Using Multi-Satellite as Repeaters.....	4-3

LIST OF ILLUSTRATIONS (Continued)

<u>Figure</u>	<u>Title</u>	<u>Page</u>
4.1.1-1	Path Diversity Configuration for Line Distribution Network.....	4-4
4.1.1-2	30 GHz Percent Outage Versus Attenuation for Washington, at Elevation Angle of 20°.....	4-9
4.1.1-3	Percent Maximum Diversity Gain Versus Site Separation.....	4-9
4.3	Block Diagram of Adaptive Polarization Correction Network.....	4-19
5.2-1	Basic Network Architecture (2 Sheets).....	5-3
5.2-2	Typical Digital European Backbone (DEB) Multiplex Configuration.....	5-5
5.2-3	Typical DCS Multiplex Configuration European Area.....	5-6
5.2-4	Japan DCS Configuration.....	5-7
5.2-5	Hawaii DCS Configuration.....	5-8
5.2-6	Type B Architecture.....	5-10
5.2-7	Type C Architecture.....	5-10
5.2-8	Type D Architecture.....	5-10
5.2-9	Type E Architecture.....	5-11
5.2-10	Type F Architecture.....	5-11
5.2-11	Type G Architecture.....	5-12
5.2-12	Type H Architecture.....	5-12
5.2-13	Network Availability Versus Per-Link Jamming Probability for a 10-Existing-Node Network With Architecture Type as a Parameter.....	5-18
5.2-14	Network Availability Versus Per-Link Jamming Probability for a 50-Existing-Node Network With Architecture Type as a Parameter.....	5-19
5.2-15	Network Availability Versus Per-Link Jamming Probability for a 100-Existing-Node Network With Architecture Type as a Parameter.....	5-20
5.2-16	Normalized Network Cost Versus Number of Existing Nodes for Several Network Architectures....	5-21
5.2-17	Relative Network Cost for Several Choices of Added-Link, Added Node, and Existing Node Costs for Various Network Architecture Types (100 Existing Node Network).....	5-25
6.2.1-1	Temporal Reference Adaptive Array.....	6-4
6.2.1-2	Reflector Feed Adaptive Null-Steering Hardware Diagram.....	6-5
6.2.2	Calculation of Feed Horn Response to a Broadband Jammer.....	6-9

LIST OF ILLUSTRATIONS (Continued)

<u>Figure</u>	<u>Title</u>	<u>Page</u>
6.2.3-1	Two Feed Horn Null Depth for a 20 Percent Bandwidth Jammer.....	6-12
6.2.3-2	Three Feed Horn Null Depth for a 20 Percent Bandwidth Jammer.....	6-14
6.2.3-3	Five Feed Horn Depth for a 20 Percent Bandwidth Jammer.....	6-15
6.2.3-4	Five Feed Horn Null Depth for Two 20 Percent Bandwidth Equal Power Jammers (Jammer 1 at 0°).....	6-16
6.2.3-5	Combined Feed Horn Response for Two Jammers Within the Main Beam for a Five Feed Horn System....	6-17
6.2.4-1	Adaptive Sidelobe Cancellation Antennas.....	6-18
6.2.4-2	Beam Pattern Cancellation Between the High Gain Beam and Low Gain Beam.....	6-19
6.3-1	Far Field Angular Positioning of Field Horn Patterns..	6-21
6.3-2	Antenna Patterns Before and After Adaption to a Jammer at 0.4°.....	6-22
6.3-3	Antenna Patterns Before and After Adaption to a Jammer at -0.25°.....	6-23
6.3-4	Antenna Patterns Before and After Adaption to a Jammer at 0.04°.....	6-25
6.3-5	Adaptive S/N Improvement as a Function of Jammer Angle of Arrival.....	6-26
6.4-1	Dual Phase Shifter Complex Weight.....	6-29
6.4-2	RF Weight Implementations.....	6-30
6.4-3	Low Loss Dual Phase Shifter RF Weight.....	6-31
6.4-4	Multitap Time Delay Weighting Network.....	6-33
6.4-5	Realizable Low Loss Combining Network Using Three Port Dual Phase Shifter Weights.....	6-34
7.1-1	Millimeter Wave Link Model.....	7-1
7.1-2	MWAR Study Link Curves - Receiver IF BW = 63 dB.....	7-5
7.1-3	MWAR Study Link Curves - Receiver IF BW = 76 dB.....	7-6
7.1-4	MWAR Study Link Curves - Receiver IF BW = 84.8 dB.....	7-7
7.2.1-1	Typical Digital European Backbone (DEB) Multiplex Configuration.....	7-12
7.2.1-2	Typical DCS Multiplex Configuration European Area.....	7-13
7.2.1-3	Korea DCS Configuration.....	7-14
7.2.1-4	Japan DCS Configuration.....	7-15
7.2.1-5	Hawaii DCS Configuration.....	7-16
7.2.3-1	Typical Space Diversity Terminal with Frequency Diversity Capability.....	7-19
7.2.3-2	Typical Frequency Diversity Terminal.....	7-20
7.2.3-3	Single Node Point-to-Point Path.....	7-21

LIST OF ILLUSTRATIONS (Continued)

<u>Figure</u>	<u>Title</u>	<u>Page</u>
7.2.3-4	Hub and Wheel Architecture.....	7-22
7.2.3-5	Bidirectional Ring Architecture.....	7-23
7.3-1	High Rate PN Code Generation Using Syncopated Shift Registers.....	7-29
7.3-2	A DS Design Example Using Syncopated PN Code Generators.....	7-32
7.5.1	Total Absorption Coefficient for the Model Atmosphere in Reference for Surface Water Vapor Density ρ_0 of 7.5 g/m ³ (60% RH at 60°).....	7-37
7.5.2	Net Gain of a 38 GHz System with Respect to an 8 GHz System Versus Rainfall Rate With Link Path Length as a Parameter.....	7-39
7.5.4	Coherence Bandwidth Considerations in Spread Spectrum Systems.....	7-41
7.5.7-1	Aliased (One-Sided) Spectrum of a BPSK Signal With Square Wave Data Input.....	7-60
7.5.7-2	One Term Square Wave No Filtering.....	7-61
7.5.7-3	Two Term Square Wave No Filtering.....	7-62
7.5.7-4	Two Term Square Wave $f_{cut} = 1.95$ GHz.....	7-63
7.5.7-5	Three Term Square Wave No Filtering.....	7-64
7.5.7-6	Three Term Square Wave $f_{cut} = 1.95$ GHz.....	7-65
7.5.7-7	Three Term Square Wave $f_{cut} = 2.93$ GHz.....	7-66
7.5.7-8	Four Term Square Wave No Filtering.....	7-67
7.5.7-9	Four Term Square Wave $f_{cut} = 1.95$ GHz.....	7-68
7.5.7-10	Four Term Square Wave $f_{cut} = 2.98$ GHz.....	7-69
7.5.7-11	Computer Program Listing for Aliasing and Bandlimiting Effects Upon BPSK.....	7-70
8.1.1	Comparative Performance of Different Modulation Methods for a BER of 10 ⁻³	8-3
8.1.2	Error Probability Curves of 2- and 4-Level CPSK and DCPSK.....	8-5
8.1.3.3.4-1	Single Conversion Frequency Plan IF BW = 1 GHz (IF BW = 2 GHz).....	8-10
8.1.3.3.4-2	Dual Conversion Frequency Plan IF BW = 1 GHz (IF BW = 2 GHz).....	8-11
8.1.3.3.5-1	Single Conversion In-Band Spur Calculator Printouts...	8-12
8.1.3.3.5-2	Double Conversion In-Band Spur Calculator Printouts (2 GHz BW).....	8-13
8.1.3.3.5-3	Double Conversion In-Band Spur Calculator Printout (1 GHz BW).....	8-14
8.2.1-1	Block Diagram of Millimeter Wave Transmitter/Receiver.....	8-20
8.2.1-2	Wideband Millimeter Wave Frequency Hopping Synthesizer.....	8-23

LIST OF ILLUSTRATIONS (Continued)

<u>Figure</u>	<u>Title</u>	<u>Page</u>
8.2.1-3	Power Output Versus Frequency of CW IMPATT Diode (April, 1979).....	8-25
8.2.2.3-1	Modem Block Diagram Receive Section.....	8-37
8.2.2.3-2	Modem Block Diagram Transmitter Section.....	8-38
8.2.2.3-3	Tapped Delay Line Matched Filter.....	8-41
8.2.2.3-4	Basic Delay Lock Loop.....	8-43
8.2.2.3-5	Delay Lock Loop for Sequence Inversion Modulation.....	8-44
8.2.2.5-1	500 MHz Code Generator.....	8-47
8.2.2.5-2	Code Sequence Multiplexer.....	8-48
8.2.2.5-3	Digital Filter.....	8-49
8.2.5	Block Diagram of Harris Model 4359 13-Channel Fiber-Optic Concentrator.....	8-52
8.2.7-1	Half-Power Beamwidth Versus Aperture Size.....	8-57
8.2.7-2	Spatial Sweep Acquisition.....	8-60
8.2.8-1	Quantizer Output Probability.....	8-64
8.2.8-2	Quantizer Magnitude Detection Probabilities.....	8-65
8.2.8-3	Quantizer Monitor.....	8-66
8.2.8-4	Practical Quality Monitor.....	8-67
8.2.8-5	Accumulator Distribution (2 Sheets).....	8-69
8.3-1	Nonregenerative Repeater for Millimeter Wave Tactical Radio.....	8-71
8.3-2	Regenerative Repeater for Millimeter Wave Tactical Radio.....	8-72
8.3-3	Illustration of Cylindrical Passive Reflection Mirrors.....	8-73
8.3.1.2-1	Near Field Definition.....	8-77
8.3.1.2-2	Near Field Radius Versus Aperture Size.....	8-78
8.3.1.2-3	Near Field Passive Reflectors.....	8-80
8.3.1.2-4	Maximum Spacing of Double Passive Reflectors for Loss < 1 dB in Near Field.....	8-81
8.3.1.3-1	Three Passive Repeater Approaches.....	8-83
8.3.1.3-2	Added Node Link Connectivity.....	8-84
8.3.1.3-3	Signal Paths Geometry.....	8-85
8.3.1.3-4	η_A Versus 2ϕ	8-91
8.3.1.3-5	Passive Repeater Geometry.....	8-92
8.3.1.3-6	Single Reflector (Two-Hop) Gain.....	8-94
8.3.1.4-1	Space Loss for Multihop Systems.....	8-96
8.3.1.4-2	Loss Versus Frequency.....	8-97
8.3.1.4-3	Loss Versus Frequency.....	8-99
8.3.4	Microstrip Q-Band Mixer, Bandpass Filter and Lowpass Filter Using 10 Mils Thick Fused Quartz Substrates.....	8-103
8.3.5	Push-Pull IMPATT Diode Amplifier.....	8-107
8.4	Millimeter Wave RF - Channel Arrangements.....	8-108

LIST OF TABLES

<u>Table</u>	<u>Title</u>	<u>Page</u>
2.1.3	Propagation Attenuation Due to Precipitation.....	2-7
2.1.5	Rain Effects Versus Communication System Performance..	2-11
2.5.1	Calculations of Rain Attenuation Margin.....	2-37
2.5.2	Preparation of Rain Outage Charts.....	2-38
3.4-1	Characteristics of Some Typical Synthesizers.....	3-10
3.4-2	Wideband Frequency Synthesizers.....	3-12
4.2	Methods to Counteract the Rain-Effects for Millimeter Wave Communications.....	4-15
5.2-1	System Availability as a Function of Number of Nodes and Probability of Link Disruption p.....	5-16
5.2-2	System Complexity as a Function of Existing Number of Nodes, Added Nodes Links, and Associated Weighting Factors.....	5-17
7.1-1	Transmitter Power and Antenna Gains.....	7-8
7.1-2	Link Allocation.....	7-10
7.2.3	Comparison of Basic Topological MWAR Architecture.....	7-24
7.2.4	Operating Aspects Criteria for MMW Architecture Suitable for DCS Alternate Routing.....	7-25
7.3-1	Direct Sequence QPSK Processing Gain.....	7-27
7.4-1	Total Gain (Antenna and Spread Spectrum Processing Against a CW Jammer).....	7-34
7.4-2	ΔG_{ANT} Versus Frequency and Antenna Diameter.....	7-35
7.5.2	Additional Rain Loss Incurred Over a 10 km Link When Operating at 38 GHz Rather than 8 GHz.....	7-37
7.5.6	Spectrum Allocations for 21.2 GHz to 275 GHz.....	7-45
8.1.3.1	Spectrum Allocations for Frequency Above 30 GHz.....	8-6
8.1.3.3.3	Pros and Cons of Single and Dual Conversion Scheme for 36-38.6 GHz Band.....	8-9
8.1.3.3.5-1	Spur Analysis Summary (IF BW = 1 GHz).....	8-16
8.1.3.3.5-2	Spur Analysis Summary (IF BW = 2 GHz).....	8-16
8.2.1-1	Comparison of Solid-State Millimeter Wave LO Active Devices.....	8-21
8.2.1-2	40 GHz Glass Cavity-Controlled Source.....	8-21
8.2.1-3	Comparison of Millimeter Wave Local Oscillators.....	8-22
8.2.1-4	High Power Q-Band IMPATT Diode.....	8-26
8.2.1-5	MMW IMPATT Diode Amplifier Using Combining Technique..	8-27
8.2.1-6	Above 20 GHz GaAs MESFET Amplifier.....	8-29
8.3	Comparison of High Data-Rate Active and Passive Repeaters.....	8-74

1.0 INTRODUCTION

This final technical report documents the results of the Millimeter Wave Alternate Route (MWAR) Study, performed in accordance with RADC contract number F30602-79-C-0055, during the period 18 December 1978 to 18 February 1980.

The introduction provides an overview of the nature of the study, a description of the study approach, the organization of the final report, and a summary of the conclusions.

1.1 Overview of the Nature of the Study

Currently the centimeter wavelength frequency bands are highly congested, and the assigned frequency allocations and bandwidths make high data-rate, wideband spread-spectrum communication systems difficult to implement. The millimeter wave (MMW) frequencies, on the other hand, are relatively uncongested with wide available bandwidths, offering solutions for both jam-resistant tactical and strategic communications applications. In addition, the high antenna gains and narrow antenna beamwidths available at MMW frequencies, as compared to centimeter wavelength frequencies, provide further antijam (AJ) benefits.

In contrast to these benefits, there are shortcomings associated with MMW transmission not present at the lower frequency bands. These center about the high attenuation experienced by MMW transmission due to rain scattering and absorption. They are manifested in decreased link availabilities for MMW links as compared to centimeter wavelength links that are identical (same link margin, distance, modulation, and coding scheme) except for RF frequency. However, there are fundamental approaches available to alleviate these shortcomings. Each of these approaches, increasing link margin, decreasing link distance, using alternate path routing, etc., has been explored during the study. The goal has been to provide quantitative measures of the effectiveness of combatting excess link

attenuation. In addition to the system related problems, there are questions to be investigated related to the implementation of MMW systems. The Study has addressed the applicable technologies, feasibility of approaches, etc., providing a basis for later detailed design activities.

1.2 Description of the Study Approach

Performance of work on the MWAR Study has been in accordance with the following summary tasks:

- a. Study and analyze the effects of rain at MMW frequencies and 8 GHz, (Task 1) and provide estimates of link availabilities.
- b. Survey AJ techniques and determine the effects of jamming at MMW frequencies (Task 2).
- c. Evaluate the use of multiple path diversity to increase system availability as affected by rain and other weather effects, and topology (Task 3).
- d. Evaluate multiple path diversity for countering jamming signals and increasing system availability (Task 4).
- e. Investigate adaptive phased array antenna techniques for maintaining antenna alignment and improving AJ capabilities (Task 5).
- f. Investigate route architectures and select an architecture which effectively uses MMW frequencies as an alternate routing technique for the DCS system (Task 6).
- g. Study and select an architecture which effectively uses MMW to improve the AJ capability in tactical communication systems (Task 7).

- h. Perform a hardware analysis to determine the MMW band(s) which can most effectively satisfy system requirements, from a cost/implementation and system availability point of view (Task 8).

1.3 Organization of the Study Final Report

The final report is organized into nine sections plus one appendix. Sections 2.0 through 6.0 follow the order of the tasks reporting the work done to satisfy Tasks 1 through 5, Section 7.0 reports on the work of Tasks 6 and 7, and Section 8.0 satisfies the requirements of Task 8. Section 9.0 discusses recommendations resulting from this study. These are additional efforts we believe should be initiated to ensure that terrestrial MMW systems can eventually be realized. The appendix contains adaptive array data, additional to that of Section 6.0.

1.4 Study Summary

The MWAR Study has entailed a medley of study tasks and system analyses. The individual tasks have required extensive literature searches and reconsideration of much work, valid at microwave frequencies but requiring modification at MMW frequencies.

The conclusions of this work tend to urge the reader/user to utilize certain techniques during the design and implementation of terrestrial, line-of-sight communication systems, for operation at MMW frequencies.

1.4.1 Transmission Frequency

The absorption of atmospheric oxygen and water vapor, and the attenuation of communications signals by rainfall are the primary factors influencing MMW propagation. Rainfall has little effect on signals at microwave frequencies (e.g., 8 GHz) but markedly reduces communication capabilities when frequencies enter the millimeter wavelength region.

The atmospheric absorption spectrum, shown in Figures 1.4.1 and 2.1, contains transmission windows centered about frequencies of 35, 94, 140, and 240 GHz. The 35-45 GHz band is the lowest absorption region in the spectrum, and it also has relatively low rainfall attenuation compared with other windows. Table 7.5.6 contains extracts from the U.S. Government Table of Frequency Allocations, with assignments for international and U.S. usage. Page 7-47 shows that the frequency band of 36.0 - 38.6 GHz is allocated for fixed and mobile usage within international and U.S. sectors. Therefore, the co-existence of a spectrum allocation and a transmission window suggests consideration of the 36.0 - 38.6 GHz band for military, terrestrial, LOS, communications systems.

1.4.2 Antijam Techniques

Antijam techniques fit into two general classes: spread spectrum and adaptive antenna. The spread spectrum AJ techniques addressed are: chirp (linear FM), frequency hopping (FH), direct sequence (DS), and hybrid techniques.

QPSK DS systems are generally preferred due to limited degradation from system nonlinearities. The DS QPSK signal cannot be completely suppressed by a strong jammer in a hard limiter. The QPSK DS technique is the most effective for the terrestrial, LOS application.

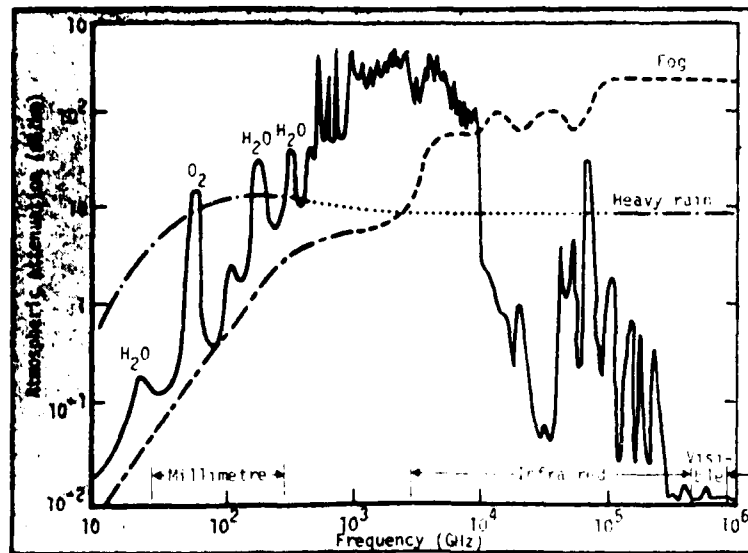


Figure 1.4.1. Atmospheric Attenuation as Function of Frequency

1.4.3 Path Diversity to Alleviate Rain Effects

Alternative diversity approaches were considered as means of alleviating rain effects:

- a. Path diversity.
 1. Tandem.
 2. Multipath.
- b. Space diversity.
- c. Transmitter power diversity.
- d. Frequency diversity.

e. Bandwidth diversity.

f. Transmission delay.

The most favorable approaches for MMW tactical systems are path diversity and adaptive transmitter power diversity. A performance comparison between these two approaches is included as Table 4.2.

1.4.4 Multiple Path Diversity to Alleviate Jamming Effects

Four types of network architectures are the building blocks of current DCS system configurations, including the Digital European Backbone:

a. Tandem link.

b. Hub and wheel.

c. Bidirectional ring.

d. Packet-and-priority.

Section 5.0 contains system availabilities and the derivation of a "relative complexity metric (C)" for various alternate route architectures. The choice of an architecture type depends upon the perceived jamming threat, the required communication reliability, and the level of complexity (cost) that can be supported.

1.4.5 Investigations of Adaptive Phased Array Antenna Techniques

An alternative to the customary sidelobe canceller has been introduced and described in Section 6.0. The reflector feed null steering concept is capable of providing broadband nulls, including nulling within the main lobe; about three orders of magnitude greater null depth bandwidth product performance is obtained when compared with the customary sidelobe

canceller. Additionally, the reflector feed adaptive approach avoids the necessity of auxiliary elements which are often located around the periphery of the principal reflector.

A primary disadvantage of the reflector feed adaptive approach is the fact that the number of degrees of freedom (hence, independent jammer sources that can be nulled) is limited by the number of feed elements. In new designs, this does not present a particular problem; however, in modification of existing installations, one is probably limited to three or four degrees of freedom.

When the reflector feed adaptive RF circuitry is coupled with a digital controller which obtains performance information from the system receiver intermediate frequency output, a very cost effective and computationally powerful algorithm can be realized. Using such a hybrid analog-digital approach, an existing unprotected reflector antenna could be converted to a fully adaptive antenna system by the addition of a digital controller, RF weights and interface circuitry, a very minimal modification.

1.4.6 System Architectural Studies

Section 7.0 commences with an examination of the millimeter wave link model, and the associated factors which must be considered to ensure link closure. Figures 7.1-2 through 7.1-4 depict allowable link distances as a function of terminal characteristics, selected link availability, and receiver IF bandwidth (data rate).

The connectivities of these links or the communications network architectures are further influenced by the expected jamming threats. Section 7.0 discusses two types of alternate route architectures (ARA) which are feasible for the DCS digital network, hardware and topological. The hardware ARA approaches are power level diversity, space diversity, time diversity, and frequency diversity. The topological ARA approaches for

complicated networks such as the DCS consist of combinations of the point-to-point, hub on wheel, star, bidirectional ring, and earth satellite. A comparison of the basic topological architectures is contained in Table 7.2.3.

Additional system considerations of importance are discussed such as atmospheric absorption, differential rain loss, antenna beamwidth, coherence bandwidth, acquisition and tracking, bandlimiting and aliasing, and spectrum allocations. The preferred spectrum allocations in the MMW range, based on propagation characteristics and governmental frequency assignments, is the 36.0-38.6 GHz band.

1.4.7 Hardware Analysis

Section 8.0 contains analyses and design approaches associated with definition of the MMW nodal and repeater terminals.

Previous sections have defended the selection of 36.0-38.6 GHz as the frequency band of use. An additional advantage is the availability of hardware and the maturation of fabrication techniques for components in that frequency range.

Paragraph 8.2 discusses options and preferences in the definition of the nodal terminal. It is recommended that the transmitter/receiver use a microstrip configuration, a MESFET or InP Gunn Diode LNA, and a solid-state HPA. The spread spectrum modem is discussed in detail, with block diagrams of the receiver and transmitter sections shown in Figures 8.2.2.3-1 and 8.2.2.3-2. Fiber-optic interconnection is considered for the linkage between the transmitter/receiver and antenna and for any local area data distribution. This concept is reiterated in Section 9.0 as a potential R&D project.

The initial alignment and maintenance of alignment are key problems for nodal terminal antennas. The most attractive technique for initial alignment utilizes an unspoiled beam and a spatial sweep procedure in conjunction with a CW carrier. Maintenance of alignment may eventually be provided by adaptive antenna techniques, but this will be difficult while attempting to simultaneously null jammers. Therefore, the interim solution is utilization of rigid antenna support structures; that is, until additional study and development of the adaptive antenna approach can be accomplished.

Three candidate approaches to link quality measurement were considered, and the preferred approach involves estimation of the probability density function of signal, noise and jammer. The technique described in Paragraph 8.2.8 is characterized by rapid response, low complexity, and operation with random data.

Paragraph 8.3 presents definition of the repeater terminals; both regenerative and nonregenerative. There is considerable discussion of the performance of passive repeater configurations.

Inexpensive passive reflector repeaters can achieve alternate route capability with acceptable link losses. The constituent elements of the repeater terminal are similar but simpler than the nodal terminal.

The section also includes discussions of frequency channel arrangements and spurs analyses.

2.0 ANALYSIS OF RAIN EFFECTS

Increasing congestion in the frequency bands, in the microwave spectrum, allocated to point-to-point wideband communications links, makes it desirable to investigate the feasibility of using millimeter waves for high data rate digital transmission. EHF propagation through the atmosphere is influenced by a 22 GHz resonance of water vapor and dominated by the millimeter wave spectrum of oxygen centered at 60 GHz. Attenuation, phase dispersion, and thermal noise associated with these molecular effects of air impose ultimate propagation limitations as well as affording unique system opportunities (e.g., transmission security and remote sensing of atmospheric variable). In spite of many well known advantages of millimeter wave communications systems, some propagation problems still exist and need to be understood, prevented, or corrected. In the past thirty years, the problem of establishing a reliable correlation between clear air EHF transfer properties and meteorological variables has been tackled by laboratory measurements¹ and refinement of the theory.² More detailed discussion of this problem will be given in this section.

2.1 Atmospheric Effects on Millimeter Wave Propagation

The absorption of atmospheric oxygen and water vapor and the attenuation by rainfall are the primary effects influencing millimeter wave (MMW) propagation. The increases of atmospheric emission temperature, refraction, and attenuation by clouds, fog, and snow are all secondary effects. The absorption coefficient of oxygen molecules and water vapor depends on the frequency, pressure, temperature and water-vapor density at the point in the atmosphere. Normally, the properties of the altitude

¹H.J. Liebe, W.M. Welch, and R. Chandler, "Laboratory Measurements of Electromagnetic Properties of Atmospheric Gases at Millimeter Wavelengths," IEEE Conference Pub. No 98, Propagation of Radio Waves at Frequencies above 10 GHz, April 1973, pp. 244-250.

²W.M. Welch, "Molecular Parameters of O₂," Phys. Rev., June 1972, p. 2692.

dependence of the absorption coefficient decrease approximately with increasing heights. Consequently the integrated path attenuation will increase steeply when the antenna elevation angle approaches zero degrees for satellite communications links.

On a clear day at ground level, the MMW absorption spectrum is depicted as H₂O and O₂ absorptions in Figure 2.1. The water vapor absorption peaks take place at 22.3 GHz, 120 GHz and 190 GHz while the oxygen molecular absorption occurs at 60 GHz. Besides these oxygen resonance and H₂O dipole interaction peaks, the atmospheric absorption spectrum also results in some transmission windows centered about frequencies of 35, 94, 140, and 240 GHz.

The rainfall-introduced attenuation severely limits the MMW propagation and can produce communications outages. In contrast, rainfall has little effect on signals at 8 GHz.

2.1.1 Cause Mechanisms

The attenuation increase within the MMW band due to oxygen, water vapor, rain and other forms of precipitation has different cause mechanisms. The absorption of MMW energy by oxygen results from magnetic dipole interactions with the incident radiation due to the oxygen molecule's permanent magnetic dipole moment, which produces transitions between molecular fine structure levels of the allowed rotational states. Contrastly, the energy absorption by water vapor results from electric dipole interactions, dipole rotations, and reflection. The attenuation due to rainfall will be treated separately in Paragraph 2.1.3 since the distribution of rain along the propagation path is generally unknown and unpredictable, making the results of rain attenuation calculations quite qualitative. The rain induced attenuation is mainly caused by reflection, refraction, scattering and absorption; therefore, the drop-size for rain distribution, temperature variation and effects of the vertical components of wind velocity all affect the attenuation. The attenuation changes with temperature variation because the water dielectric constant and loss tangent

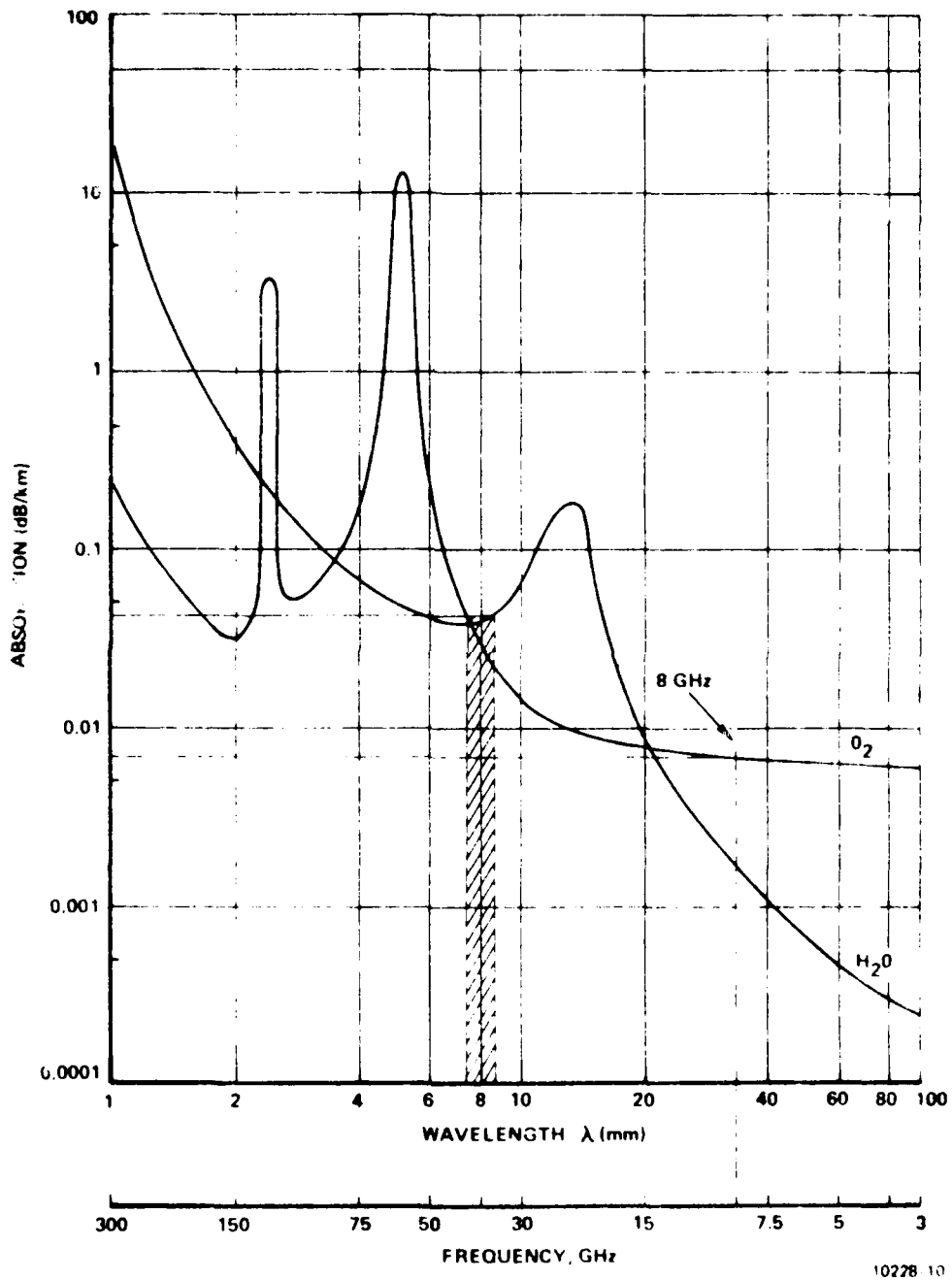


Figure 2.1. Atmospheric Attenuation Due to Water Vapor and Oxygen Absorption

are functions of temperature. The scattering effect and the oblate shape of raindrops also depolarize the signal and thereby differential phase shift and differential attenuation. Ice and dry snow will generate scattering, reflection and refraction losses but low absorption loss. The water vapor attenuation at the saturation pressure has been experimentally measured and empirically fits in units of

$$\alpha_w \approx \left[(4 \pm 1) P_w (300/T)^{2.5} (f/61) + (0.8 \pm 0.1) P_w^2 (300/T)^{10} (f/61)^{2.6} \right] \cdot 10^{-3} \quad (2.1.1)$$

dB/km, where frequency f is in GHz and the pressure P_w in torr. The P_w^2 term points to pressure-induced polarization effects most likely to be associated with molecular complexes in water vapor.

Wideband communications near 60 GHz, despite its attractiveness for security communication, is almost impossible due to oxygen molecular resonance induced high phase dispersion. Figure 2.1.1 displays the attenuation and phase dispersion of dry air from 10 to 140 GHz for a distance of 10 km. It is obvious that the phase dispersion changes rapidly in the vicinity of 60 Hz. Besides, the temperature and pressure effects broaden the oxygen resonance and make phase fluctuation unpredictable from 52 GHz to 68 GHz.

2.1.2 Utilization of Millimeter Wave Spectrum

The transmission windows at 35, 94, 140, and 240 GHz are attractive for communications, radio and radiometry application because of their relatively low absorption. Particularly, the 35 to 45 GHz band is the lowest absorption region in the MMW spectrum and it also has relatively low rainfall attenuation compared with other windows. The use of high absorption peaks due to oxygen at 60 GHz has often been suggested to provide security for short-distance line-of-sight terrestrial and shipboard communications; also, for aircraft/aircraft and aircraft/satellite links. Actually, the

resonance peak happens at 60.306 GHz. Since the attenuation fluctuates severely between 55 and 64 GHz, practical system design must be exercised with extreme caution and is not recommended for wideband operation.

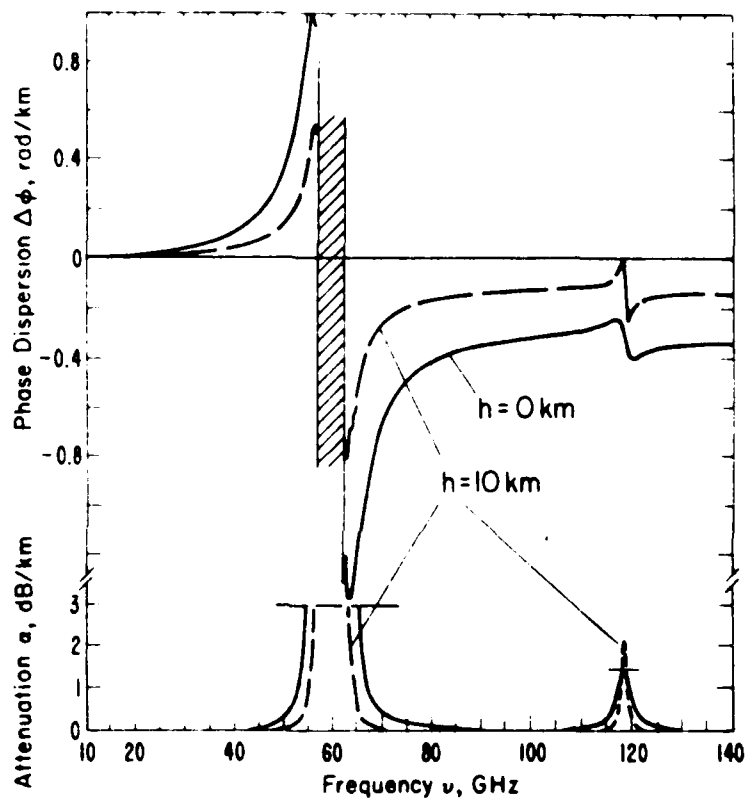


Figure 2.1.1. Dispersion and Attenuation of Dry Air in the Wings of O_2 Resonance for Homogeneous Path at Horizon and 10 km (After J.H. Liebe and W.M. Welch)

2.1.3 Rain Type and Rain Effects

Precipitation in the forms of rain and thunderstorms, which has little effect on signal at 8 GHz, will produce outage at the higher frequencies; especially, for the MMW band. Other precipitation forms such as hail, sleet, snow, fog and wet snow contribute much less attenuation effects compared with rainfall.

In the past 30 years, the rainfall effects in the MMW frequencies have been investigated thoroughly by numerous people. The MMW rain effects can be summarized as follows:

- Attenuation
- Dispersion
- Depolarization due to scattering
- Multipath due to scattering
- Sky temperature
- Random fading
- Doppler shift and phase fluctuation¹ - refractive index fluctuations cause transit time variation.

The attenuation induced by fogs and various rainfall rates at both 8 GHz and 38 GHz are tabulated in Table 2.1.3. It is obvious that 8 GHz has extremely low propagation attenuation under fog and rain. At 38 GHz, the loss becomes significant when the rain rate is above 10 mm/hour.

¹E. Vilar and P.A. Matthews, "Propagation Noise and Frequency Stability at 36 GHz," Conference Digest on Propagation of Radio Waves at Frequencies above 10 GHz, April 1973, London, pp. 83-89.

Table 2.1.3. Propagation Attenuation Due to Precipitation

	Attenuation (dB/km) at	
	8 GHz (37.5 mm)	38 GHz (7.9 mm)
Very Thick Fog 0.5 - 1.0 (Comparable to 2.5 mm/hr) 5 mm/hr rain	<0.05	0.9
Medium Thick Fog 0.25 g/m ³	<0.01	0.15
Thin Fog 0.01 g/m ³	Negligible	<0.01
Rain (mm/hr)		
0.2 } Drizzle	<0.001	0.06
0.4 } Drizzle	0.0015	0.1
1.0 } Light Rain	0.007	0.2
10.0 } Light Rain	0.1	2.8
20.0 } Medium Heavy Rain	0.28	5.7
40.0 } Heavy Rain	0.7	11.0
100.0 - Tropical Downpour	2.0	28.0

As a consequence of increased absorption by the atmosphere as frequency increases, the noise emission or apparent-brightness temperature of the sky is increased. The sky temperature at 30 GHz and 10° elevation is about 135°K compared to less than 30°K at 8 GHz, and the obtainable signal-to-noise ratios will be consequently reduced. This effect also works to slight advantage in the terrestrial and earth/satellite detection problem, since the would-be interceptor on the horizon must look through a nearly 300°K sky toward the transmitter. The sky temperature varies not only with rain rate and size of rainfall, but also with frequency, thickness of cloud, polarization and incident angles.

The attenuation caused by the thin water layer accumulated on the antenna radome may be considered as an indirect rain effect. An electromagnetic wave incident on a layer of water experiences both absorption and reflection loss; the resulting overall degradation in transmission is shown in Figure 2.1.3 as functions of layer thickness for several frequencies calculated by Hogg and Chu.¹

2.1.4 Attenuation Due to Clouds

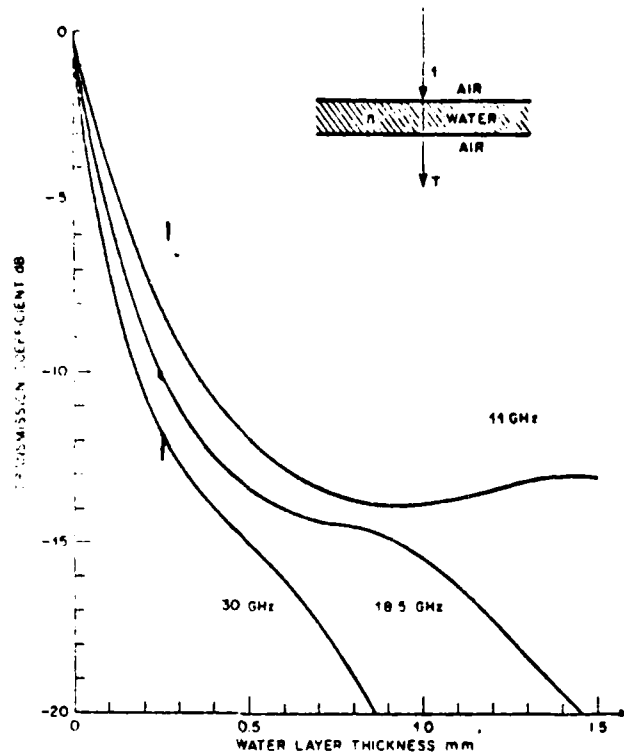
For millimeter wave satellite-earth links, the attenuation due to clouds, A_c , has to be evaluated.² A simplified global formula of empirical A_c is:

$$A_c = k \rho r \quad (2.1.2)$$

where ρ denotes the water content of clouds, in g/m^3 , and r represents the signal path length through the cloud, in km.

¹D.C. Hogg and T.S. Chu, "The Role of Rain in Satellite Communications," Proc. of IEEE, Sept., 1975, pp. 1308-1331.

²W. Holzer, "Atmospheric Attenuation in Satellite Communications", Microwave Journal, March 1965, pp. 119-125.



A90401-69

Figure 2.1.3. Transmission Through a Layer of Water at Various Common Carrier Frequencies (After Hogg and Chu)

The coefficients of attenuation (k , in dB/km/g/m³) of water clouds and ice clouds can be expressed as the following equations, respectively, as functions of frequency (f in GHz) and temperature (T , in °C):

$$k_w = fb_w \cdot \exp [a_{ow} (1 + mT)] \quad (2.1.3)$$

$$k_i = fb_i \cdot \exp [a_{oi} (AT^2 + BT + 1)] \quad (2.1.4)$$

where a_{ow} , b_w , a_{oi} , b_i , m , A , and B are all empirical constants, approximately given as:

<u>Water Cloud</u>	<u>Ice Cloud</u>
$a_{ow} = -6.866$	$a_{oi} = -8.261$
$b_w = 1.95$	$b_i = 1.006$
$m = 0.0045$	$A = -4.374 \times 10^{-4}$
	$B = -1.767 \times 10^{-2}$

2.1.5 Rain Effects Versus Communication Systems

The most fundamental obstacle encountered in design of communication systems at frequencies above 10 GHz is rain effects. Individual rain effects contribute to the degradation affecting the systems' performance. Table 2.1.5 summarizes the performance versus various rain effects. The multipath effect due to scattering can be a very serious problem for millimeter wave digital communications. It not only degrades system LPI, but also fluctuates BER and limits the operational bandwidth. The system designer must exercise procedures for estimating the probability of excessive attenuation, scattering, and depolarization as functions of MMW frequency, geographical location, path length and system margin.

For a digital system, a large number of very short interruptions caused by deep fading may be potentially more damaging to the information content of the transmissions than the same total interruption time occurring in one period. Multipath fading caused by rain and by atmospheric anomalies, contributes the degradation of higher error rate, due to the reduction of received signal level and the resultant intersymbol interference arising from the echo structure of the multipath transmission. The estimation of the error rate in particular cases must consider not only the incidence of multipath fading but also the amplitudes and delays of the echos contributing to the multipath activity.

Table 2.1.5. Rain Effects Versus Communication System Performance

Rain Effects	System Performances
<ul style="list-style-type: none"> ● Rain Attenuation ● Rain Dispersion ● Depolarization ● Scattering ● Sky Temperature (Black Body Radiation) ● Multipath ● Flat Fading 	<ul style="list-style-type: none"> ● Propagation Loss <ul style="list-style-type: none"> - Antenna Size - Link Distance - System Noise Temperature, S/N, BER - Link Margin, AJ/LPI ● Antenna Radome Performance <ul style="list-style-type: none"> - Gain, sidelobe, matching ● Pulse Spread <ul style="list-style-type: none"> - Modulation Waveform - BW, Data Rate, BER ● Cochannel Interference of Dual-Polarization Transmission ● Attenuation and Phase Shift of Cross Polarization ● Cross Talk ● Propagation Loss ● Security ● System Temperature, G/T, S/N, BER

The multipath dispersion of the millimeter wave propagation may limit the system operation bandwidth. Regardless of the cause of multipath, the limiting value of multipath spread is determined by the effective beamwidth of the antenna. For a 3 dB beamwidth β , and a path length L , the multipath spread is:

$$T = \frac{\beta^2 L}{8C} \quad (2.1.5)$$

where C is the velocity of propagation. At 35 GHz, an antenna beamwidth of 10 milliradian is obtained from an antenna diameter of 1.2 meters (4 feet). Thus, according to Figure 2.1.5, including normal multipath fading, the 35 GHz channel should have a correlation bandwidth of several GHz. It also is realizable that, from Figure 2.1.5, the antenna diameter must be larger than 0.24 meters in order to achieve 1 GHz bandwidth and 10 km link distance.

The development of digital millimeter wave systems may ultimately require the use of orthogonal polarizations of the same carrier frequency over the same hop. This consideration has prompted an increase of interest recently in the cochannel cross-polar discrimination preference of millimeter wave systems. However, the cross polarization of dual-polarization digital transmission can be degraded significantly during multipath fading.^{1,2}

¹S.H. Lin, "Impact of Microwave Depolarization During Multipath Fading on Digital Radio Performance," B.S.T.J., May 1977, pp. 645-674.

²T.O. Mottl, "Dual-Polarized Channel Outages During Multipath Fading," *ibid.*, pp. 675-701.

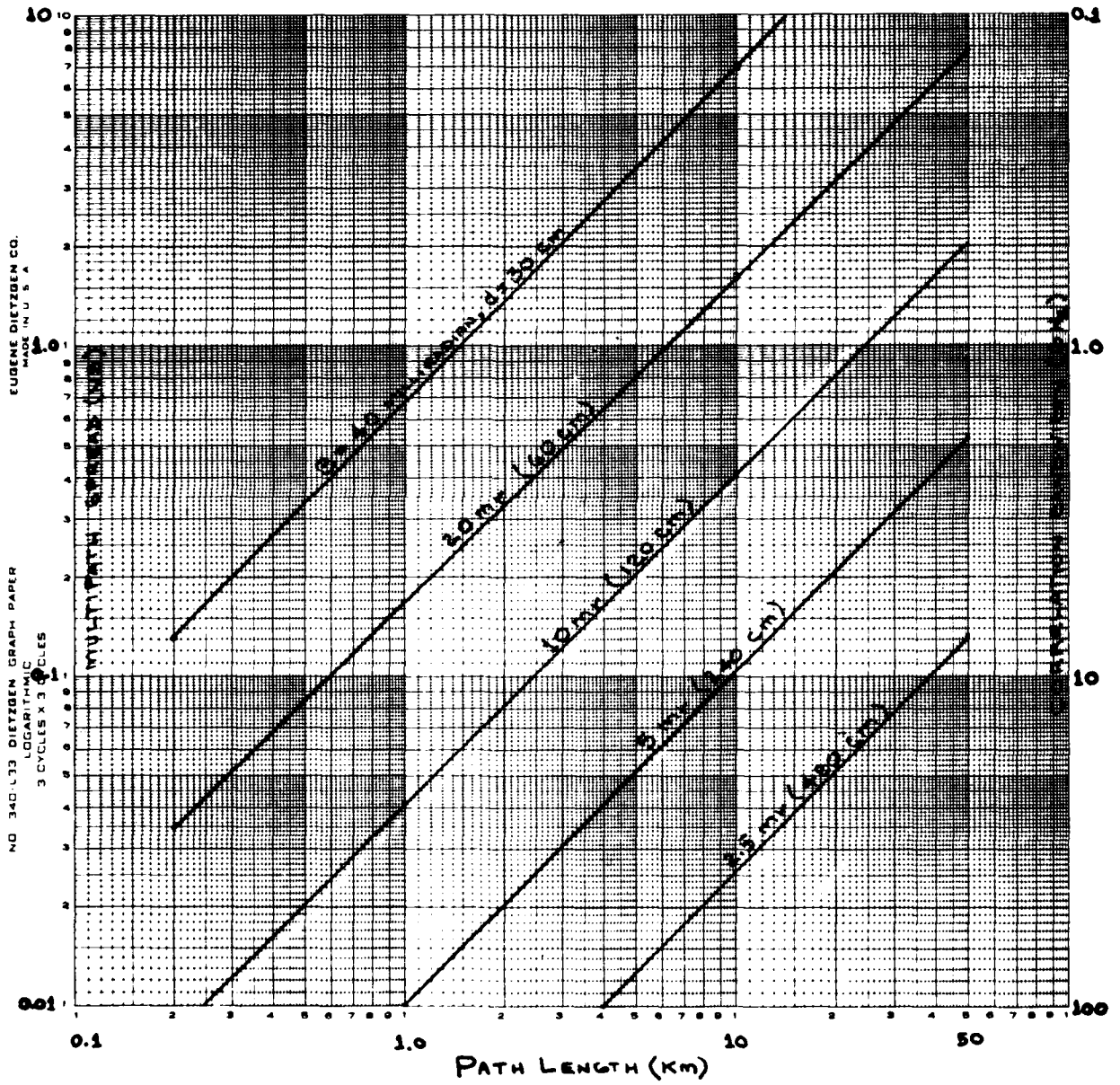


FIGURE 2.1.5. Geometrical Upper Bound on Multipath Delay Spread

2.2 Rain-Induced Attenuation and Rain Statistics

2.2.1 Rain Parameters

The theoretical classical treatment of rainfall attenuation expresses an incident plane wave, a scattered wave, and a transmitted wave as spherical functions; while the coefficients of the expanded solutions are fitted to the boundary conditions at the surface of a spherical raindrop. Obviously, the classical estimation of rain induced attenuation is far away from reality, because the rain effects vary according to the following parameters:

- Rain rate, rainfall probability, and integration time.
- Storm size.
- Rain - drop size and distribution.
- Wind velocity and rain - drop shape.
- Temperature effect.
- Height at which the rain originates.
- Chronic rain statistics (versus geographical location).
- Rain attenuation versus frequency.

Since so many parameters are involved, the total attenuation due to the rainfall is then related to the rainfall rate using an empirically based model of the drop size versus number distributions as functions of rain rate by summing the attenuation due to the various size drops, neglecting the effect of multiple scattering.

Besides the importance of rain-rate in the area of communication links, the system designer has to decide the simultaneous effect of the rainfall distribution for the complete link path. Therefore, the storm size becomes an important parameter of rain effects. Convective showers have an average diameter of 8 - 10 km (maximum diameter of storm cell in Europe is 22 km), and peak rainfall rates in such storms usually do not cover the entire area under the storm simultaneously. There will be considerable variation in rates with both time and location under the storm cells. In an area where squall lines (lines of severe thunderstorms) are known to occur, however, it may be the possibility that a line of heavy showers exceeds the length of the millimeter wave link.

The instantaneous path attenuation, caused by an isolated storm 10 km in diameter will be the same if the entire storm cell moves across a 10 km path or a 50 km path. Reducing the length of a millimeter-wave link will, therefore, not always reduce the path fade depth caused by rainfall, but the annual outage time can be expected to be greater on the longer path because there will be a greater probability of a shower moving across the longer path on any particular rainy day. Also, if a shower moves along the path, the longer path will be affected for a greater period of time.

2.2.2 Rain Statistics

The statistics of attenuation by rain measured at a given location are unique for several reasons: the total amount of precipitation varies from one place to another, as does the duration of the storms, the geometry, and the height at which the rain originates. It is also true that attenuation measurements must be made continuously for several years to obtain data sufficient for an engineer to design a system with confidence.

Point rain data can be obtained from the records of many weather stations located throughout the U.S. and abroad. These records usually give the depth of water accumulated versus elapsed time, either in graphical or tabular form, and must be differentiated to yield the rain-rate. Since rain

varies rapidly with time, the raw data contain too much information to be generally useful and are therefore processed to reveal their long term statistical characteristics. Then, the cumulative distribution functions, which show the fraction of time a certain rain-rate is not exceeded, are utilized in the rain-rate calculation.

The point rain-rate cumulative distribution function is approximated as:¹

$$P(R \geq r) \approx \frac{P_0}{2} \cdot \operatorname{erfc} \left[\frac{\ln(r) - \ln(R_m)}{\sqrt{2} S_R} \right] \quad (2.2.1)$$

where

$P(R \geq r)$ = Probability that rain-rate exceeds r (mm/hr)

P_0 = Probability that rain is falling at the point of interest

erfc = Complementary error function

R_m = Median value of point rain-rate during raining time

S_R = Standard deviation of $\ln(R)$ during rain time

¹S.H. Lin, "A Method for Calculating Rain Attenuation Distributions on Microwave Paths," Bell system Tech. J., July - August, 1975, pp. 1051-1086.

2.2.3 Rain Attenuation

The instantaneous relationship obtained between the point rain rate $R(\underline{S}, t)$ located at \underline{S} and the corresponding rain attenuation gradient $\beta(\underline{S}, t)$ depends upon the particular distributions of raindrop sizes, shapes, orientations, the speed and local direction of the wind, and the rain temperature. However, the average relationship between rain rate R and rain attenuation gradient can be simplified and approximately described by:

$$\beta = r(\lambda) R \zeta(\lambda) \quad \text{dB/km} \quad (2.2.2)$$

where $r(\lambda)$ and $\zeta(\lambda)$ are parameters dependent on the polarization and frequency of the radio signal, and rain temperature. R is in terms of mm/hr. The validity of the theoretical method is now fairly well established, and calculations have been carried out for a wide range of frequencies.^{1,2,3} The empirical values of γ and ζ have been given by many authors.^{4,5,6} Its complexity, however, makes it impractical for

¹K.L.S. Gunn and T.W.R. Est, "The Microwave Properties of Precipitation Particles," Quart. J. Roy. Meteor Soc., 1954, pp. 522-545.

²R.G. Medhurst, "Rainfall Attenuation of Centimeter Waves: Comparison of the Theory and Measurement," IEEE Trans. On AP, July 1965, pp. 550-564.

³R.L. Olsen, D.V. Rogers and D.B. Hodge, "The aR^b Relation in Calculation of Rain Attenuation," IEEE Trans. on AP, March 1978, pp. 318-329.

⁴S.H. Lin, B.S.T.J., July - Aug 1975, pp. 1051-1086.

⁵J.T. DeBettencourt, "Statistics of Millimeter Wave Rainfall Attenuation," J. Rech. Atmos., Aug 1974, pp. 89-119.

⁶B.N. Harden, et al, "Attenuation/Rain-Rate Relationships on Terrestrial Microwave Links in the Frequency Range 10-40 GHz," Elect Lett, 2 March 1978, pp. 154-155.

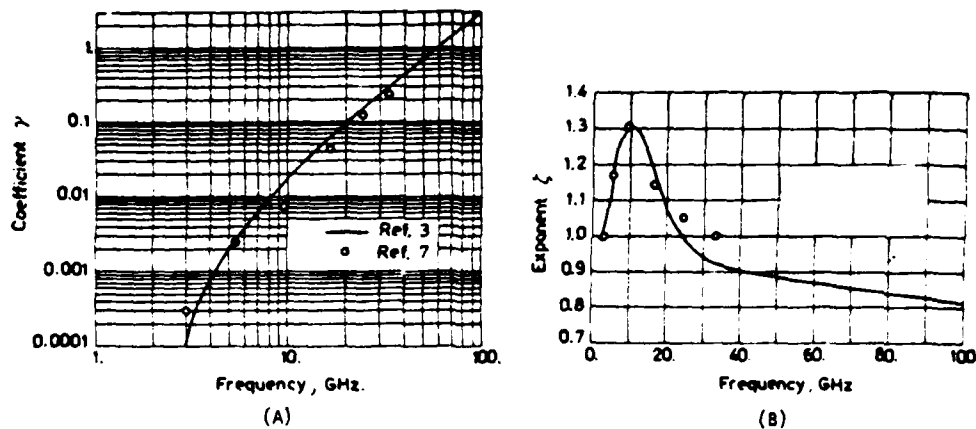
direct use by systems designers. Consequently, the calculation has commonly been given in the form of graphs or tables, such as the curves given by CCIR¹ illustrated in Figure 2.2.3. This solution, although satisfactory for applications requiring only a few calculations, is unsuitable for those requiring calculation at a wide frequency range. It also lacks the simplicity of empirical procedure based on Equation 2.2.2, which is still used by many workers for this reason. The approximate validity of the linear form of Equation 2.2.2 with $\zeta = 1$ was first pointed out by Ryde² on the basis of his early Mie scattering calculations; Gunn and Est³ later proposed the more general nonlinear relation. In 1965, Medhurst⁴ reviewed the experimental results to that date and pointed out serious discrepancies with the theoretical calculations. Although he concluded that the accuracy of the theoretical approach "cannot be said to be demonstrated," it is now generally accepted that most of the discrepancies were due to a combination of the spatial nonuniformity of actual rain and the limitations in the rain-rate sampling techniques employed in the early experiments.

¹CCIR, Programmes d'Etudes 191 (V) et 192 (V), Documents de la Xe Assemblée Plénière, Vol. II.

²J.W. Ryde, "The Attenuation and Radar Echoes Produced at Antimeter Wavelengths by Various Meteorological Phenomena," 1946.

³K.L.S. Gunn and T.W.R. Est, "The Microwave Properties of Precipitation Particles," Quart. J. Roy. Meteor. Soc., 1954, pp. 522-545.

⁴R.G. Medhurst, "Rainfall Attenuation of Centimeter Waves: Comparison of the Theory and Measurement," IEEE Trans. On AP, July 1965, pp. 550-564.



A90401-109

Figure 2.2.3. Coefficients γ and ζ of Rain Attenuation (After CCIR)

Lately, Olsen et al.¹ utilized an approximation of a more general relation

$$\beta = aR^b \left[1 + \sum_{n=2}^{\infty} c_n f^n R^{nd} \right] \quad (2.2.3)$$

to expand and cover very wide frequency range (1 - 1,000 GHz) and raindrop sizes. In Equation 2.2.3; a , b and the coefficient c_n are functions of frequency, rain temperature, and the parameters of a general drop size distribution; d is a constant depending on the parameters of the drop size distribution. The equation implies that Equation 2.2.3 is exact, with γ and ζ independent of R , as $f \rightarrow 0$ (realistically, for $f \leq 1$ GHz) and also to

¹R.L. Olsen, D.V. Rogers and D.B. Hodge, "The aR^b Relation in Calculation of Rain Attenuation," IEEE Trans. on AP, March 1978, pp. 318-329.

be true in the infrared region $f \rightarrow \infty$. Values of γ and ζ of various drop size distributions, including wide spread rain of high rate, thunderstorm distribution and drizzle distribution, are analyzed extensively and given by Olsen¹ at different frequencies and temperatures. Olsen et al. also made the comparison between measured and calculated values of γ , ζ , a , and b over a wide range of frequencies, that provides an added measure of confidence in their theory and the experimental results.

In the design of systems operating at frequencies in the millimeter wave region where rain attenuation is severe, it is recommended that the convective, widespread rain distribution at temperature of 0°C be utilized for all rain rates. The calculations for the other drop size distributions and rain temperatures can be used in the regions where they are known to apply, or to provide appropriate bounds.

2.3 Rain-Induced Polarization Degradation

2.3.1 Polarization Degradation Effects Frequency Reuse Communications Systems

Frequency reuse via orthogonally polarized channels can double the bandwidth efficiency of communication systems. The 3 dB increase in bits/Hz of spectrum is accomplished with a corresponding 3 dB increase in transmitted power and no resultant degradation in the quality of communications. Unfortunately, the nonideal antenna and nonideal transmission media create the cross polarization degradations which reduce the signal-to-interference ratio (S/I) and increase crosstalk. The rainfall in the transmission path will worsen the millimeter wave S/I further due to a decrease of S as opposed to an increase in I.

2.3.2 Rain-Induced Cross Polarization

Cross coupling is due to rain results from the differential phase shift and differential attenuation of electrical field components, parallel and perpendicular to the main axis of oblate spherical raindrops. If raindrops were perfectly aligned with the transmitted polarization, that is, if one polarization was parallel to the major axis of the raindrops and the orthogonal polarization parallel to the minor axis, there would be no crosspole coupling due to rain. Also, if raindrops were perfectly spherical, again, there would be no crosspole coupling. Obviously, however, since these situations are far from reality, the diffraction and scattering, reflection, and refraction of millimeter wave signals from the oblate shape of raindrops will cause both differential phase shift and differential attenuation between vertical polarization and horizontal polarizations. Consequently, crosstalk and degradation of S/I result.

Since the realistic raindrop shape is determined by wind velocity, gravitation, inertia, drop size and many other factors; the canting angle distribution of raindrops becomes too complicated to estimate. However, there are several characteristics of rain-induced cross polarization listed below:

- Insensitive to rain rate.
- For a given rain fading,¹ the cross polarization decreases with increases in frequency.
- The cross polarization discrimination of circularly polarized waves is much poorer than that of linearly polarized waves (Except 0 - 45°).
- Varies with canted angle.

¹T.S. Chu, "Rain-Induced Cross-Polarization at Centimeter and Millimeter Wavelengths," B.S.T.J., Oct. 1974, pp. 1557-1579.

2.3.3 Rain-Induced Attenuation and Phase Shift

As described previously, the cross coupling between vertical and horizontal polarizations occurs as a result of the differential attenuation and differential phase shift between two polarizations I and II, perpendicular and parallel to the major axis of the oblate raindrops. The rain-induced attenuation and phase shift obtained from the forward scattering function $S(0)$ are¹

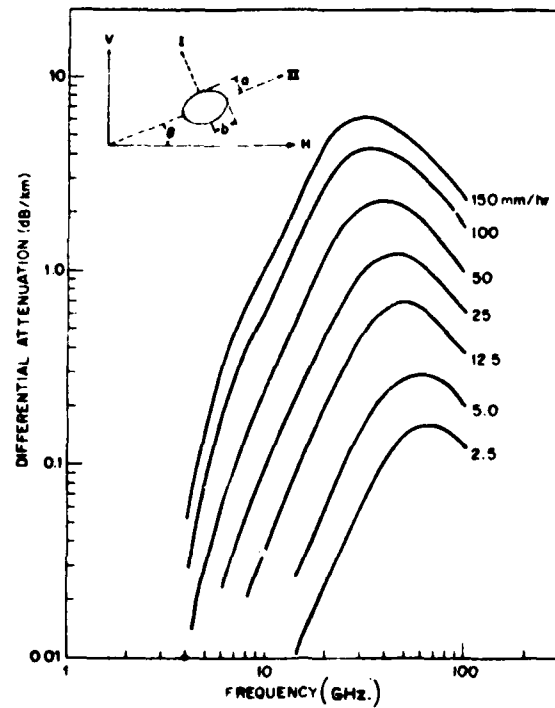
$$A_{I,II} = 0.434 \frac{\lambda^2}{\pi} \sum \text{Re } S_{I,II}(0) n(\bar{a}) \quad \text{dB/km} \quad (2.3.1)$$

$$\theta_{I,II} = -36 \frac{\lambda^2}{\pi} \sum \text{Im } S_{I,II}(0) n(\bar{a}) \quad \text{deg/km} \quad (2.3.2)$$

where $n(\bar{a})$ is the number of drops with equal volume spherical radius \bar{a} , per cubic meter. The calculated differential attenuation and differential phase shift between polarizations II and I for various rain rates and frequency are given in Figure 2.3.3-1 and Figure 2.3.3-2, respectively.

For a given fade, the differential shift declines sharply with the increase of frequency, whereas the normalized differential attenuation is relatively insensitive to frequency. Therefore, the differential attenuation becomes increasingly important as the frequency increases. The sharp descent of differential phase shift also implies less depolarization at frequencies above 20 GHz for a given fade.

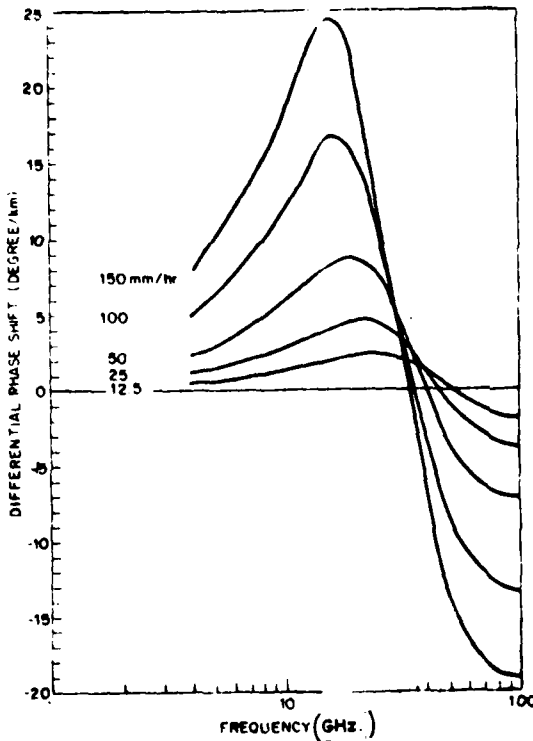
¹D.C. Hogg and T.S. Chu, "The Role of Rain in Satellite Communications," Proc. of IEEE, Sept. 1975, pp. 1308-1331.



A90401-71

Figure 2.3.3-1. Rain-Induced Differential Attenuation Between Polarizations I and II for Various Rain Rates (After Hogg and Chu)

As the rain rate decreases, the normalized differential attenuation of each frequency decreases. On the other hand, the differential phase shift per dB of fading generally increases with the decrease of the rain rate. These two opposite trends tend to keep the depolarization relatively insensitive to the rain rate.



A90401-72

Figure 2.3.3-2. Rain-Induced Differential Phase Shift Between Polarizations I and II for Various Rain Rates (After Hogg and Chu)

From differential attenuation and differential phase shift at given frequency, rain rate and path length, the cross polarization coupling and phase difference can be calculated from the following equations.

Cross Polarization Coupling (dB)

$$C = 20 \log \left[\frac{(\cos \theta \sin \theta - \alpha \cos \theta \sin \theta \cos \beta)^2 + (\alpha \cos \theta \sin \theta \sin \beta)^2}{(\cos^2 \theta + \alpha \sin^2 \theta \cos \beta)^2 + (\alpha \sin^2 \theta \sin \beta)^2} \right]^{1/2} \quad (2.3.3)$$

Phase Difference Between Copolarized Signals

$$\delta \phi = \left| \tan^{-1} \left[\left(\frac{-\alpha \cos \theta \sin \theta \sin \beta}{\cos \theta \sin \theta - \alpha \cos \theta \sin \theta \cos \beta} \right) \right] \right. \\ \left. - \tan^{-1} \left[\left(\frac{\alpha \sin^2 \theta \sin \beta}{\cos^2 \theta + \alpha \sin^2 \theta \cos \beta} \right) \right] \right|$$

where

α = Differential attenuation

β = Differential phase shift

θ = Raindrop canting angle

Consequently, a cross polarization isolation factor for circularly and linearly polarized waves can be expressed as below:

Circularly Polarized Waves Cross Polarization Isolation

$$I_c = 20 \log \left| \frac{1 - e^{-L(\alpha + j\beta)}}{1 + e^{-L(\alpha + j\beta)}} \right| \quad (2.3.5)$$

Linearly Polarized Waves Cross Polarization Isolation

$$I_c = 20 \log \left| \frac{1 - e^{-L(\alpha + j\beta)} \tan \theta}{1 + \tan^2 \theta e^{-L(\alpha + j\beta)}} \right| \quad (2.3.6)$$

where L path length in rain

It is noted that for 45° raindrop canting angles, the linear and circular crosspolar isolation factors are identical. At mean time, the depolarization can also be expressed by Chu¹ in terms of cross polarization discrimination or crosstalk discrimination. For example, Figure 2.3.3-3 illustrates the polarization crosstalk ratio as a function of frequency and path length at 100 mm/hr rain rate. According to Chu,¹ the calculated data in Figure 2.3.3-3 and Figure 2.3.3-4 for linear and circular polarized waves agree fairly well with measured data by many other authors.

2.4 Millimeter Wave Propagation Over the Water

For short distances, line-of-sight millimeter wave links may not have the multipath problem due to earth curvature. Overwater paths, undesirable because of reflections, are sometimes unavoidable. The experimental works of overwater propagations of millimeter wave frequencies have been investigated by several authors.^{2,3} At 37 GHz, 30 km distance, the fade depth (due to multipath caused by reflection) of 8 dB is typical, although fade depths as great as 14 dB were observed by Vagnali. The fading generally displays a fast and a slow component with typical average values of about 0.5 fade per second and 1.5 fades per minute. The corresponding

¹T.S. Chu, "Rain-Induced Cross Polarization at Centimeter and Millimeter Wavelengths," BSTJ, Oct. 1974, pp. 1557-1579.

²A.J. Mondloch, "Overwater Propagation of Millimeter Waves," IEEE Trans on AP, Jan 1969, pp. 82-85.

³J.A. Vignali, "Overwater Line-of-Sight Fade and Diversity Measurements at 37 GHz," IEEE Trans on AP, July 1970, pp. 463-471.

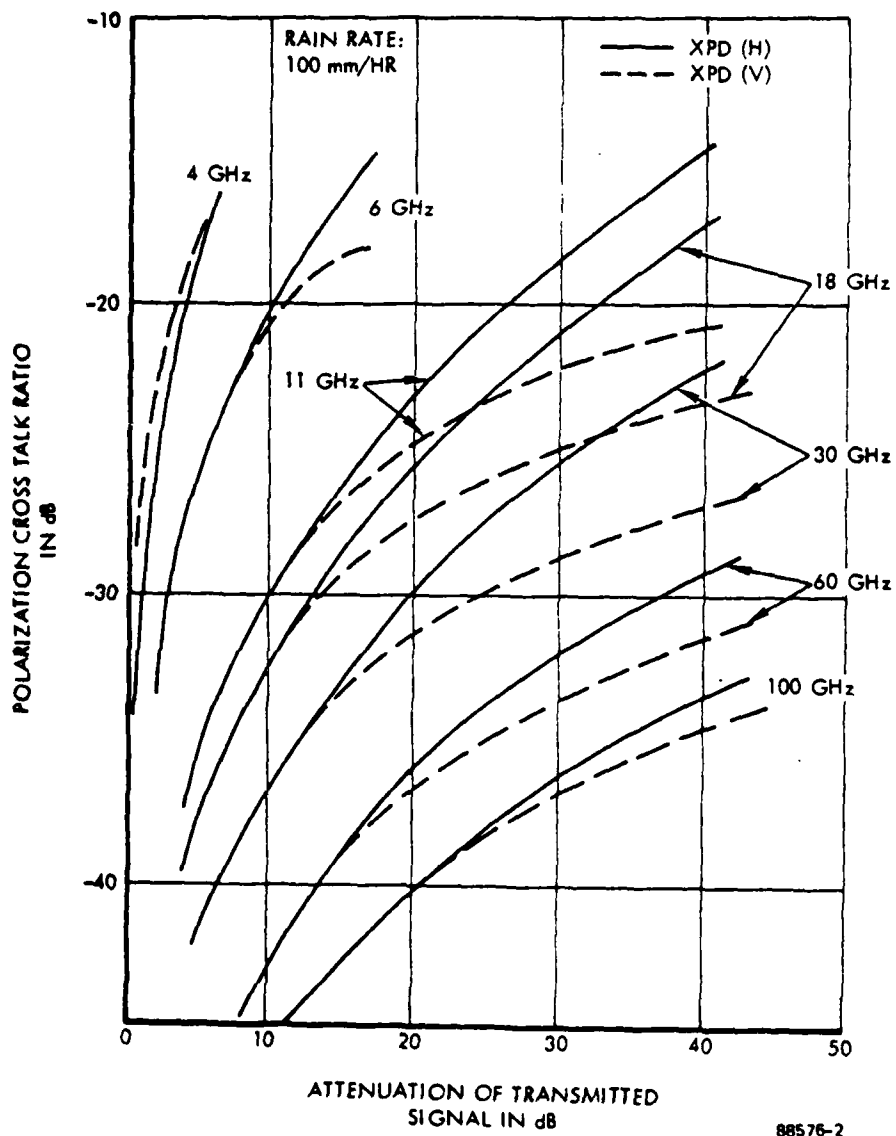


Figure 2.3.3-3. Calculated Rain-Induced Cross Polarization of Horizontally and Vertically Polarized Waves (After Chu)

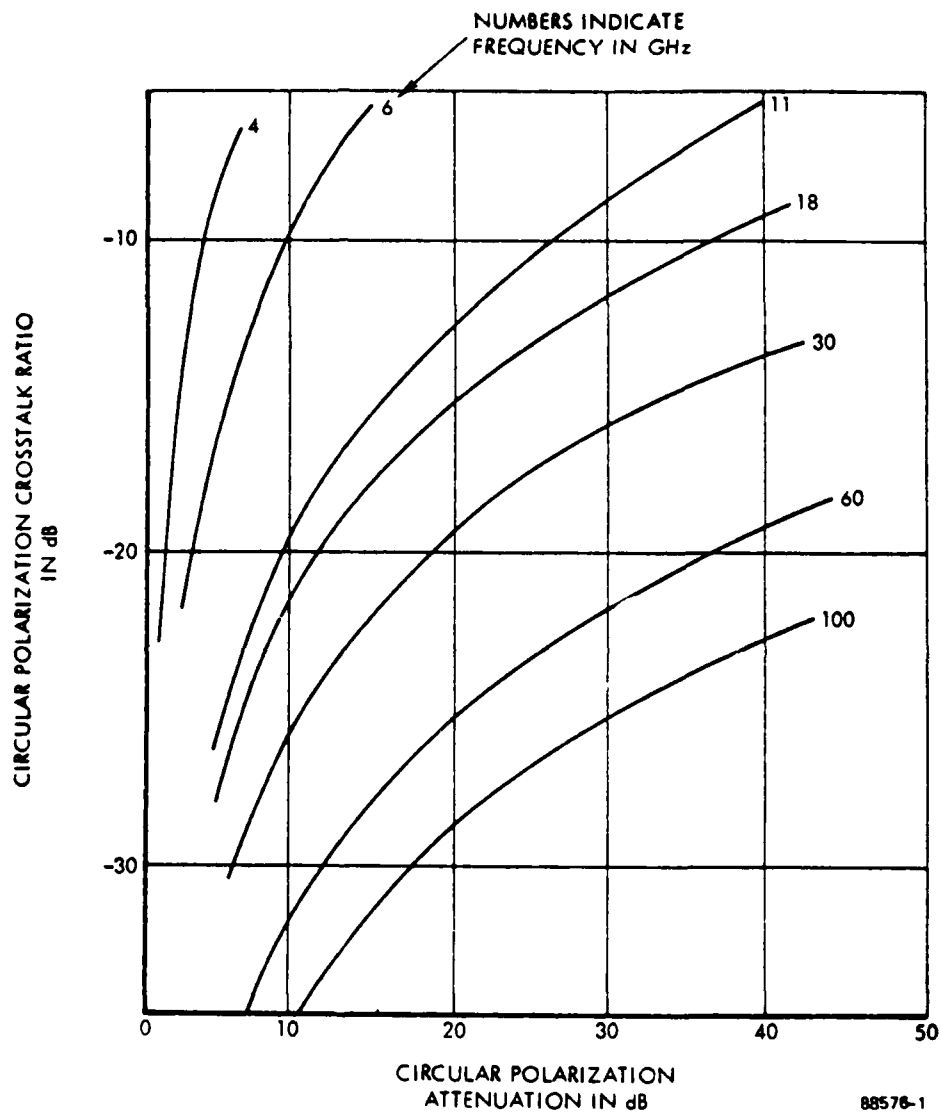


Figure 2.3.3-4. Calculated Rain-Induced Cross Polarization of Circularly Polarized Waves (After Chu)

average fade durations were 1 second and 20 seconds, respectively. The importance of the specular reflection from the water surface was clearly evident in the results. The typical value of the specular reflection coefficient is about 0.7, but extreme values varied from almost 0 to 1. The reflection coefficient of the diffusely scattered component showed less variation and is typically about 0.25.

The use of a 15 dB fade margin would be sufficient to overcome at least 98 percent of short term fading (no rain effects are included) for every sample of data examined. With a 10 dB fade margin, the 98 percent value would be exceeded during typical fading, but a value of only 93 percent would be achieved during the worst fading periods.

2.5 Link Availability and System Design

2.5.1 System Availability and Path Availability

In order to quantitatively assess the usefulness of path diversity and system performance at millimeter wave frequencies, it is desirable to establish system availabilities. The system availability, A_S , can be expressed as

$$A_S = A_T \cdot \bar{A}_p \cdot A_R \quad (2.5.1)$$

where the subscripts T, P, and R represent transmitter, propagation medium and receiver. A_T and A_R are estimates from the MTBF and MTBR of transmitter and receiver's electronics, while A_p is determined by rain effects, jammer, vegetation and geographical circumstances.

In modern communications systems, the outage time of transmitter and receiver equipment can be made negligibly small by using standby equipment and automatic protection switching systems. Protection against some propagation outages can also be achieved by providing an alternate path

or channel and automatic switching; with protection against multipath fading provided by space or frequency diversity. However, in the millimeter wave frequency range, attenuation by rain can cause outage which is not easily eliminated by an alternate path or channel, because rain attenuation is relatively constant with frequency across the common carrier bands, attenuates both polarizations, and covers a fairly large area. Then, the availability of the link path becomes critical to the budget of system design.

For path diversity systems, A_p is readily computed from

$$A_p = A_{TR} \cdot A_{RE} \cdot A_{RR} \quad (2.5.2)$$

where

and A_{TR} = Propagation availability of radio path between transmitter and repeater

A_{RE} = Repeater availability

A_{RR} = Propagation availability of radio path between repeater and receiver

and a single repeater is assumed. The path diversity related A_p will be discussed further in Section 4.0. Since the rain effects increase the path attenuation, cross polarization and multipath fading, the radio path propagation availability due to rain effects will be

$$A_p = \frac{k_1 A_{att}}{k_1} \times \frac{k_2 A_{cp}}{k_2} \times \frac{k_3 A_{mf}}{k_3} \quad (2.5.3)$$

where

$$k_1^1 = k_1 \quad \text{for frequency above 10 GHz}$$

$$= k_1 A_{\text{att}} \quad \text{for frequency below 10 GHz}$$

$$k_2^1 = k_2 \quad \text{for dual-polarization system}$$

$$= k_2 A_{\text{cp}} \quad \text{for single-polarization system}$$

$$k_3^1 = k_3 \quad \text{for link distance } < 10 \text{ km}$$

$$= k_3 A_{\text{mf}} \quad \text{for link distance } > 10 \text{ km}$$

$A_{\text{att}} =$ availability due to excess rain attenuation, including the wet radome loss

$A_{\text{cp}} =$ availability due to cross-polarization degradation

$A_{\text{mf}} =$ availability due to multipath fading

All A_{att} , A_{cp} and A_{mf} are dependent upon the frequency and rain rate. If rain rate, operation frequency and link distance are given, the path propagation availability can be obtained. An example will be presented later in this section. Multi-antennas can be utilized for a single station. Vigants¹ has defined a "space diversity improvement factor"

$$I_{sd} = \frac{7.0 \times 10^{-5} \times f \times S^2 \times 10^{-F/10}}{D} \quad (2.5.4)$$

where

f = frequency in GHz

S = Vertical antenna spacing

F = Fade margin associated with the second antenna

D = Path length in miles

For a single polarization system, the unavailability for a non-diversity hop, U_{nd} , is the probability that fade margin will be exceeded and is defined as:

$$U_{nd} = br \times 10^{-F/10} \quad (2.5.5)$$

where F is fade margin in dB, r is the probability of exceeding path attenuation due to rain effects at given rates and operation frequency, and b is a constant which depends on geographical condition, multipath fading, etc. The path availability, A_p , then is given by:

$$A_p = 1 - U_{nd} \quad (2.5.6)$$

¹A. Vigants, "Space-Diversity Performance as a Function of Antenna Separation," IEEE Trans on Comm. Dec. 1968.

Assume for calculation purposes an 8 GHz space diversity system with a 30 mile path, 40 dB fade margins, and 40 foot antenna spacing, then the unavailability of space-diversity is:

$$U_{sd} = \frac{U_{nd}}{I_{sd}} = \frac{1/4 \times 10^{-5} \times 8/4 \times (30)^3 \times 10^{-4}}{7 \times 10^{-5} \times 8 \times (40)^2 \times 10^4 / 30}$$
$$= 5 \times 10^{-8}$$

or

$$A_{ps} = 1 - 5 \times 10^{-8}$$

However, it is suggested in this report that no direct comparison of path availability between 8 GHz and millimeter wave frequencies should be given because the MMW spectra has many inherent advantages which an 8 GHz system could not possess. The advantages, as mentioned previously, are high antenna gain, small size/weight, wide bandwidth, low LPI, low antenna tower required, etc.

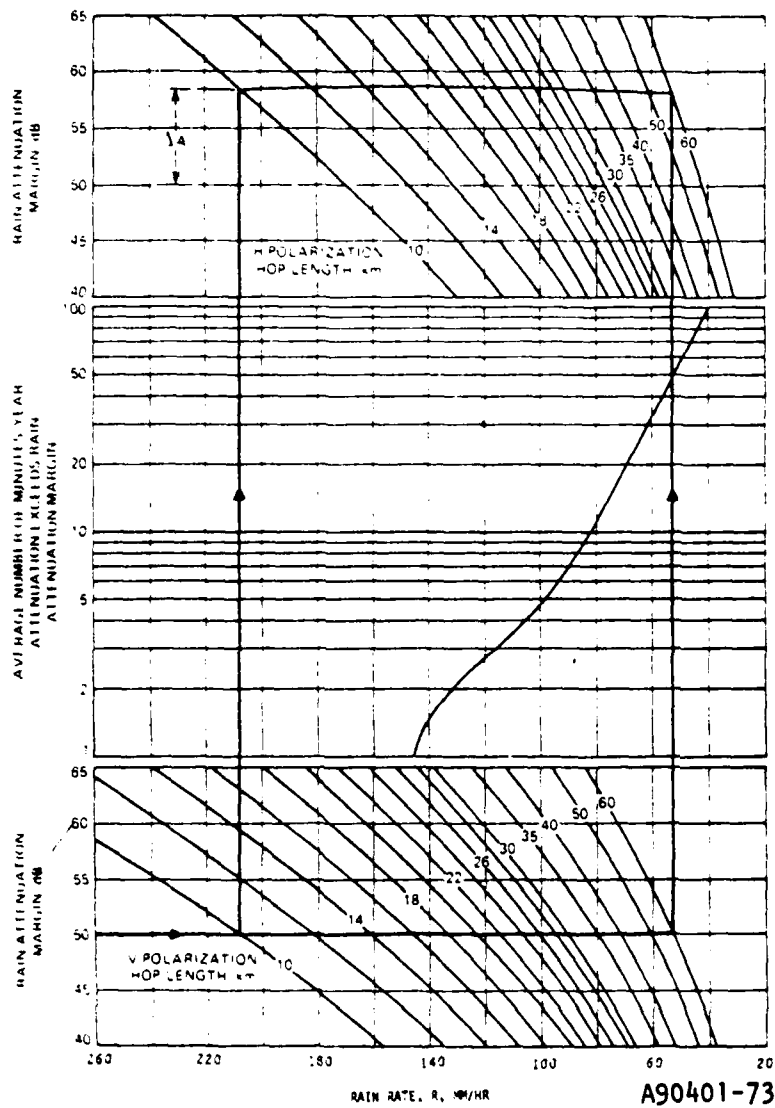


Figure 2.5.1. Rain Outage Chart (After T.L. Osbourne)¹

¹T.L. Osbourne, "Application of Rain Attenuation Data Rate to 11-GHz Radio Path Engineering," B.S.T.J., Nov. 1977, pp. 1605-1627.

The rain induced propagation loss at 8 GHz is almost negligible. The path availability of 8 GHz radio is definitely higher than millimeter wave frequencies. However, 8 GHz radio cannot provide wide bandwidth or high data rate capability without extremely difficult dispersion equalization processing. The multipath fading problem of 8 GHz operations is reducible by using space diversity.

2.5.2 System Budget Design Including Rain Effects

The use of route diversity has been considered to provide an alternate propagation path. Unavoidable tradeoffs of economics-versus-reliability is required to determine whether the alternate route approach is practical or economical, because of the cost of providing a complete standby system and the uncertainty of whether the designer can vary parameters adequately in the proper range to obtain an optimum rain attenuation margin.

Using either alternate routing or direct link, the designer must evaluate the attenuation induced by rain and provide sufficient system margin to reduce the amount of rain outage time below some outage objective to achieve a reliable communication system. In this section, procedures of millimeter wave system budget design are summarized based upon the works of T.L. Osbourne.¹ In the design procedures, the outage caused by rain attenuation and cross polarization are addressed, but not other causes such as multipath fading or equipment failure. The procedures are summarized as follows:

- a. Calculate Rain Attenuation Margin
- b. Generate the Rain Outage Charts
- c. Graphically find the following parameters

¹T.L. Osbourne, "Application of Rain Attenuation Data Rate to 11-GHz Radio Path Engineering," B.S.T.J., Nov. 1977, pp. 1605-1627.

(see example illustrations)

- Outage time (from attenuation margin and hop length)
- Differential attenuation between the horizontal and vertical polarizations
- Maximum allowable hop lengths for a particular system
- Radio receiver limitation due to AGC
- Others

The first step is to determine the available rain attenuation margin from the link distance and the specification of the equipment; such as antenna, transmitter, receiver, random, interface transmission line, etc. The computation of the rain attenuation margin is sequentially listed in Table 2.5.1. The depolarization performance degradation only applies to the digital system using dual polarized frequency channels. The depolarization by heavy rain causes cochannel interference. The right column of Table 2.5.1 indicates the design manipulability.

The second step is to prepare a Rain Outage Chart such as Figure 2.5.³ The steps of preparation of Rain Outage Charts are depicted in Table 2.5.2. The detail information is described and illustrated in References 1, 2 and 3.

¹S.H. Liu, "Nationwide Long-Term Rain Rate Statistics and Empirical Calculation of 11-GHz Microwave Attenuation," B.S.T.J., November 1977, pp. 1581-1604.

²T.S. Chu, "Rain Induced Cross Polarization at Centimeter and Millimeter Wavelengths," B.S.T.J., October 1974, pp. 1557-1579.

³T.L. Osbourne, "Application of Rain Attenuation Data to 11-GHz Radio-Path Engineering," B.S.T.J., November 1977, pp. 1605-1627.

Table 2.5.1. Calculations of Rain Attenuation Margin

System Parameter	Symbol	Calculation (dB)	Design Manipulability
System gain* at given BER or S/N	G _S		Yes
Loss between TX and TX Antenna	L _{TA}		Yes
Loss between RX Antenna and RX	L _{RA}		Yes
Free-space path loss (including rain effects)	L _p		Yes
TX Antenna gain	G _T		Yes
RX Antenna gain	G _R		Yes
Section loss	L _S	$L_S = G_T + G_R - L_p - L_{TA} - L_{RA}$	Yes
Total fade margin available for rain fading	M _T	$M_T = G_S - L_S$	Yes
Wet Radome Loss	L _R		No
Depolarization Performance Degradation (for dual-polarization system only)	L _{XP}		No
Foreign system interference degradation	L _I		No
Rain attenuation margin	M _R	$M_R = M_T - L_R - L_{XP} - L_I$	Yes

*G_S: Difference in signal levels between TX output and RX input.

Table 2.5.2. Preparation of Rain Outage Charts

Step	Equations	References
<p>1. Long-term appropriately averaged, point rain rate distributions are derived from weather bureau data at a given location. These distributions show the number of minutes per year, T, that the 5-minute point rain rate, R, exceeds a given value, and can be described by</p>	$T = g(R)$	<p>1</p>
<p>2. The radio path attenuation, α, for a given hop length, L, and polarization is related to the 5-minute point rain rate, R</p> <p>($\bar{L}(R)$ is the characteristic path length, determined by geographical location)</p>	$\alpha_v = \gamma_v R \zeta^v / (1 + L/\bar{L}(R))$ $\alpha_h = \gamma_h R \zeta^h / (1 + L/\bar{L}(R))$	<p>1,2</p>
<p>3. Since we are interested in the amount of time, the path attenuation exceeds the rain attenuation margin, M_r and obtain (setting X equal to M_r)</p>	$R = f_v(\lambda, M_r, L)$ $R = f_h(\lambda, M_r, L)$	<p>3</p>

¹S.H. Liu, "Nationwide Long-Term Rain Rate Statistics and Empirical Calculation of 11-GHz Microwave Attenuation," B.S.T.J., November 1977, pp. 1581-1604.

²T.S. Chu, "Rain Induced Cross Polarization at Centimeter and Millimeter Wavelengths," B.S.T.J., October 1974, pp. 1557-1579.

³T.L. Osbourne, "Application of Rain Attenuation Data to 11-GHz Radio-Path Engineering," B.S.T.J., November 1977, pp. 1605-1627.

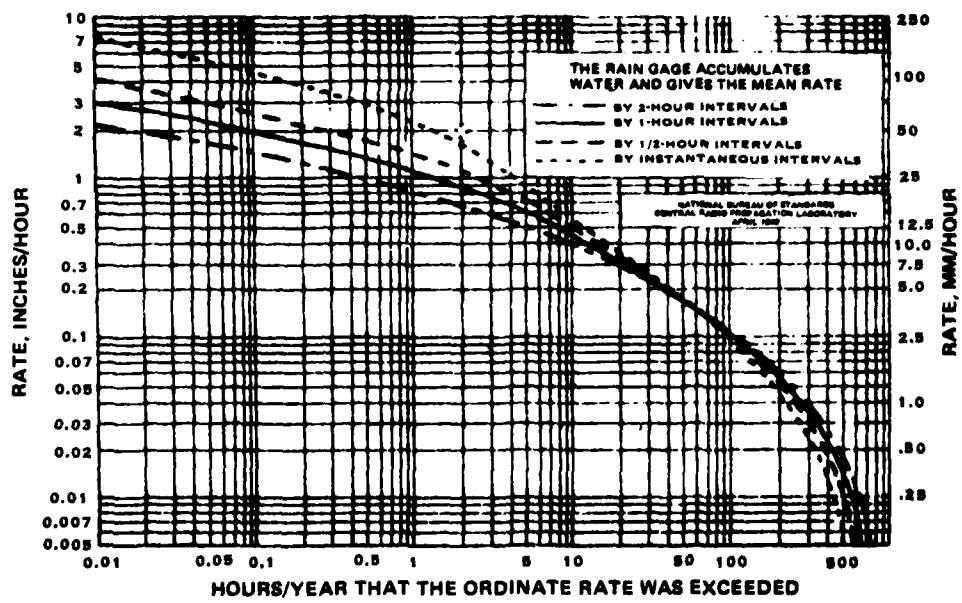
Table 2.5.2. Preparation of Rain Outage Charts - Continued

Step	Equations	References
4. From Step 3, generate rain outage charts for vertical and horizontal polarizations (see example)		

Considerable detail is given by T.L. Osbourne to compute the link outage time by a step-by-step graphical method and will not be repeated in this report. When the annual outage time due to rain is determined, then propagation path availability is equal to $(1 - \text{probability of total outage})$.

Systems with path availability better than 99 percent require considerable system margin to compensate for rain-induced path attenuation, particularly for the link distances over 10 km. Since the cumulative rainfall distribution for point rates at Washington, D.C. is known (depicted in Figure 2.5.2-1), then the path availability versus required system margin can be derived according to the previously described procedures. Figure 2.5.2-2 is the availability as a function of system margin for various link distances at 38 GHz and 44 GHz, respectively. At 38 GHz, a 10 km link may need 12 dB system margin to achieve 99.9 percent availability while 20 km links require 27 dB margin. From a hardware dynamic range viewpoint, even with automatic gain control (AGC), the millimeter wave communication is not recommended for a long distance (e.g., 20 km at 99.9 percent availability). However, if the system can tolerate 53 minutes outage annually (or 99 percent availability), a longer distance such as a 50 km link is still feasible.

Referring to Figure 2.5.2-2, annual path availabilities of better than 99.9 percent at 38 GHz and 44 GHz are achievable without path diversity in the vicinity of Washington, D.C. for link distance of 5 km. With an extra repeater for path diversity purposes, the link distance of the same path availability may extend to 10 km.



A90401-74

Figure 2.5.2-1. Cumulative Rainfall Distribution for Point Rates at Washington, D.C.

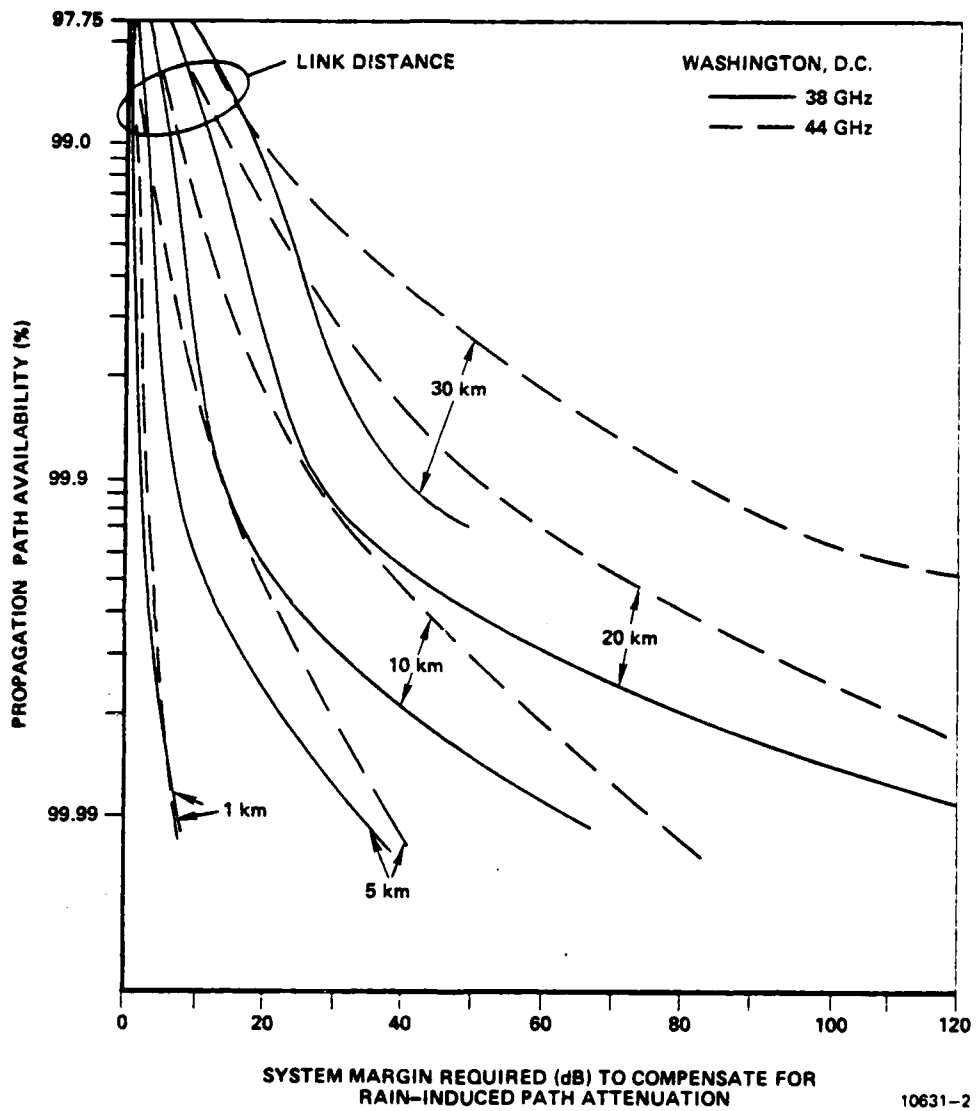


Figure 2.5.2-2. 38 and 44 GHz Path Availability Versus System Margin in Vicinity of Washington D.C.

3.0 SURVEY OF ANTIJAM TECHNIQUES AND JAMMING EFFECTS

3.1 Introduction

Antijam (AJ) techniques fall into two classes: spread spectrum techniques and adaptive antenna techniques. Spread spectrum techniques rely solely upon desired signal waveform in order to discriminate against jammers, whereas adaptive antennas discriminate against jammers on the basis of their angular (equivalently, spatial) separation from the desired signal transmitter. The discussion below deals only with spread spectrum techniques; additional AJ protection afforded by virtue of null-steering adaptive antenna arrays is the subject of another study task, the results of which will be integrated with the results of the spread spectrum survey task. The AJ capability that may be obtained at MMW frequencies will be compared to that available at 8 GHz, accounting for available spectrum and state-of-the-art device technology.

In the past, spread spectrum AJ protection has typically been applied to data rates on the order of tens of kilobits/sec with chip rates in the Mb/s to tens of Mb/s, range, to yield processing gains on the order of 20 to 30 dB. However, since the data rates of interest in this study are 1 Mb/s to 20 Mb/s, and 150 Mb/s, obtaining large processing gains becomes much more difficult to achieve due to the difficulty of implementing large chirp range SAW devices, high chip rate PN generators, or sufficiently fast frequency hoppers. The limitations on achievable processing gains imposed by implementation considerations will be explored subsequently.

3.2 Figure of Merit for Spread Spectrum Communication Systems

The spread spectrum AJ techniques to be discussed are

- a. Chirp (linear FM)
- b. Frequency Hopping (FH)

c. Direct Sequence (DS)

d. Hybrid Techniques

The figure of merit for a spread spectrum protected communication system is the antijam (AJ) protection in dB. The AJ protection for a spread spectrum communication system is defined as

$$AJ \text{ dB} = \left[G_p - (E_b/N_0)_{\text{required}} \right] \text{ dB}$$

where, in general,

$$G_p = \frac{\text{spread bandwidth}}{\text{data bandwidth}} = \text{processing gain}$$

For the three basic types of spectrum spreading in linear channels, the processing gain is given by:

DS

$$G_p = \text{chip rate/bit rate} = R_c/R_b$$

FH

$$G_p = N = \text{number of hop frequencies}$$

Chirp

$$G_p = \text{chirp frequency range/data rate}$$

Since the AJ figure of merit may be trivially calculated once the processing gain is determined, we will hereafter deal primarily with processing gain when characterizing a spread spectrum system. The parameter AJ, or equivalently, G_p , characterizes the system performance; it is also desirable to characterize the severity of the jamming environment. This is done by specifying the jammer-to-signal power ratio J/S at a given point in the communication receiving system. The J/S ratio after spectrum despreading is improved by a factor of G_p with respect to the J/S ratio prior to despreading.

One important concern in any spread spectrum system is the linearity of the system. Some systems utilize highly nonlinear saturated TWT repeater amplifiers (e.g., satellite systems) whereas other systems are nominally linear. However, for very high power jammer situations the receiver may be driven into a nonlinear region of operation. It is therefore important to understand the effects of limiters on spread spectrum system performance. It turns out that for $J/S \ll 1$ the effect of the hardlimiter is to actually suppress the weak jammer by 3 dB.

While this effect is beneficial, it is of little practical significance since the usual jamming situation is characterized by $J/S \gg 1$. The effect of a limiter upon the J/S ratio is summarized below for $J/S \Big|_{in} \gg 1$ in DS and FH systems.¹

NOISE JAMMER (BROADBAND): FH AND DS SYSTEMS

$$J/S \Big|_{out} = J/S \Big|_{in} + 1 \text{ dB}$$

¹D.G. Mueller, F.A. Perkins, E.F. Smith, C.L. Zahm, Spread Spectrum Communications, Technical Report No. 38, Advanced Systems Operations, Radiation, Inc., pp. 5-20, 5-29, July, 1970.

CW JAMMER

FH SYSTEM

single sinusoid jammer

$$J/S \Big|_{out} = J/S \Big|_{in} + 6 \text{ dB}$$

multiple sinusoid jammer (approaches noise jammer case)

$$J/S \Big|_{out} = J/S \Big|_{in} + 1 \text{ dB}$$

DS System with CW or Replica Jamming

- BPSK - inphase jammer captures the limiter and obliterates the desired signal
- QPSK - 6 dB signal suppression so that

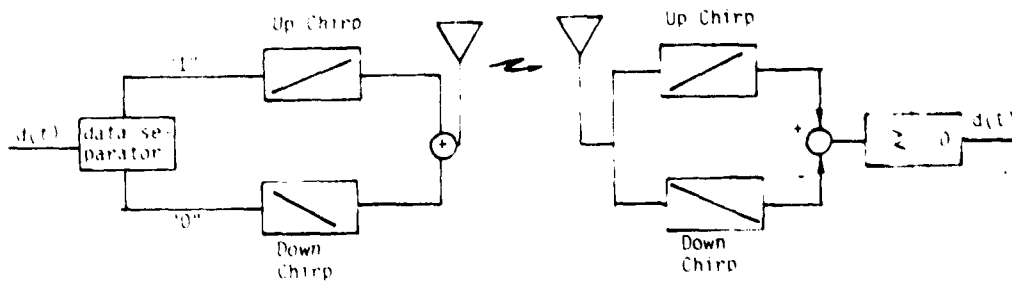
$$J/S \Big|_{out} = J/S \Big|_{in} + 6 \text{ dB}$$

- Staggered QPSK² - 12 dB signal suppression under certain conditions unlikely to be fulfilled in practice; 6 dB signal suppression otherwise.

Having now discussed the figures of merit that characterize spread spectrum systems and the jamming environment that they operate in, we now examine each of the fundamental types of spread spectrum systems.

²William E. Toms, Jr., Investigation of Offset QPSK Modulation in Conjunction with Spread Spectrum Communications (U), prepared for DCA by Computer Sciences Corporation, Contract No. DCA 100-73-C-0008 Task Order No. 0308, Part 3, October 1974 (Confidential).

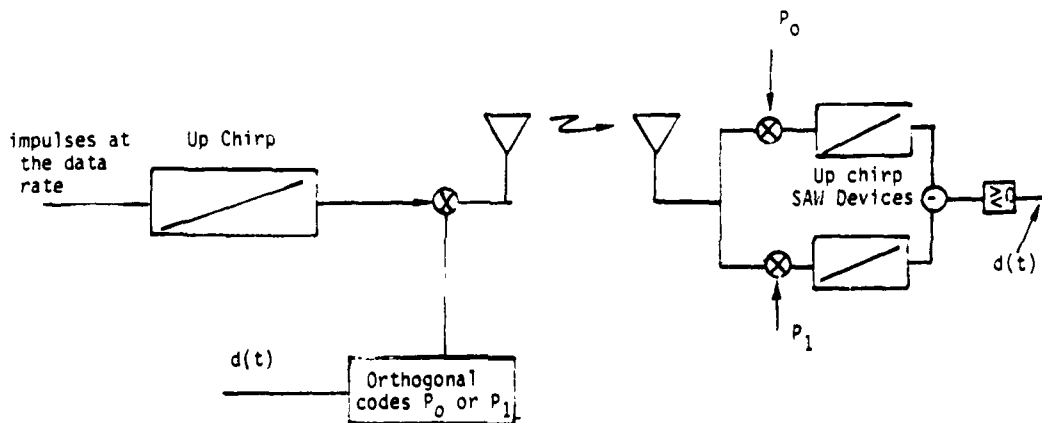
Figure 3.3-1 is a conceptual block diagram which is intended to show how an up/down chirp system operates. The key element of this system is a surface acoustic wave (SAW) device, which generates a linear FM wave (upchirp or downchirp) when an impulse is applied to its input. In the simple block diagram of Figure 3.3-1 the data separator block distinguishes data "1's" from "0's" and applies impulses to either the upchirp SAW device or the downchirp SAW device accordingly. Identical SAW devices perform a matched filter correlation operation at the receiver. A received upchirp, for example, yields a large, time compressed pulse at the receiver's upchirp SAW device output; since the upchirp is orthogonal to the downchirp, no output appears at the output of the receiver downchirp SAW device output. A comparator with zero threshold makes data decisions. The advantages of chirp systems include high processing gains (at suitably low data rates), low cost, low weight and simplicity of implementation. The disadvantage of the system of Figure 3.3-1 is that the upchirp and downchirp SAW device characteristics do not track well over time and temperature. Since the output pulse is greatly compressed in time by the factor G_p , small timing discrepancies between upchirp and downchirp output pulses can lead to intolerable performance degradation.



A90401-1

Figure 3.3-1. Up/Down Chirp System Using SAW Devices

The system of Figure 3.3-2 is designed to circumvent this tracking problem by eliminating downchirp devices. The chirp property still provides the same spectral spreading and hence the same G_p as before; the data "1's" and "0's" are transmitted by biphase modulating the chirp with one of two orthogonal codes. The corresponding matched filter process is implemented at the receiver as shown conceptually in Figure 3.3-2; in practice the multiplication by P_0 or P_1 at the receiver could be accomplished by suitably etching the SAW substrate. The biphase modulation by P_0 or P_1 also provides some additional protection against chirp jammers, unless the chirp jammer is also modulated with P_0 or P_1 .



Advantages: fewer SAW Devices, better temperature tracking
Some additional AJ protection against chirp jammers

A90401-2

Figure 3.3-2. Up Chirp Orthogonal Code System Using SAW Devices

The principal disadvantage of the chirp approach in high data rate applications is that sufficiently large processing gain cannot be realized. The figure of merit for SAW devices is the BT product, i.e., the bandwidth of frequency chirp multiplied by the chirp duration. Since we associate one chirp with one data bit and the reciprocal of the bit duration is the data bandwidth, it may be shown that the BT product is the same as the processing gain:

$$BT = \frac{f_{\max} - f_{\min}}{R_B} = G_p$$

The state of the art is such that BT products as high as 10,000 or 20,000 can be obtained. A typical example is 200 MHz chirp range within a 50 μ sec duration (corresponding to 20 Kb/s) for a processing gain of 40 dB. However, as the chirp duration is made smaller the chirp range cannot be indefinitely increased in order to maintain the BT product, or equivalently, the processing gain.

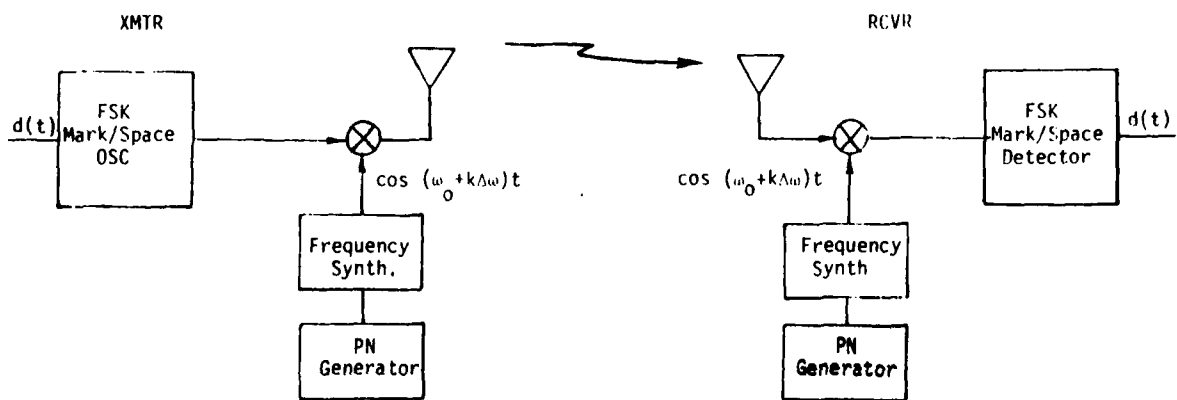
In other words, for high data rate applications, the upper limit on achievable chirp range B constrains the processing gain. For the MMW study data rates the achievable bandwidth is probably on the order of B = 600 MHz so that the processing gains are smaller than 40 dB as indicated below.

1 Mb/s:	(600 MHz) (1 μ sec) = 600	$G_p = 27.8$ dB
20 Mb/s:	(600 MHz) (0.05 μ sec) = 30	$G_p = 14.8$ dB
150 Mb/s:	(600 MHz) (6.6 Nanosec) = 4	$G_p = 6$ dB

These results show that chirp system G_p decreases as the reciprocal of the data rate for the data rates of interest in the MMW study.

3.4 Frequency Hopping Spread Spectrum Communication System

A FH FSK spread spectrum system is shown in Figure 3.4. Basically, the local oscillator frequency at both transmitter and receiver vary pseudorandomly but synchronously. Since the jammer does not know the hopping sequence, the jammer must be content with jamming one or more frequencies constantly in hopes of interrupting communications.



NOTE: DIRECT FREQUENCY SYNTHESIZERS ARE CAPABLE OF FASTER HOPPING RATES THAN INDIRECT FREQUENCY SYNTHESIZERS, BUT HAVE HIGHER IMPLEMENTATION COMPLEXITY.

A90401-3

Figure 3.4. FH FSK Spread Spectrum System

Ideally, one would like to associate several PN chips (i.e., hops) with each data bit in order to make majority vote decisions for each bit and thus effectively combat multiple frequency jammers. Unfortunately, this is not possible if the data rate is more than one-third of the hop rate capability of the frequency synthesizer. If the data rate is equal to the hop rate capability, i.e., one chip or hop per data bit, then the BER is equal to j/n where n is the total number of hopping frequencies and j is the number of jammer frequencies for which J/S is large enough to cause bit errors. In the MMW study the lowest data rate far exceeds the hopping rate capability of indirect or even direct synthesizers, so that many data bits are transmitted at a single hop frequency. The average BER is still given by j/n , but in this case the bit errors occur in long bursts, rather than singly at random; this may not be a serious drawback depending upon the nature of the data.

Another result of the fact that the data rate exceeds the synthesizer hopping rate capability is that some form of data buffering is required at both the transmitter and receiver. This requirement exists because the frequency synthesizer cannot instantaneously change its output frequency; some settling time, corresponding to many data bit intervals in the application at hand, is required for the frequency of the synthesizer output to stabilize at its new value after receipt of a command to change frequency. This settling time may be minimized by utilizing direct frequency synthesis rather than indirect frequency synthesis, but at the expense of additional complexity for the same number of available hopping frequencies. For the data rates of interest in this study even direct frequency synthesis would not allow one hop per bit; in view of this fact the lower complexity indirect synthesizer approach is appropriate.

Table 3.4-1 indicates the range of frequencies and settling times for several synthesizers that have been developed in the past. Table 3.4-2 shows the parameters for several coarse resolution, wide frequency range, indirect frequency synthesizers; two of these are discussed in final reports as noted in the table.

Table 3.4-1. Characteristics of Some Typical Synthesizers

Type	Frequency Range	Oscillator	Phase Noise	Settling Time	Spurious Response (dBc)	Power (Watts)	RF Output Power (dBm)	Step Size
Indirect	300 to 650 MHz	Varactor	10° rms	10 ms	-60	1.2	0-+4	250 kHz
Direct	8 to 8.8 MHz	NA	Not Measured	20 ms	-45	5	0	200 Hz
Indirect	150 to 230 MHz	Varactor Tuned	2° rms	30 ms	-88	4.3	+3	1/32 MHz
Indirect	2800 to 3400 MHz	YIG Tuned	2° rms	50 ms	-80	5	0	500 kHz
Indirect	22 to 2600 MHz	Varactor Tuned	4° rms	NA	-76	4.0	+7	500 kHz
Indirect	2000 to 4000 MHz	YIG Tuned	3° rms	50 ms	-80	10	0	500 kHz
Indirect	3500 to 6400 MHz	YIG Tuned	2.0 rms	10 ms	-90	10	+11	1.0 MHz
Indirect	218 to 270 MHz	Varactor Tuned	0.1° rms	NA	-50	4.6	0	156.250 kHz

Table 3.4-1. Characteristics of Some Typical Synthesizers (Continued)

Type	Frequency Range	Oscillator	Phase Noise	Settling Time	Spurious Response (dBc)	Power (Watts)	RF Output Power (dBm)	Step Size
Digital	0 to 3 MHz	NA	1.00 rms	5 ms	-50	3	+4	4 Hz
Indirect	28 to 44 MHz	Varactor Tuned	0.050 rms	5 ms	-60	1.5	-10	40 kHz
Indirect	4000 to 6500 MHz	YIG Tuned	2.00 rms	10 ms	-90	10	+11	500 kHz
Digital/Indirect	3.8 to 4.3 GHz	NA/Varactor	40 rms	10 ms	-70	7	+10	10 Hz
Digital/Indirect	2.5 to 3.5 GHz	NA/Varactor	0.50 rms	55 ms	-70	7	+10	1 kHz
Digital	250 kHz \pm 13 kHz	NA	1.00 rms	5 ms	-50	3	+4	1/4 Hz

Table 3.4-2. Wideband Frequency Synthesizers

Coarse Resolution, Wide Frequency Range Indirect Frequency Synthesizers

X-band Indirect Synthesizer

$$\tau_s = 200 \mu\text{sec settling time}$$

$$\Delta f = 40 \text{ MHz frequency resolution}$$

$$f_H = 5 \text{ Khops/sec hopping rate}$$

$$N = 16 \text{ channels for 640 MHz hopping range}$$

X-band Indirect Synthesizer

$$\tau_s = 300 \mu\text{sec settling time}$$

$$\Delta f = 4 \text{ MHz frequency resolution}$$

$$f_H = 3.3 \text{ Khops/sec hopping rate}$$

$$N = 1000 \text{ channels for 4 GHz hopping range}$$

WATKINS-JOHNSON WJ-1204-1 Frequency Synthesizer, 0.1 - 26 GHz

Settling time (digital sweep mode):

$$\tau_s = 10 \text{ msec for } f = 1 \text{ MHz}$$

$$\tau_s = 20 \text{ msec for } f = 10 \text{ MHz}$$

$$\tau_s = 40 \text{ msec for } f = 100 \text{ MHz}$$

Frequency resolution:

$$\Delta f = 10 \text{ kHz for } 100\text{-}250 \text{ MHz}$$

$$\Delta f = 100 \text{ kHz for } 250\text{-}2000 \text{ MHz}$$

$$\Delta f = 1 \text{ MHz for } 2 \text{ GHz} - 26 \text{ GHz}$$

Table 3.4-2 Wideband Frequency Synthesizers (Continued)

<p><u>Preliminary Design of an Experimental Modem for SHF/EHF Communication-</u> <u>Vol I, TR prepared by Raytheon on Contract N00014-75-C-0408, 25 Feb 75</u></p> <p>25 Khops/sec</p> <p>2 GHz</p> <p>1000 channels</p> <p>2 MHz resolution</p> <p>indirect synthesizer</p>
<p><u>Investigation of Special Techniques Related to Satellite Communication-</u> <u>Vol II - Task 2, "mmWave Technology," Contract DCA 100-77-C-0059, 25 Aug 73</u></p> <p>36 - 38 GHz</p> <p>direct synthesizer</p> <p>1.5 μsec settling time</p> <p>fhop = 666 Khops/sec</p>

As was previously mentioned, the fact that the data rate is higher than the hopping rate prohibits the use of the highly advantageous majority vote decoding scheme. There is another disadvantage as well: data buffers are required at both transmitter and receiver in order to accommodate bits that occur during the settling time of the frequency synthesizers. The size of the buffer required is equal to the product of the data rate and the settling time, and ranges from 10 Kb/s to 1.5 Mb/s if 10 ms settling time is assumed.

Since extremely wide hopping ranges are possible it is important to account for the frequency dependence of the absorption coefficient in determining link closure; this dependence is discussed in the Paragraph 7.5.1 and will not be re-examined here. Unlike chirp or direct spread systems operating over tens of GHz, frequency hop systems will not be adversely affected by frequency dependent transmission loss, assuming link closure.

The difference lies in the fact that for FH systems only a small fraction of the wide spectrum is used to transmit one bit of information, whereas in chirp and DS systems the entire spectrum is utilized to transmit one bit. Thus nonflat transmission loss will lead to degradation due to frequency selective distortion in DS or chirp systems. Note that each channel or hopping frequency in a FH system is associated with two adjacent frequencies corresponding to mark or space; since bit decisions are based upon the difference in received power in the mark and space filters, the frequency dependence of the absorption coefficient is unimportant for adjacent frequencies.

In the FH system design example below the processing gain G_p is computed for each of the following data rates: 1 Mb/s, 20 Mb/s, and 150 Mb/s. Although extremely large processing gains are obtained by virtue of the very large (25 GHz) assumed hopping range it is important to understand that the computed processing gains are based upon the assumption that the jammer equally distributes his available power over all the hopping frequencies. If this is true, the jamming has no effect unless the total jamming power at each hopping frequency exceeds the power of the desired signal. It is much more advantageous for the jammer to estimate the power level of the received desired signal and then attempt to place a slightly larger (CW) power level in as many hopping frequencies as his available jamming power will permit. Thus, the jammer sets the system BER at

$$BER_{FH} = (1/2) n/N = (1/2) \frac{\# \text{ of jammer frequencies}}{\# \text{ of hopping frequencies}}$$

assuming that received jammer power at each hop frequency is greater than desired signal power, i.e., $J > S$. In this way a multiple frequency jammer can severely disrupt communications in a FH system even in the face of very large processing gain. As mentioned earlier this situation may be greatly ameliorated using majority vote (i.e., multiple frequency hop) bit decisions; however, this option is not possible here due to the large data rates compared to the available hopping rates.

A very wide range FH system design example is summarized below.

FH Design Examples

Assumptions

- 25 GHz hopping range (e.g., 20 GHz to 45 GHz)
- 10 ms settling time
- 0.1 second dwell time
 - implies 11% increase in channel data rate and 0.7 hours between visits to the same frequency.
- FSK modulation with mark and space tones one bit rate apart

$$\text{Recall that BER} = 1/2 \frac{\# \text{ jammer frequencies}}{\# \text{ hopping frequencies}} = \frac{n}{2N}.$$

1 Mb/s

- resolution of 2 MHz
 - implies $N = 12,500$ hop frequencies
- $G_p = 10 \log N = 41 \text{ dB}$; $\text{BER} = \frac{n}{2(12,500)} = (4n) \times 10^{-5}$
- 10 K bit buffer required

20 Mb/s

- resolution of 40 MHz
 - implies 625 hop frequencies
- $G_p = 28 \text{ dB}$; $BER = \left(\frac{1.6}{2} n\right) \times 10^{-3}$
- 200 K bit buffer required

150 Mb/s

- resolution of 300 MHz
 - implies 83 hop frequencies
- $G_p = 19.2 \text{ dB}$; $BER = (0.6 n) \times 10^{-2}$
- 1.5 Mb buffer required

The disadvantages associated with the FH system approach are:

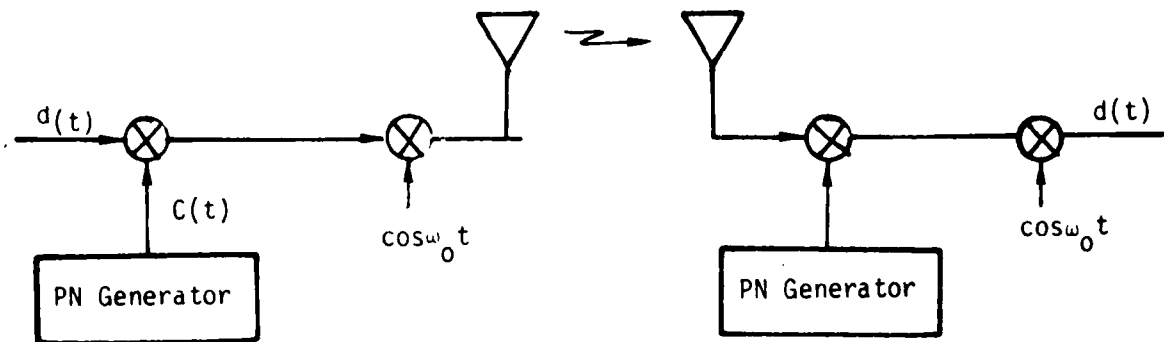
- a. Majority-vote, multiple-hop-per bit technique cannot be used; thus, this FH approach is very susceptible to multiple frequency jammers and computed processing gain is not realized.
- b. Errors occur in long bursts, regardless of BER.
- c. Data buffers are required, which implies memory, additional overhead bits for reacquisition of bit and word timing and increased transmission rate. This is a result of the fact that the data rate is much higher than the frequency hop rate; consequently, many data bits are produced at the source during the transition/settling times of the FH oscillator.

These bits must be buffered at both transmitter and receiver, and in addition, the signal sync must be reacquired after each hop.

- d. Jammer may find and jam each hop frequency in real time, i.e., follow the hopping sequence of the desired signal.
- e. FH synthesizers are very expensive.

3.5 Direct Sequence Spread Spectrum Systems

Direct sequence spread spectrum systems are perhaps the most widely used because of their simplicity and versatility. The simplest form of a direct sequence system is shown in Figure 3.5-1. As before, filters and acquisition and tracking circuitry are not shown in this conceptual diagram.



$$d(t) = \pm 1 \text{ data bits}$$

$$c(t) = \pm 1 \text{ pseudo random chips from PN Generator}$$

Figure 3.5-1. BPSK Direct Sequence Spread Spectrum System

In this system the product of the pseudorandom chip sequence and the input data is used to phase shift key (PSK) the carrier by $(0, \pi)$ radians (BPSK). The processing gain afforded by this DS system against a jammer $J(t) \cos(\omega_0 t + \psi)$ is given by

$$G_{\text{BPSK}} = R_C/R_B \left(\frac{1}{\cos^2 \psi} \right)$$

where

R_C = chip rate

and

R_B = bit rate

The most effective jammer against a DS system is a CW jammer, i.e., one for which $J(t) = \text{constant}$; thus the processing gain given above represents a lower bound on performance.

The shortcoming of the system shown in Figure 3.5-1 is that if the system contains a hardlimiter, a strong co-phased jammer ($\psi = 0$) can capture the limiter and completely suppress the desired signal. If the jammer frequency is slightly offset from that of the desired signal, i.e., $\psi = \Delta\omega t + \psi_0$, then the jammer phase repeatedly "slides" through the desired signal phase and effectively renders the channel useless if the jammer strength is larger than the product of (R_C/R_B) and the signal's strength; this occurs in spite of the fact that the processing gain is infinite when averaged over uniformly distributed jammer phase.

An alternative direct sequence spread spectrum system whose processing gain is independent of jammer phase is the QPSK DS system of Figure 3.5-2. It may be shown that the processing gain for this DS QPSK technique is given by:

$$G_{\text{QPSK}} = R_C/R_B$$

The most important feature of DS QPSK is that the DS QPSK signal cannot be completely suppressed by a strong jammer in a hard limiter. It can be shown that the DS QPSK signal suffers 6 dB degradation in a hardlimiter due to the presence of a strong jammer.

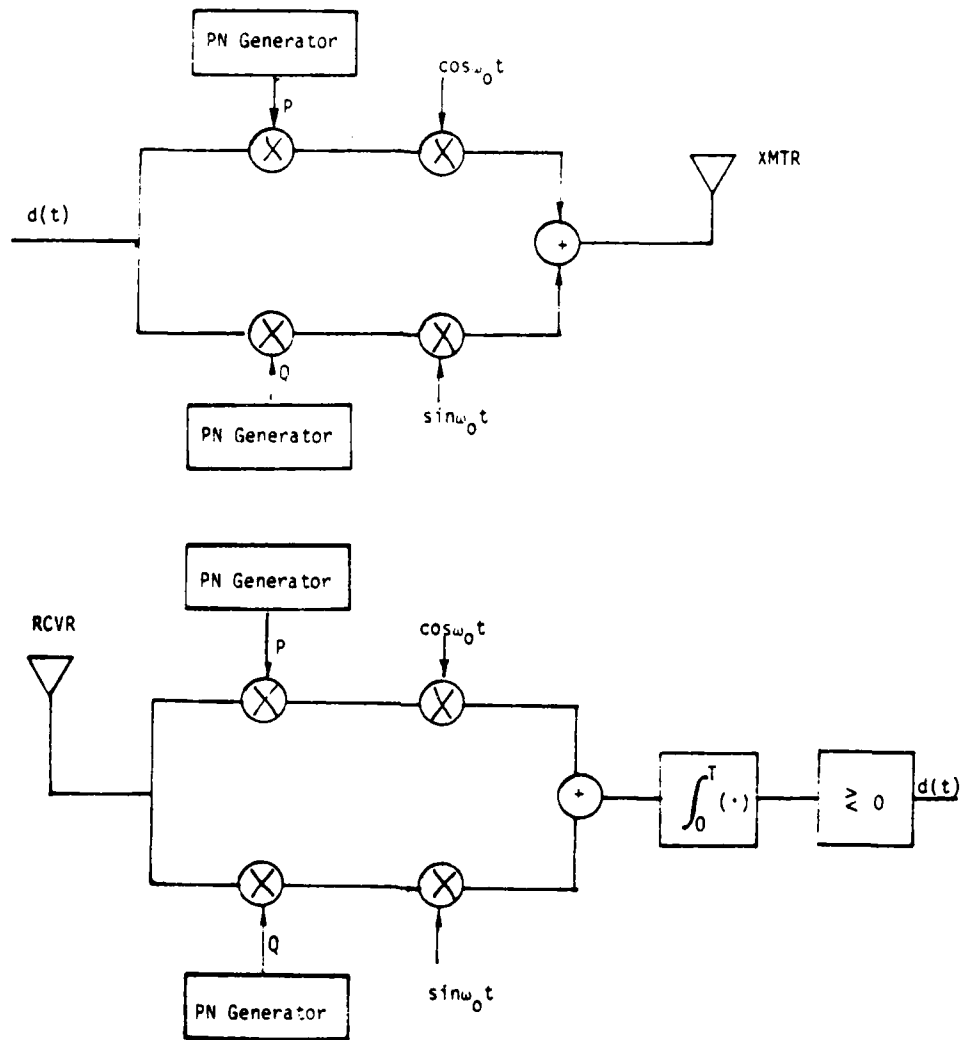
QPSK actually has poorer performance than BPSK in linear systems but is often preferred since the performance in jammer-induced hardlimiting is superior.

A third DS alternative, which we called DS interleaved QPSK for convenience, is shown in Figure 3.5-3. An analysis shows that the processing gains associated with the two quadrature channels before interleaving the bit streams at the receiver are:

$$G|_{\text{Q channel}} = 2 R_C/R_B \left(\frac{1}{\sin^2 \psi} \right)$$

and

$$G|_{\text{P channel}} = 2 R_C/R_B \left(\frac{1}{\cos^2 \psi} \right)$$



A90401-5

Figure 3.5-2. QPSK DS System

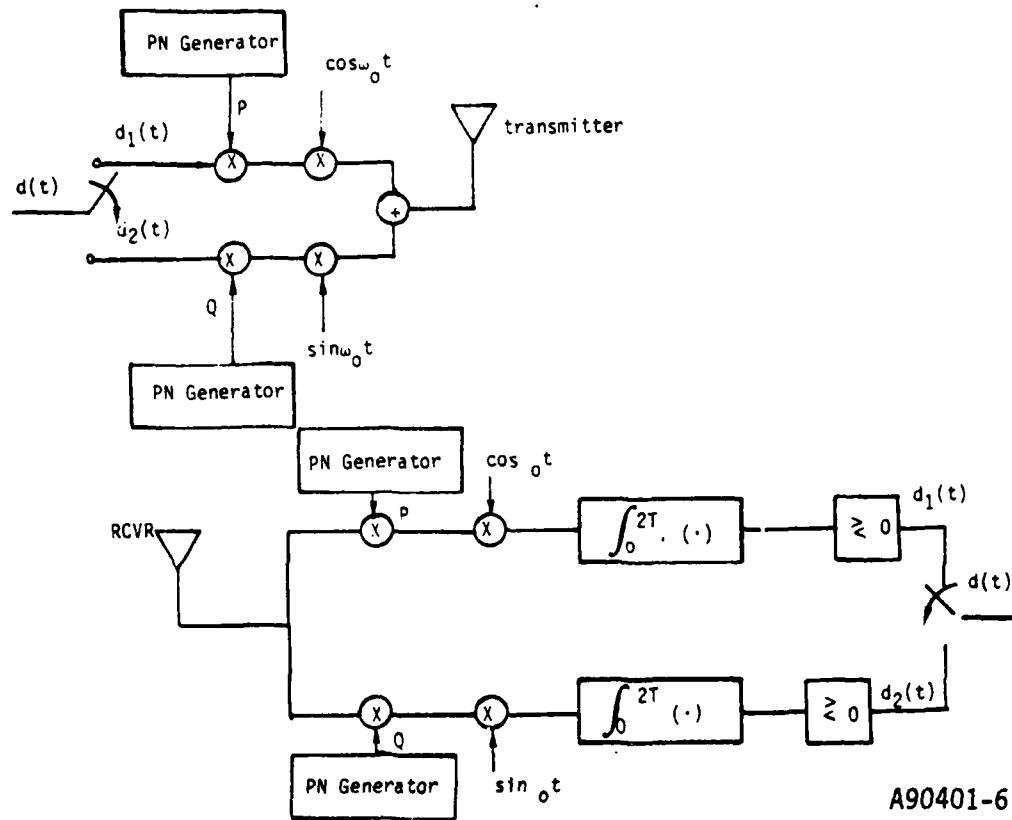


Figure 3.5-3. Interleaved One-Half Data Rate QPSK System

Thus, for $\psi = 0$ or $\psi = \pi/2$, one channel has infinite processing gain while the processing gain of the other channel is at its minimum. As in the DS BPSK system the processing gain is infinite for the Q and the P channels when averaged over uniformly distributed jammer phase; this fact is of little practical interest. For severe jamming ($J/S \gg G_p$) the limiting BER is $1/4$ rather than $1/2$; either BER renders the communication link useless and the 3 dB advantage of DS 1QPSK over DS QPSK does not seem to be worth the additional circuit complexity.

In general, QPSK DS systems are preferred because of their limited degradation due to system nonlinearities (either inherent or jammer induced limiting). Assuming 1 Gb/s chip rates the processing gain ranges from 30 dB at 1 Mb/s data rate to 8.2 dB at 150 Mb/s data rate. The implementation and design of a DS QPSK spread spectrum communication system is discussed in more detail in Paragraph 7.3.

Hybrid spread spectrum techniques consist of combinations of two of the three basic techniques. For certain TDMA systems with many users the hybrid processing gain is the sum of the processing gains associated with each of the constituent techniques. However, process gain computed in this way can lead to erroneous results when predicting AJ protection against particular signals. To see why this is true, consider a hybrid FH/DS system operating against a single frequency CW jammer. When the hop frequency is such that the CW jammer is within the receiver bandwidth, the processing gain is only that associated with the DS process. System performance would be better if the total processing gain were obtained via DS rather than from a combination of DS and FH.

3.6 Selection of Candidate Spread Spectrum AJ System

Having surveyed the basic spread spectrum AJ techniques, the next step is to select the one which is most cost effective for the data rates of interest.

Recall that state-of-the-art SAW devices used in chirp systems are limited in bandwidth to about 600 MHz. For the chirp durations associated with the required high data rates, the resulting processing gain did not approach the 40 dB (BT product) processing gain inherent in SAW devices because of SAW device bandwidth limitations. The achievable processing gains are somewhat lower than those associated with the DS approach.

FH systems that cannot rely upon several hops per bit to implement majority vote decoding are very susceptible to multiple frequency jamming. The data rates required for the MMW system are orders of magnitude faster than the available frequency synthesizer hop rates. Another consideration is the very high cost of wideband, coarse resolution frequency synthesizers.

DS systems are inherently superior to FH systems for the same J/S as shown in Figure 3.6. In addition, different data rates are easily accommodated without changing the chip rate. As will be shown in Paragraph 7.3, very high chip rates can be economically obtained via syncopation to achieve processing gain that exceeds that of the chirp systems that were discussed.

Hybrid combinations of spread spectrum techniques can be used to achieve larger processing gains than can be obtained using any single technique. One such hybrid technique is FH/DS. However, since synthesizer hop rates are much lower than the minimum data rate, the FH/DS approach loses much of its appeal, because of the required buffers, overhead data bits, and increased channel data transmission rate. These disadvantages result from the fact that many bits must be buffered during the transition/settling times between successive hop frequencies, and that the data sync must be reacquired after each hop.

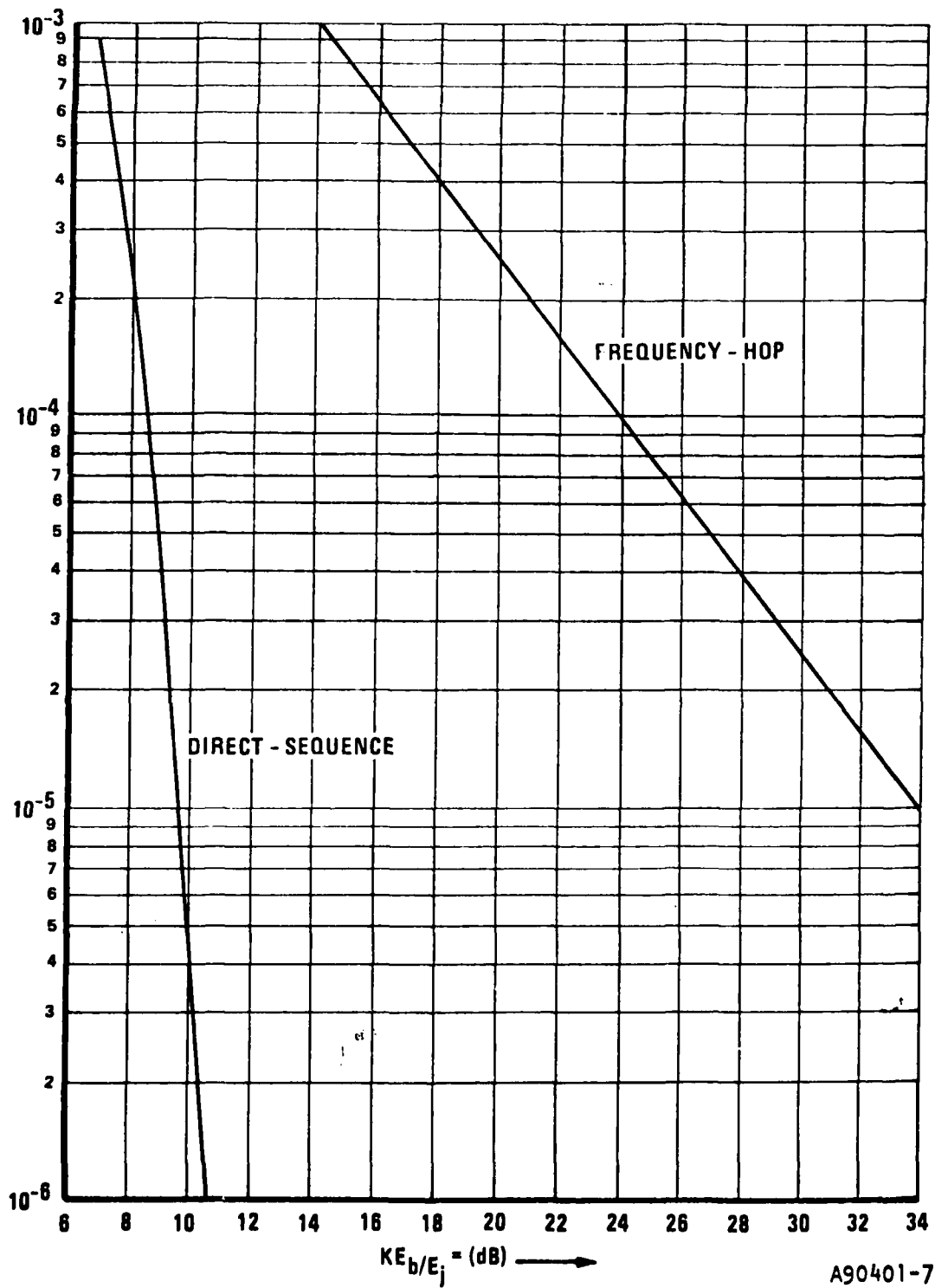


Figure 3.6. Comparison of Direct-Sequence and Frequency-Hop Techniques (Quadrphase Data Modulation and Replica Jamming Assumed)

In view of all the above considerations, it appears that a DS approach is the most straightforward and effective. In order to combat the effects of limiting in the receiver we choose the QPSK DS technique. The implementation and system parameter considerations are presented in Paragraph 7.3. It will be shown there that 1 Gb/s chip rates can be easily implemented to obtain high jamming margins.

4.0 EVALUATION OF PATH DIVERSITY TO ALLEVIATE RAIN EFFECTS

Reliable application of millimeter wave communication is sometimes frustrated by attenuation due to rain and other effects. In order to maintain an expected service availability, provide system design flexibility, and reduce the amount of rain outage, the following alternative approaches have been considered:

- a. Path diversity.
 1. Tandem path diversity.
 2. Multipath diversity.
- b. Space (antenna heights) diversity.
- c. Transmitter power diversity.
- d. Frequency diversity.
- e. Bandwidth diversity.
- f. Transmission delay (temporary storage).

Each of these diversity methods has its relative advantages and disadvantages. Besides system factors such as variation of fade margin with hop length, merging of the diversity at switching points, the nature of the attenuation distributions, and the degree of independence of two lateral separated paths versus separation, the designer must evaluate the crucial factor of economics versus reliability. These factors depend on the statistical occurrences, hardware practicalities, and costs.

Time diversity and polarization diversity also have been examined during the study; however, these two diversity methods can not effectively counteract the rain effects and will only be discussed briefly in this section. Antenna height diversity is useful in compensating multipath fading on long links: multipath fading is not a serious problem for short distance tactical communication links.

Millimeter wave tactical communications routes in tough geographical locations or long distance strategical communications (such as the European backbone system and future global positioning system) may utilize communication satellite or satellites as repeater, as illustrated in Figures 4.0-1 and 4.0-2, to extend the terrestrial hop distance and to improve link availability.

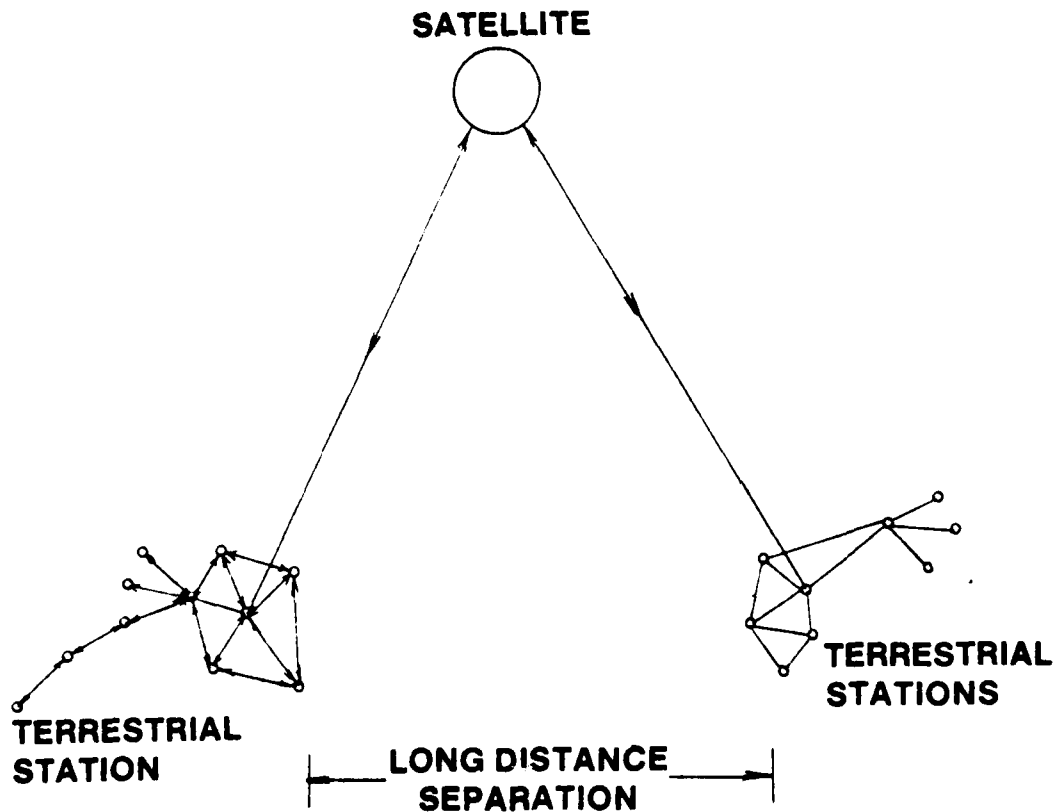


Figure 4.0-1. Long Distance Millimeter Wave Communication Using Satellite as a Repeater

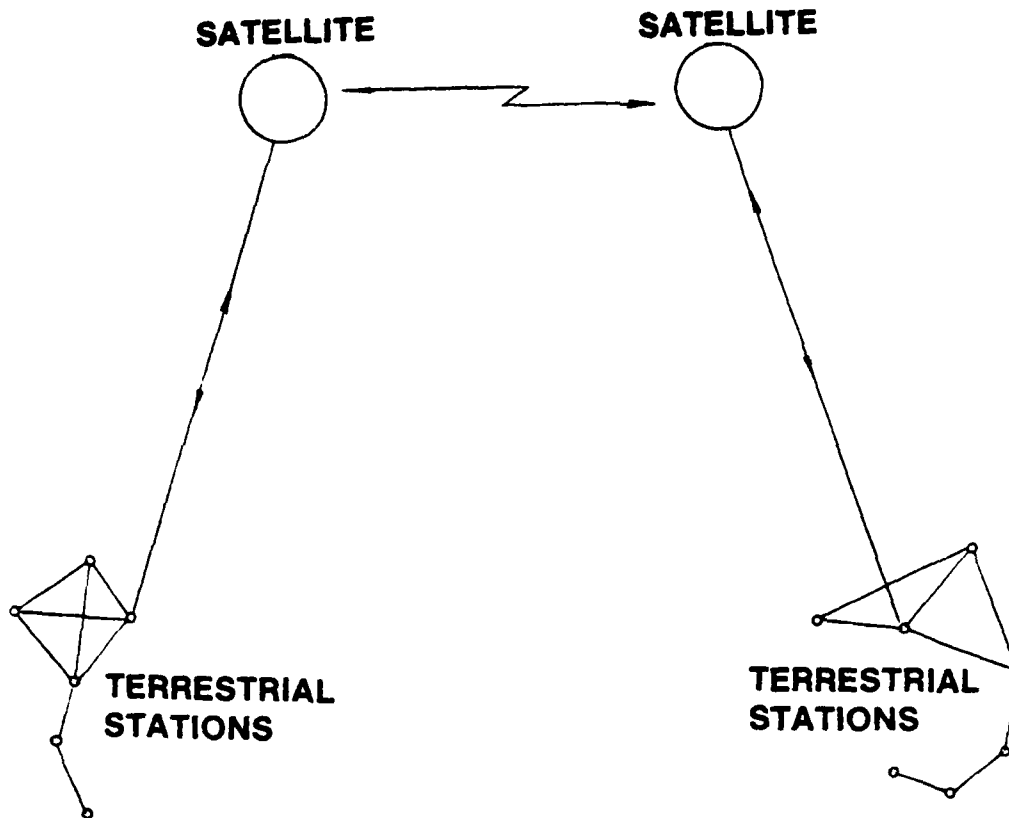


Figure 4.0-2. Long Distance Millimeter Wave Communication Using Multi-Satellite as Repeaters

4.1 Diversity Methods

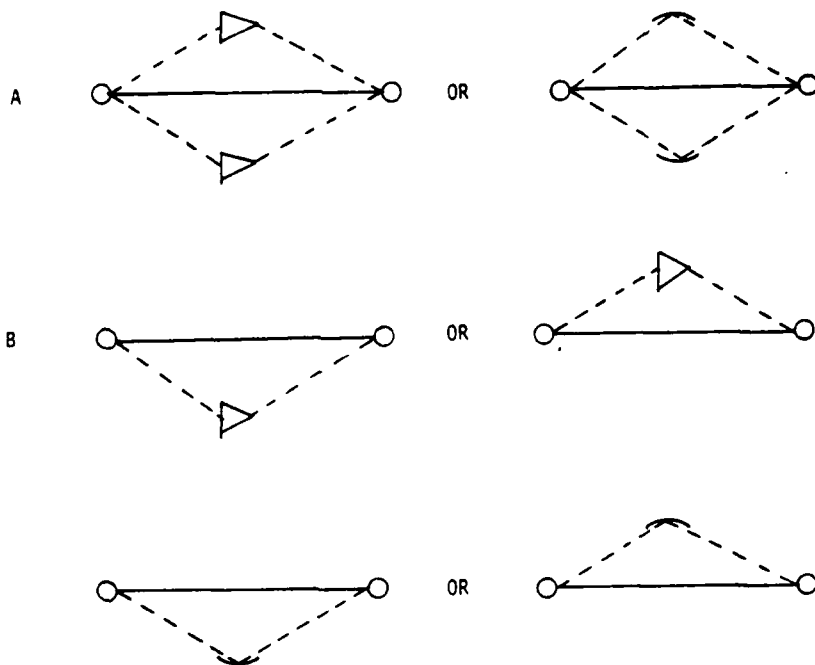
4.1.1 Path Diversity

The rain outage performance of tandem path (non-diversity) and multipath diversity systems depends entirely on the probability distribution of rain induced attenuation on a path of given length and on the joint distribution for multiple paths of different lengths and separations. Multi-disjoint paths connecting two stations, using either an active repeater or a passive repeater, as depicted in Figure 4.1.1-1, will not only reduce the rain outage but also improve link redundancy (namely, when an

1. TANDEM SYSTEM



2. DIVERSITY SYSTEM



○ TERMINAL

▷ ACTIVE REPEATER

- - - ACCESSORILY ALTERNATIVE ROUTE

— MAIN LINK ROUTE

⌒ PASSIVE REPEATER

A90401-105

Figure 4.1.1-1. Path Diversity Configuration for Line Distribution Network

active link fails, traffic rerouting will re-establish connection between stations). This path diversity approach may provide better performance, but also has some disadvantages such as:

- The cost of the alternate route system (antenna and repeater).
- The cost of switching equipment.
- The uncertainty of the amount of joint fading on the route.

If the same repeaters are being utilized in both tandem and diversity systems, the performance of these systems can be evaluated by its rain outage time probability (p_t) or the path availability ($1-p_t$). The p_t of each system may be computed in the following manner:

a. Tandem System

For equally spaced sections the rain outage time of the tandem section is:

$$P_t = 1 - (1 - p_t)^{N_t}$$
$$\approx N_t p_t \quad (4.1.1)$$

where N_t is the number of repeaters in the hop length S with spacing of L_t , and

$$N_t = S/L_t . \quad (4.1.2)$$

The fade margin of each of the tandem hops is

$$\alpha_t = \alpha_s - 20 \log L_t \quad (4.1.3)$$

where α_s is the fade margin of the standard repeater on a 1 km hop. The rain attenuation probability distribution is approximately

$$P_t(R \geq r) \approx \frac{P_0}{2} \cdot \operatorname{erfc} \left[\frac{\ln(r) - \ln(R_m)}{\sqrt{2} S_R} \right] \quad (4.1.4)$$

The designation of these symbols have been described in Paragraph 2.2.2. The outage time of the section determines the tandem repeater spacing, L_t , for a system with a specified total outage time, T , is:

$$L_t = \frac{ST}{P_t} \quad (4.1.5)$$

b. Diversity System

Similarly, analysis of a tandem system can apply to the diversity system. However, for calculating the outage time of a diversity system, joint probability distributions for two parallel laterally separated hops of equal length are needed for different hop lengths and path separations. Since no such directly measured attenuation distributions are available, these distributions must be assumed. Fortunately, because of the assumed symmetry of diversity systems (such as case 2.A of Figure 4.1.1-1), the distributions for two special cases can be derived from the individual distributions. Let event a_i be the fading of the i th diversity hop and event b_j be the fading of a hop in the

opposite path of the diversity system; the joint probability of both events is $P(a_i, b_j)$. Since the hops are identically contributed, i.e., $P(a_i) = P(b_j) \equiv p$, and only the cases when the variables take the same values are considered, in the special cases of complete dependence [$P(a_i | b_j) = P(b_j | a_i) = 1$] and statistical independence the joint probabilities are $P(a_i, b_j) = p$ and $P(a_i, b_j) = p^2$, respectively. Joint probabilities between and including these two cases represented by:

$$P(a_i, b_j) = p^c \quad 1 \leq c \leq 2 \quad (4.1.6)$$

where $c = 1$ gives the case of complete dependence and $c = 2$ gives the case of statistical independence

c. Path Diversity for Satellite Communications

The path diversity has not only been used in terrestrial communication links, it also has applied to satellite-ground communication to reduce rain outage time, and has been discussed by many authors^{1,2}. To ascertain the effectiveness of the diversity techniques for satellite-earth links, it is necessary to define bounds on the expected performance for such systems. Figure 4.1.1-2 shows a typical yearly percent outage versus fade level curve for Washington, D.C. area at 20° elevation angle. The corresponding rainfall rate to the attenuation (X-axis) can be converted easily. One measure of potential improvement is to consider

¹D.C. Hogg, "Path Diversity in Propagations of Millimeter Waves Through Rain," IEEE Trans on Antenna & Prop, May, 1967, pp. 410-415.

²D.B. Hodge, "Path Diversity for Earth-Space Communications Links," Radio Science, May - June, 1978 pp. 481-487.

AD-A102 303

HARRIS CORP MELBOURNE FL GOVERNMENT COMMUNICATION SY--ETC F/6 17/2.1
MILLIMETER WAVE ALTERNATE ROUTE STUDY. (U)

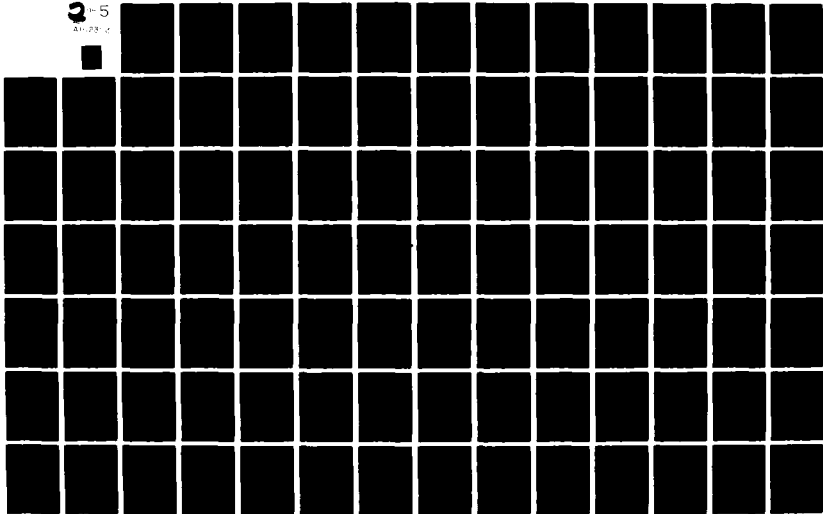
APR 81 W C ADAMS, J J PAN, W C WHITEHEAD
RADC-TR-81-42

F30602-79-C-0055
NL

UNCLASSIFIED

2-5

AD-79-2



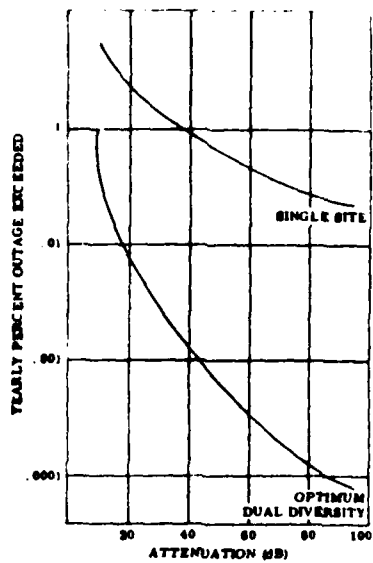
the joint probability for occurrence of independent signal fading as for a path diversity case. The lower curve indicates the optimum dual site diversity improvement which is possible for the Washington area. The optimum performance requires the proper inter-station baseline orientation and spacing in order to obtain statistical independence of the two signals. Figure 4.1.1-3 shows the sensitivity in maximum available diversity gain¹ versus baseline separation. Statistical analysis indicates that signals with a correlation of about 0.6 can achieve 80 to 90 percent of the maximum diversity gain. Therefore, complete decorrelation of the two signal paths is not necessary to obtain useful results. These results show that a minimum baseline separation of 10-25 km is necessary for useful diversity gains (in the Washington D.C. and meteorologically similar areas). These results, however, may vary with changes in the detailed meteorological conditions and anomalies at site specific locations.

The diversity gain not only depends on the baseline separation, but also varies with the geometrical approach and the shape of rain cells. Mass² and Goldhirsh³ sensed this problem and also pointed out that experimental results show a definite and quite large difference between orientations of the baseline. The detailed discussion has been given by Mass and Goldhirsh and will not be repeated in this report.

¹Diversity Gain was defined by D.B. Hodge as $G(A) = a(1-e^{-bD})$, where D is ground terminal separation distance, and constants a and b depend upon the single site attenuation A.

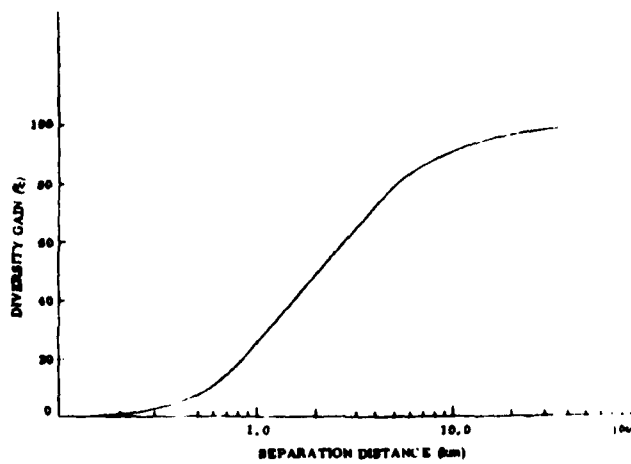
²J. Mass, "Diversity and Baseline Orientation," IEEE Trans on Ant. & Prop. Jan 1979, pp. 27-30.

³J. Goldhirsh, "Path Attenuation Statistics Influenced by Orientation of Rain Cells," IEEE Trans on Ant. & Prop. Nov 1976, pp. 792-799.



A90401-77

Figure 4.1.1-2. 38 GHz Percent Outage Versus Attenuation for Washington, at Elevation Angle of 20°



A90401-78

Figure 4.1.1-3. Percent Maximum Diversity Gain Versus Site Separation

4.1.2 Adaptive Transmitter Power Diversity

System margin, in many occasions, is not sufficient to offset the rain attenuation and to maintain continuity of service. Adaptive transmitter power diversity can be considered in both terrestrial and satellite communications systems to extend the system margin even further. Up to 10 dB rain-induced attenuation can be readily overcome by a temporary increase of transmitter power. However, when the attenuation exceeds 10 dB, this method becomes progressively less attractive, since transmitters with very high peak power capabilities would be required. Furthermore, the automatic gain control (AGC) circuit in the receiver has to have extra gain control capability. Normally, the AGC has a control range of 20 to 30 dB. In the future, the AGC level may be extended to 50 to 60 dB by using GaAs low noise amplifier in front-end dual-gate variable gain amplifier to IF gain control. High Power Amplifiers (HPA's), used in the transmitter (whether tube or solid state) are often operated at saturation levels. In this case the tuning range will be small unless the gain of the HPA driver is controlled or operation is changed to the class A mode. In such a case, the combination of adaptive transmitter power with relatively wide system margin may provide reasonable power diversity capability to counteract the rain effects.

For satellite communications, one must distinguish between the uplink and downlink cases. For uplinks, the transmitter power at each ground station need only be increased to compensate for its own path attenuation. For downlinks, the satellite transmitter must provide enough power to overcome the highest attenuation observed by any one of the ground stations it serves simultaneously. Thus, a satellite transmitter serving a very large number of ground stations must operate near peak power all the time.

In principal, the bandwidth (B) can be traded for signal power (S) in accordance with the well-known channel capacity (C) relation

$$C = B \log_2 \left(\frac{S + N}{N} \right) \text{ bits per second} \quad (4.1.7)$$

where N is noise power and B bandwidth in Hz. When $S \gg N$, a small percentage increase in bandwidth can effectively compensate for a much larger percentage decrease in signal power. Therefore, it may be possible to reduce the information bandwidth slightly to conserve the signal power by a few dB to upgrade system margin, offsetting rain attenuation.

4.1.3 Millimeter Wave/Microwave Frequency Diversity

The use of frequency diversity (or protection channel) techniques provides the ability to use a high (link) availability channel on a lower frequency (microwave) to provide a means of transferring high priority traffic during temporary high rain-rate. Since microwave frequency has relatively smaller available bandwidth than millimeter wave, this scheme implies a reduction in the throughput available due to bandwidth constraints when the frequency is switched from millimeter wave to microwave. The selection of microwave frequency (preferable from 8 GHz to 18 GHz because of the wide bandwidth capability) is dependent upon rain-rate statistics, link distance, antenna size and the tolerance of interception. The antenna size necessary for a given gain and beamwidth at microwave frequencies is larger than that required for millimeter waves (antenna size is proportional to λ^2). However, the disadvantage of antenna gain may be offset by the smaller path loss at microwave frequency.

It is a straightforward process to compute the link availability from one terminal to another terminal. But, if one terminal links to more than one terminal simultaneously (or TDMA) through a single-link-per-transponder, the link availability has to be considered in a different manner. Then, the availability, A, can be obtained from:

$$A = (1 - p) + \sum_{n=1}^N \frac{(1 - p)^{M-n} p^n (M - 1)!}{(M - n)! (n - 1)!} \quad (4.1.8)$$

where p is the probability of rain attenuation exceeding the clear-weather margin for any one link

M is the number of links served simultaneously by one terminal; (statistical independence is assumed).

N is number of microwave transponders.

For systems in which several stations want to receive the same transponder signal, the transponder must be switched to low frequency operation whenever the clear-weather margin is exceeded. Then, the probability that the microwave transponder transmitter must be switched is:

$$P_m = 1 - (1 - p)^m \quad (4.1.9)$$

where m is the number of stations served simultaneously.

4.1.4 Transmission Delay Diversity

When real-time operation is not mandatory, service can be maintained by temporarily storing the data during the rain-induced fade and transmitting them after the fade has ended.

The service availability (SA) of this transmission delay diversity is:

$$SA = 1 - P [T(A) \geq t] \cdot P(A \geq X \text{ dB}) \quad (4.1.10)$$

where

$P(A \geq X \text{ dB})$ = probability that signal fade exceeds clear weather margin of X dB

and

$P [T(A) \geq t]$ = probability that fade duration exceeds t minutes.

Thus, when the temporary storage capability operation frequency, rain-rate, and link distance are given, SA can be readily calculated.

4.2 Diversity Design Consideration

From the foregoing discussion of various diversity approaches it should be clear that no single diversity method is "best" for all conceivable circumstances. The choice can, in general, be made only after the following information is known:

- Topological and architectural preference
- Availability of satellite diversity selection
- Geographical information
 - Vegetation
 - Terrain and topographical map
 - Lake and river

- Rain data
- Threat information (threat type, jamming power, direction, etc.)
- System availability specification
- Hardware (antenna tower, G/T, transmitter power, receiver sensitivity, etc.)
- System approach (AJ method, modulation format, etc.)
- Cost budget.

Among these diversity methods, the most favorable approaches for millimeter wave tactical systems are path diversity and adaptive transmitter power. Each of them has different merits and are compared in Table 4.2. Unfortunately, neither of these approaches can compensate the sky temperature increase due to rain effect. The AGC diversity design is relatively more straightforward than the path diversity. However, the designer must include the following geographical considerations during the design process:

- a. No vegetation, buildings or hills should be higher than the straight line between the two line-of-sight antenna towers.
- b. Calculate the midpath clearance considering antennas heights and earth curvature. The radius of the radio path should be smaller than midpath clearance¹.

¹C.L. Ruthroff, "Rain Attenuation and Radio Path Design," B.S.T.J., Jan 1970, pp. 121-135.

Table 4.2. Methods to Counteract the Rain-Effects for Millimeter Wave Communications

Performance	Path Diversity		Automatic Control ⁺ (Adjustable Tx Power ⁺⁺ and Rx AGC)
	Terrestrial Repeaters	Satellite as Repeater	
Cost	Very High	High when no satellite available Medium when satellite is available	Low/Medium
Probability of Being Jammed and Intercepted	Medium-Low	High	N/A
Area Coverage		Large	
Phase Correction Requirement*	Yes	No	Yes
Antenna Tower Requirement	Yes	No	Yes
Repeater Availability (Reliability)	Relatively Low	Relatively High	
Sky Temperature During Rain	High	Low**	High
Lake or River Effects	Yes	No	Yes

⁺Terrestrial space diversity with Automatic Control schemes will increase the link distance.

⁺⁺With large systems margin.

*Due to rain-effect dispersion and multipath fading (for high data-rate only).

**Due to propagation angle.

And then, practice the design disciplines according to the following procedure:

- a. Survey the geography, topology, threat and climate at the given communication area.
- b. Determine hardware availability, system rain attenuation margin, and system dynamic range.
- c. Calculate outage probability and outage time.
- d. Evaluate and compare the path attenuation and diversity gain of various alternate routes, including the geographic limitations.
- e. Compare sky temperature versus elevation angle (for satellite path diversity only).
- f. Select the optimum architectural configuration - trade-off between performance and cost.
- g. Select the diversity scheme. Terrestrial Satellite or Terrestrial Satellite Combination - between performance and cost trade-off.
- h. System design (including the considerations of AGC, highly sensitive Rx, adjustable Tx power adaptive system, etc.).

4.3 Adaptive Polarization Correction to Counteract Rain-Induced Cross Polarization

Frequency agility and frequency reuse via an orthogonally polarized channel can double the bandwidth of a communications system. Rain, water vapor turbulence, multipath, and imperfect antenna cause polarization crosstalk in the orthogonal polarization channels. Several methods can be used to reduce the cross polarization problem.

a. Canting Angle Correction Method

For linear polarization, rain depolarization can be minimized by rotating the polarization of the communications antennas such that the effect of the canting angle of rain is always near the minimum. In other words, the polarization is always in the same direction of the major and minor axes of the elliptically shaped rain drops. However, this technique is not very practical for millimeter wave tactical applications since it requires antenna rotation.

b. Differential Phase-Shift and Attenuation

Chu^{1,2} has demonstrated that a differential phase shifter followed by a differential attenuator can restore orthogonality. The correction circuitry is most easily implemented preceding the orthomode transducer and low noise amplifier. However, as a consequence, the noise figure is degraded in direct proportion to the differential attenuation (which, in turn is proportional to the degree of non-orthogonality).

¹T.S. Chu, "Restoring the Orthogonality of Two Polarizations in Radio Communications System, I," BSTJ Nov. 1971, p. 3063.

²T.S. Chu, "Restoring the Orthogonality of Two Polarizations in Radio Communications System, II," BSTJ Mar. 1973, pp. 319-327.

Besides the shortcomings of differential phase-shift and attenuation, the millimeter wave radios prefer an all electronic, light weight, and low cost correction network, operational over wide temperature range and wide frequency bandwidth. Then the adaptive polarization method becomes more practical and attractive.

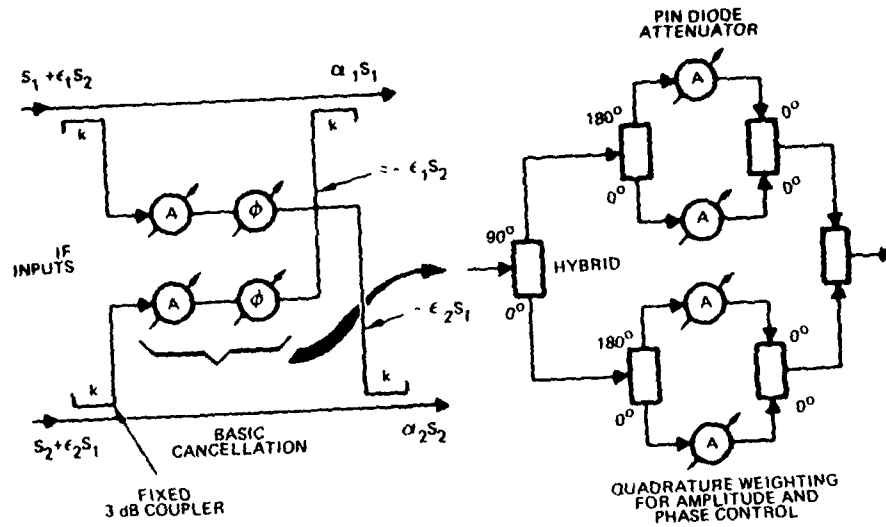
c. Adaptive Polarization Technique

The adaptive circuits employing couplers interconnected via series phase shifters was first introduced by DiFonzo¹, and extensively investigated and verified by Baird and Pelchat². The theoretical detail of this adaptive approach will not be repeated in this report. A typical IF correction network is illustrated in Figure 4.3. It is a straightforward network that cross-couples each signal into this other channel cancelling the polarization error in the channel. Variable coupling in both amplitude and phase is achieved with in-phase and quadrature phase variable attenuators, using PIN diodes. This network has been demonstrated successfully with a bandwidth of more than 700 MHz, at IF frequencies of both S- and L-Bands. With analog control, approximately -36 dB crosstalk cancellation has been achieved.³

¹D. DiFonzo, "Adaptive Antennas for Polarization Isolation in Frequency Reuse Systems," COMSAT Internal Memo T CLT/71-2085, July 15, 1971.

²C.A. Baird and G. Pelchat, "Cross Polarization Techniques Investigation," Final Technical Report RADC-TR-77-244 July 1977.

³G.G. Rassweiler, et al, "Adaptive Polarization Separation Experiments," Final Report, Aug 1976, AAFE Contract NASI-13942.



88911-5A

Figure 4.3. Block Diagram of Adaptive Polarization Correction Network

5.0 EVALUATION OF MULTIPLE PATH DIVERSITY TO ALLEVIATE JAMMING EFFECTS

5.1 Introduction

Strategic and tactical communications networks currently in use are vulnerable to intentional jamming because of the nonredundant nature of the network architecture; a jammer that disables one link or node of the network effectively disables the network. The vulnerability of a communication network to jamming can be decreased by utilizing spread spectrum techniques, null steering adaptive antennas, or by introducing redundancy into the network in the form of additional nodes and links. The spread spectrum and null steering antijam (AJ) techniques are the subjects of Section 3.0, Section 6.0, and Appendix A and will not be treated here. The subject of the present task is the use of multiple path diversity, i.e., alternate routes, to combat jamming and increase system availability.

As is the case with the spread spectrum and null steering techniques, the AJ protection obtained using alternate routes is not without its price. The AJ advantage of using alternate routes must be balanced against the additional cost of the attendant links, nodes, and associated switching equipment. The issues involved in this trade-off between AJ protection and alternate routing architecture complexity are:

- Distance
- Availability
- AJ Performance
- Cost of Links and Nodes
- Configuration Control
- Flexibility

The organization of this section is as follows. In Paragraph 5.2 communications network architectures that afford protection against jamming are discussed and analyzed in terms of system availability and complexity (or equivalently, cost). A specific alternate route architecture is selected as being a reasonable compromise between AJ protection and

complexity (cost). In Paragraph 5.3 the trade-off between active and passive repeaters at the added nodes is addressed in some detail and some specific examples of each are presented. In Paragraph 5.4 there is a brief discussion of other pertinent systems engineering considerations that were not addressed because they are common to systems not having an alternate route capability.

5.2 Communications Network Architecture

In this section the generic architecture types are introduced and related to existing DCS networks. Possible alternate route architectures are discussed and analyzed in terms of jamming vulnerability and system complexity and cost. A single alternate route approach is selected as being a reasonable compromise between AJ capability and system complexity.

Basic Network Architectures and Typical Networks

Four generic network architectures of importance are illustrated in Figure 5.2-1: tandem link, hub and wheel, bidirectional ring, and packet-and-priority. These four types of configurations of links and nodes may be identified as the building blocks of actual communications networks. This fact is borne out by Figures 5.2-2, 5.2-3, 5.2-4, and 5.2-5 which show the network architecture for the Digital European Backbone (DEB), and the DCS configurations of Europe, Japan and Hawaii. (These architectures are illustrative of the networks but do not necessarily show the current configurations.)

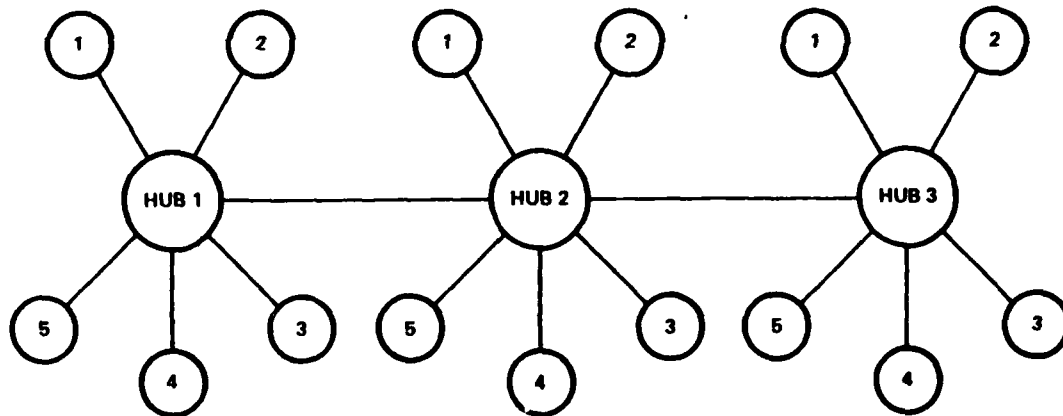
Candidate Alternate Route Approaches

The protection against jamming afforded by alternate communication links is obtained at the expense of additional complexity and, therefore, additional cost. The relative amount of additional cost incurred depends upon the degree of redundancy introduced into the network which, in turn, is related to the degree of protection against jamming.



10228-11

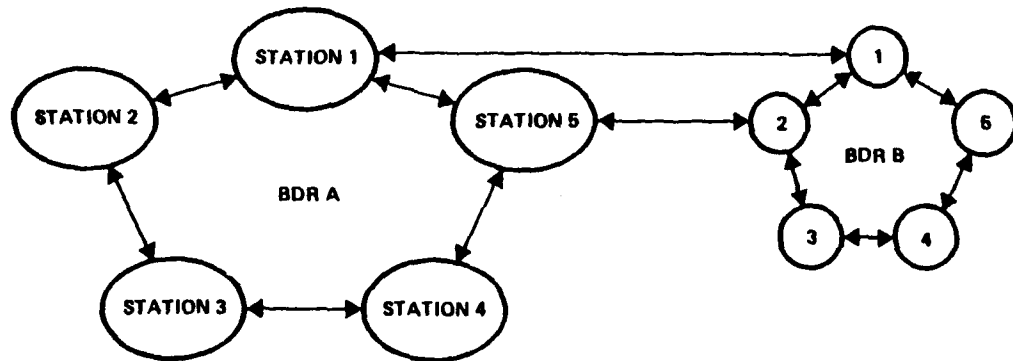
A. TANDEM LINK ARCHITECTURE



10228-13

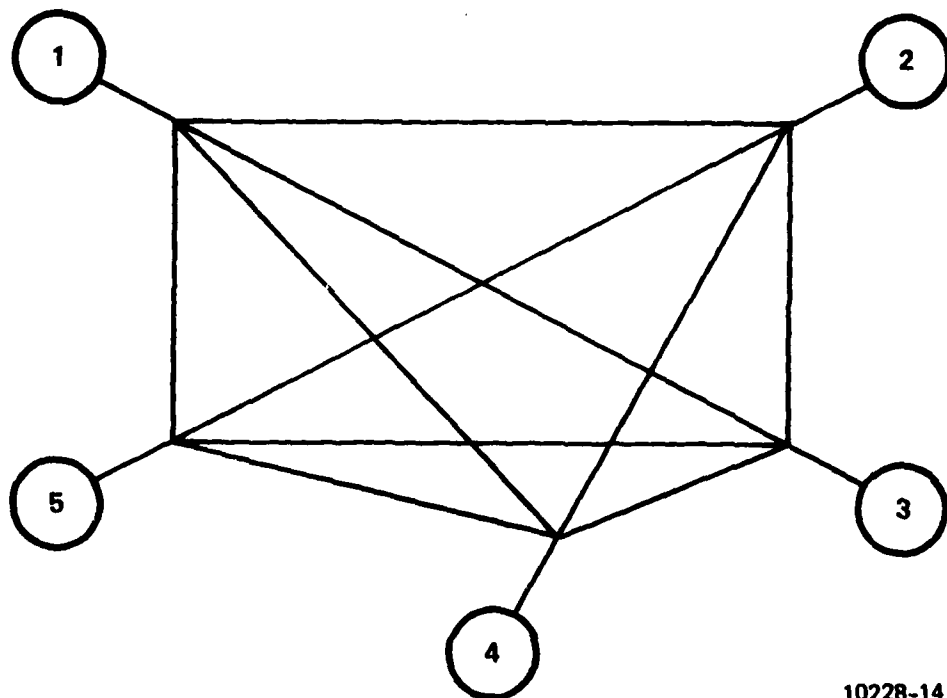
B. HUB AND WHEEL ARCHITECTURE

Figure 5.2-1. Basic Network Architecture (Sheet 1 of 2)



10228-12

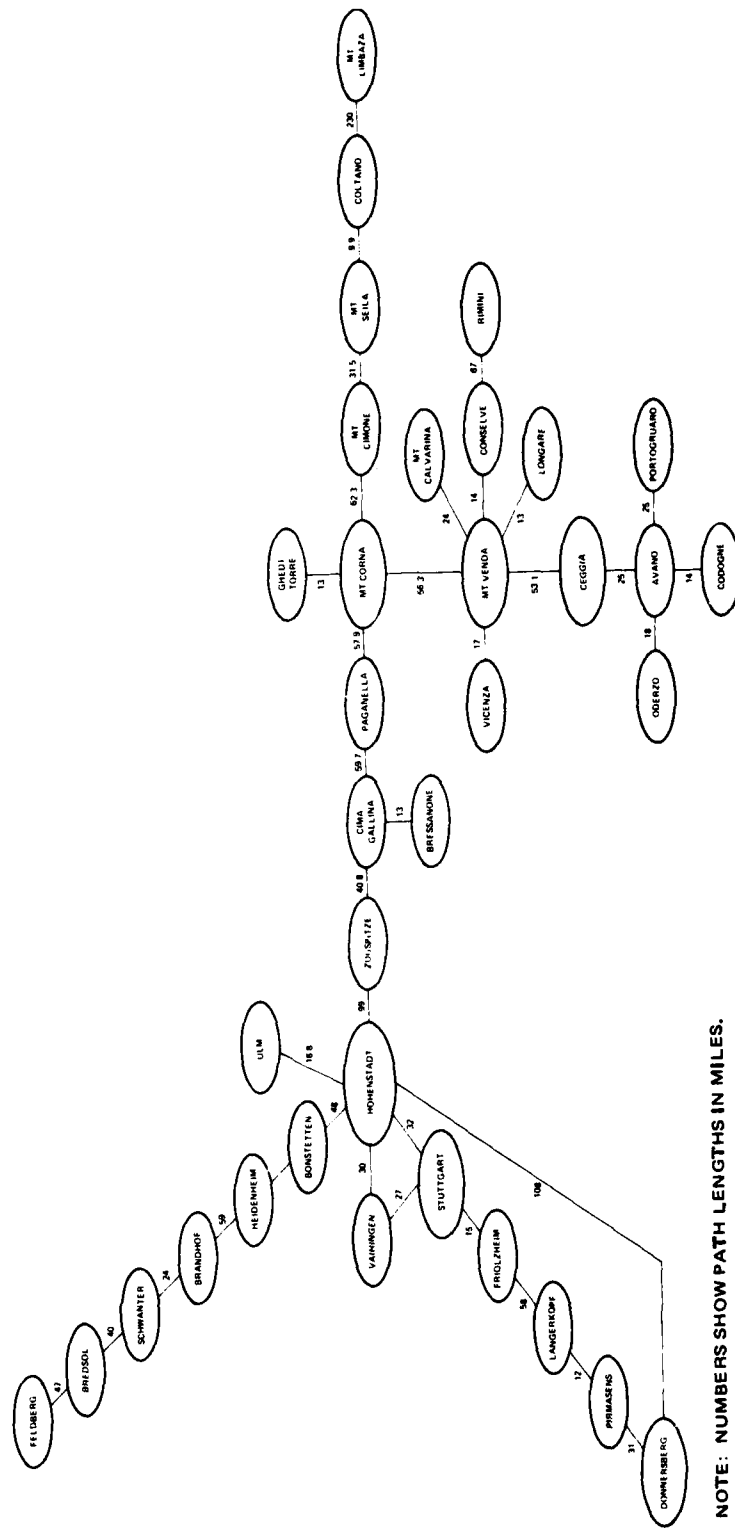
C. BIDIRECTIONAL RING ARCHITECTURE (TWO CONNECTED BDR'S)



10228-14

D. FULLY CONNECTED NODES" NETWORK

Figure 5.2-1. Basic Network Architecture (Sheet 2 of 2)



NOTE: NUMBERS SHOW PATH LENGTHS IN MILES.

Figure 5.2-2. Typical Digital European Backbone (DEB) Multiplex Configuration

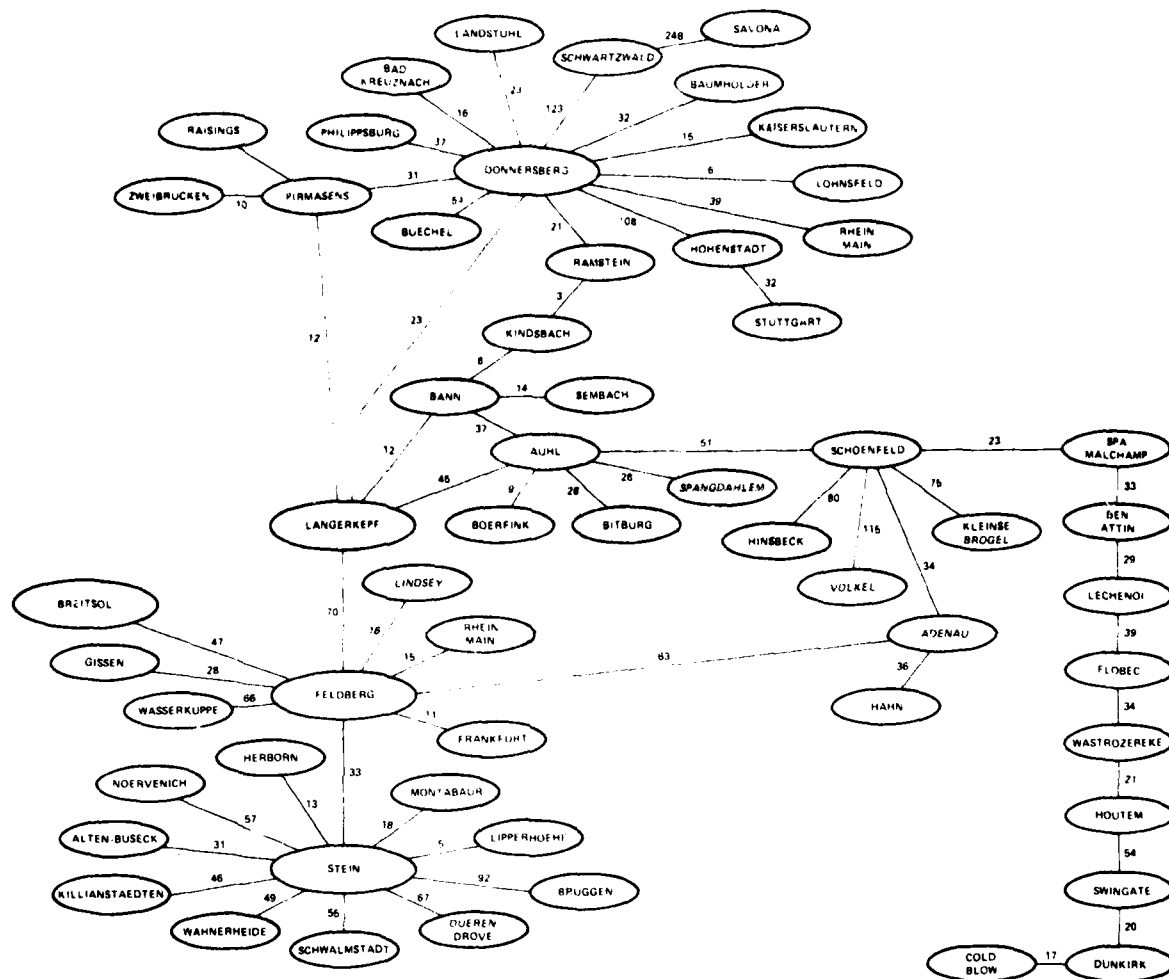
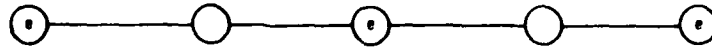


Figure 5.2-3. Typical DCS Multiplex Configuration European Area

In Figures 5.2-6 through 5.2-12 several alternate routing schemes of various degrees of complexity and therefore cost in terms of numbers of required nodes and links are illustrated; the symbol "e" appearing at some of the nodes indicates "existing node" and shows how nodes and links could be added to an existing tandem-like network in order to provide multiple path diversity to combat jamming. The architecture types in Figures 5.2-6 through 5.2-12 are identified with alphabetical letters for ease of reference in later figures. Architecture type "A" (not shown) refers to a tandem link consisting of only "existing nodes" and looks like that of Figure 5.2-6 except that all nodes would contain the symbol "e".

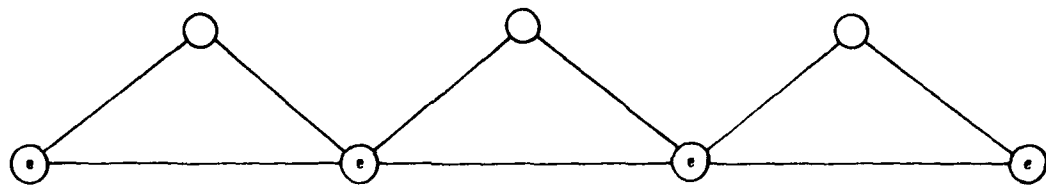
Although in practice communication networks of interest are rarely "pure," e.g., purely hub-and-wheel or purely tandem, we restrict our attention in this study to the advantages and relative cost of augmenting an existing purely tandem network. The rationale for this approach lies in the belief that the communications networks of interest are likely to have a tandem flavor. This seems especially likely for millimeter wave frequencies which may require several repeater stations between manned nodes because of the rain attenuation characteristic at these frequencies. Thus, even if the manned nodes form a hub-and-wheel architecture, the use of repeaters to ameliorate the rain attenuation problem could lead to "spokes" of the wheel that are purely tandem in nature. In any event, the use of a tandem link leads to alternate route architectures that are amenable to quantitative analysis regarding system availability and relative system cost for the augmented, alternate route structure built around an existing tandem link.



A90401-8

"e" DENOTES EXISTING NODE

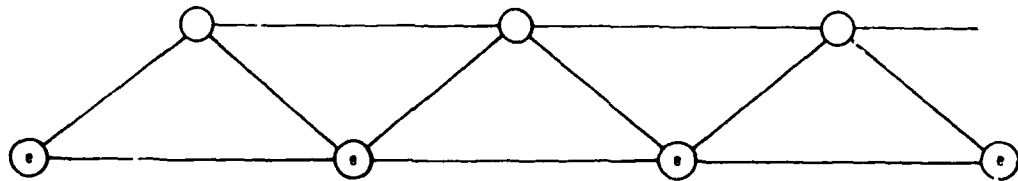
Figure 5.2-6. Type B Architecture



A90401-9

"e" DENOTES EXISTING NODE

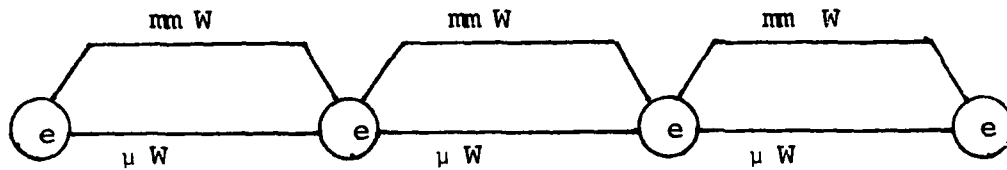
Figure 5.2-7. Type C Architecture



A90401-10

"e" DENOTES EXISTING NODE

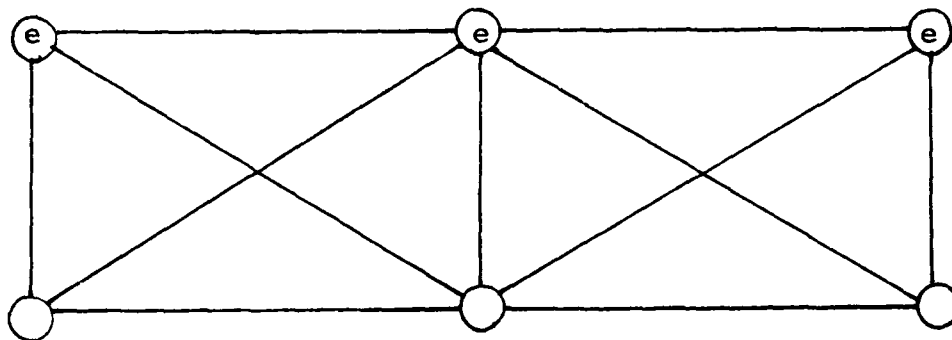
Figure 5.2-8. Type D Architecture



A90401-11

"e" DENOTES EXISTING NODE

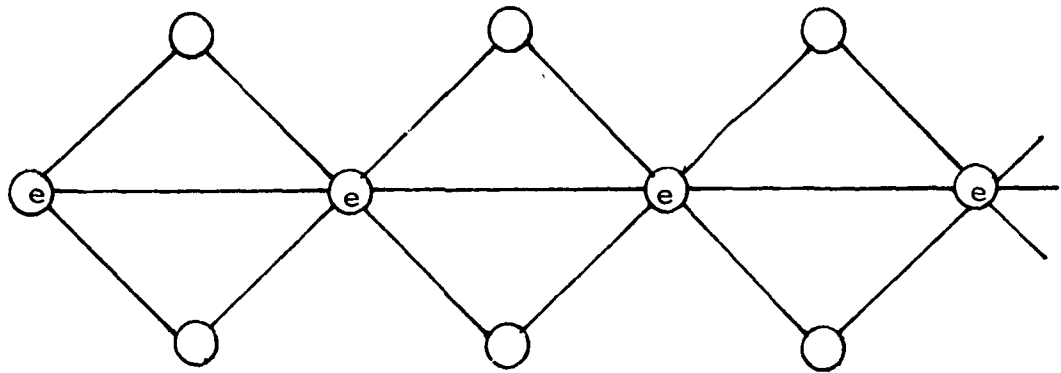
Figure 5.2-9. Type E Architecture



A90401-12

"e" DENOTES EXISTING NODE

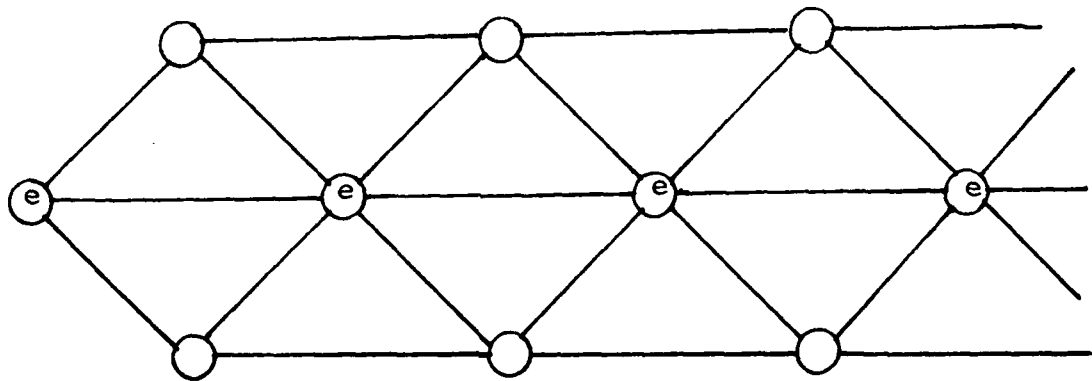
Figure 5.2-10. Type F Architecture



A90401-13

"e" DENOTES EXISTING NODE

Figure 5.2-11. Type G Architecture



A90401-14

"e" DENOTES EXISTING NODE

Figure 5.2-12. Type H Architecture

Note that the link of Figure 5.2-6 does not properly fit into the class of "alternate route architectures" since it possesses no alternate routes. It is shown only to illustrate the following point:

If an existing tandem network of N nodes is to be augmented by N additional nodes, these additional nodes should be used to form alternate routes, not to merely decrease the distance between nodes while retaining a tandem network. Although there will be twice as many nodes to attack (jam) in either case, successful jamming of one link is ineffective in the former case and catastrophic in the latter.

The above point illustrates that then halving the link distance with additional nodes to combat jamming is of little use. A more effective strategy is to utilize the additional nodes to form alternate routes: if one link is jammed then an alternate route (link) to the destination is pressed into service. This approach has the advantage that one or more links can be rendered useless by jamming with no effect on the network's ability to communicate. The penalty for this jamming protection is the higher system cost due to the redundant links.

In order to evaluate the performance of the various alternate route network configurations that have been presented, it is necessary to define a meaningful performance metric. For our purposes we choose network availability as our metric and use the following definition:

The network is said to be available if and only if every "existing node" can communicate with every other "existing node" in the network. The network availability metric is defined as the probability that the network is available, conditioned upon a specified probability assignment of link disruption.

This definition of network availability may seem somewhat overly restrictive in that losing communication with one node does not imply loss of communications among the remaining nodes. On the other hand, if the lost node is the originating node, or a militarily important node such as HQ, then losing one node could be catastrophic and the above definition of availability then seems appropriate. This definition of availability also makes the analysis more tractable.

In order to simplify the formulation of the availability results we will assume that the network under consideration has a total of N nodes, N_e of which are "existing nodes," and that each link has unconditional probability p of being disrupted. We may now compute system availability in terms of p and N_e for all of the architectures presented previously. The assumption that each link has equal probability p of being disrupted (i.e., successfully jammed) seems appropriate in the absence of any other a priori information. A more flexible approach would be to assign probability P_k that the k th link would be disrupted; the analytical results could still be obtained in this case but would require that many more degrees of freedom be specified. The results would be hard to evaluate since they would be a function of many arbitrarily assigned independent variable values. The approach that was taken, i.e., $P_k = p$, all k , should lead to a relative performance ranking that is meaningful.

Another parameter of interest is the relative cost of the various alternate route architectures. A relative complexity metric C may be defined which is the weighted sum of the number of existing nodes, added nodes, and links normalized by the weighted sum of the number of nodes (denoted by "e" in the figures) and links in the existing system network:

$$C = \frac{W_{n_e} (N_a - N_e) + W_{n_e} (N_e) + W_1 L_a}{W_{n_e} N_e + W_1 L_e}$$

where

C = Relative complexity metric (= 1 for existing system)

N_a = Number of nodes in alternate route system

N_e = Number of nodes in existing system

$N_a - N_e$ = Number of added nodes

L_a = Number of links in alternate route system

L_e = Number of links in existing system

W_{n_e} = Cost associated with an existing node: transmitter, receiver, building, land, tower, maintenance

W_{n_e} = Cost associated with an added node

W_l = Cost associated with a link: antennas and link switching equipment. It may be appropriate to incorporate link switching equipment cost into the node cost.

The availability and complexity metrics associated with several of the alternate route architectures are shown in Table 5.2-1 and Table 5.2-2, respectively. The first entry in these tables, "existing tandem network," consists of N_e nodes and $(N_e - 1)$ tandem links: it is included in the table for comparison purposes since it represents the existing tandem network prior to adding alternate routes. The availability as a function of p with architecture type as a parameter, is plotted in Figures 5.2-13, 5.2-14 and 5.2-15 for $N_e = 10, 50, \text{ and } 100$, respectively. The system complexity, or equivalently, cost, is plotted in Figure 5.2-16 for $W_l = W_{n_e} = 1$. The alphabetical letters in these figures refer to the architecture types as defined in Figures 5.2-6 through 5.2-12.

Table 5.2-1. System Availability as a Function of Number of Nodes and Probability of Link Disruption p

ARCHITECTURE TYPE	AVAILABILITY
A Existing tandem network	$A = (1 - p)N_e - 1$
B See Figure 5.2.6	$A = (1 - p)^2(N_e - 1)$
C See Figure 5.2.7	$A = [1 - P(P + p)]N_e - 1$
D See Figure 5.2.8	$A^* = [1 - \{ (N_e - 2) p^4 + 2p^2 \}]$
E See Figure 5.2.9	$A = [1 - p^2]N_e - 1$
F See Figure 5.2.10	$A^* = [1 - \{ (N_e - 2) p^5 + 2p^3 \}]$
G See Figure 5.2.11	$A = [1 - P(2P)(2P)]N_e - 1$
H See Figure 5.2.12	$A^* = [1 - \{ (N_e - 2) p^6 + 2p^3 \}]$

*valid only if $P \ll 1$

N_e = Number of existing nodes

p = Probability of link disruption

Table 5.2-2. System Complexity as a Function of Existing Number of Nodes, Added Nodes Links, and Associated Weighting Factors

COMPLEXITY	
A Existing tandem network	$C = 1$
B See figure 5.2.6	$C = \left\{ W_{ne} N_e + W_{ne} (N_e - 1) + W_1 (2N_e - 2) \right\} / CD$
C See figure 5.2.7	$C = \left\{ W_{ne} N_e + W_{ne} (N_e - 1) + W_1 3(N_e - 1) \right\} / CD$
D See figure 5.2.8	$C = \left\{ W_{ne} N_e + W_{ne} (N_e - 1) + W_1 [4(N_e - 2) + 3] \right\} / CD$
E See figure 5.2.9	$C = \left\{ W_{ne} N_e + W_1 (2(N_e - 1)) \right\} / CD$
F See figure 5.2.10	$C = \left\{ W_{ne} N_e + W_{ne} N_e + W_1 [5(N_e - 1) + 1] \right\} / CD$
G See figure 5.2.11	$C = \left\{ W_{ne} N_e + W_{ne} [2N_e - 2] + W_1 5(N_e - 1) \right\} / CD$
H See figure 5.2.12	$C = \left\{ W_{ne} N_e + W_{ne} [2N_e - 2] + W_1 [7(N_e - 2) + 5] \right\} / CD$
	W_{ne} = Relative cost of existing node
	W_{ne} = Relative cost of <u>added</u> nodes
	W_1 = Relative cost of link
	N_e = Number of existing nodes
	CD = Complexity of existing network = $W_{ne} N_e + W_1 (N_e - 1)$

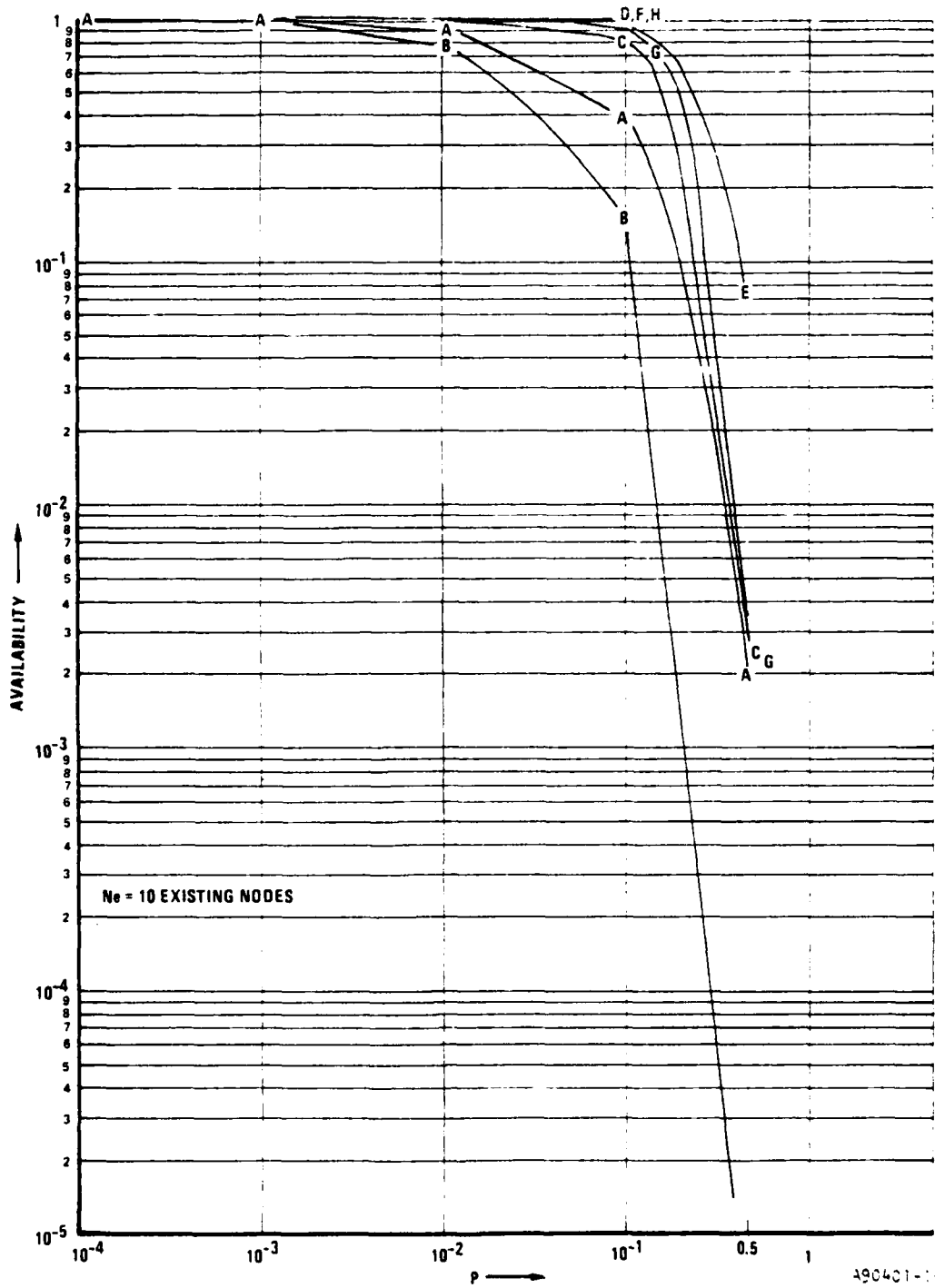


Figure 5.2-13. Network Availability Versus Per-Link Jamming Probability for a 10-Existing-Node Network With Architecture Type as a Parameter

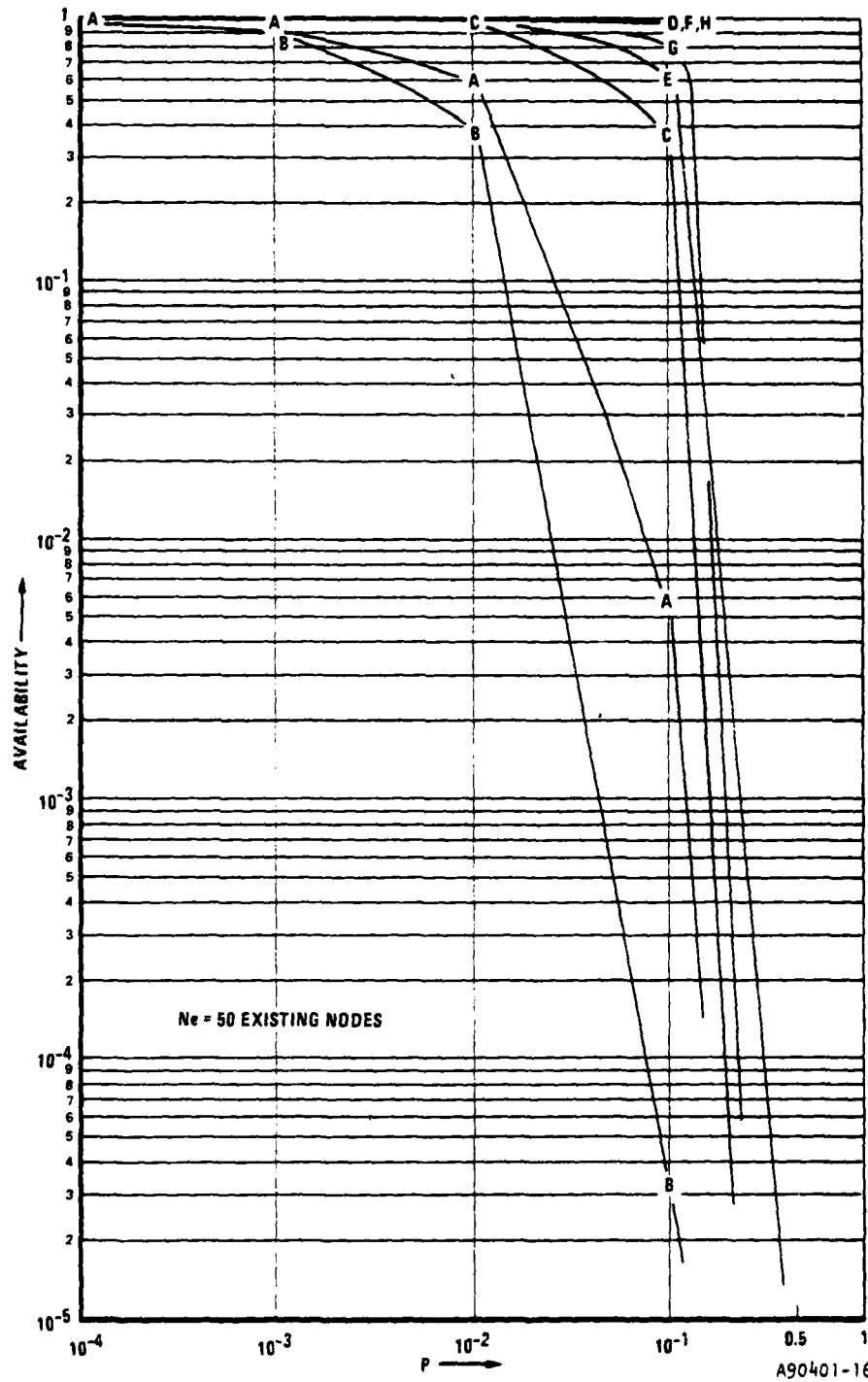


Figure 5.2-14. Network Availability Versus Per-Link Jamming Probability for a 50-Existing-Node Network With Architecture Type as a Parameter

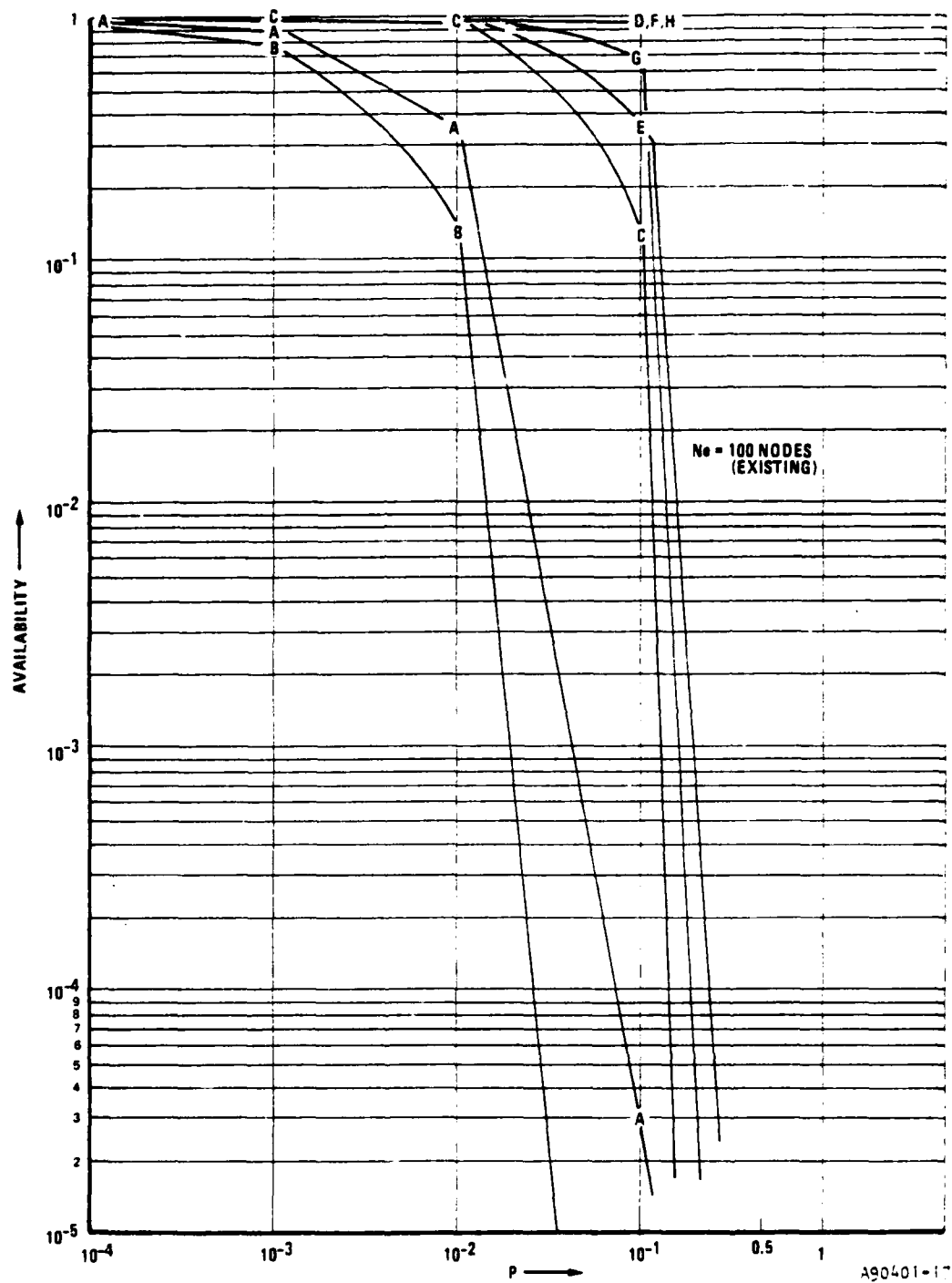
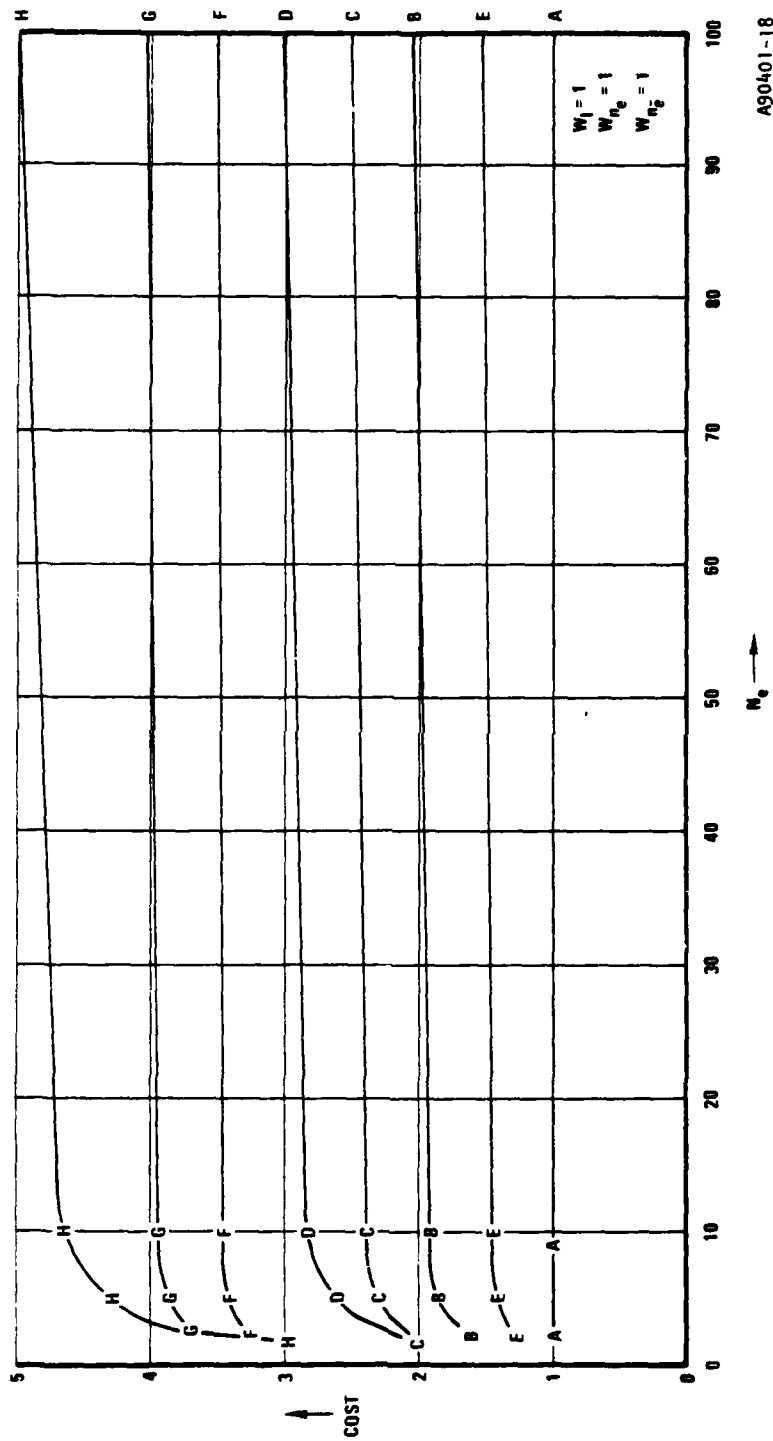


Figure 5.2-15. Network Availability Versus Per-Link Jamming Probability for a 100-Existing-Node Network With Architecture Type as a-Parameter



A90401-18

Figure 5.2-16. Normalized Network Cost Versus Number of Existing Nodes for Several Network Architectures

There are several aspects of the availability curves (Figures 5.2-13, 5.2-14, 5.2-15) worthy of comment.

- a. The availability function for architecture types D, F, and H are valid only for $p \ll 1$; consequently, no data for $p > 0.1$ is plotted for these architecture types.
- b. Architecture types D, F, and H are among the most complex; indeed, this is the reason that only approximate availability functions could be formulated which are invalid for p approaching unity. One would expect the most complex architecture to have the most favorable availability characteristic; this is borne out in Figures 5.2-13 through 5.2-15.
- c. Architecture type B consistently exhibits poorer availability performance than type A for equal probability of link disruption p . This seemingly anomalous behavior may be explained by recalling that architecture type B is not of the alternate route type, technically speaking; recall that it was introduced for purposes of comparison. It differs from all the other types in that the link distances are all one-half of the distance between "existing" nodes; this should have the effect of decreasing the probability of link disruption p to the extent that the availability will exceed that of the original existing network A. Of course, a somewhat different viewpoint may also be taken; the architecture of type B has twice as many vulnerable links as type A, albeit they are each less likely to be disrupted. The crucial point here, however, is that the tandem nature of the type B link leaves this architecture extremely vulnerable to a strong jammer. Our interest will lie mainly with architecture types C through H, which should be compared to the existing tandem network, type A.

- d. Note that the availability characteristics exhibit a knee or threshold effect; this is especially pronounced for the more complex architecture types.
- e. The availability metric of the more complex networks, types C, D, F, G, and H, is dominated by the higher jamming vulnerability of the outermost two existing nodes. These two outermost nodes are more vulnerable to jamming because they have fewer links connecting them to the remainder of the network and thus fewer alternate routes available. Recall that our definition of availability assumes that:
 1. all links are duplex links
 2. the system is defined to be "unavailable" to a node if that node cannot communicate to any other node in spite of unlimited rerouting capability

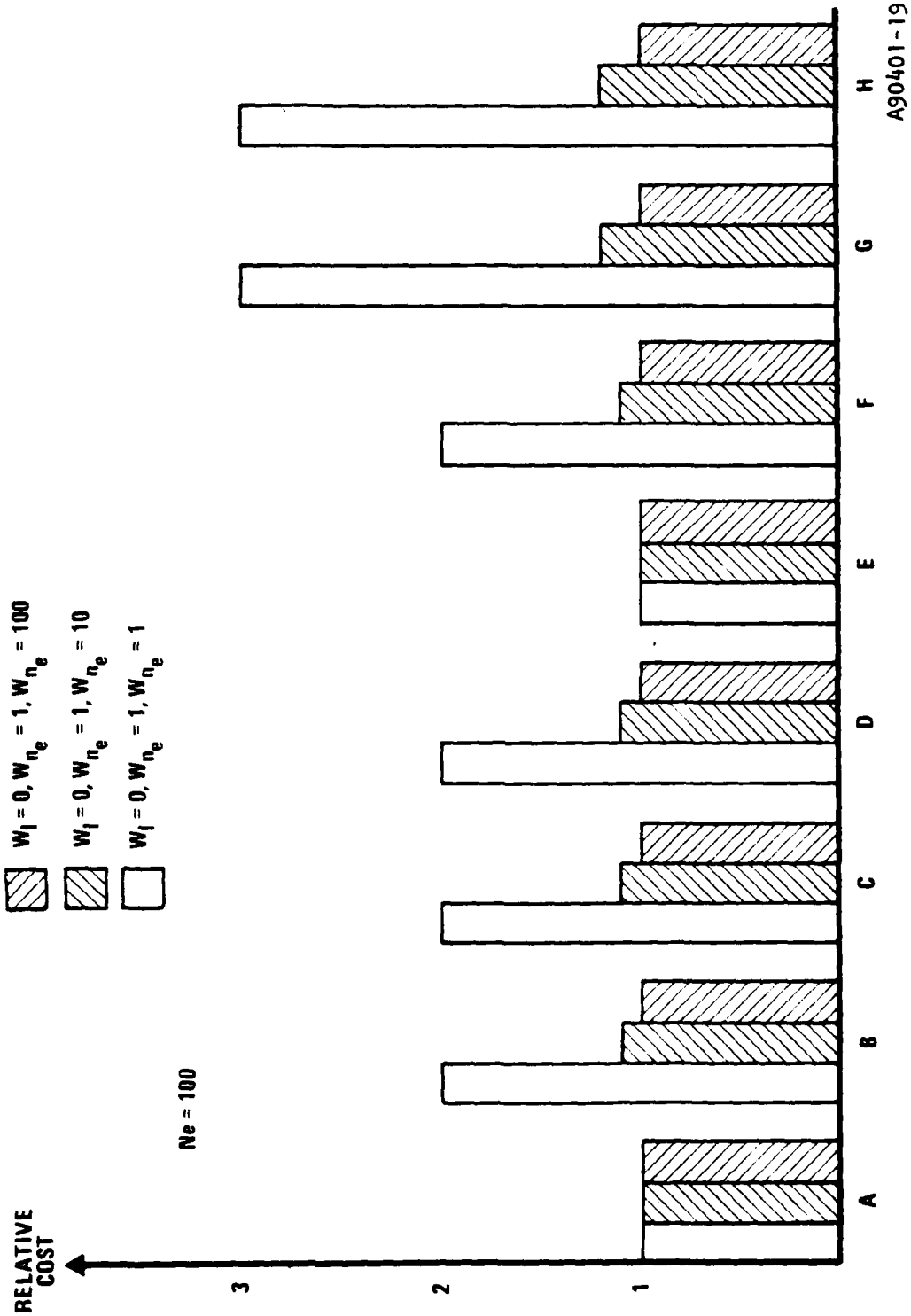
In order for the alternate route approach to be most effective, the two outermost nodes must be made less vulnerable to jamming than the inner node. This could be achieved using higher link (i.e., jamming) margins for all links connected to the two outermost nodes.

The complexity (cost) versus N_e curves, Figure 5.2-16, are based upon the assumption that "new" nodes, "existing" nodes and links all have the same relative cost; this is not likely to be true in practice. Different relative weights for these three costs affect the asymptotes of these cost versus N_e curves but not the shape, since the cost function for each architecture type is normalized by that of the existing network, type A. The complexity curves sharply decrease for $N_e < 10$ because of the network end effects: there are fewer links and added nodes per existing node for the existing nodes at each end of the network. These end effects become negligible as the number of existing nodes N_e becomes large.

The bar graphs of Figure 5.2-17 show the relative costs ($N_e = 100$) for all the network architecture types for three more realistic choices of relative cost for the network elements. The cost of the links was assumed to be negligible for each choice of relative weights. This may be reasonable since we attribute only the cost of the additional antenna to the link and absorb the cost of the automatic switching function within the node cost.

Since the cost functions of Figures 5.2-16 and 5.2-17 have been normalized by the cost of the existing network which contains only existing nodes, it is clear that the relative cost increases as the cost of an added node (relative to an existing node) increases. One may infer from Figure 5.2-17 that if link costs (i.e., antennas) are negligible and added nodes cost 1/10 (assumed) the cost of existing nodes, then even the most complex alternate route network costs only 20% more than the existing network. One situation in which added nodes might cost only a fraction of what existing nodes cost could occur if the added nodes were unattended and the existing nodes were not unattended, i.e., existing nodes were staffed. Another such situation in which the added node costs are small would arise if the added nodes consisted only of passive reflectors properly oriented with respect to the existing nodes. The rain margin would be somewhat reduced due to the passive reflection efficiency and the longer effective length of the alternate link, but since high rain margins are required at millimeter wave frequencies this may be an acceptable tradeoff.

The bar graph of Figure 5.2-17 dramatically illustrates that the key to a high performance, low cost alternate route communication network is the use of inexpensive added nodes and links. The cost of added nodes relative to the cost of existing nodes depends upon whether the added nodes are manned or unmanned and whether the repeaters are regenerative or non-regenerative. Regenerative repeaters demodulate the received signal and remodulate a strong carrier with the demodulated data, whereas non-regenerative repeaters simply amplify and rebroadcast the received signal without demodulating it; thus, regenerative repeaters are more expensive than non-regenerative repeaters.



A90401-19

Figure 5.2-17. Relative Network Cost for Several Choices of Added-Link, Added Node, and Existing Node Costs for Various Network Architecture Types (100 Existing Node Network)

Since passive reflectors are non-regenerative and may be unmanned, they represent a cost effective way to add nodes and links to an existing network in order to obtain an alternate routing capability. In view of the importance of passive reflection type "repeaters," some of the system considerations of a passive reflector alternate route system will be examined in Paragraph 8.3.

If we anticipate that the relative cost of added nodes and links can be made quite small by using passive repeaters at the added nodes, then it becomes cost effective to select a relatively complex alternate route architecture such as type D, F, G, or H. The choice of an architecture type depends upon the perceived jamming threat, the required communication reliability, and the level of complexity (cost) that can be supported.

6.0 INVESTIGATIONS OF ADAPTIVE PHASED ARRAY ANTENNA TECHNIQUES

6.1 Introduction

It is well known that adaptive array null steering can provide substantial system antijam capability. Because of the difficulty of working with millimeter wave frequencies, little of the potential of this technology has been realized. The subject of this section is a new approach to adaptive array signal-to-noise ratio maximization which is particularly applicable to the millimeter wave bands. Specifically, this approach adaptively combines inputs from a reflector antenna's feed elements. In many cases, existing feed and antenna designs or hardware can be easily modified for this purpose. Resulting adaptive array performance is orders of magnitudes superior to the customary sidelobe canceller approach, both in bandwidth and null depth.

At frequencies between 1 and 10 GHz, communications links begin to use reflector antennas in place of individual lower gain antenna elements; thus, the need for new approaches is established. At millimeter wave frequencies, reflectors are almost always the first choice because their conveniently achievable high gain reduces required transmitter power, provides inherent spatial antijam properties, and reduces the probability of intercept. Consequently, the Adaptive Array Feed Concept reported here is expected to be of special usefulness in millimeter wave links. The drawbacks associated with using multiple low-gain antenna elements in a phased array at millimeter wave frequencies are discussed in some detail in Appendix A.

Specific goals of the investigation were as follows:

- Adaptive signal-to-noise maximization including main beam interference cases.
- Use of customary reflector and feed elements, etc.

- Minimize impact of adaptive circuits (size, weight, power and cost).
- Broadband operation (greater than 10% bandwidth) capability.

While we will cover this topic in greater detail in Paragraph 6.2, we note that the reflector feed null steering anti-jam technique is potentially superior to the customary sidelobe canceller from the standpoints of achievable null depth, convenience of use, and the inability of the sidelobe canceller to null jammers in the main beam.

The organization of this section is as follows. Fundamentals of the adaptive reflector feed concept are presented in Paragraph 6.2. Paragraph 6.2.1 introduces the concept on a block diagram level, while Paragraph 6.2.2 gives considerations to the analytical approach. Performance calculations showing feasibility of the approach are given for a simple one-dimensional feed structure in Paragraph 6.2.3. A brief comparison with the customary approach, a sidelobe canceller, follows in Paragraph 6.2.4.

Paragraph 6.3 is devoted to a two-dimensional five-horn feed which was designed specifically for millimeter wave communications links. A threat of up to two significant jammers was postulated. Antenna nulling performance is shown as a function of jammer angle of arrival with respect to the desired signal for several different cases.

Paragraph 6.4 is devoted to a discussion of the critical RF component, a low-loss weight. A design approach which was realized in hardware at X-band is presented.

The conclusions of the millimeter wave adaptive antenna investigations are presented in Paragraph 6.5.

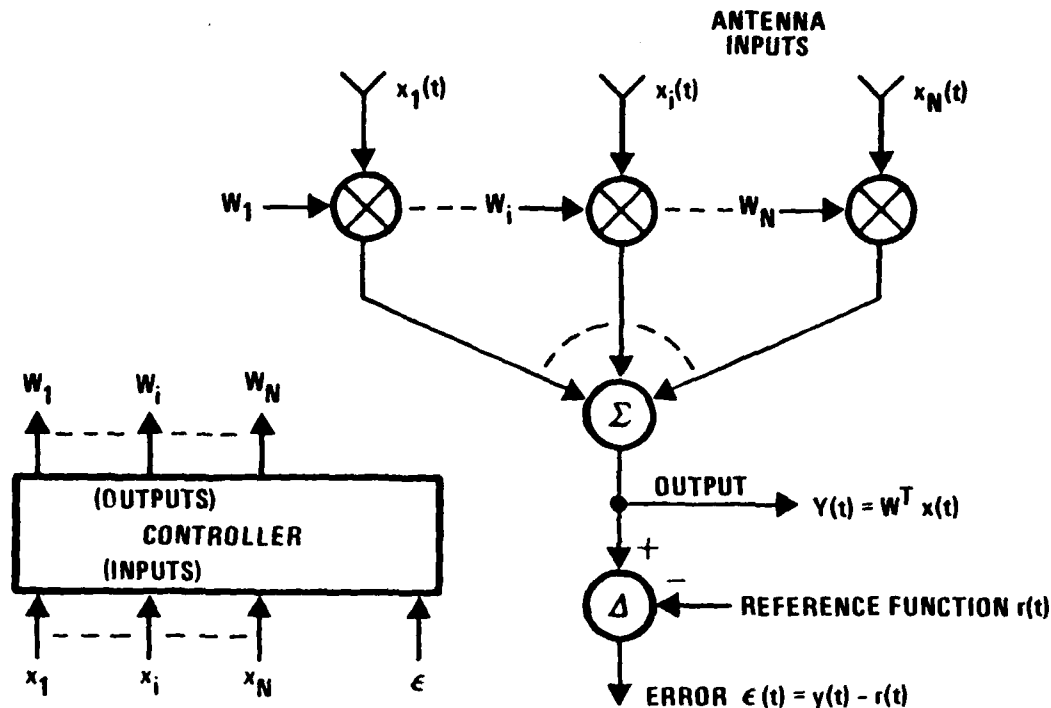
6.2 Reflector Feed Adaptive Null Steering

In the following paragraphs, adaptive weighting and controlling of reflector feed elements as an antijam technique is briefly described and compared conceptually with a sidelobe canceller. Following this, a detailed description of the new technique is given. Paragraph 6.2.2, Analytical Approach, discusses some of the problems encountered in analyzing and operating such an array structure. Following this in Paragraph 6.2.3 is a presentation of calculated nulling performance for a simple one-dimensional suppression-type algorithm. Such calculations are useful in that they establish the basic feasibility of the approach. Simulated performance of a feed design suitable for the millimeter wave communications link is presented separately in Paragraph 6.3.

6.2.1 Description of the Approach

An adaptive array processor can be diagrammed conceptually as shown in Figure 6.2.1-1. A number of inputs are shown at the top of the figure, for signals which are weighted by weights W_1 through W_N . The weighted sum of these inputs is the array output. The problem faced by the adaptive processor is to adjust the weights in such a manner that the output signal most nearly matches a desired response. A temporal reference type adaptive array is illustrated in the figure. In such a circuit, an array error is formed by subtracting a desired response of the reference function from the array output. The task of the adaptive processor, then, is to minimize the error function.

Formation of an error function and topics that generally treat how the adaptive processor adjusts the weights are well understood theoretical problems and will not be discussed here.



A90401-108

Figure 6.2.1-1. Temporal Reference Adaptive Array

Basically, the reflector feed adaptive null steering circuit is formed much as illustrated in Figure 6.2.1-1 by using the feed elements of a reflector antenna as though they were ordinary elements in a conventional adaptive array. A diagram of such a representative configuration is given in Figure 6.2.1-2. This figure illustrates a Cassegrain-type reflector where the feed horns illuminate the subreflector, and thus, indirectly illuminate the main reflector. In a non-adaptive feed system, the horn outputs would be combined "fixed weighted" and summed so as to produce the desired sum and difference patterns (only one output is shown in Figure 6.2.1-2). In the reflector feed adaptive approach, the fixed weighting conventionally used is replaced by low loss RF weighting devices that are capable of being adjusted to arbitrary amplitude and phase values.

In this manner, in the absence of interference to be nulled, the weights would take on the values needed to achieve the conventional feed pattern. Thus, in the absence of jamming, performance of the antenna system is essentially unchanged. Alternatively, when interference is present, it is possible to adjust the weights in such a manner that the interference is nulled while retaining a useful degree of signal response, provided that the signal and jammer are not too close in angle. We will show in Paragraph 6.3 that this approach provides for nulling interferences within the main beams of the feed system in contrast to the sidelobe canceller which cannot achieve useful main beam nulls.

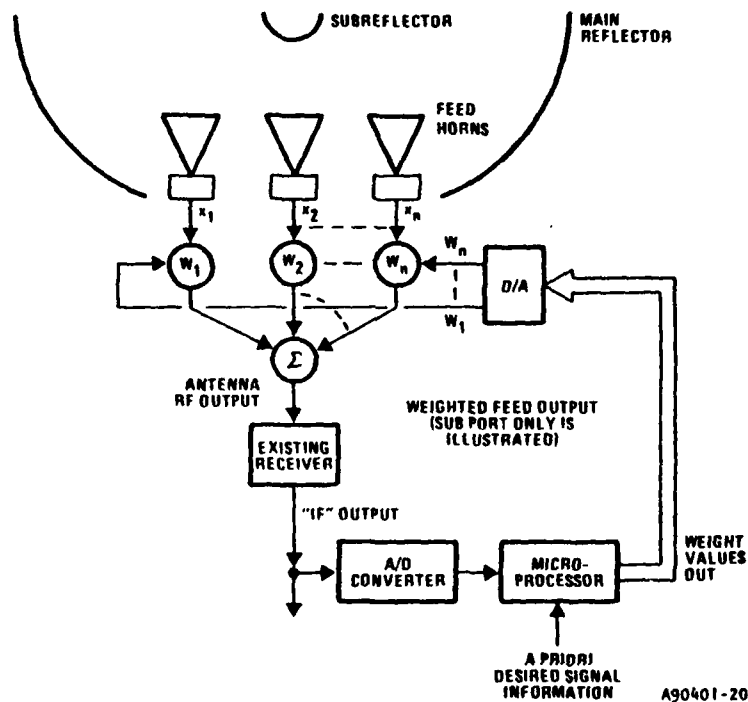


Figure 6.2.1-2. Reflector Feed Adaptive Null-Steering Hardware Diagram

The output of the feed system is directed to the usual receiver as required by the system to provide necessary amplification and band limiting of desired signals. The adaptive processor controller, shown in Figure 6.2.1-2, is an analog-digital hybrid circuit. A question of whether to use analog-digital or hybrid analog-digital adaptive processors can be answered by a study of system requirements. In most cases, the analog-digital hybrid is a very cost effective and powerful approach. As a matter of interest, most sidelobe cancellers use analog controls.

Continuing with the block diagram in Figure 6.2.1-2, desired signals at the IF output of the receiver are processed as required by the system with the exception that a tap has been provided for the adaptive algorithm controller. Information from the receiver's IF output is obtained in a digital format by means of an analog-to-digital converter which periodically samples the receiver's output. The microprocessor/controller through a systematic perturbation of the RF weights used in place of the fixed weighted combining structure can obtain sufficient information to realize a performance-optimizing adaptive algorithm. Details of this algorithm are given in the report "Application of the Correlation Discriminant Operator to Perturbational Adaptive Algorithms," RADC-TR-79-44 April 1979 (RADC Contract Number F30602-77-C-0073).

Note that the analog-to-digital converter need only sample at a rate sufficiently rapid to satisfy the adaptation bandwidth needs of the algorithm. It is unnecessary to sample at such a rate that the amplitude and phase of the IF output itself is coherently retained.

Observe that use of this digital perturbational type algorithm allows the receiver ordinarily required by the system to be used as an integral part of the entire adaptive nulling approach. Thus, amplification and band limiting required by the adaptive processor is handled automatically by the required system receiver. This is contrast with the customary approach wherein expensive and bulky analog correlators are used along with special purpose receivers to realize the null forming circuits.

Through the use of the perturbational approach, great savings in size, weight, power and dollars are possible at the expense of somewhat slower adaptation response and somewhat reduced null depth performance. Regardless, hybrid-digital-analog approaches are capable of achieving 35 to 40 dB nulls in a few hundreds of microseconds. This is as good as many existing analog circuits.

The minimal hardware impact of the hybrid-analog-digital adaptive null steering approach is emphasized. As can be seen in Figure 6.2.1-2, the only hardware required beyond that in the customary system is a replacement of the fixed feed horn combining network with a variable weighted combining network, an intermediate frequency output tap from the system receiver which may already be present, an A/D converter, microprocessor with adaptive algorithms, and D/A converter to drive the RF weights.

Design of the RF weight is a critical matter and will largely determine whether or not the hybrid approach will be useful. This topic is covered in Paragraph 6.4 of this report.

6.2.2 Analytical Approach

In a conventional adaptive antenna processor, the several inputs are obtained from an array of antenna elements which directly view the electromagnetic environment. In this application, inputs are obtained from an array of antenna elements that view the external environment through a system of subreflector and main reflector. Thus, certain transformations occur which are not present in the conventional application.

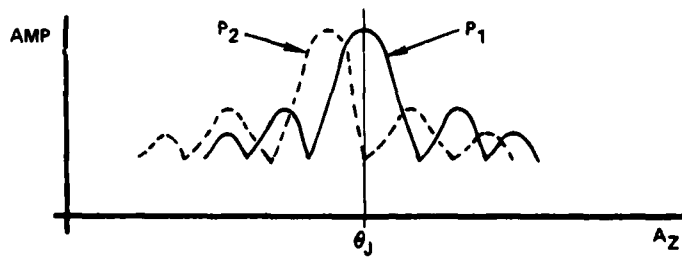
In order to predict achievable null-steering performance for both idealized and actual circuit designs over the wide bandwidths of interest, it has been necessary to modify and expand existing analytical computer programs. A very important mathematical parameter in these programs is the cross-correlation matrix of the several input waveforms. This matrix is a function of the chosen weighting network, the antenna feed and the reflector

antenna, as well as the spectral properties of the interference sources. Through the use of measured feed horn scattered patterns and a fast Fourier transform, the output of each horn as a function of a frequency for a given interference source can be computed. When a given broadband weighting structure is specified, the cross-correlation matrix is then computed numerically, thus facilitating use of standard null computing programs.

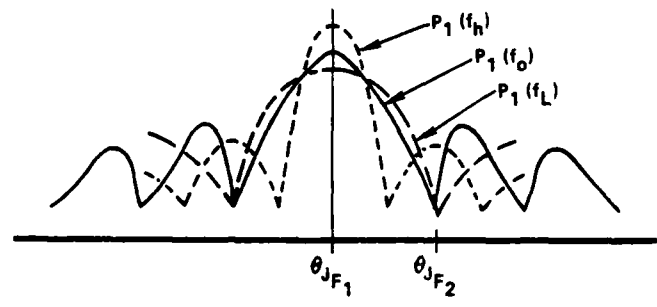
An illustration of the problem being addressed is given in Figure 6.2.2. At the top of the figure in Part A, the pattern for two horns is given as a function of azimuth. In this particular feed design, the horns are offset in position; thus, the azimuth patterns of their far field maximum responses do not coincide. In Part B of the figure, a response of one of these horns is shown as a function of frequency. Observe that as frequency increases, the lobe becomes narrower and exhibits increased on axis-gain.

We can use this single horn response as given in Part B to calculate the response of the two different horns to the jammer considered earlier in Part A. We assume for this example that the far field response, P_2 , of horn Number 2 is the same as that of horn Number 1 except offset in angle. Thus the response for F_2 is found approximately by examining the pattern in Figure 6.2.2 at the angle θ_{JF1} ; likewise, the output of F_2 is found by evaluating the same pattern at the angle θ_{JF2} .

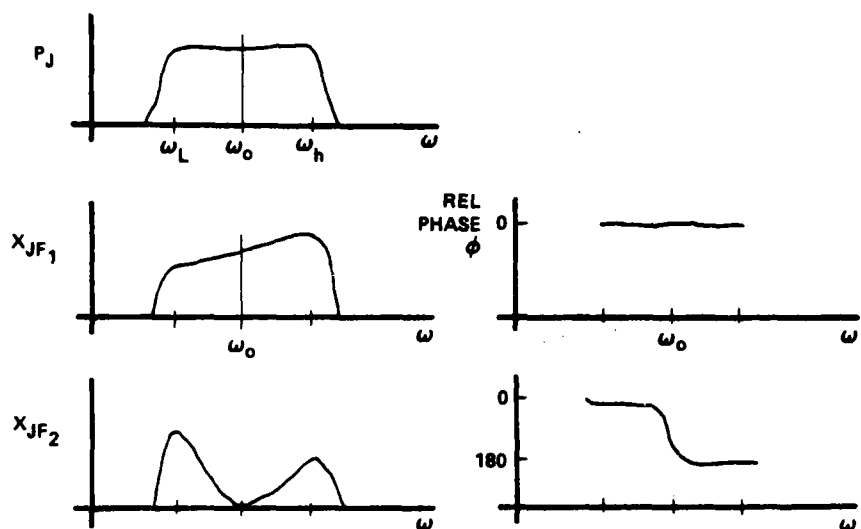
Part C of the figure shows the spectral response of the two horns to this jammer. The uppermost spectral diagram is the assumed jammer amplitude as a function of frequency. The second level of the diagram shows amplitude and phase of the first horn signal as a function of frequency. (We assume the lobes of the pattern in Figure 6.2.2 to alternate in phase although the phase response is not illustrated.) Since the jammer is centered on the peak response of horn 1, the higher frequency spectral terms of the jammer emerge from the feed at greater amplitude than the lower frequency terms. Relative phase is essentially constant. The lowest set of diagrams show the amplitude and phase response of the jammer emerging from



A. TWO FEED HORN PATTERNS VERSUS AZIMUTH AT CENTER FREQUENCY



B. FEED HORN RESPONSE AS A FUNCTION OF FREQUENCY .



C. FEED HORN OUTPUT AS A FUNCTION OF FREQUENCY FOR TWO DIFFERENT JAMMER ANGLES OF ARRIVAL

10509-30

Figure 6.2.2. Calculation of Feed Horn Response to a Broadband Jammer

horn 2. In this case, the pattern at the jammer's lowest spectral frequency is wide enough to incorporate those jamming terms inside the main lobe of the feed. At a higher frequency, the pattern has narrowed enough that the first null of the pattern is seen for those spectral terms. Finally, the highest frequency spectral terms of the jammer are received on the first sidelobe of horn 2's pattern. Since the antenna pattern lobes are approximately reversed in phase, the spectral energy in the jammer's lower frequencies in the second feed horn output are essentially in phase with those emerging from the first feed horn; however, at the highest frequencies, a 180 degree phase reversal is seen.

While it is evident that no single amplitude and phase when applied to the signal emerging from horn Number 2 is sufficient to cancel the energy arriving from horn Number 1, surprisingly good results can be obtained over certain jammer angles of arrival. Furthermore, the presence of several horns rather than just two provide additional degrees of freedom which can be useful in obtaining the necessary spectral contributions for cancellation of such interference.

Due to the fact that the horn response is largely characterized by nearly constant amplitude and phase over large portions of a particular sidelobe structure, a simple amplitude and phase weighting circuit is suggested as being more useful than one might imagine. More complicated tapped delay line and weighting circuits are discussed later.

6.2.3 Calculated Nulling Performance

In this section, the basic nulling capability of the adaptive reflector feed configuration is calculated. In this portion of the analysis, we address the problem of forming nulls only. Signal to noise ratio maximization is treated later in Paragraph 6.3 where a design specific to millimeter wave communication links is presented.

The results here show the nulling performance obtainable with up to five feed horns. In this first set of calculated performance data, we assume only two horns located at slightly offset physical positions such as might be used in forming a monopulse sum and difference pattern for azimuth only. The horn element producing a maximum response at a relative azimuth of zero in the far field was chosen as a reference element. Weights connected to the other elements were adjusted so as to minimize jammer power emerging from the combination of inputs. In all of the examples given here, a main reflector producing a 3 dB beamwidth of 0.30 degrees is considered. Furthermore, the RF bandwidth is 20 percent. It is assumed that the antenna is pointed at a relative azimuth angle of 0 degrees. A jammer is assumed having an arbitrary azimuth angle of arrival falling somewhere between -1.2 and $+1.2^{\circ}$. This limitation on assumed jammer angle of arrival was assumed for computational convenience. It is noted, however, that at very large angular separation from the main pointing angle of the antenna, the measured and computed data is likely to be substantially in error. For this reason, broadband nulling performance outside of the first six or seven sidelobes cannot easily be extrapolated from the computed data presented here.

A jammer suppression performance curve for a two feed horn system is illustrated in Figure 6.2.3-1. In this example, the horns produce far field patterns which have maxima at the azimuth angles indicated. For example, the referenced feed horn has a far field maxima at an azimuth of 0, while the second feed horn has a far field maxima at an azimuth of about 0.37 degree. This response corresponds to a readily achievable feed horn spacing in the antenna feed structure. The ordinate of the graph in the figure is null depth achieved. The meaning of null depth is clarified by the following example. Suppose that only the reference feed horn were present, then the jammer would produce a particular output from this reference feed horn as a function of angle. If the jammer were to move from -1.2 to $+1.2^{\circ}$ and the power output of the feed horn were to be measured, then the relative shape of the output curve would be the far field pattern of that feed horn. Then in order to achieve the null pattern, a second feed horn is connected to a weighted combining network so as to sum with the

reference horn output. By means of amplitude and phase adjustment of the second feed horn's output, one minimizes the total output of the combining network. Null depth, then, is interpreted as the difference between output of the reference horn and output of the combining network.

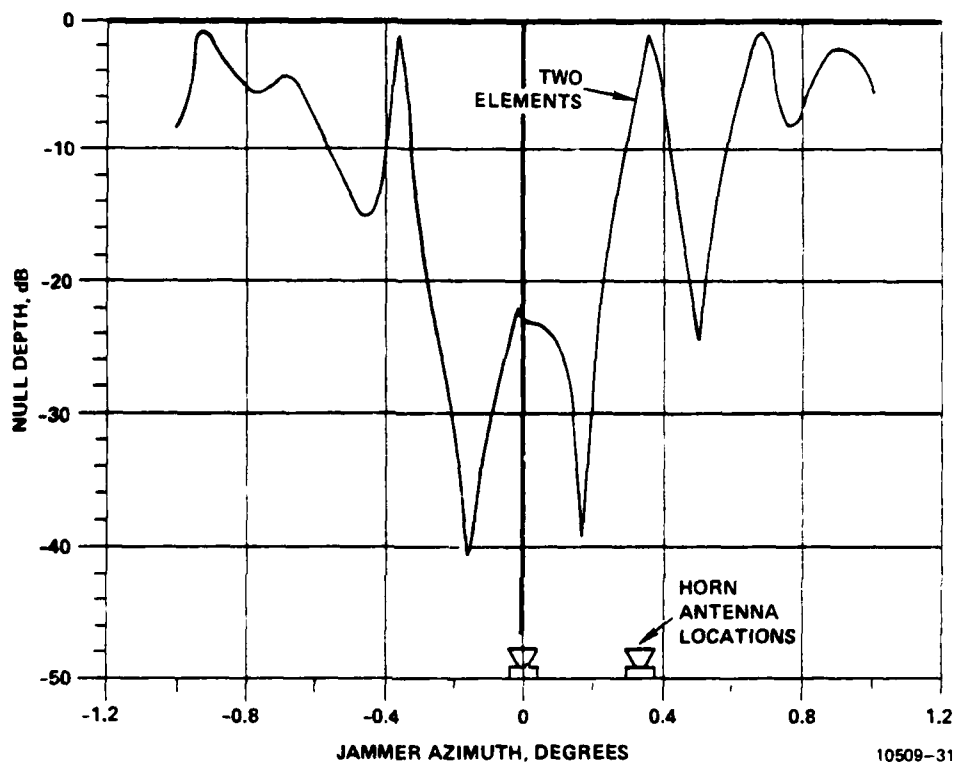


Figure 6.2.3-1. Two Feed Horn Null Depth for a 20 Percent Bandwidth Jammer

As expected, relatively good null depths are achieved when both the reference element and the secondary horn have the jamming source coming in on the primary lobe or first sidelobes. This is because these lobes have relatively uniform amplitude and phase response. As the jammer moves toward the third and fourth sidelobes, substantially reduced nulling performance is obtained because of the severe dispersion present in these lobes. As a matter of substantial importance, note in Figure 6.2.3-1 that a null depth of only about 2 dB is achieved at the azimuth of the second horn, about 0.37 degree.

At first, one might think that the total antenna performance would be rather poor at this angle. In fact, it turns out that the reference horn has a null in its pattern at this particular angle. Consequently, even though only about 2 dB suppression of the reference antenna output was obtained, this output was in fact very low to begin with since it was due to the jammer arriving at the reference horn's first null position. Since the first null depth (not shown) was about 30 dB, the array output is about 32 dB below the mainlobe peak in this case. Consequently, as far as system performance goes, the 22 dB null seen at a jammer azimuth of 0 degree represents a more severe condition in that total array output is only 22 dB below the main antenna peak at this point.

The results just shown indicate that a two horn weighting adaptive circuit can provide a useful system null of 20 or more dB depending upon the jammer angle or arrival. At relatively wide jammer angles of arrival, achievable null depth deteriorates to only a few dB below the response of the reference horn. Thus, the sidelobe cancelling performance of this particular arrangement, while not poor, is not especially good either. As shown in the next paragraph, this performance is dramatically improved by the addition of more horns to the array. Figure 6.2.3-2 shows the results obtained when three horns instead of two are used to form the adaptive circuit.

Note that a much broader area of deep nulls is obtained. In this case, nulls 20 dB below reference lobes are obtained over most of the jammer angles of arrival. Over the interior 0.8 degree, null depths approaching 40 dB are calculated. Specifically, note that a jammer arriving at 0 degree in azimuth (exactly on the reference mainlobe) is suppressed by 40 dB. The reference horn response at its first null is also additionally suppressed by 22 dB as contrasted to the 2 dB obtained with only two elements. Such improved performance is obtained because the third element provides an additional degree of freedom; that is, it provides alternative amplitude and phases of various parts of the spectrum needed to augment the first elements response in cancelling the reference horn waveform. Although the results will not be presented here, if two jammers are considered for the

three-element case, each individual jammer would be suppressed about as much as shown in the first example, the two horn case. Thus, while the three horn configuration could in principle do some nulling of two jammers, this would not be desirable, in that substantially degraded performance is obtained compared to the null achievable on a single interferer.

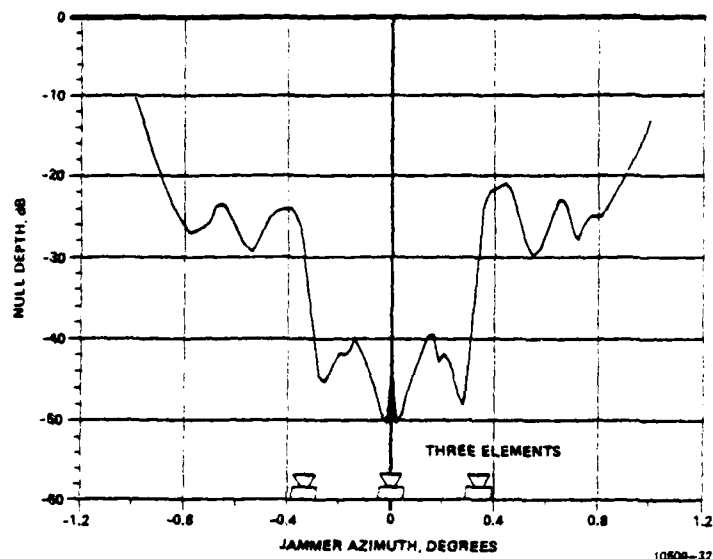


Figure 6.2.3-2. Three Feed Horn Null Depth for a 20 Percent Bandwidth Jammer

Even more impressive results are obtained when five elements are employed to null a single jammer. These calculations are shown in Figure 6.2.3-3. For comparison purposes, the two element null depth curve is also shown on this figure. Note that achievable null depth is better than 40 dB below any point of the reference horn's pattern over the entire angular area of interest. It turns out that with five horns, it is possible to do a very good job of nulling two jammers. A two jammer case for five horns is illustrated in Figure 6.2.3-4. The first jammer is assumed to arrive at an angle of 0 degree, that is, directly on the mainlobe of the reference element. The second jammer's azimuth is allowed to vary from 1.2° to -1.2° . Since nulling of both jammers simultaneously affects the null depth achievable on both of these jammers simultaneously, it is necessary to

plot the array output for the individual jammers even though only Jammer Number 2 is varied in azimuth. As can be seen in the figure, the worst-case obtained is a null of about 25 dB on one jammer simultaneously with a null of about 35 dB on the second jammer. Consequently, output is probably dominated by the minimally nulled jammer. Over most of the angular space, however, both jammers are nulled 30 dB or more, often as much as 35 or 40 dB. Keep in mind that both jammers have a bandwidth of 20 percent. Consequently, the performance predictions shown in this figure are considered to be good.

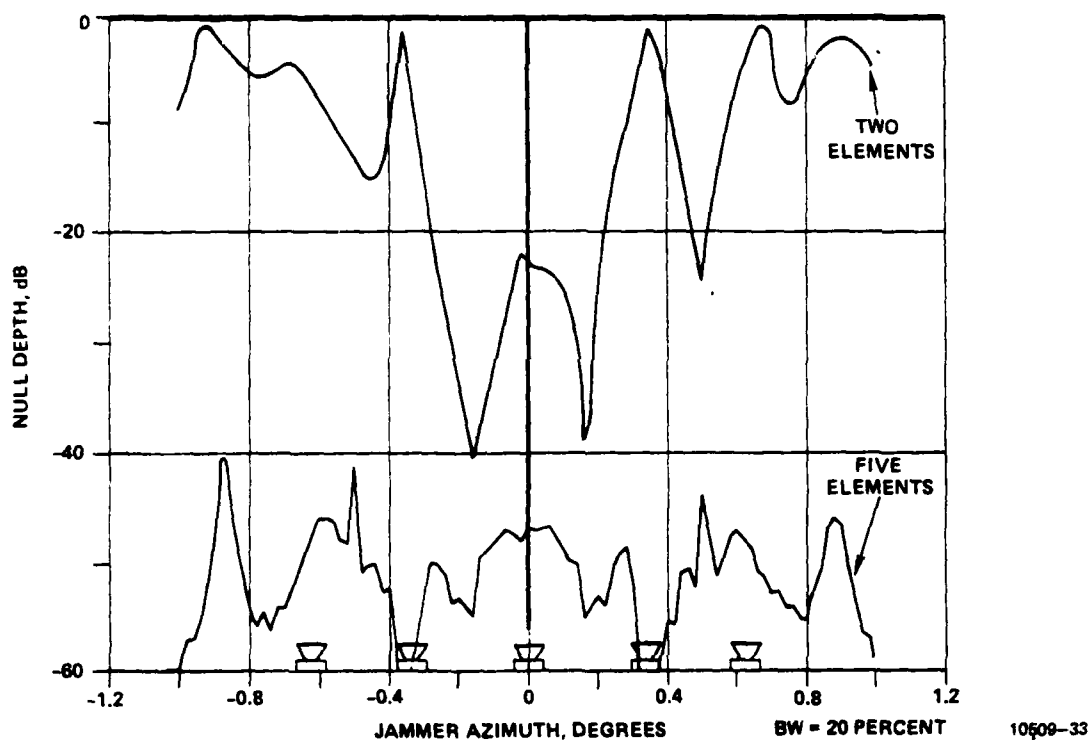
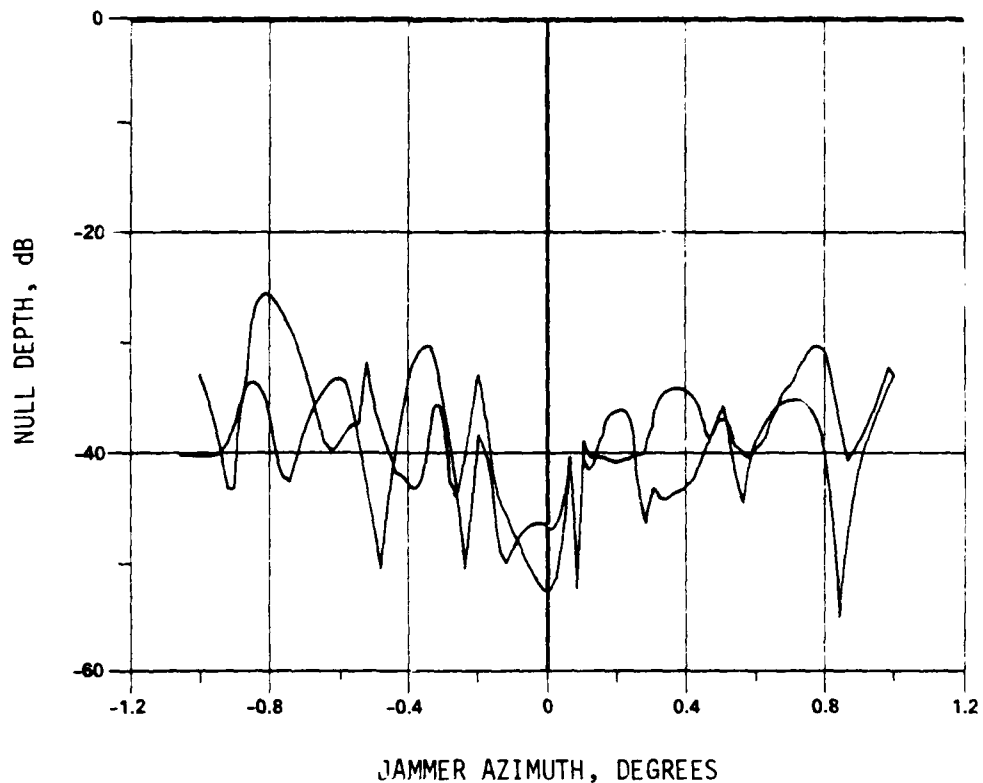


Figure 6.2.3-3. Five Feed Horn Depth for a 20 Percent Bandwidth Jammer



10509-34

Figure 6.2.3-4. Five Feed Horn Null Depth for Two 20 Percent Bandwidth Equal Power Jammers (Jammer 1 at 0°)

A resultant antenna pattern for this five horn configuration is shown in Figure 6.2.3-5. The illustrated case is for Jammer Number 1 at 0.0 degree and Jammer Number 2 at 0.2 degrees. As can be seen, relatively good nulls are obtained completely within the mainbeam. Since this is a single frequency antenna pattern (center of the band) null depths do not agree exactly between this curve and those of Figure 6.2.3-4, the latter being an integrated null depth calculation.

Obviously, signal and jammers must be separated in angle if null steering is to be useful. In this case, an angular separation of about one beamwidth is required in order that no desired signal gain be lost (as expected from other considerations). Alternatively, if reduced signal gain is tolerable, closer angular approach is permitted.

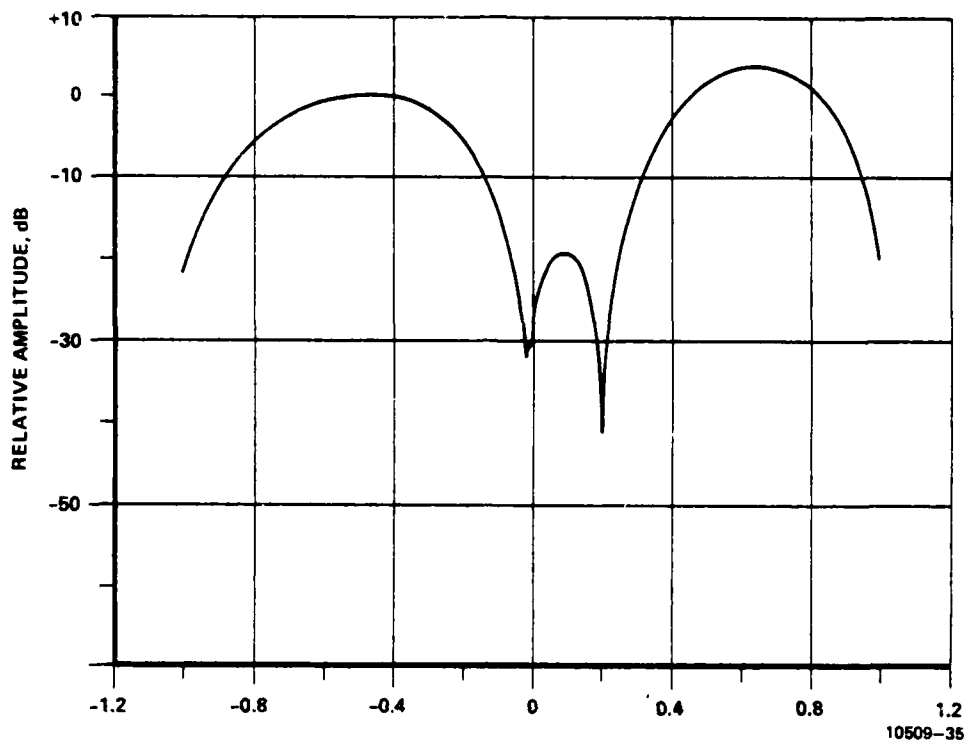


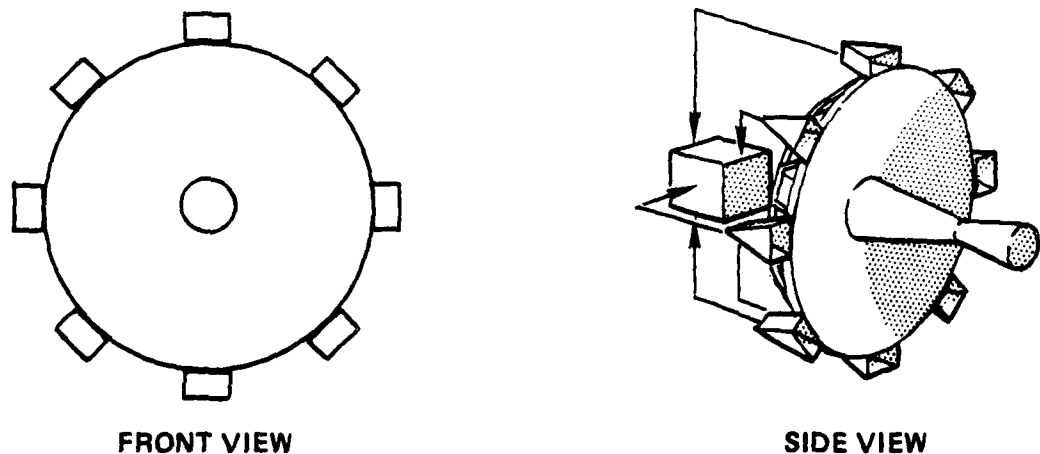
Figure 6.2.3-5. Combined Feed Horn Response for Two Jammers Within the Main Beam for a Five Feed Horn System

Finally, it is noted that sharper nulls and thus a closer signal/jammer approach are obtained with a S/N maximization algorithm and two dimensional feeds (azimuth and elevation). This subject is discussed in Appendix A.

6.2.4 Comparison With a Sidelobe Canceller

A typical sidelobe canceller has several low gain antenna elements on the rim of the main dish which serve as inputs to the adaptive processor. A representative configuration is shown in Figure 6.2.4-1. Ordinarily, the gain of the auxiliary elements is roughly that of the gain

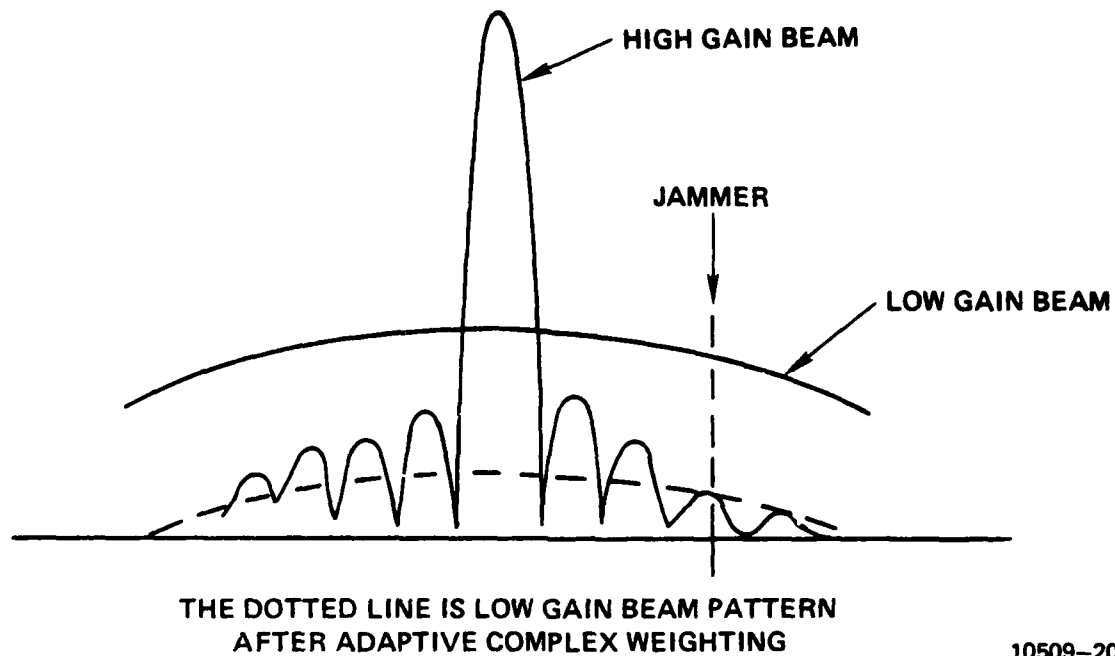
of the first sidelobe of the main beam pattern. Therefore, by correct amplitude and phase adjustment of the inputs from the auxiliary elements, interferers entering the main antenna through sidelobes can be cancelled without severe degradation of the antenna's response to the desired signal. This is illustrated in Figure 6.2.4-2.



A90401-106

Figure 6.2.4-1. Adaptive Sidelobe Cancellation Antennas

Sidelobe canceller performance is primarily limited by the fact that the extra cancelling elements are usually located along the antenna's periphery or on the back of the subreflector. Given such a configuration, substantial time-of-arrival differences are present in jammer signals arriving at the auxiliary element versus those arriving at the feed elements. Since these time-of-arrival differences are a function of the angle of arrival of the interference, no fixed time delay compensation is possible. Consequently, the sidelobe canceller can either achieve good nulling only at a particular jammer angle of arrival or only over a narrow frequency band.



10509-20

Figure 6.2.4-2. Beam Pattern Cancellation Between the High Gain Beam and Low Gain Beam

Sidelobe cancellers also are incapable of achieving useful nulls within the main beams of the antenna system. This is due to the fact that the aperture size of the auxiliary cancelling elements is much less than the aperture of the main reflector. Therefore, if nulling within the mainbeam is allowed, either substantial attenuation of the desired signal from the main antenna or substantial amplification of the relatively noisy desired signal from the auxiliary elements is necessary in order to achieve cancellation of the interference. Under these conditions, the desired signal is severely degraded. For this reason, most sidelobe canceller circuits have limitations placed on the auxiliary element weights to prevent nulling within the main beam.

6.3 Millimeter Wave Adaptive Feed Design

While the preceding section presented details of the new adaptive array feed nulling approach and performance data for a linear type feed configuration, such a feed configuration is not suitable for use in a general communication link design. The principal flaw in such an approach is that no degrees of freedom exist in the direction orthogonal to the axis of the one-dimensional feed structure. In order to provide nulling in both azimuth and elevation directions, an array having two dimensions is required.

An array feed design which has shown to be useful in preliminary evaluations is given in Figure 6.3-1. Five elements are used with the fifth element being a centrally located one. Spacing of the elements is chosen to provide beams crossing in the far field at about the 6 dB points. In this evaluation, all feed elements were assumed to have similar gains, although in a future design, it is possible that the auxiliary elements can be reduced in gain compared with the central element.

Incorporation of the central element is an important factor in the design. If this element were missing, jammers in the azimuth plane for 0° elevation or in the elevation plane for 0° azimuth would, in effect, be nulled with only one degree of freedom. This is due to the fact that pairs of elements would receive similar signals. Resulting performance would be essentially that presented earlier for the two-element null steerer in Paragraph 6.2.

Some results of computer simulation of the five element configuration are given in the following paragraphs. A single jammer and a single desired signal were assumed. The desired signal is presumed to arrive on boresight while the jammer angle of arrival was calculated for a large number of points located in planes which cut through the far field pattern of the feed elements at 0, 22-1/2, and 45 degrees as illustrated in Figure 6.3-1. Due to the symmetry of the feed arrangement, similar results would be obtained for the remaining octants of the structure.

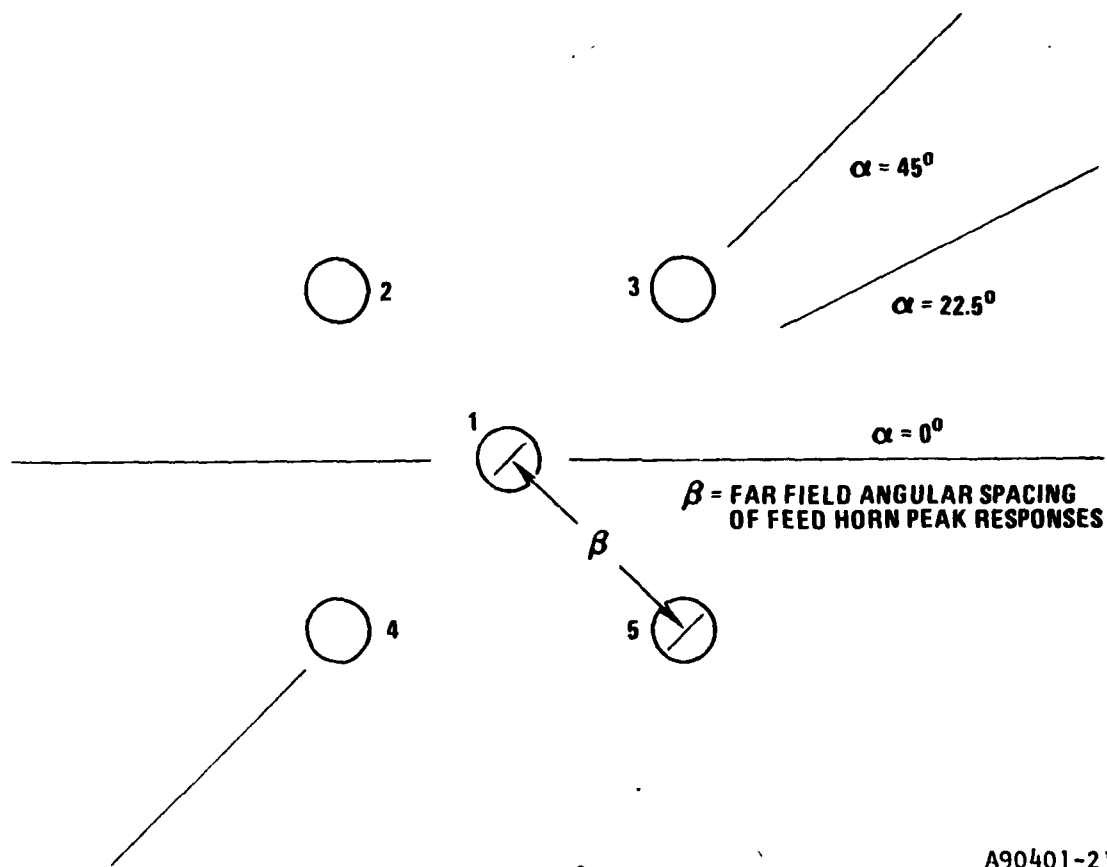
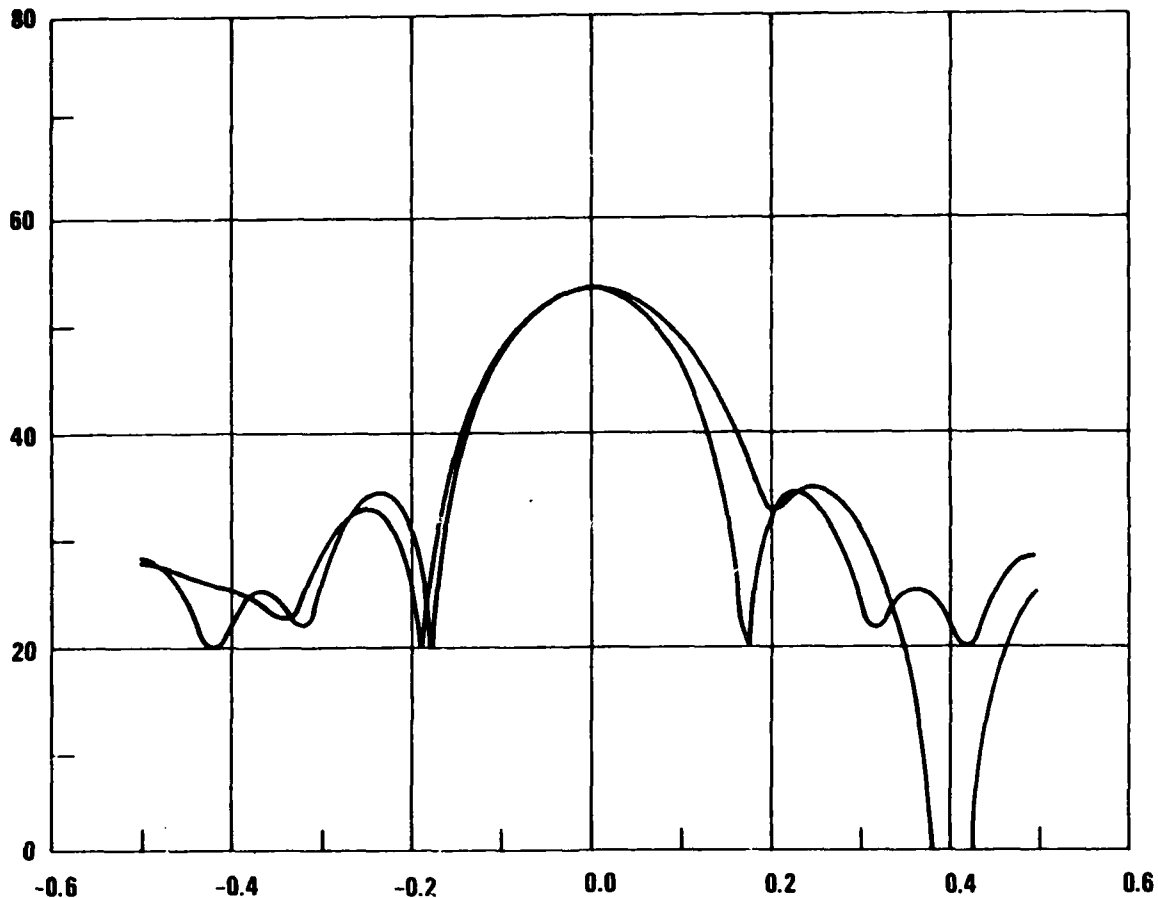


Figure 6.3-1. Far Field Angular Positioning of Field Horn Patterns

Significantly, bandwidth in all of these simulations was assumed to be 20 percent. We note that the achievable null depth-bandwidth product for this reflector feed null steering approach is roughly three orders of magnitude superior to that of the sidelobe canceller. Jammer power in these simulations was 30 dB greater than desired signal power and 40 dB greater than thermal noise in an individual feed element. A reflector having a 3 dB beamwidth of 0.15° was chosen. Similar performance would be obtained with different reflector sizes.

Processing results for a jammer arriving at an angle of 0.4° (near the second sidelobe) are given in Figure 6.3-2. Two curves are drawn by the computer. The first, approximately symmetrical, is the response of the antenna system in the presence of only the desired signal. The second

curve shows the response of the antenna system as a function of angle for the jammer located at 0.4° . As can be seen, a null considerably in excess of 20 dB has been formed on the jammer while desired signal gain is largely unaffected.

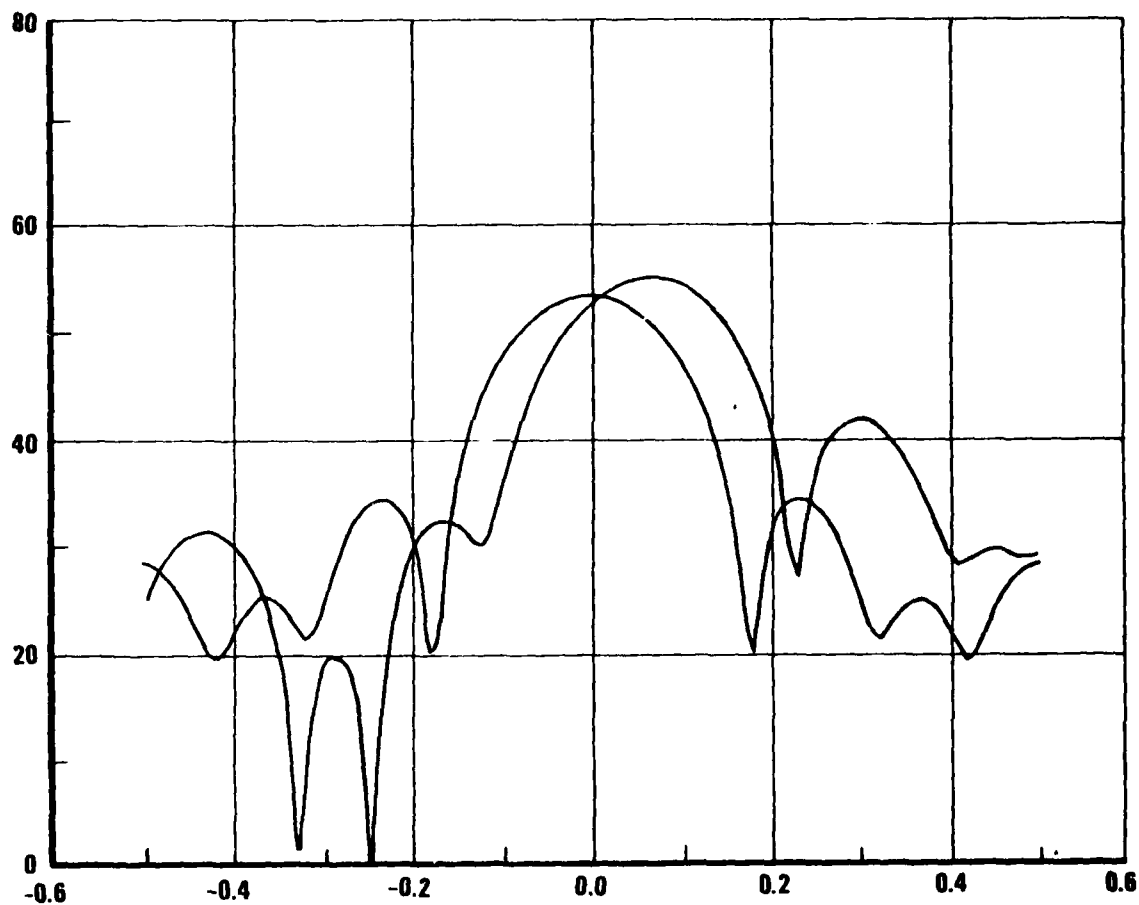


A90401-22

Figure 6.3-2. Antenna Patterns Before and After Adaptation to a Jammer at 0.4°

In Figure 6.3-3, response of the antenna system is shown for a jammer located near the peak of the first sidelobe at an angle of arrival of about -0.25° . A null depth of about 35 dB is achieved with only a 1 or 2 dB loss in desired signal gain. Note that the resultant antenna pattern has several dB greater gain off axis than the best gain it can place on axis in

the absence of a jammer. This is due to the fact that five equal gain horns are used in the feed design. A better feed design would utilize a principal central feed element surrounded by lower gain peripheral elements. The use of five equal gain feed elements positioned for the far field response depicted in Figure 6.3-1 is not optimal for on-axis desired signal performance.



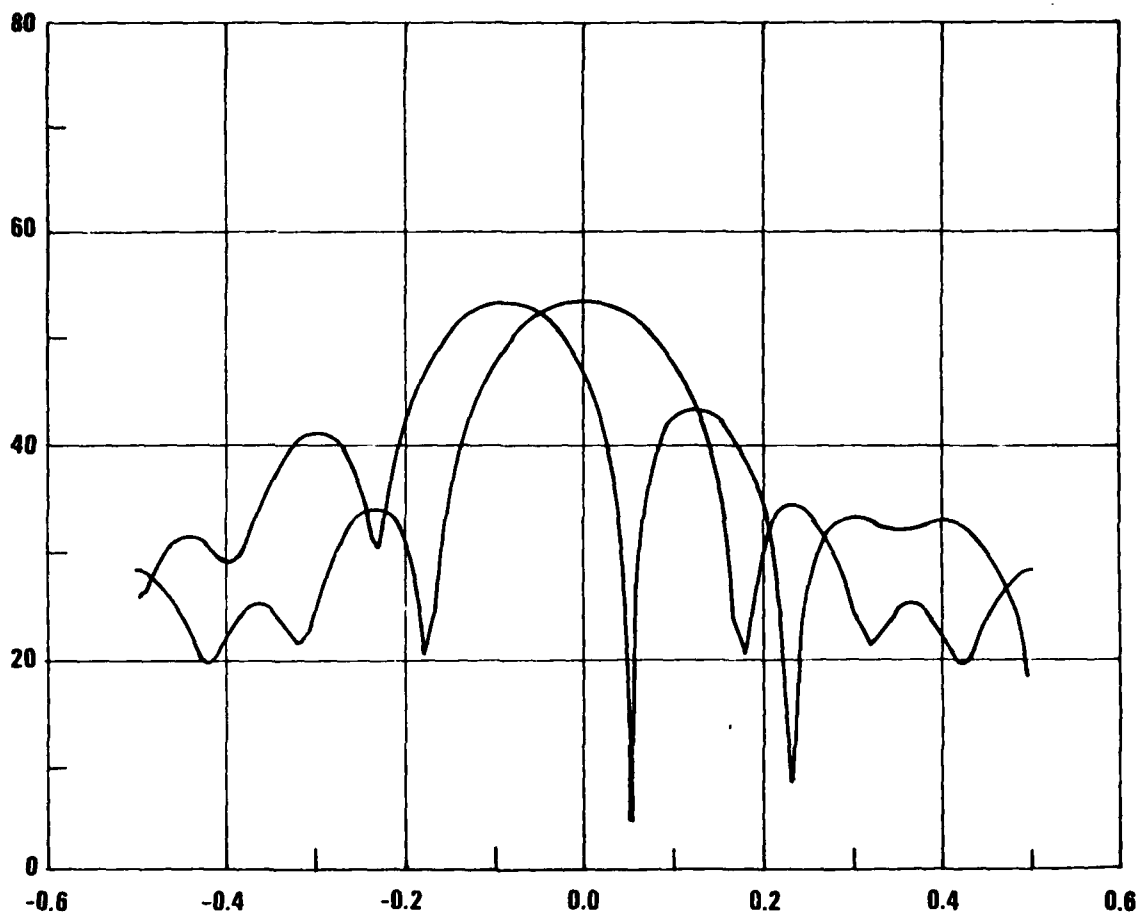
A90401-23

Figure 6.3-3. Antenna Patterns Before and After Adaption to a Jammer at -0.25°

Response of the antenna system to a main beam jammer is illustrated in Figure 6.3-4. In this instance, the jammer is arriving near the 3 dB point on the central element's pattern. Although a very deep null has formed, the desired signal gain has also dropped, in this case by about 10 dB. Nevertheless, signal-to-noise ratio improvement will be in the order of 35 dB. Such a loss in desired signal gain is not necessarily detrimental to system performance, provided that a degree of margin exists in the system. Such margin is often designed to provide for rain attenuation and other factors. Unless the jamming is coincident with additional external propagation disturbances, it is likely that good system performance will be obtained in spite of the desired signal gain loss.

We observe that since this adaptive feed nulling approach can easily provide nulling well within the main beam, it is necessary to use an algorithm capable of signal-to-noise ratio maximization in order to prevent nulling of the desired signal as well as for its optimization. Details of algorithms suitable in this respect, such as the PSF (positive signal feedback) are described in an RADC report TR-79-44 entitled, "Application of the Correlation Discriminate Operator to Perturbational Adaptive Algorithms," the Harris Corporation Final Report on Contract Number F30602-77-C-0073.

With such an approach for nulling within the main beam, dramatic results for signal-to-noise ratio improvement can be obtained. (Again, it is important to recognize that desired signal gain may be lost as the jammer approaches the desired signal.) The adaptive algorithm knows how to optimally trade loss of desired signal gain with jammer nulls. Thus, a good system design would take into account margin required for the closest jammer approach as well as for propagation anomalies.

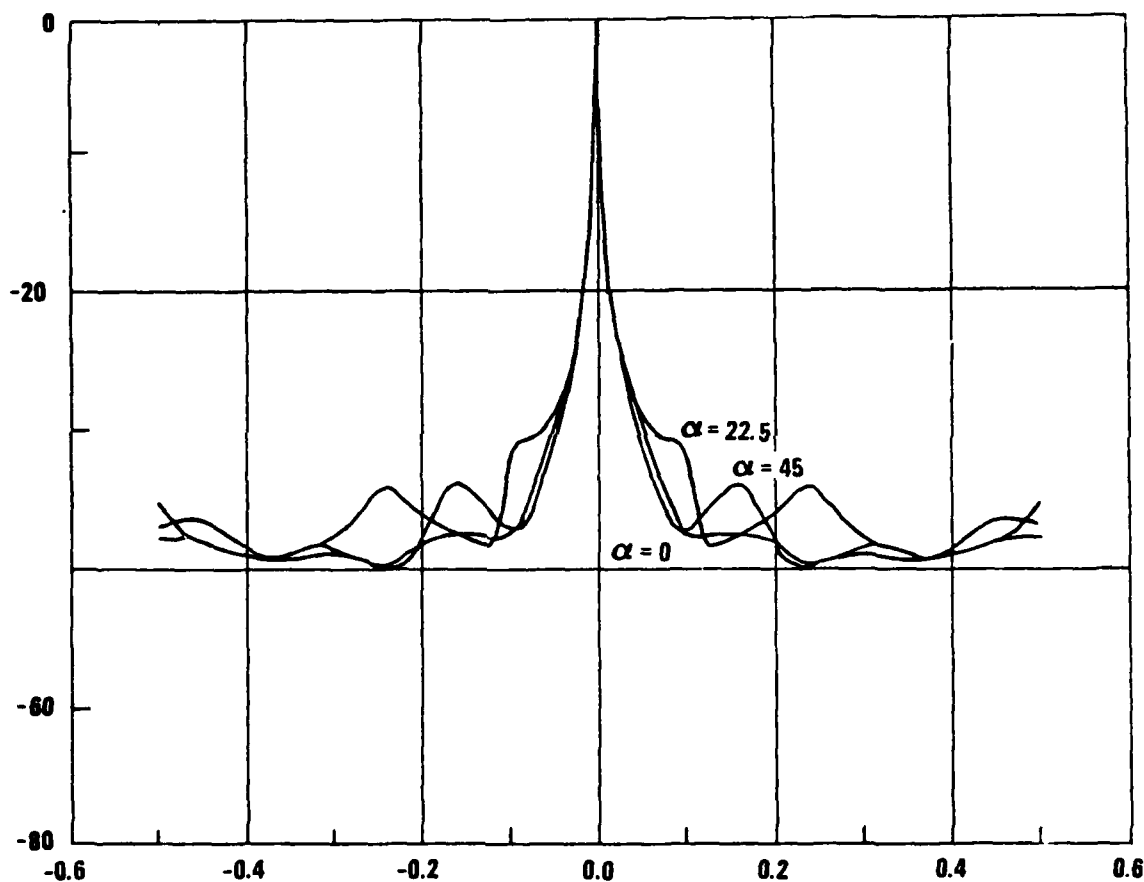


A90401-24

Figure 6.3-4. Antenna Patterns Before and After Adaption to a Jammer at 0.04°

Signal-to-noise ratio improvement obtained as a function of jammer angle of arrival is shown in Figure 6.3-5. We define signal-to-noise ratio improvement as the signal-to-noise ratio obtained by the adaptive system configured to optimally receive the desired signal in the presence of jamming divided by the signal-to-noise ratio obtained by the unadapted antenna pattern. As can be seen in Figure 6.3-5, signal-to-noise ratio improvements in excess of 20 dB are obtained for jammer angles of arrival

approximately 0.02° (about one fifth of a beamwidth) away from the desired signal. Null depths from 35 to 40 dB are obtained from roughly the 6 dB point outward. Note that three curves are shown in Figure 6.3-5. Those are for jammers arriving in planes of 0, 22-1/2, and 45 degrees, as depicted in Figure 6.3-1. It can be seen that signal-to-noise ratio improvement is not significantly dependent upon the plane in which the jammer is located.



A90401-25

Figure 6.3-5. Adaptive S/N Improvement as a Function of Jammer Angle of Arrival

In summary, we note that very good signal-to-noise ratio improvement properties have been predicted for the five element array design specific to the millimeter wave length study. However, we also note that since this is a five element design, reduced nulling capability will be obtained when more than one jammer is present. Due to the limited nature of the study, performance was not calculated for more than one jammer, but it is expected that results similar to those presented in Paragraph 6.2 for the linear array will be seen. It is certainly true, however, that if more than two jammers are a significant threat, then increased numbers of feed elements will be required in order to achieve useful performance. Such an analysis and design is recommended for a future effort.

6.4 Low Loss RF Weights

A critical component in the hybrid-analog-digital adaptive processing approach (illustrated in Figure 6.2.1-2) is the RF weighting device. Unless the RF weights combine the characteristics of very low minimum insertion loss with very low amplitude and phase dispersion, then inadequate performance will result. Excessive loss in the weights will degrade system noise performance while excessive amplitude and phase dispersion will limit the ability of the system to form good jammer nulls. It is noted that amplitude tracking across a band to within 0.5 dB and rms phase tracking across the same band of 0.9° limits one to achieving null depths less than 35 dB.

This section is devoted to a presentation of a weighting scheme which has promise in the millimeter wave application. We refer to the approach as a "paired phase shifter" weight. This weighting scheme, developed on IR&D funds, is capable of generating any complex weight value less than unity. Thus, it is no less general than attenuator type weights. Its primary advantage is that it can be set for zero attenuation in contrast to the attenuator type weight which may have as much as 10 dB attenuation in its minimum weight setting condition. In order for either of these weighting schemes to achieve weight values greater than unity, amplification

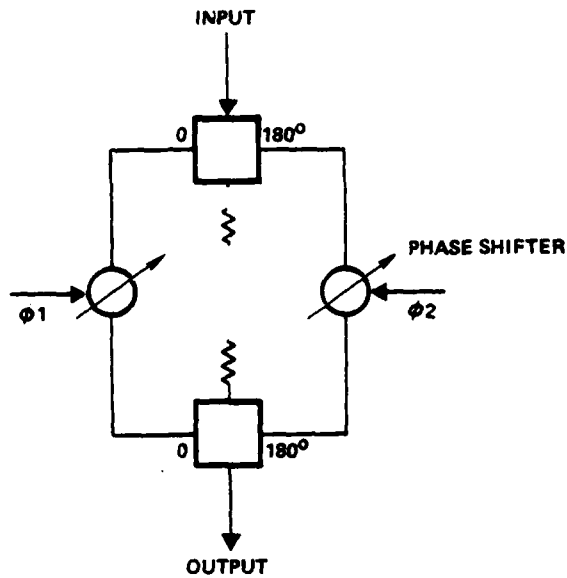
is necessary. However, it is expected that the microcomputer's program can scale the weights as a function of time so that the largest weight is always unity. Then, the paired phased shifter weight is capable of meeting antenna array weighting requirements without the need for amplification. Alternatively, attenuator type weights would each require at least a 10 dB gain RF amplifier.

The weighting device, described later in this section, was designed by Harris Corporation and built by Microwave Associates Group. The weight operates in X-band. Minimum loss is about 0.2 dB and amplitude and phase dispersion is adequate to provide between 35 and 40 dB nulls across a 20% bandwidth. A weight of this type would be highly suitable for use in millimeter wave adaptive circuitry. While waveguide losses increase with frequency, the performance of the ferrite phase shifting devices improves. Consequently, the overall performance of a millimeter wave weighting circuit should be about the same or possibly better than the X-band device.

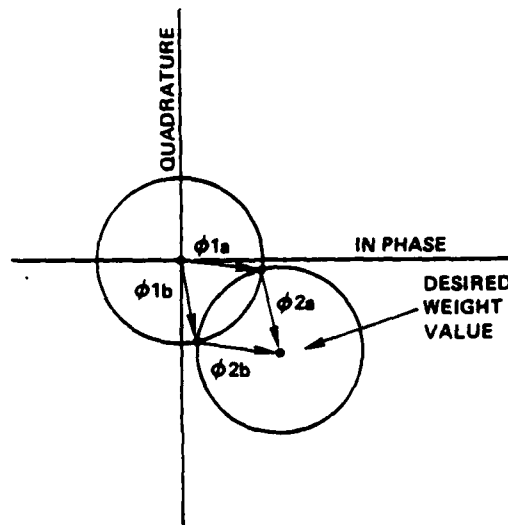
A circuit diagram and a phasor diagram of the "Paired Phase Shifter Weight" are given in Figure 6.4-1. Part (a) of the figure shows an input to be weighted being fed through a power dividing hybrid. This divided signal is then routed to two different phase shifters ϕ_1 and ϕ_2 . Control lines lead to these phase shifters, the voltage of which determines phase shift. Thus the phase shifted signals are combined in a second hybrid to provide the weighted output.

The phasor diagram given in Part (b) of the figure illustrates how the paired phase shifter weight works. A point has been selected in the fourth quadrant of the complex plane as the desired weight value. Inspection of the diagram shows that either $\phi_{1a} + \phi_{2a}$ or that $\phi_{1b} + \phi_{2b}$ can achieve this value. The circles are unity amplitude and represent the locus of points achievable by the two phase shifters, respectively. One circle is drawn at the origin of the diagram and the second is drawn at the desired weight value. Therefore, the intersections of these two circles determined the pair of phase shifter values which will give the required complex

weight. Inspection of this diagram will also reveal that the maximum allowed weight value is obtained when the phase circles just touch. This, of course, is a sum of two but when it is recognized that the input power was divided by two, the input/output attenuation assuming no loss in the hybrids or phase shifters is 0 dB.



(a) BLOCK DIAGRAM

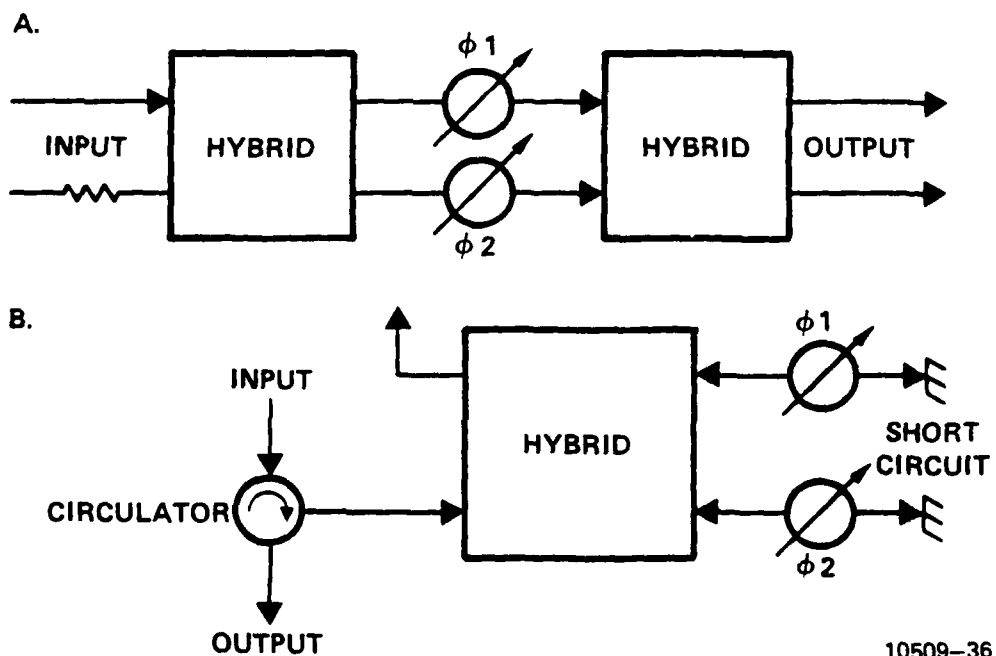


(b) PHASOR DIAGRAM

10191-18

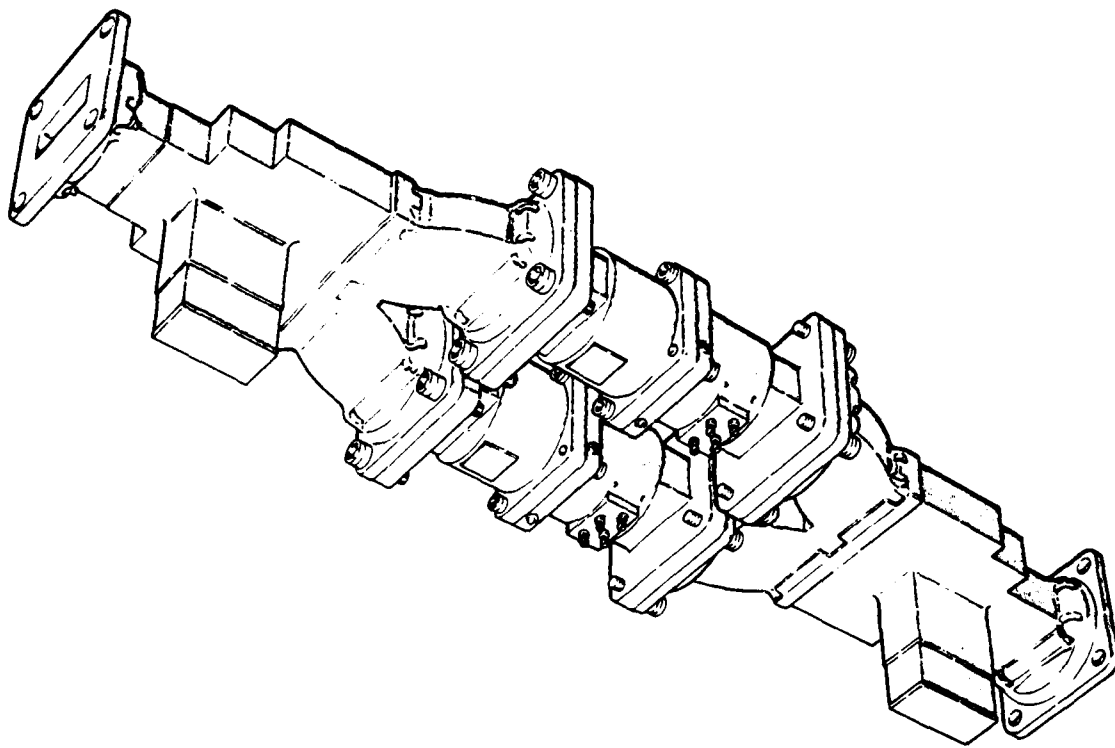
Figure 6.4-1. Dual Phase Shifter Complex Weight

Schematic realization of the dual phase shifter weighing approach are shown in Figure 6.4-2. For microwave frequencies, the hybrid is realized as a magic T. The phase shifters are very low-loss ferrite devices (0.2 dB) which, because of their particular design, are also rather insensitive to temperature variations. The configuration shown in Part A for the figure has been realized in a breadboard form using ferrite phase shifters supplied by Microwave Associates Group using our basic design. A photograph of the complete weighting device is given in Figure 6.4-3. Note that an important property of this weighting scheme is that input power which is not used in the weighting process is available at the difference port of the output hybrid. Consequently, for broader bandwidth weighting approaches, this unused output power can be subsequently weighted itself and combined as needed.



10509-36

Figure 6.4-2. RF Weight Implementations

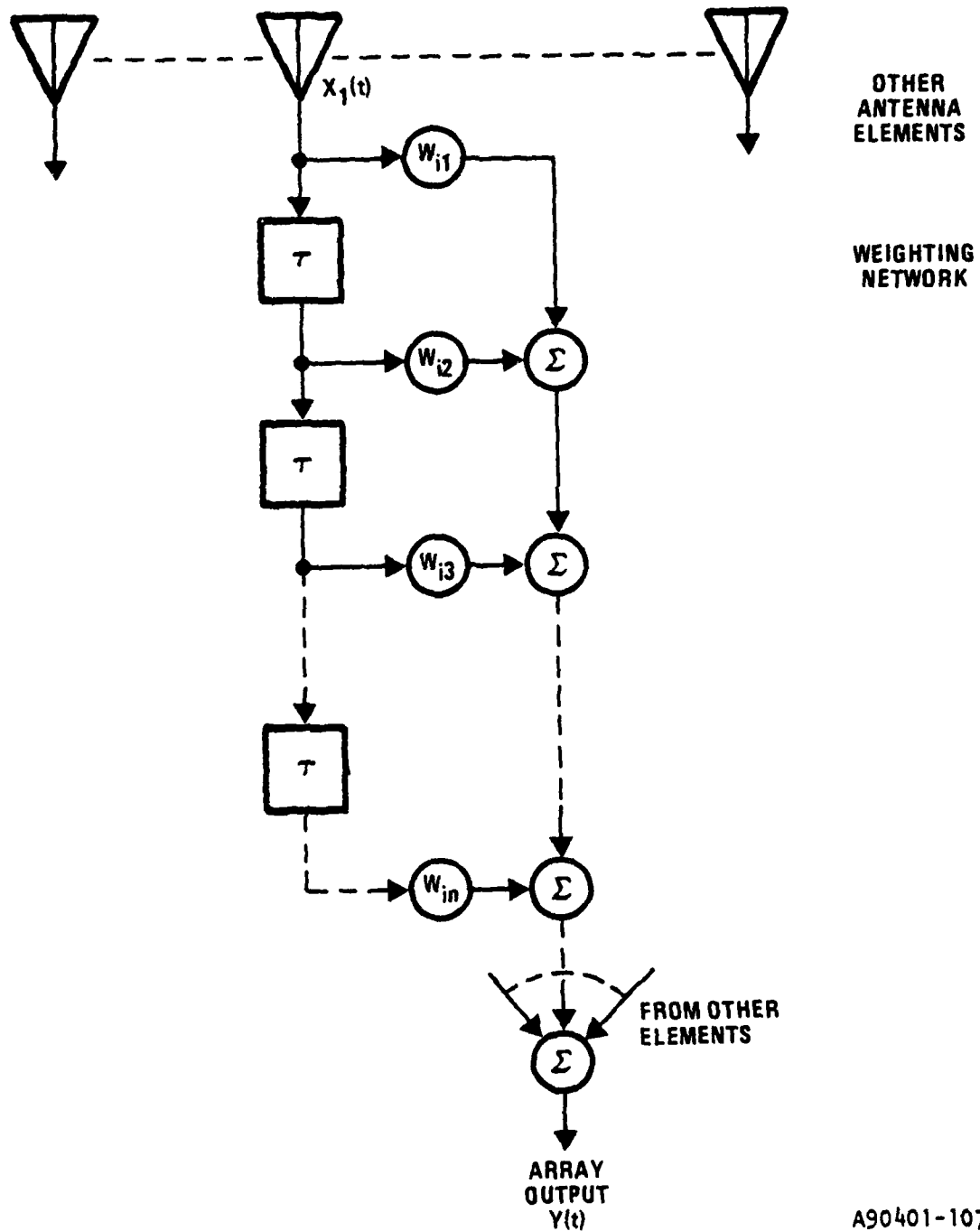


AP0481-26

Figure 6.4-3. Low Loss Dual Phase Shifter RF Weight

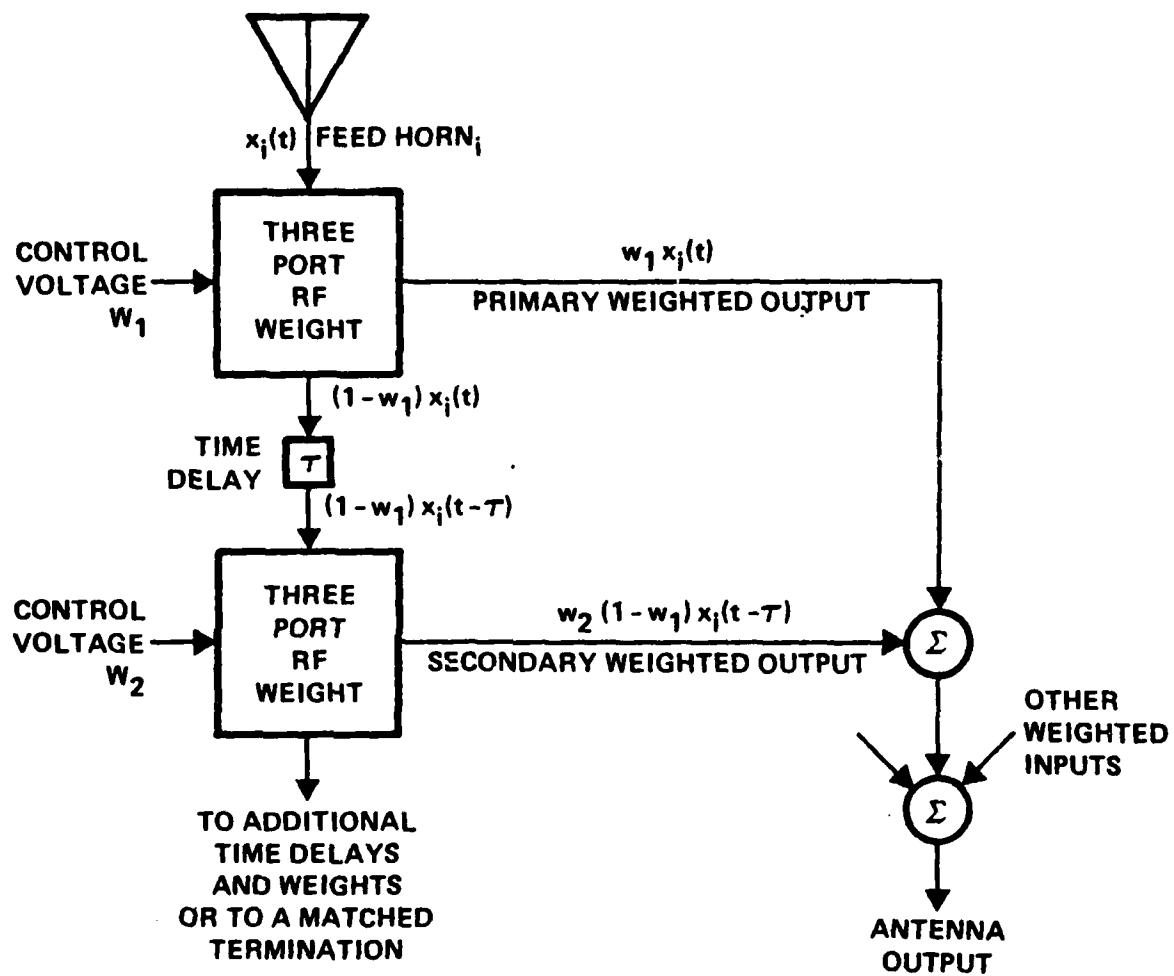
An alternative equivalent weight implementation is shown in Part B of Figure 6.4-2. RF signals from the feed are inputted to the circulator which then delivers power to the hybrid and phase shifter combination. Depending upon settings of the phase shifters which are working into a short circuit, some of the incident energy will be reflected to the circulator while other parts of the incident energy will appear at the difference port of the hybrid. Power reflected to the circulator appears in the circulator's output and is the desired RF weighted output. As in the earlier circuit, power available from the difference hybrid can be time delayed and additionally weighted if broader bandwidth nulling capability is desired.

In applications where the number of horns is limited, it is desirable to obtain broader bandwidth nulls by utilizing a multitapped, weighted delay line circuit. This is the conventional approach to obtaining an arbitrarily dispersed and weighted waveform. Essentially, voltages present at the taps of a multiply tapped delay line are weighted and summed. This circuit is diagrammed in Figure 6.4-4. It is essentially unrealizable in the case of RF weightings. In effect a zero impedance output from the antenna element is assumed. Each of the taps, therefore, provides a voltage sample of the appropriately delayed input. In a real circuit operated at RF frequency, power division would be necessary and substantial losses would result. For example, those weights having small or near zero values would effectively waste the power available at that port. In order for such a scheme to work effectively, large amounts of low noise amplification would have to be provided for each antenna element input. Alternatively, the new RF weighting scheme helps to minimize the problems associated with this broadband combining network. Basically, the taps and weights on the ideal combining circuit have been replaced with a cascade of the three-port weight shown in Figure 6.4-2, Part A. A block diagram of the modified combining network is shown in Figure 6.4-5. RF power from the feed, labelled here as $X_i(t)$, is delivered to a three port RF weight. The primary output of this weight is $W_1 X_i(t)$, given a control voltage input to the weight of W_1 . Unused power from this first weight is then



A90401-107

Figure 6.4-4. Multitap Time Delay Weighting Network



10509-37

Figure 6.4-5. Realizable Low Loss Combining Network Using Three Port Dual Phase Shifter Weights

time-delayed and delivered to a second three-port weight. This power is also time delayed so as to provide the necessary parallel with the ideal broadband weighting circuit shown earlier in Figure 6.4-4. After the second control voltage W_2 is applied, the secondary weighted output is $W_2(1-W_1) x_i (t-\tau)$.

As can be seen from the figure, a potential drawback of this approach is that the RF power available at progressive delayed taps is reduced by an amount proportional to the weights of the preceding stages. This means that input signal cross correlation matrices will be a function of the weights, resulting in a nonlinear control algorithm unless some form of compensation can be used within the algorithm itself. A possible approach in this regard is to make the individual loop gains of a weighting circuit proportional to the inverse of the coefficient of the delayed waveform. Regardless, this approach is considered to have some merit in that it avoids the use of RF amplification.

6.5 Conclusions

An alternative to the customary sidelobe canceller has been introduced and described in the preceding sections. The reflector feed null steering concept is capable of providing broadband nulls, including nulling within the main lobe; about three orders of magnitude greater null depth bandwidth product performance is obtained compared with the customary sidelobe canceller. Additionally, the reflector feed adaptive approach avoids the necessity of auxiliary elements which are often located around the periphery of the principal reflector.

A primary disadvantage of the reflector feed adaptive approach is the fact that the number of degrees of freedom (hence, independent jammer sources that can be nulled) is limited by the number of feed elements. In new designs, this does not present a particular problem; however, in modification of existing installations, one is probably limited to three or four degrees of freedom.

When the reflector feed adaptive RF circuitry is coupled with a digital controller which obtains performance information from the system receiver intermediate frequency output, a very cost effective and computationally powerful algorithm can be realized. Using such a hybrid analog-digital approach, an existing unprotected reflector antenna could be converted to a fully adaptive antenna system by the addition of a digital controller, RF weights and interface circuitry, a very minimal modification.

Except for a low loss RF weight which has been designed, constructed and tested, the remainder of the reflector feed adaptive null steering approach has been simulated on general purpose computers. On the basis of the promising simulation results obtained, the technology should be further advanced. It is suggested that a specific system design be formulated and in a following phase constructed and tested. Important steps in this process would be:

- Feed Design. A reflector feed specifically meeting the requirements of a particular millimeter wave communication link would be designed. This design would take into account the jammer threat expected as well as desired signal gain.
- Simulations/Performance Predictions. The feed design established in the first task would be examined using the simulation computer programs with the result being curves of expected performance of the design against the postulated jammer threats. Weaknesses in the initial design would be corrected in this phase. Additionally, performance predictions established will be useful for later comparison with actual test results.

- Millimeter Wave Weight Design. A critical component in the reflector feed null steering concept is the RF weighting device used in the feed combining networks. A low loss high performance millimeter wave weighting device would be designed using the approach taken earlier in the design and construction of the X-band weight for the IR&D program.

Given completion of the above tasks, the paper design of a specific system could be accomplished. A logical further development step would then be the construction and testing of breadboard hardware to prove the design approach. Suggested tasks in this development are:

- Detailed Hardware Design. Block diagram level paper designs from the previous effort would be expanded to a component level. Critical parts would be ordered.
- Construction. Assembly of the various components into a breadboard test setup would be accomplished in this phase.
- Test and Comparison. Testing of the reflector feed nulling concept would proceed with conditions being established in the experiment similar to those postulated in the original system design problem. Null depth and rate of adaptation would be measured and compared with simulation results also produced in the first design phase.

At the completion of these activities, the adaptive reflector feed null steering concept would be proven and ready for use as required in communications links using reflector antennas at millimeter wave frequencies.

7.0 SYSTEM ARCHITECTURAL STUDIES

7.1 System Link Budget Considerations

In this section a typical set of link allocations for a millimeter wave radio frequency link is presented. Link budget curves are given which account for most of the components of propagation loss (e.g., free-space path loss, rainfall absorption, and atmospheric multipath) in the MWAR system link. Selection of the remaining system parameters (some of which may be variable) allows one to then determine the terminal separation distance at which link closure may be achieved.

Link Analysis

A simple model for a millimeter wave transmission system is illustrated below in Figure 7.1-1.

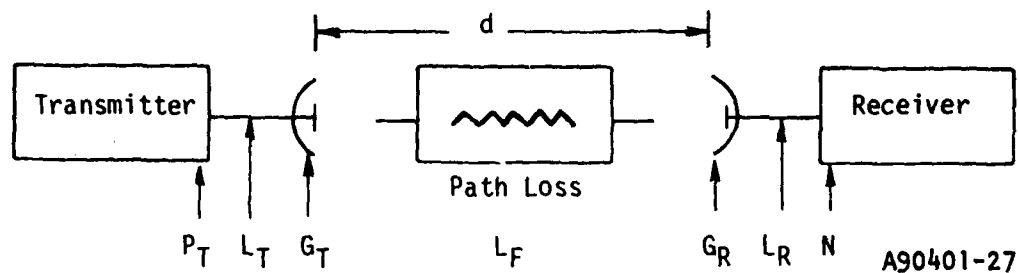


Figure 7.1-1. Millimeter Wave Link Model

The symbols in Figure 7.1-1 are defined as follows:

P_T = transmitter power

L_T = transmitter feed loss

G_T = transmitter antenna gain

L_F = free-space transmission loss

G_R = receiver antenna gain

L_R = receiver feed loss

N = receiver noise threshold

d = link separation distance

The objective of this link analysis is to investigate how the key system parameters vary in the MWAR link. In an effort to produce some meaningful curves, some of the very slowly varying parameters will be assigned fixed values. In order to keep the allocation relatively simple, the following link entries are selected:

- Transmitter power (P_T)
- Transmitter feed loss (L_T)
- Transmitter antenna gain (G_T)
- Free-space path loss (L_F)
- Multipath and scintillation (M)

- Rainfall loss (L_{RF})
- Atmospheric absorption loss (L_A)
- Receiver antenna gain (G_R)
- Receiver feed loss (L_R)
- Noise density (kT_0)
- IF bandwidth (B)
- Implementation loss (L_I)
- Noise figure (NF)

The carrier signal level in dB, C , at the receiver input (before further processing) is given by

$$C = P_T + L_T + G_T + L_F + M + L_{RF} + L_A + G_R + L_R$$

By convention all loss terms will be taken as negative.

The receiver noise threshold in dB, N , is given by

$$N = kT_0 + B + L_I + NF$$

For our purposes we define link closure as the condition that

$$C \geq N$$

To be useful the carrier signal level must satisfy the condition

$$C - N \geq E_b/N_0 | \text{required}$$

This fact must be kept in mind when interpreting the link budget results presented later in this section.

First, the free-space path loss is plotted in Figures 7.1-2 through 7.1-4 using the familiar equation

$$L_F = 32.5 + 20 \log_{10} f + 20 \log_{10} d \text{ dB}$$

Where f is the transmission frequency (MHz), and d is the hop or path length (km). Most of the signal multipath at these frequencies is a consequence of scintillation fading in the troposphere. (Scintillation refers to the random amplitude and phase fluctuations of the signal.) The multipath curves plotted in Figures 7.1-2 through 7.1-4 result from data found in Lane¹. Rainfall attenuation is computed by knowing the dependence of path average rainfall rates on the "effective rainbearing distance" and the required link availability^{2,3}. These curves are based on a total annual rainfall of 1 m in a continental temperate climate (typical, e.g., of the Federal Republic of Germany) and are utilized to produce rainfall attenuation curves as illustrated in the figures. The sum $L_F = M + L_{RF} + L_A$ is then plotted as three curves in Figures 7.1-2 through 7.1-4. Thus, we have curves of propagation loss ($L_R + M + L_{RF} + L_A$) plotted versus terminal separation distance for link availabilities of 99, 99.9, and 99.99 percent (percentage of time for link closure).

¹J. A. Lane, "Scintillation and Absorption Fading on Line-of-Sight Links at 35 and 100 GHz," IEE Conference on Tropospheric Scatter Propagation, London, October 1968.

²P. L. Rice, A. G. Longley, K. A. Norton, and A. P. Barsis, "Transmission Loss Prediction for Tropospheric Communication Circuits," NBS Tech. Note 101, Vol. I, ITSA, revised January 1967.

³J. W. Reid, Jr., "A Tropospheric Propagation Model for Ground/Ground Low Elevation Angle LOS Systems," HESD Tech. Rpt. 9331-77-001, May 1977.

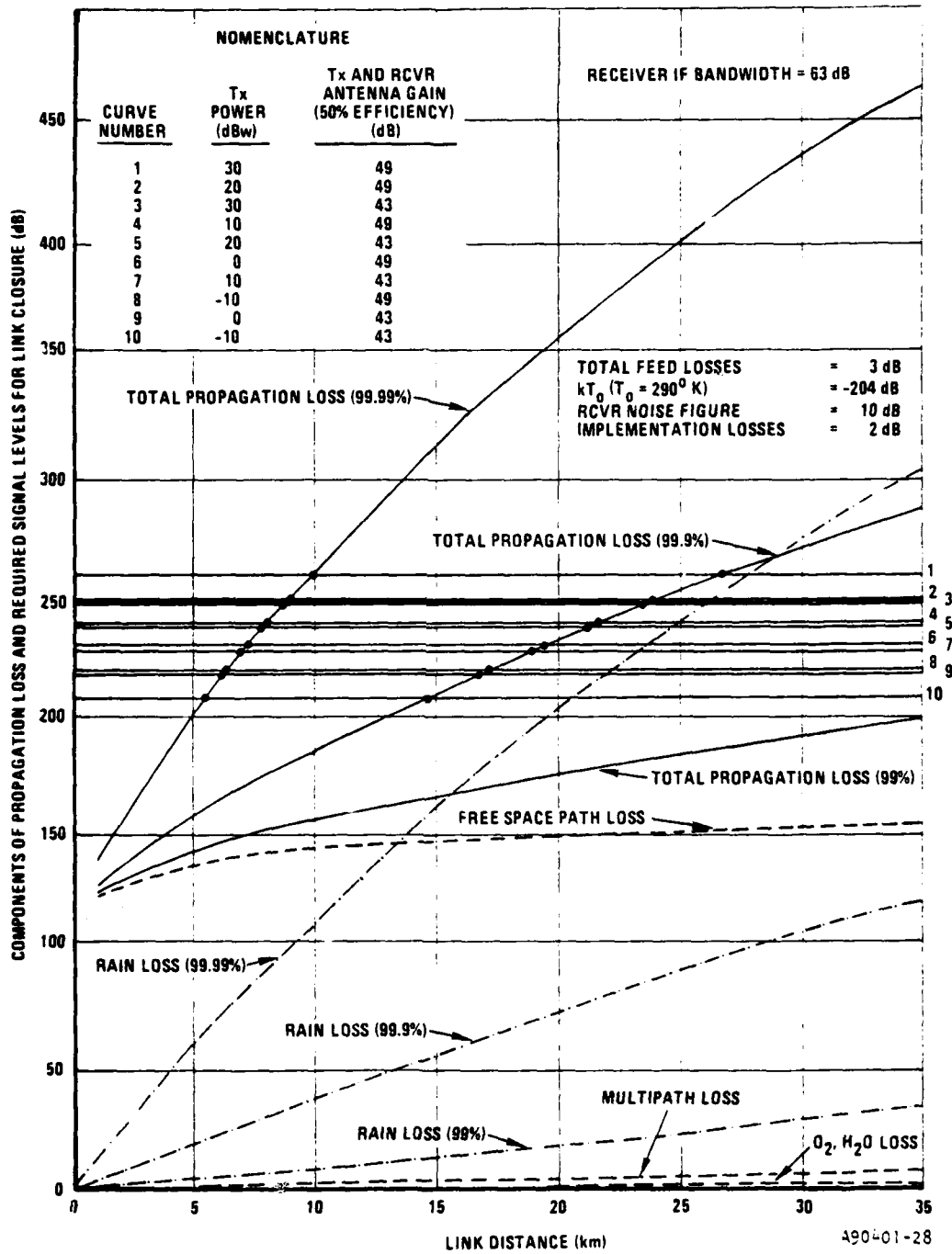


Figure 7.1-2. MWAR Study Link Curves - Receiver IF BW = 63 dB

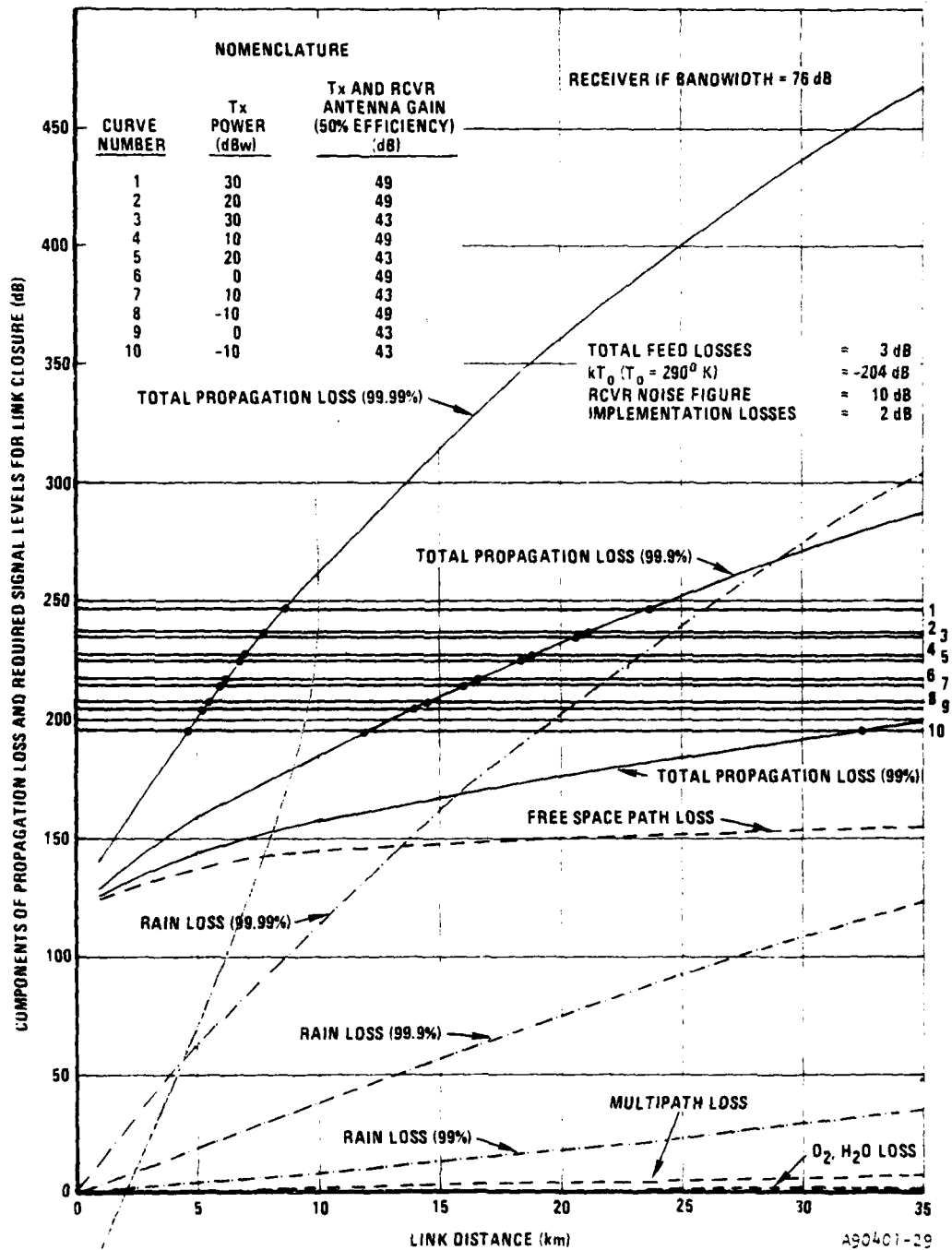


Figure 7.1-3. MWAR Study Link Curves - Receiver IF BN = 76 dB

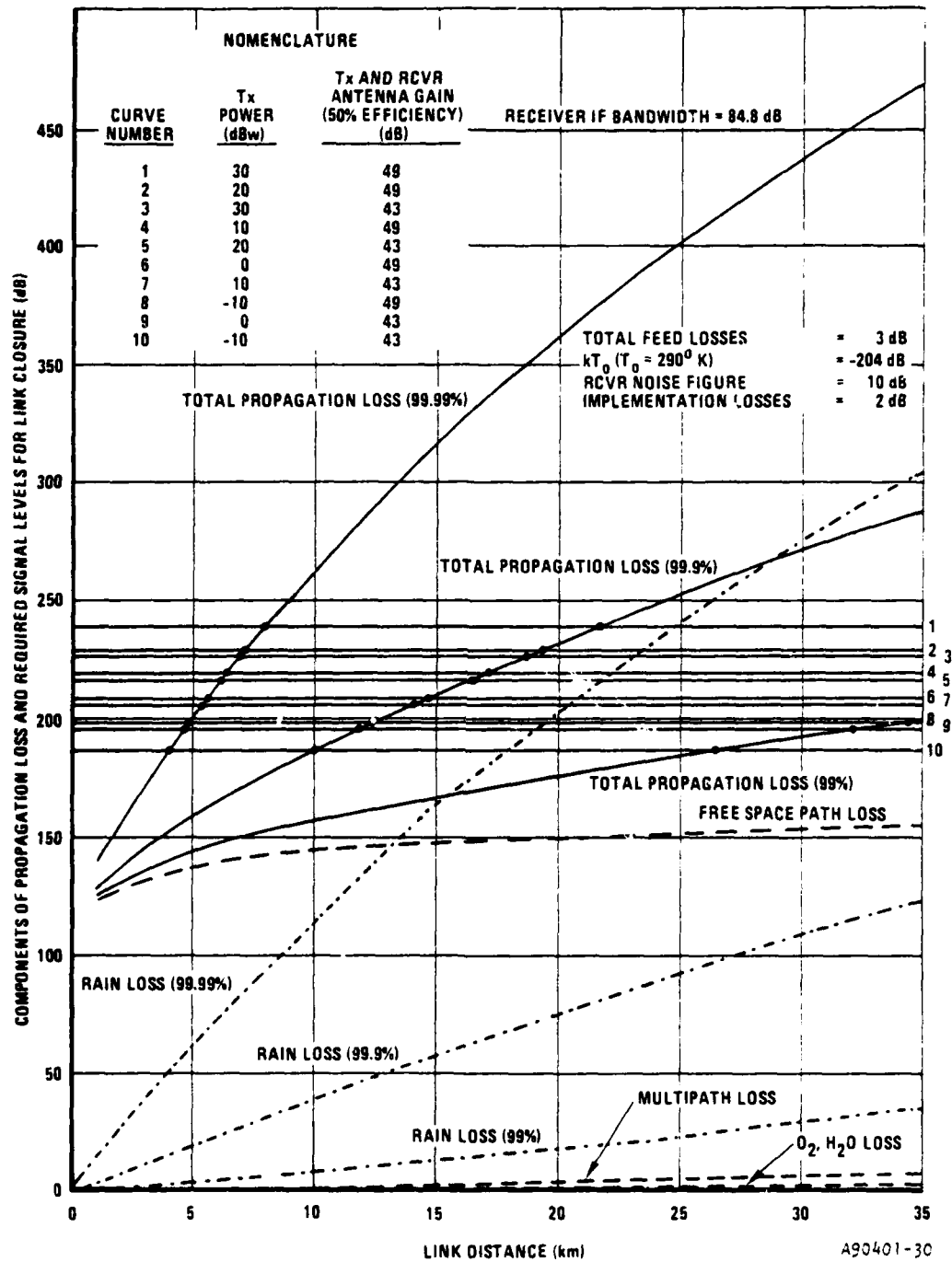


Figure 7.1-4. MWAR Study Link Curves - Receiver IF BW = 84.8 dB

Next we set the system parameters exhibiting least variation as fixed values:

$$L_T = 1.5 \text{ dB} \quad K T_o = -204.0 \text{ dBw} \quad (T_o = 290^{\circ}\text{K})$$

$$L_R = 1.5 \text{ dB} \quad \text{NF} = 10.0 \text{ dB}$$

$$L_I = 2.0 \text{ dB}$$

The above values represent reasonable values in a practical millimeter wave system.

In Figures 7.1-2 through 7.1-4, the following combination of transmitter power and antenna gains is considered (Table 7.1-1):

Table 7.1-1. Transmitter Power and Antenna Gains

Transmitter Power (dBw)	Transmitter and Receiver Antenna Gains (dB)
-10	43
-10	49
0	43
0	49
10	43
10	49
20	43
20	49
30	43
30	49

When the antenna efficiency is 50%, a 0.5 m diameter antenna yields 43 dB gain, whereas a 1 m diameter antenna yields 49 dB gain.

All that remains is to consider the receiver IF bandwidth. In a "first-cut" effort to minimize bit-error rate (BER), the receiver IF bandwidth is selected to be twice the bit-rate bandwidth. Hence, the bandwidth B becomes 63 dB, 76 dB, and 84.8 dB when the bit rate is 1, 20 and 150 Mb/s, respectively. Figures 7.1-2, 7.1-3, and 7.1-4 correspond to transmission rates of 1, 20, and 150 Mb/s.

Hence, for a given link availability, the signal level at the receiver input just balances the receiver noise threshold when the horizontal lines cross the total propagation loss curves. This means that to achieve link closure (as defined previously), one must operate at terminal separation distances less than or equal to the distance at which the curves intersect (denoted by large points on the figures).

Link Allocations

The link allocation of Table 7.1-2 is applicable for a 30 km link with 99 percent propagation availability.

7.2 Alternate Routing Technique for DCS

The purpose of this task element of the study program is to develop a recommended architecture which effectively uses millimeter waves as an alternate routing technique for the DSC System. This recommended architecture will be based upon consideration of:

- a. The effects of rain on the transmission
- b. Antijam techniques against various jammer types

Table 7.1-2. Link Allocation

System Parameter	Budget	Comments
Transmitter Power	10.0 dBw	-
Transmitter Feed	-1.5 dB	-
Transmitter Antenna	43.0 dB	0.5 m diameter dish, 50% efficiency at 38 GHz
Free Space Path Loss	-153.6 dB	30 km link at 38 GHz
Atmospheric Absorption	-1.0 dB	30 km link
Rainfall Attenuation	-30.0 dB	30 km link, 99% availability
Atmospheric Multipath	-7.0 dB	30 km link
Receiver Antenna	43.0 dB	0.5m diameter dish, 50% efficiency at 38 GHz
Receiver Feed	-1.5 dB	-
Subtotal	98.6 dBw	-
Receiver Noise Density	-204.0 dBw	kT_0 with $T_0 = 290^{\circ}K$
Noise Figure	10.0 dB	-
Implementation Loss	2.0 dB	-
IF Bandwidth	84.8 dB	150 Mb/s; IF BW = 2 X BR BW
Noise Threshold	-107.2 dBw	-
Link Margin	8.6 dB	-

- c. Multiple path diversity to counter rain and other climatic conditions
- d. Multiple path diversity to counter jamming. An information rate of 25.856 Mb/s will be used as a basis for any DCS node in arriving at the recommended configuration.

7.2.1 DCS

In assessing the effectiveness of using millimeter waves for alternate routing on the DCS one must first have some knowledge of this system. Shown in Figure 7.2.1-1 is a typical nodal topology for the DCS Digital European Backbone (DEB) multiplex system with the number of miles between stations. Note that the nodes form patterns that represent the architectures of point-to-point, hub and wheel, and bidirectional ring.

Figure 7.2.1-2 is also a European area multiplex configuration. As before, the number of miles between stations is shown. Note that in this figure the station configuration around Stein is of the hub and wheel type and that the route from Schoenfeld to Cold Blow is the single node point-to-point type.

Not only is the European area a candidate for alternate routing techniques but so also is the Pacific connectivity, particularly Korea, shown in Figure 7.2.1-3; Japan, shown in Figure 7.2.1-4; and Hawaii, shown in Figure 7.2.1-5.

Each of the European and Pacific regions has areas where there are many bases closely located where the potential for frequency congestion is very high, thus requiring close repeater spacing. The architecture not only necessitates topological analysis as has been discussed, but also the investigation of hardware architecture.

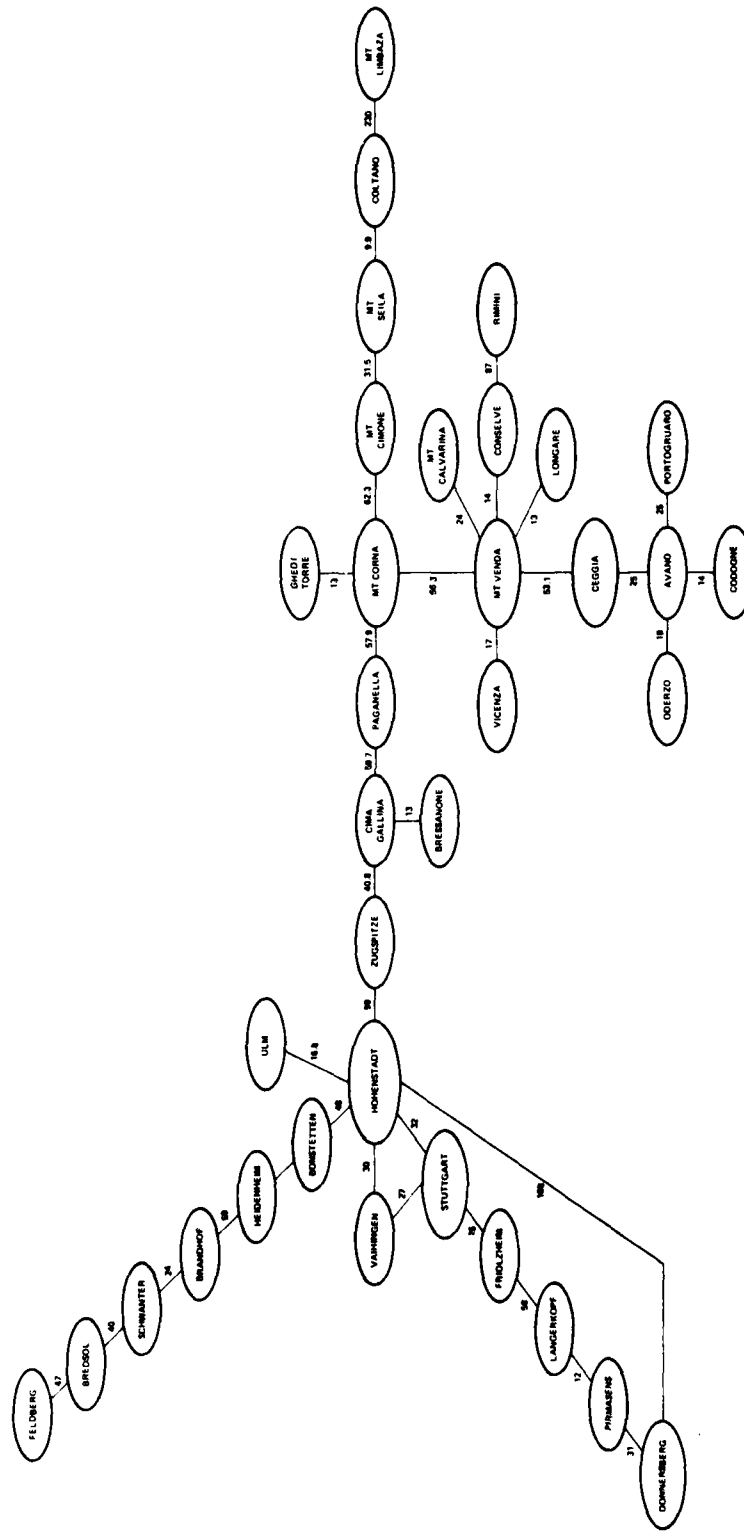
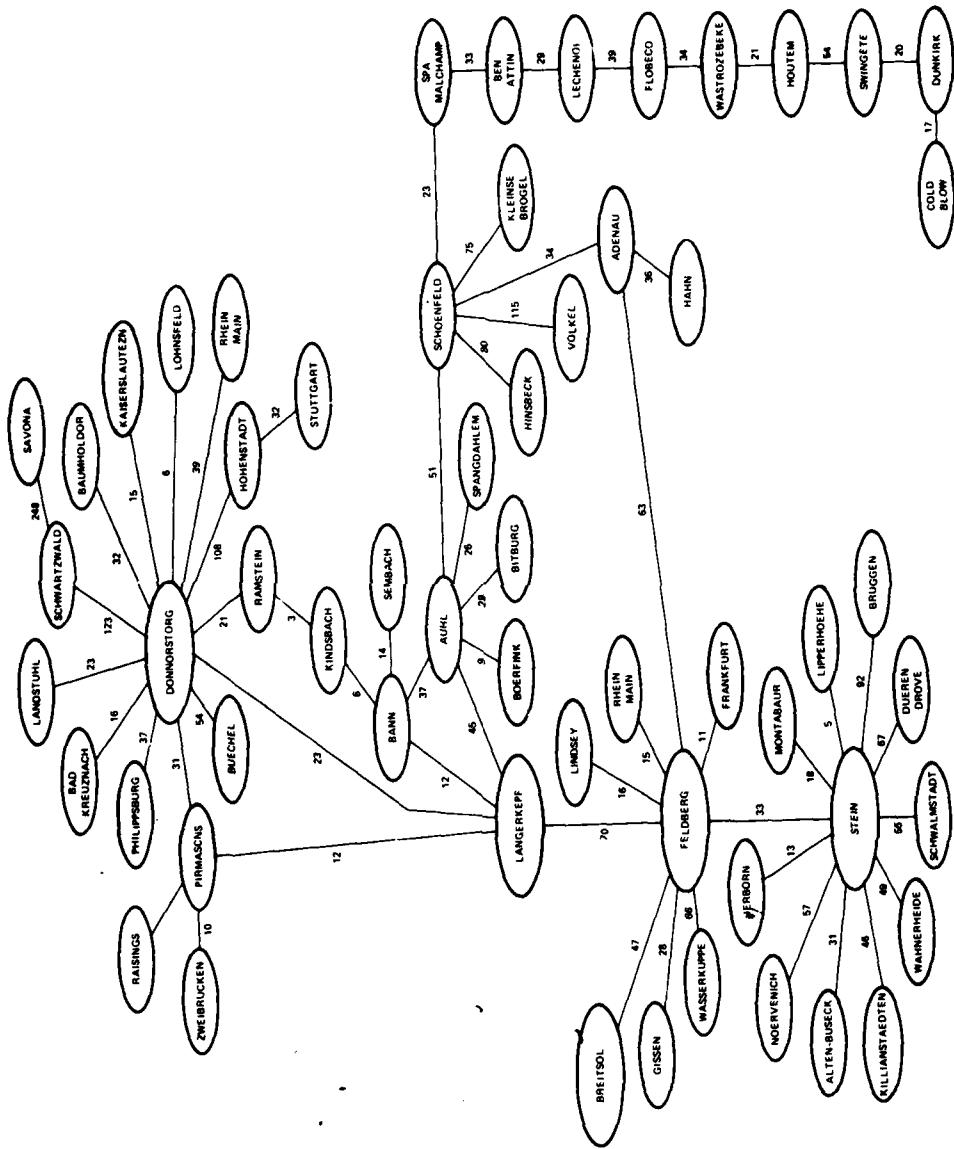
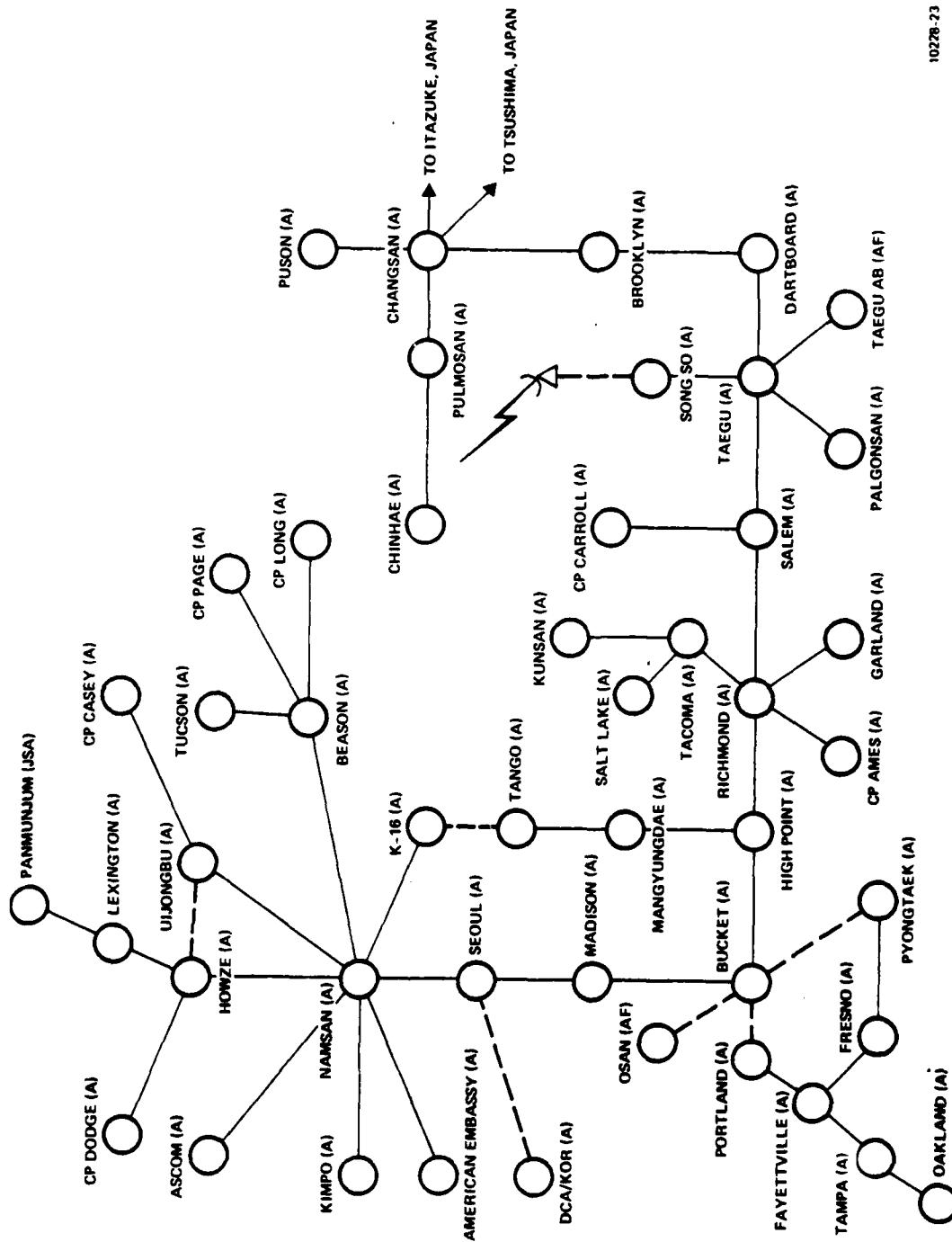


Figure 7.2.1-1. Typical Digital European Backbone (DEB) Multiplex Configuration



1074

Figure 7.2.1-2. Typical DCS Multiplex Configuration European Area



10278-23

Figure 7.2.1-3. Korea DCS Configuration

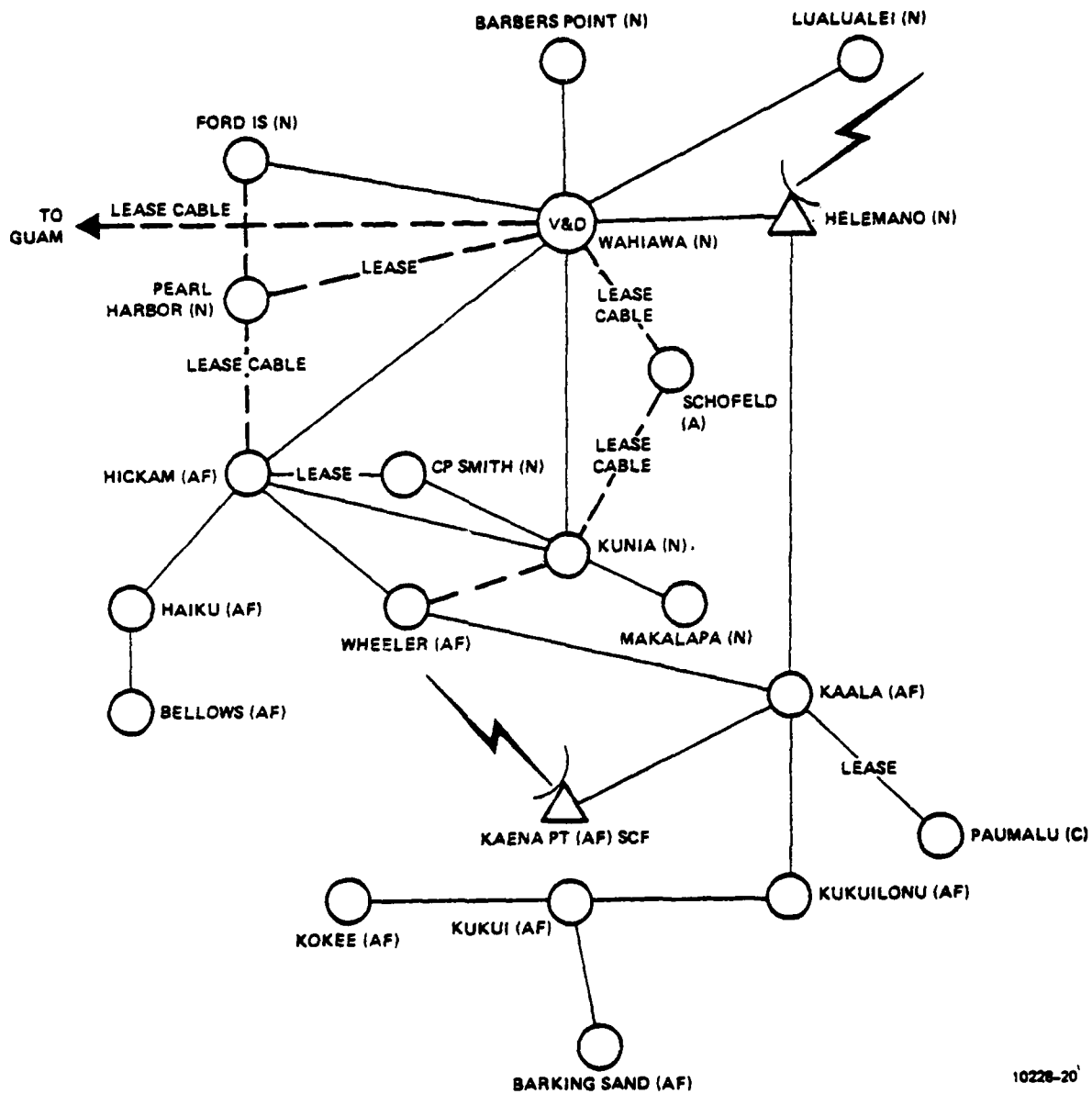


Figure 7.2.1-5. Hawaii DCS Configuration

7.2.2 Millimeter Wave Alternate Routing to Counteract Rain Effects

Based upon the analysis of millimeter wave (MMW) rain effects discussed in Section 2.0, it can be concluded that the MMW communications is suitable for short distance (less than 30 km) tactical application with or without alternate routing, and 99.9% availability is achievable at reasonable system margin. For the DCS digital transmission network some links between two nodes are much greater than 30 km; then the alternate routing approach (AR) and repeater have to be considered in the system design. From counteracting rain-effects viewpoint, the communication satellite functioning as a repeater is more efficient than the terrestrial repeater, particularly for a great coverage area. Also, various system architectures may be helpful to establish adequate routing for DCS at different geographical regions.

7.2.3 Millimeter Wave Link Architectures

Both hardware alternate route architecture (ARA) and topological alternate route architecture are feasible for DCS digital network. Hardware ARA has the following approaches some of which are discussed in Section 4.0:

- a. Power Level Diversity
 - Antenna of variable gain
 - Adaptive transmitter (Tx) power
 - AGC in receiver (Rx)
 - Combination of adaptive Tx and Rx
- b. Space Diversity
 - Use of alternate paths

c. Time Diversity

Information storage for later transmission

d. Frequency Diversity

- MMW only
- MMW and Microwave (Mw)
- MMW and Fiber Optics (FO)
- MMW - MW - FO

Power Diversity at MMW frequencies is straightforward; no further discussion is given here.

The specified DCS nodal information rate of 25.856 Mb/s is assumed to be composed of a multiplex of two mission bit streams (MBS). The essential components of the terminal for a typical space diversity configuration are shown in Figure 7.2.3-1. The upper portion of the diagram depicts a multiplexer, modulator, upconverter, and antenna operating at 8 GHz. A second chain provides the capability to record data over a different path thus providing space diversity. For a millimeter wave architecture with AJ capability one could connect a modem and up/downconverters between the video and rf switches to provide both space and frequency diversity. The modem by itself could provide AJ with the 8 GHz antenna. Further protection resulting from the narrow beamwidth and higher gain of the millimeter wave system could be incorporated by adding another up/downconverter for 8 GHz/38 GHz operation. Two such chains would provide path diversity at millimeter waves for enhanced alternate routing. Other architectural schemes are feasible including the use of a single feed in the 6-foot, 8-foot, 10-foot diameter antennas that would allow operation

at both 8 GHz and 38 GHz. This approach not only can counteract rain induced outage but also provide the hardware redundancy particularly attractive to the link. Unfortunately, it loses the advantage of high transportability of MMW equipment.

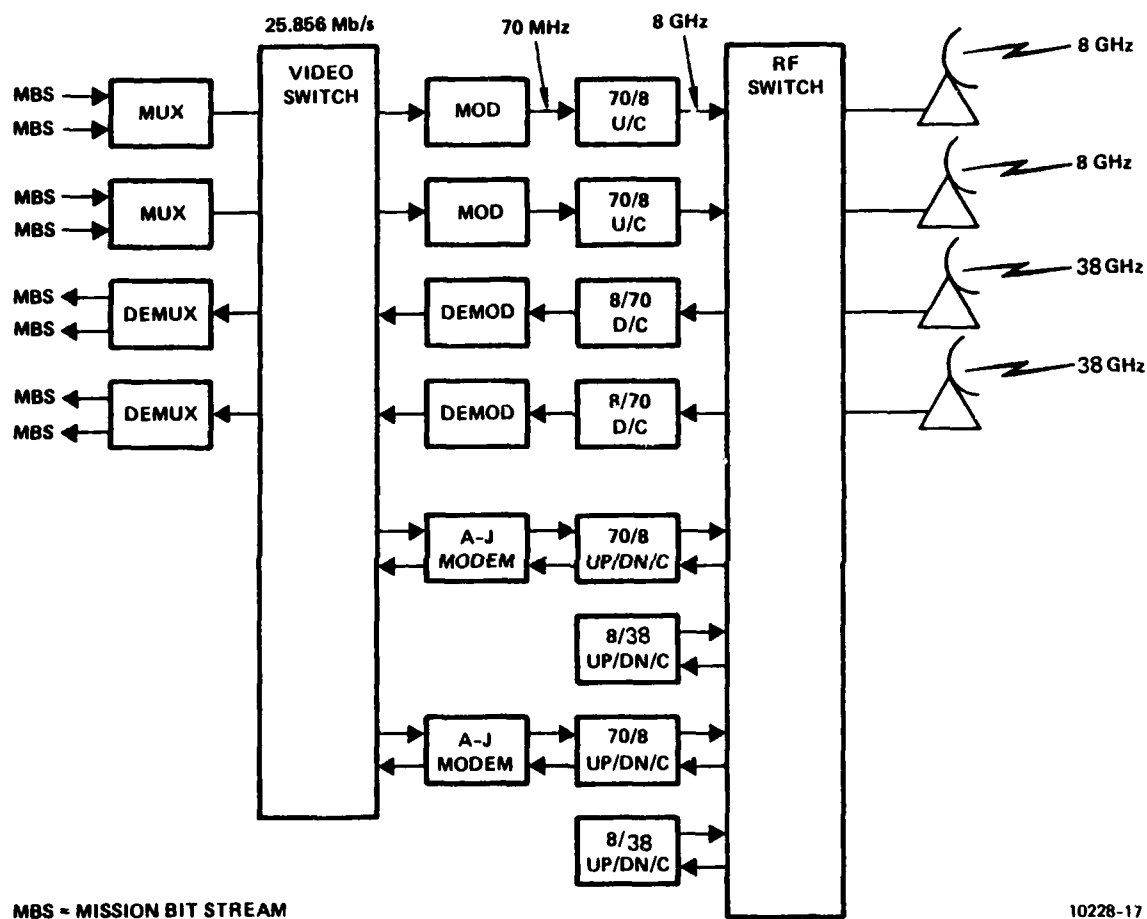
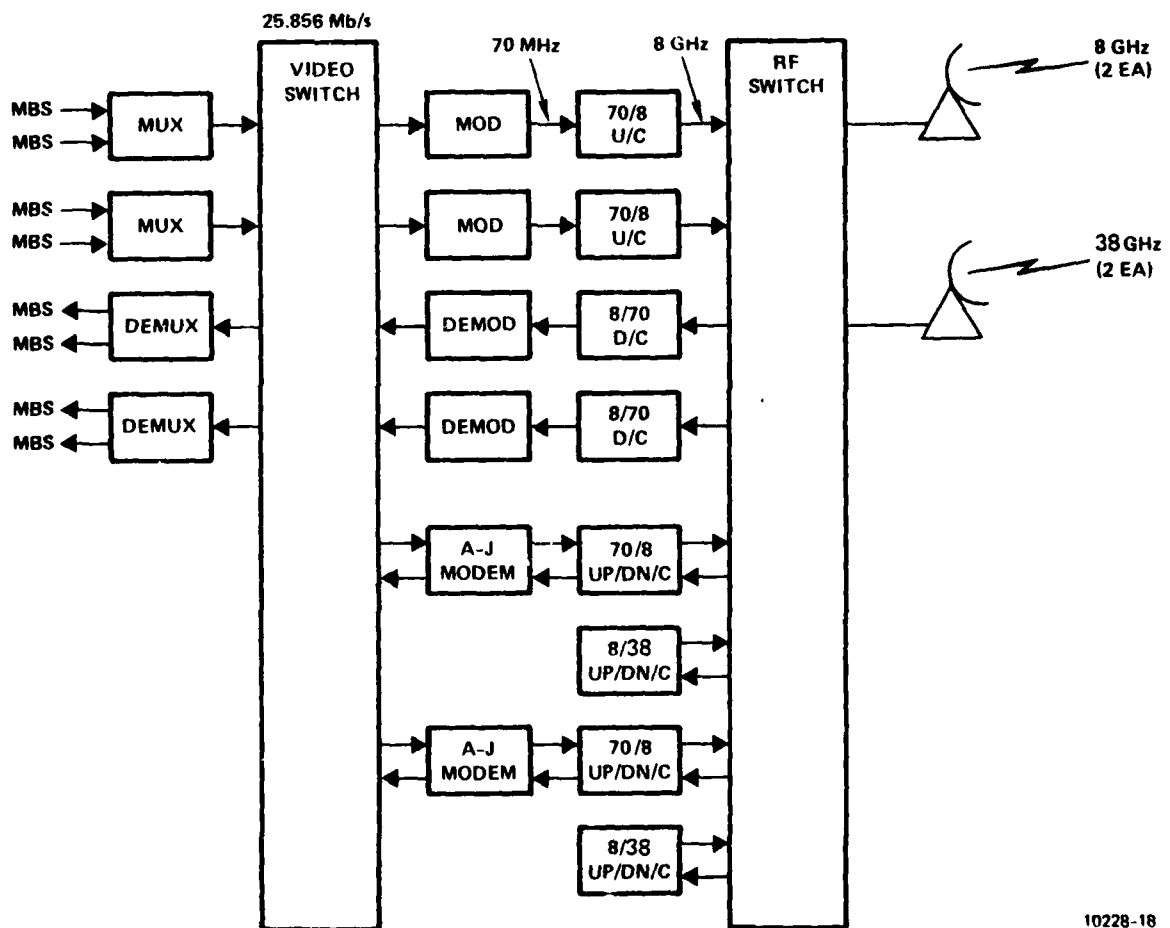


Figure 7.2.3-1. Typical Space Diversity Terminal with Frequency Diversity Capability

Time diversity using temporary storage is the most economical ARA. However, it depends on the system requirement whether it can accept the non-real-time information transfer. For the multi-Megabit/sec rate of interest here the required storage is not feasible.

A fourth type of architecture is envisioned for a terminal that presently employs frequency diversity. As shown in Figure 7.2.3-2 a single antenna operating at 8 GHz (actually 7.125 GHz - 8.4 GHz) is connected to the two chains of transmitters and receivers. As for the space diversity architecture the addition of A-J modems with the appropriate up/downconverters and 38 GHz antenna represents a millimeter wave architecture that can provide alternate routing for the DCS system.



10228-18

Figure 7.2.3-2. Typical Frequency Diversity Terminal

The topological MMW ARA is dependent upon the terminal cities and local distributions. Generally, it can divide as the following categories:

- Point-to-point
- Hub on wheel
- Star
- Bidirectional ring
- Combination of the above schemes
- Earth-satellite

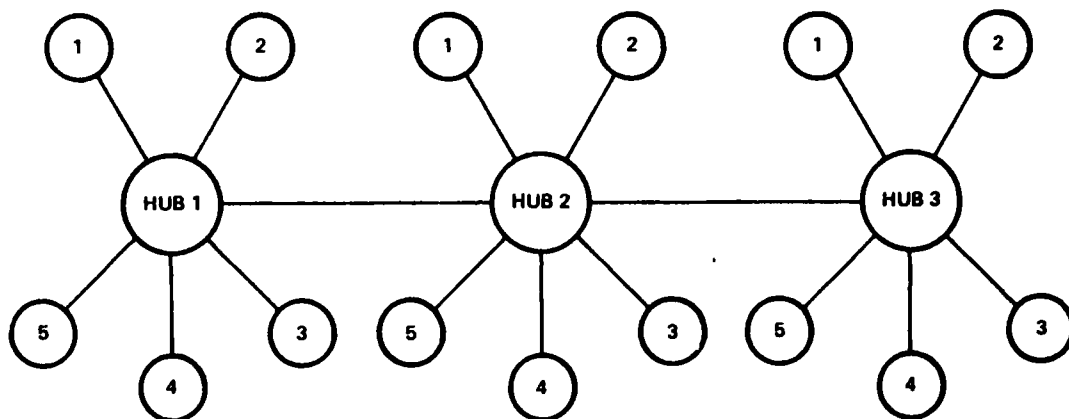
A single node point-to-point system as shown in Figure 7.2.3-3 is the most vulnerable to jamming. In this type message system, communications from Station A to Station F are routed serially through Stations B, C, D, and E. The message is vulnerable to jamming at any one of the six stations (i.e., at the transmitter, receiver, or any other station in the serial chain). Reductions in susceptibility to jamming and rain effects can be realized by increasing the path diversity or network switch diversity.



10228-11

Figure 7.2.3-3. Single Node Point-To-Point Path

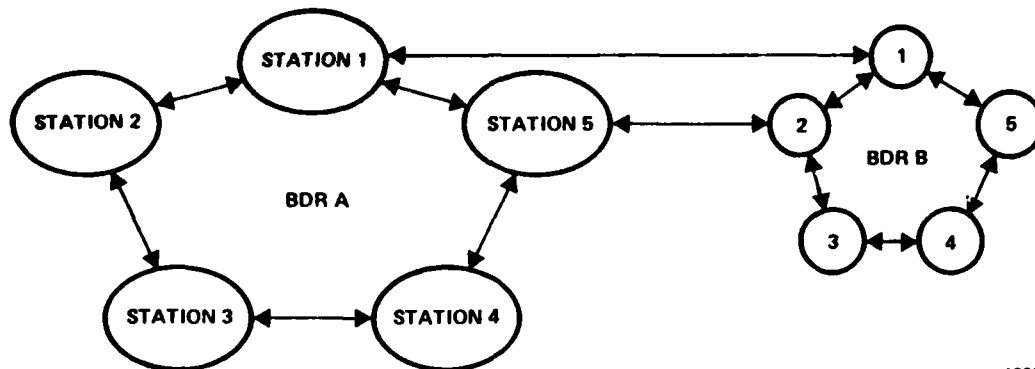
Figure 7.2.3-4 depicts a hub and wheel architecture in which the primary stations on the main trunk act as hubs for the secondary stations that form wheels. Messages are collected at the hub for all the stations of a wheel and then routed to other hub stations. This configuration suffers from the same deficiencies as the single node point-to-point system in that the hubs act as a serial chain which allows the message to be jammed at any hub station. Reduced message susceptibility to jamming would result if the hubs were connected as bidirectional ring architecture.



10228-13

Figure 7.2.3-4. Hub and Wheel Architecture

The star architecture is morphologically similar to the hub configuration, and earth-satellite links may be considered as this family. On the bidirectional ring network architecture, as illustrated in Figure 7.2.3-5, each station is connected to two other stations by two full duplex links. The total connection is such that a loop is formed containing all stations, thus providing a connection between any two stations in two different directions. The actual geography is an important parameter in determining the feasibility of any configuration.



10228-12

Figure 7.2.3-5. Bidirectional Ring Architecture

The data routing is such that each station sends messages in both directions on the bidirectional ring (BDR). When one station receives a message from another station it determines whether the message has been previously received in the opposite direction and if it has then discards the message. Otherwise, the message is forwarded to the adjacent station in the ring. This procedure allows all messages to proceed in both directions on the BDR and to be discarded when duplicates cross. In order to increase throughput, major trunks connect adjacent BDR's at two locations. Message routing is accomplished using package format and the appropriate communications protocol.

The comparison of these various topological MMW ARA is given in Table 7.2.3. Note the high jamming vulnerability of satellite systems: this is due to the fact that a single successful, uplink jammer renders the entire communication system useless.

Table 7.2.3. Comparison of Basic Topological MWAR Architecture

Architecture	Performance						Expand-ability*
	Reliability	Hardware Requirement	Cost	Jamming Vulnerability	Link Distance		
Point-to-Point (PTP)	Poor	Nominal	Nominal	Low	Normal	Good	
Hub or Wheel	Good	Multibeam or Multiple Antennas and Switch Matrix	Slightly High	Low	Large	Good	
Star	Good	Nominal	Slightly High	Low	Nominal	Very Good	
Bidirectional Ring	Excellent	Nominal	Nominal	Low	Nominal	Good	
Earth Satellite	Fair-Poor	Satellite Required	Extremely High	High	Extremely Large	Very Good	
Ring-Wheel Combination	Excellent	Multibeam or Multiple Antennas and Switch Matrix	High	Low	Large	Good	

*Expandability to other architectures is not included.

7.2.4 Selection of Millimeter Wave Architecture for DCS

Selection of a recommended architecture for DCS system is dependent on the relative merits of the operating aspects of various candidates. Table 7.2.4 lists some of the more important criteria. The selection of the most suitable approach will be made on the basis of performance versus desired characteristics employing these criteria. The system designer may assign different weighting functions to these criteria.

Table 7.2.4. Operating Aspects Criteria for MMW Architecture Suitable for DCS Alternate Routing

- Cost
- Link Distance
- Topological, Geographical and Meteorological factors
- System Performance Availability Requirement
- Flexibility and Expandability Requirements
- Spectral Availability and Congestion Condition
- Availability of Satellite
- Information Volume
- Jamming
- Message Delivery Time

7.3 AJ Improvements in Tactical Communications Systems Using Direct Sequence QPSK Spreading

The DS QPSK system discussed in Section 3.0 is straightforward and can achieve useful processing gain using available components. The PN generators must be designed so that the PN code repetition rate is lower than the lowest frequency of interest in the information bandwidth. Since the data rates of interest are 1 to 20 Mb/s and 150 Mb/s, we will consider three data rate cases: 1, 20 and 150 Mb/s. We will examine three chip rates: 500 Mb/s, 750 Mb/s and 1000 Mb/s. The 500 Mb/s chip rate is well within the state-of-the art since it was achieved in 1973 in the Harris Model 4335 QPSK modulator and demodulator. Implementation complexity of 500 Mb/s chip rate PN generators can be reduced by using Fairchild high speed logic: the F100141 8-bit shift register operates at 500 MHz and can be used in conjunction with the F100107 exclusive or gate to build high speed PN generators.

The processing gain for QPSK at each of the data rates of interest is tabulated in Table 7.3-1. It should be pointed out that there is a point of diminishing returns for this direct sequence spectrum spreading implementation; while the 500 Mb/s PN generators can be implemented using 8-stage shift register devices (F100141), the 750 Mb/s PN generator (assuming direct generation) would use one-stage shift registers (i.e., flip-flops) capable of operating at 750 Mb/s. This implies an eight-fold increase in implementation complexity of the PN generator to obtain only 1.8 dB of additional processing gain.

The 1 Gb/s (1000 Mb/s) PN code rate is not amenable to direct generation with presently available logic, although the state-of-the-art is rapidly advancing.

Table 7.3-1. Direct Sequence QPSK Processing Gain

Data Rate (R_B)	Chip Rate (R_C)	$G_p = 10 \log_{10} (R_C/R_B)$
1 Mb/s	500 Mb/s	27.0 dB
20 Mb/s	500 Mb/s	14.0 dB
150 Mb/s	500 Mb/s	5.2 dB
1 Mb/s	750 Mb/s	28.8 dB
20 Mb/s	750 Mb/s	15.8 dB
150 Mb/s	750 Mb/s	7.0 dB
1 Mb/s	1 Gb/s	30.0 dB
20 Mb/s	1 Gb/s	17.0 dB
150 Mb/s	1 Gb/s	8.2 dB

NOTES

1. $R_C = 500$ Mb/s may be economically realized using Fairchild F100141 8-stage shift register packages.
2. $R_C = 1$ GHz may be realized via syncopation of two 500 Mb/s PN generators, each constructed with Fairchild F100141 8-stage shift register packages.
3. $R_C = 750$ MHz may be realized via syncopation or directly using Fairchild flip-flops capable of operating at clock rates of 750 MHz (Fairchild F11C06).
4. Exclusive OR gates are Fairchild F100107 devices.

However, chip rates of 1 Gb/s (or the 750 Mb/s mentioned above, if desired) can be obtained by using a syncopated register technique described by R. W. Dixon¹. Consider two PN code generators, each operating at $R_c/2$, but with clock phases that differ by 180° as shown in Figure 7.3-1. Combining the two outputs in an exclusive or gate results in a PN sequence with a clock rate of R_c and a period equal to the product of the periods of the individual PN sequences² (assuming these are unequal). This concept can be extended to any number of registers to generate extremely high chip rates as long as the exclusive or combining elements are fast enough.

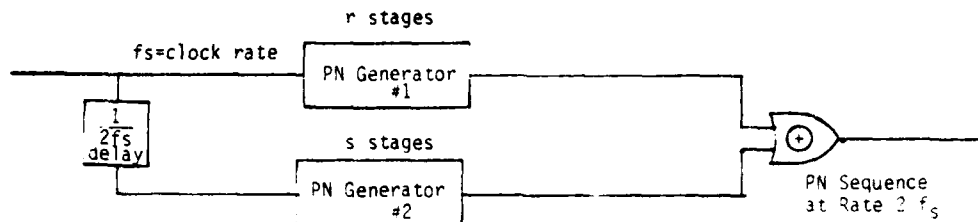
The disadvantage of syncopation is that the autocorrelation properties of such PN codes are unknown³; these properties should be investigated empirically via computer simulation for a particular set of individual codes prior to implementation. Note the distinction between syncopated codes and Gold codes:

- a. The output chip rate is $n \times f_{\text{clock}}$ for syncopated codes ($n = \#$ PN generators).
- b. Output chip rate is f_{clock} for Gold codes.
- c. Gold codes are useful in CDMA systems since they exhibit bounded cross-correlation.
- d. Cross-correlation properties among syncopated codes generated by relative shifts of the PN sequences are not necessarily bounded; they are unknown.

¹R. C. Dixon, Spread Spectrum Systems, Wiley and Sons, 1976, pp. 75-77.

²IBID.

³IBID.



NOTES:

- PN Generators #1 and #2 must have different periods, i.e., different lengths, $r \neq s$
- period of synchopated PN sequence is product of periods of individual PN Generators, i.e., $N = (2^r - 1)(2^s - 1)$
- Correlation properties of synchopated PN codes are unknown; must be determined via computer simulation
- synchopated codes are nonmaximal
- synchopation technique can be extended to k registers with clock delays of $1/kf_s, 2/kf_s, \dots, k-1/kf_s$.
- stringent speed requirements fall only on the exclusive or combining elements, not on individual shift registers.

A90401-31

Figure 7.3-1. High Rate PN Code Generation Using Syncopated Shift Registers

Recall that a 1 Gb/s chip rate yields processing gains of 30 dB, 17 dB, and 8.2 dB at data rates of 1 Mb/s, 20 Mb/s and 150 Mb/s, respectively. Assuming a 1 Gb/s chip rate generated via syncopation, it remains to specify the length and feedback connections required to generate each of the 500 Mb/s codes. The period of the composite PN code should be such that many spectral lines occupy the signal bandwidth: $T_p \gg T_{bit}$. Since the maximum value of T_{bit} is 1 μ sec we choose $T_p = 10^3 T_{bit} = 1$ ms. Thus the total number of chips in one period is given by

$$N = R_c T_p = \left(10^9 \frac{\text{chips}}{\text{sec}}\right) (10^{-3}) = 10^6 \text{ chips}$$

Recall that when using two syncopated registers the total period is the product of the periods of the individual registers having lengths r and s stages¹:

$$N = (2^r - 1) (2^s - 1)$$

Since 500 MHz shift registers are available 8 to a package, we choose $r = 15$ and $s = 7$. For a minimal number of taps, we can choose taps $[7, 1]$ for $s = 7$ and $[15, 4]$ for $r = 15$. The code period is then $N = (2^{15} - 1) (2^7 - 1) = 4,194,176$ chips or 4.2 ms.

A much longer code period is easily achieved by choosing $r = 23$ with taps $[23, 5]$ and $s = 22$ with taps $[22, 1]$. Then

$$N = 3.518 \times 10^{13} \text{ chips and } T_p = 9.77 \text{ hours.}$$

¹R.C. Dixon, Spread Spectrum Systems, Wiley and Sons, 1976, p. 77.

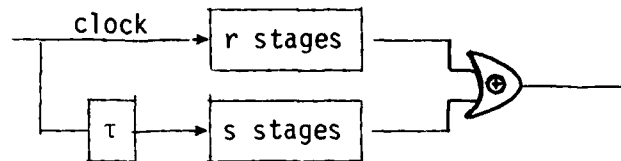
This latter code length is preferred. Using only six integrated circuit packages of 8 shift registers each we may generate a 1 Gb/s PN sequence which repeats every 9.77 hours. This $r = 23$, $s = 22$ design example is summarized in Figure 7.3-2.

Assuming that the correlation properties of the selected syncopated code are adequate, there is an advantage to using nonmaximal syncopated PN codes rather than maximal length PN codes. It is known that if one knows $(2n + 1)$ consecutive bits of a maximal length PN code generator, the shift register feedback connections can be ascertained. This means that a jammer can generate the correct PN sequence after listening to less than a few dozen bits at most, and can thus increase the jamming effectiveness. The traditional solution to this problem is to use nonlinear combinatorial functions of the shift register contents to obtain the feedback signal to obtain PN codes that cannot be cracked by jammers. The use of syncopated codes could perhaps also lead to secure PN sequences. The process of ascertaining the feedback connections and relative phasing of syncopated PN code generators is necessarily more difficult than the corresponding single PN generator case. Thus, although syncopated PN codes were used to obtain high chip rates, a beneficial side effect is that resulting code should be more difficult for a jammer to duplicate.

The syncopated register technique advocated for the generation of 1 Gb/s PN codes has the drawback that the correlation properties of syncopated codes are unknown¹. It would be desirable to generate maximal length PN sequences in the usual fashion without resorting to syncopation. The rapidly advancing GaAs technology may lead to gigabit LSI logic within the next 2 to 4 years. Hewlett-Packard has achieved switching speeds of less than 100 picoseconds in FETs and demonstrated frequency division at 4 GHz - 5 GHz. With the gigabit MSI or LSI logic that should be available within a few years, higher PN code rates can be implemented, yielding higher processing gains for DS spread spectrum systems.

¹R.C. Dixon, Spread Spectrum Systems, Wiley and Sons, 1976, p. 76.

Assume 1 Gbps PN sequence obtained via synchopation of two PN code generators.



$$\text{Period of Synchopated PN Code} = N_s = (2^r - 1)(2^s - 1)$$

where r = # stages in PN generator #1

s = # stages in PN generator #2

Let $r = 23$ and feedback taps = [23, 5]

and $s = 22$ and feedback taps = [22, 1]

Then $N_s = (2^{23} - 1)(2^{22} - 1) = 3.518 \times 10^{13}$ chips

and at 1 Gbps chip rate the code period is

$$T_p = 9.77 \text{ hours}$$

Summary

Obtained 1 Gbps PN sequence with period of 9.77 hours using only six integrated circuit packages of 8 shift registers each and three exclusive or gates. There are 3.518×10^7 spectral lines in the 1 Mbps data bandwidth.

A90401-32

Figure 7.3-2. A DS Design Example Using Synchopated PN Code Generators

7.4 Total Processing Gain Obtainable From Directive Antennas and Spectrum Spreading

In this section the values of the combined processing gain obtained from spectrum spreading and nonadaptive antenna gain are presented. The QPSK 1 Gb/s chip rate system described in Paragraph 7.3 is assumed and frequencies of 8 GHz, 38 GHz, and 80 GHz are evaluated for two antenna diameters, viz., 1 meter and 5 meters. It was shown in Paragraph 7.3 that spread spectrum processing gain for the 1 Gb/s QPSK system is 30 dB, 17 dB, and 8.2 dB at data rates of 1 Mb/s, 20 Mb/s, and 150 Mb/s, respectively. The additional protection afforded by the directivity of the nonadaptive antennas will be assumed to be the antenna gain. This assumes isotropic radiation outside the main lobe, but since beamwidths are extremely narrow a jammer may be reasonably assumed to be many sidelobes away from the main beam; therefore little error is incurred by the isotropic radiation assumption.

Table 7.4-1 gives total gain G against CW jammers (dB) for the frequencies, data rates and antenna diameters indicated. The total gain is given by the sum of antenna gain and spread spectrum gain in dB:

$$G = (G_{ANT} + G_{SS}) \text{ dB where}$$

$$G_{ANT} = 10 \log_{10} (\pi D/\lambda)^2, D = \text{antenna diameter}$$

$$G_{SS} = 10 \log_{10} (R_C/R_B)$$

Table 7.4-1. Total Gain (Antenna and Spread Spectrum Processing Against a CW Jammer)

Frequency (GHz)	Data Rate (Mb/s)	Antenna Diameter (Meters)	
		1 Meter	5 Meters
8	1	68.46 dB	82.44 dB
8	20	55.46 dB	69.44 dB
8	150	46.66 dB	60.64 dB
38	1	82.00 dB	95.98 dB
38	20	69.00 dB	82.98 dB
38	150	60.80 dB	74.78 dB
80	1	88.46 dB	102.44 dB
80	20	75.46 dB	89.44 dB
80	150	66.66 dB	80.64 dB

NOTE

All other jammer types are less effective than a CW jammer; therefore, these figures represent the lower bound for total gain against all jammer types.

Note from these expressions that G_{ANT} is independent of chip rate and data rate and that G_{SS} is independent of frequency. It is informative to compute the difference in antenna gain at the three frequencies of interest for both the 1 meter and the 5 meter antenna. If we take the 8 GHz 1 meter antenna as the 0 dB reference point we obtain the expression:

$$\begin{aligned} \Delta G_{ANT} &= 10 \log \left(\frac{D/\lambda}{D_8/\lambda_8} \right) \text{ dB} \\ &= \left[10 \log \left(\frac{\lambda_8}{\lambda} \right)^2 + 10 \log \left(\frac{D}{D_8} \right)^2 \right] \text{ dB} \end{aligned}$$

The computed values for ΔG_{ANT} are contained in Table 7.4-2.

Table 7.4-2. ΔG_{ANT} Versus Frequency and Antenna Diameter

	D = 1 meter	D = 5 meters
f = 8 GHz	0.00 dB	13.98 dB
f = 38 GHz	13.54 dB	27.52 dB
f = 80 GHz	20.00 dB	33.98 dB

7.5 Systems Considerations

In this section several system considerations of importance are discussed, including:

- a. Atmospheric Absorption
- b. Differential Rain Loss
- c. Antenna Beamwidths

- d. Coherence Bandwidth
- e. Acquisition and Tracking
- f. Spectrum Allocations
- g. Bandlimiting and Aliasing of BPSK Signals

7.5.1 Atmospheric Absorption

The 8 GHz frequency was specified as a reference frequency in the statement of work. The rationale for selecting 38 GHz and 80 GHz as candidate operating frequencies for short links is evident from Figure 7.5.1 which shows atmospheric absorption coefficient as a function of frequency¹. The 38 GHz frequency is not far removed from a local minimum in absorption coefficient. The same is true for the 80 GHz frequency. Note that the atmospheric absorption coefficient is 5 times larger at 80 GHz than at 38 GHz; thus, the 38 GHz frequency is to be preferred in order to minimize atmospheric loss.

The atmospheric loss coefficient is 0.4 dB/km larger at 80 GHz than at 38 GHz, which translates into 4 dB additional loss for a 10 km link.

7.5.2 Rain Loss

Of much more importance at MMW frequencies is the loss due to rainfall. Rainfall loss increases monotonically with frequency and rainfall rate. Table 7.5.2 shows the extra rain margin required for a 10 km link when operating at 38 GHz rather than 8 GHz. A rainfall rate of 25 mm/hr is considered a "heavy" rain and rates higher than 100-125 mm/hr are called "cloudbursts".

¹R. A. LeFande, "Attenuation of Microwave Radiation for Paths Through the Atmosphere," Naval Research Laboratory, NRL Report 6766, November 29, 1968.

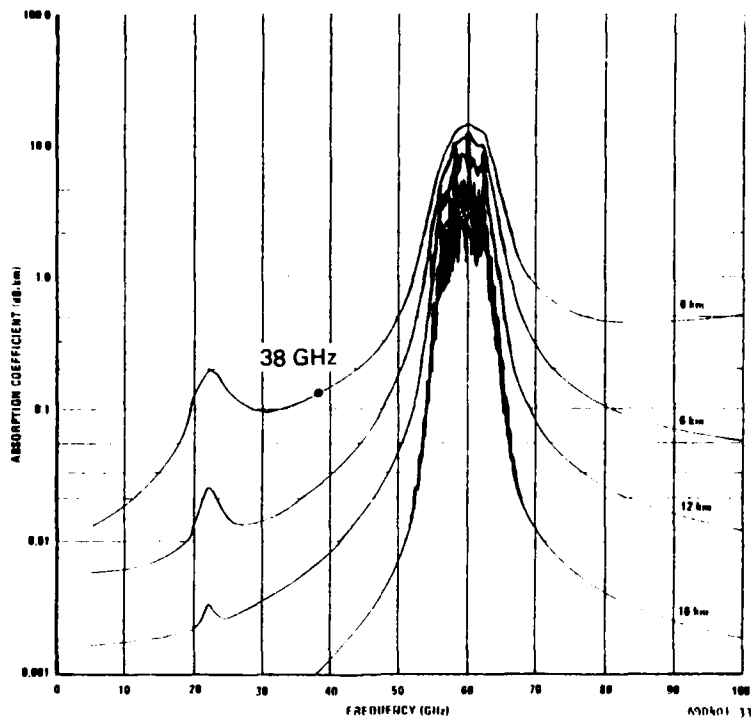


Figure 7.5.1. Total Absorption Coefficient for the Model Atmosphere in Reference¹ for Surface Water Vapor Density ρ_0 of 7.5 g/m^3 (60% RH at 60°F)

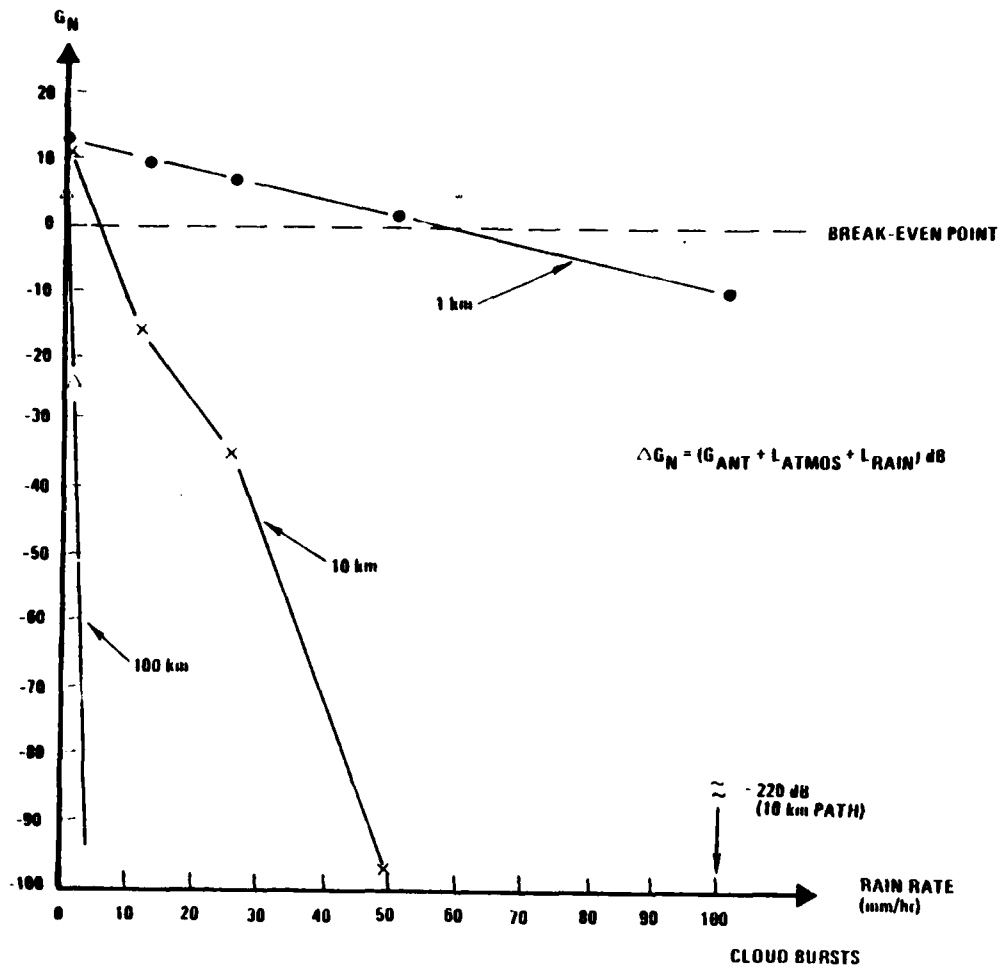
Table 7.5.2. Additional Rain Loss Incurred Over a 10 km Link When Operating at 38 GHz Rather than 8 GHz

1 mm/hr:	ΔL_{RAIN}	=	(0.32 - 0.004)	dB/km X 10 km	=	3.16 dB
10 mm/hr:		=	(3 - 0.08)	dB/km X 10 km	=	29.20 dB
25 mm/hr:		=	(6 - 0.3)	dB/km X 10 km	=	57.00 dB
50 mm/hr:		=	(12 - 0.9)	dB/km X 10 km	=	111.00 dB
100 mm/hr:		=	(25 - 2)	dB/km X 10 km	=	230.00 dB

¹R. A. LeFande, "Attenuation of Microwave Radiation for Paths Through the Atmosphere," Naval Research Laboratory, NRL Report 6766, November 29, 1968.

It is evident from Table 7.5.2 that rain attenuation and rain rate statistics will dominate system design with regard to system availability and terminal separation. A graphical illustration of rain loss versus rainfall rate for a 10 km link is shown in Figure 7.5.2. This figure plots the net gain of a 38 GHz system with respect to an 8 GHz system versus rainfall rate. The net gain includes a positive term corresponding to increased antenna gain, a (negligible) negative term corresponding to atmospheric loss and a negative term corresponding to rain loss. The breakeven (i.e., net gain equal to zero) condition is shown as a dashed line in the figure. This figure dramatically points out the importance of rainfall rate in MMW systems and shows how rapidly rain losses increase with path length between transmitter and receiver. Note that for 25 mm/hr (about 1 inch/hour) the net gain for a 20 km link is -35 dB, i.e., a loss of 35 dB is incurred at the higher frequency.

A less obvious consequence of the severe signal attenuation due to rain is that the near/far jammer problem is aggravated at MMW frequencies in the presence of rain. Consider the case in which the jammer is much closer to the receiver than the transmitter. In the presence of rain the desired signal is greatly attenuated with respect to the jammer's signal because of the much longer path length. This means that the J/S ratio would sharply increase whenever rain was present and that higher rainfall rates imply higher J/S ratios. On the positive side, MMW systems would necessarily be designed with much higher rain margin than an 8 GHz system and therefore would have an additional jamming margin in clear weather. This latter statement assumes that the system parameters are chosen such that adequate AJ protection is obtained in the presence of rain for the assumed jamming threat.



A90401-34

Figure 7.5.2. Net Gain of a 38 GHz System with Respect to an 8 GHz System Versus Rainfall Rate With Link Path Length as a Parameter

7.5.3 Antenna Beamwidths

One further result of using MMW frequencies rather than microwave frequencies is that the antenna beamwidth is smaller, given the same antenna aperture. The 3 dB beamwidth in degrees is given by

$$\theta_{3 \text{ dB}} = \left[\frac{70\lambda}{D} \right] \text{ degrees}$$

Thus, for a 1 meter dish antenna the beamwidth is 2.625° at 8 GHz and only 0.55° at 38 GHz. If a 5 meter dish antenna is assumed the values decrease by a factor of five to 0.525° and 0.11° , respectively. Narrower beamwidths are generally desirable from a low probability of intercept (LPI) point of view, although, practically speaking, there is a point of diminishing returns. For example, going from 3 dB BW = 1.0° to 3 dB BW = 0.1° decreases the cross-sectional area of the main beam by a factor of 100; however, the probability of intercepting a 1.0° wide beam is extremely low to begin with.

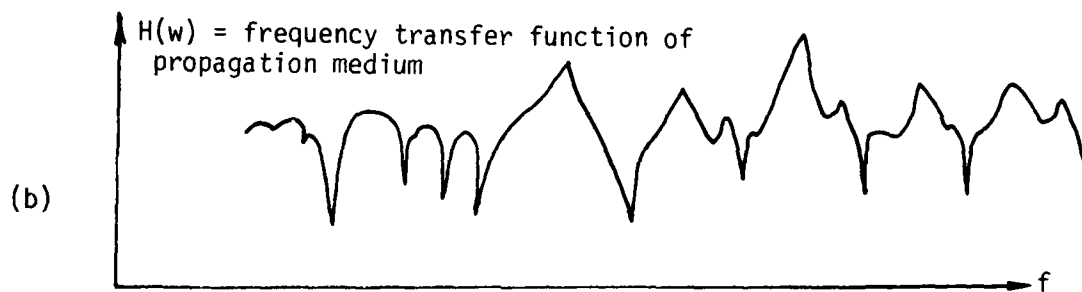
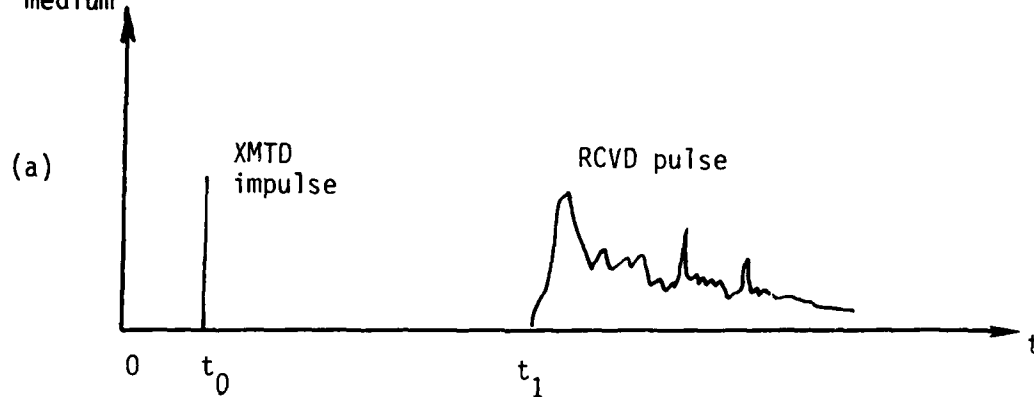
Also, the narrower beamwidths associated with MMW frequencies will tend to aggravate the spatial alignment problem and to make the antenna support rigidity requirements more severe. Adaptive arrays provide one potential solution to this problem and are discussed in Section 6.0.

Finally, the use of the higher MMW frequencies reduces the allowable antenna surface roughness tolerance. For relatively small antenna dishes this should pose no problem, and it is within the state-of-the-art to produce large antennas for use at MMW frequencies; generally, the use of higher frequencies implies smaller tolerances in tracking error, and surface roughness, which, in turn, increases the overall cost of the antenna system.

7.5.4 Coherence Bandwidth Considerations at MMW Frequencies

Coherence bandwidth is a measure of the signal dispersion and hence intersymbol interference introduced by the propagation medium. Figure 7.5.4 illustrates how an ideal transmitted impulse would be spread out or dispersed in time after propagating through a dispersive medium. The effect of multiple paths between transmitter and receiver due to reflections, refraction, scattering, etc., is evidenced in the frequency transfer function. The coherence bandwidth of a channel is defined as the frequency

$h(t) = \text{impulse response of propagation medium}$



NOTES:

- B_c is a measure of amplitude flatness of propagation medium
- $B_c \geq R_b$ implies that $\text{BER} \rightarrow \frac{1}{2}$
- Roche et al. measured B_c in the 27 to 40 GHz band for both an 8 Km link and a 32 Km link near Washington, D.C.
 - $B_c > 6$ GHz for 8 Km link
 - $B_c > 6$ GHz for 99.9% of measurements for the 32 Km link

A90401-35

Figure 7.5.4. Coherence Bandwidth Considerations in Spread Spectrum Systems

separation at which the correlation of two CW sinusoids is reduced to e^{-1} , i.e., the value of f for which $\overline{H(f) H(f + f)} = e^{-1}$. The autocorrelation of the frequency transfer function may also be obtained as the Fourier transform of the squared impulse response $h^2(t)$. The autocorrelation of the frequency transfer function may also be obtained as the Fourier transform of the squared impulse response $h^2(t)$.

The coherence bandwidth determines the maximum data rate that can be transmitted through a channel with acceptable BER. As a general rule of thumb, data rates higher than about 0.1 to 0.3 times the coherence bandwidth lead to unacceptably high BER. HF propagation over long distances is characterized by severe multipath and therefore has a very small coherence bandwidth, usually on the order of a few kHz. This is the source of the frequency-selective distortion characteristic of shortwave AM broadcasting: the transfer function is not flat over the 6 to 10 kHz RF bandwidth of AM speech signals.

For line-of-sight microwave or MMW transmission the antenna beams are relatively narrow and the number of opportunities for multipath to occur is greatly reduced or eliminated. The minimal dispersion that is observed is probably due to scattering within the volume of intersecting transmitter and receiver antenna beams. In view of the very wide bandwidths anticipated it is necessary to determine the limitations, if any, imposed upon data rate due to the coherence bandwidth of the MMW propagation medium. Fortunately, some empirical data for the 27 GHz - 40 GHz band is available for both an 8 km link and a 32 km link near Washington, D.C. Roche et al.¹ report that the coherence bandwidth always exceeded 6 GHz for the 8 km link and exceeded 6 GHz for 99.9% of the time for the 32 km link. This is reassuring since it means that data rates (chip rates in DS systems) on the order of 1 Gb/s are

¹J. Roche, H. Lake, D. Worthington, C. Tsao, and J. DeBettencourt, "Radio Propagation at 27 - 40 GHz," IEEE Trans, Antennas and Propagation, Vol. AP-18, No. 4, July, 1970.

acceptable. Coherence bandwidth is of no consequence for FH systems since the entire bandwidth is used sequentially rather than simultaneously in FH systems. The severity of the degradation to chirp systems due to constrained coherence bandwidth is unknown; at the least the waveform distortion introduced into the received chirp signal would give rise to correlation loss in the matched filter detection process.

7.5.5 Acquisition and Tracking in Spread Spectrum Systems

Acquisition and tracking is an aspect of spread spectrum communications that is of crucial importance. If transmitter and receiver locations are assumed known, acquisition can be accomplished with little difficulty. The two PN generators can be co-located, initially loaded with the same state and accurately clocked. After transporting the PN generators to their respective sites, the path delay can be computed and acquisition easily completed. An alternative approach is to acquire "in the blind" which is also easily accomplished in the absence of jamming. In this technique a sequence of N received chips is loaded into the PN generator at the receiver and the feedback connection closed; if there are no chip errors in the received sequence of N chips ($N = \#$ stages in PN generator) the receiver PN generator will be synchronized with the transmitter PN generator.

Once code acquisition has been accomplished tracking should pose no difficulty since the transmitter and receiver locations are assumed to be fixed. Loss of synchronization would only occur during rain outages (an infrequent event for a properly designed system) or due to jamming strong enough to completely disrupt the link.

In view of the fact that the system terminals are stationary and since acquisition can be accomplished once the system is installed, the code acquisition/tracking aspect of the spread spectrum systems will not be treated further.

7.5.6 Spectrum Allocations at MMW Frequencies

One of the reasons for the interest in MMW frequencies is that the microwave frequencies currently used for digital data and FDM/FM voice communications are becoming crowded and the MMW frequencies are relatively uncongested. In addition much wider bandwidths should be available at millimeter wave frequencies. Table 7.5.6 (continued over thirteen pages) shown below is extracted from the U.S. Government Table of Frequency Allocations and shows both international and national spectrum allocations for the frequency band from 21.2 GHz to 275 GHz. The notations G, NG in the National Provisions column refer to government and nongovernment, respectively.

7.5.7 The Effects of Bandlimiting and Aliasing Upon BPSK Signals

One of the operations required to generate PSK signals is the multiplication of the data sequence by a sinusoidal carrier signal, which has the effect of translating the baseband data spectrum up to the carrier frequency. For the extremely high data rates proposed for the DS QPSK system the limited bandwidth of available mixers will introduce some distortions into the PSK signal due to bandlimiting and aliasing. In order to investigate the severity of these effects a computer program was written that plots the distorted BPSK waveform under varying conditions. The BPSK results are all that are required since QPSK may be regarded as the sum of two quadrature carrier BPSK signals.

For convenience, the data was assumed to be a square wave, i.e., alternating "1's" and "0's", so that a Fourier series expression can be used. This assumption results in the widest possible signal bandwidth since the transition density is 100 percent in this case. In addition, the resulting spectrum is a line spectrum because of the periodicity but the envelope of the spectrum is the same as for purely random data. Since an ideal square wave will not be obtained in practice, only a few terms of the series are retained.

Table 7.5.6. Spectrum Allocations For 21.2 GHz to 275 GHz

INTERNATIONAL			UNITED STATES				
Region 1 GHz	Region 2 GHz	Region 3 GHz	Band GHz	National Provisions 2	Government Allocation 3	Non-Government Allocation 4	Remarks 5
21.2-22	EARTH EXPLORATION-SATELLITE (Space-to-Earth) FIXED MOBILE		21.2-22	G, NG	EARTH EXPLORATION- SATELLITE (Space-to-Earth) FIXED MOBILE	EARTH EXPLORATION- SATELLITE (Space-to-Earth) FIXED MOBILE NC107	
22-22.5	FIXED MOBILE 410A		22-23.6	G, NG 410A	FIXED MOBILE	FIXED MOBILE	
22.5-23	FIXED MOBILE	22.5-23 FIXED MOBILE BROADCASTING- SATELLITE 410B					
23-23.6	FIXED MOBILE						
23.6-24	RADIO ASTRONOMY 407		23.6-24	G, NG US72 US74	RADIO ASTRONOMY	NC107 RADIO ASTRONOMY	
24-24.05	AMATEUR AMATEUR-SATELLITE 401C		24-24.05	AMATEUR US72 US202 US211	G45	AMATEUR AMATEUR- SATELLITE	

Table 7.5.6. Spectrum Allocations For 21.2 GHz to 275 GHz (Continued)

INTERNATIONAL			UNITED STATES				
Region 1 GHz	Region 2 GHz	Region 3 GHz	Band GHz	National Provisions	Government Allocation	Non-Government Allocation	Remarks
1	2	3	1	2	3	4	5
24.05-24.25	RADIOLOCATION Amateur		24.05-24.25 (ISH 24.125 + .125 GHz)	G, NG US72 US110 US202	RADIOLOCATION	Amateur Radiolocation	
	407 410C						
24.25-25.25	RADIONAVIGATION 411 412		24.25-25.25	G, NG US72	RADIONAVIGATION	RADIONAVIGATION	
25.25-27.5	FIXED MOBILE		25.25-27.5	G	FIXED MOBILE		
27.5-29.5	FIXED FIXED-SATELLITE (Earth-to-space) MOBILE		27.5-29.5	NG		FIXED FIXED-SATELLITE (Earth-to-space) MOBILE	
29.5-31	FIXED-SATELLITE (Earth-to-space)		29.5-30	NG		FIXED-SATELLITE (Earth-to-space)	
31-31.3	409E FIXED MOBILE Space Research 412H 412I		30-31 31-31.2 31.2-31.5	G NG US100 G, NG US74 US100	FIXED-SATELLITE (Earth-to-space) G107 RADIO ASTRONOMY		
31.3-31.5	RADIO ASTRONOMY 412A						G45

Table 7.5.6. Spectrum Allocations For 21.2 GHz to 275 GHz (Continued)

INTERNATIONAL			UNITED STATES				
Region 1 GHz	Region 2 GHz	Region 3 GHz	Band GHz	National Provisions 2	Government Allocation 3	Non-Government Allocation 4	Remarks 5
31.5-31.8 SPACE RESEARCH Fixed Mobile	31.5-31.8 SPACE RESEARCH 405C	31.5-31.8 SPACE RESEARCH Fixed Mobile	31.5-31.8	G, NC US100 US211	SPACE RESEARCH	SPACE RESEARCH	
31.8-32.3	RADIONAVIGATION Space Research 412B		31.8-33.4	G, NC US69 US100	RADIONAVIGATION C35	RADIONAVIGATION	
32.3-33.0	RADIONAVIGATION						
33.0-33.4 RADIO ASTRONOMY RADIONAVIGATION	33.0-33.4 RADIONAVIGATION 412F						
33.4-34.7							
34.7-35.2	RADIOLOCATION 407 408 412 412G		33.4-36.0	G, NC 412D US100 US110	RADIOLOCATION	Radiolocation	Although the band 10000-10500 MHz presently seems most suitable as a common frequency band for such survey operations in different countries, future development, if required, should be directed to the band 34.0-35.6 GHz, within the overall band 33.4-36.0 GHz, with no new development below 10000 MHz.
35.2-36.0	RADIOLOCATION Space Research 407 408 412 412C 412D						
36-40	RADIOLOCATION 407 408 412		36.0-38.6	G	C34 FIXED MOBILE		
	FIXED MOBILE 391A 412E		38.6-40.0	US100 NC		FIXED MOBILE	

Table 7.5.6. Spectrum Allocations For 21.2 GHz to 275 GHz (Continued)

INTERNATIONAL			UNITED STATES				
Region 1 GHz	Region 2 GHz	Region 3 GHz	Band GHz	National Provisions	Government Allocation	Non-Government Allocation	Remarks
1	2	3	1	2	3	4	5
40-41	FIXED-SATELLITE (Space-to-Earth)		40-41	G, MG	FIXED FIXED-SATELLITE (Space-to-Earth) MOBILE	FIXED FIXED-SATELLITE (Space-to-Earth) MOBILE	
41-43	BROADCASTING-SATELLITE		41-43	G, MG	FIXED MOBILE	FIXED BROADCASTING- SATELLITE MOBILE	
43-48	AERONAUTICAL MOBILE-SATELLITE MARITIME MOBILE-SATELLITE AERONAUTICAL RADIONAVIGATION- SATELLITE MARITIME RADIONAVIGATION-SATELLITE		43-48	G, MG	AERONAUTICAL MOBILE AERONAUTICAL MOBILE- MOBILE- SATELLITE MARITIME MOBILE MARITIME MOBILE- SATELLITE AERONAUTICAL RADIONAVIGATION AERONAUTICAL RADIONAVIGATION- SATELLITE MARITIME RADIONAVIGATION MARITIME RADIO- NAVIGATION- SATELLITE RADIOLOCATION	AERONAUTICAL MOBILE AERONAUTICAL MOBILE- MOBILE- SATELLITE MARITIME MOBILE MARITIME MOBILE- SATELLITE AERONAUTICAL RADIONAVIGATION AERONAUTICAL RADIONAVIGATION- SATELLITE MARITIME RADIONAVIGATION MARITIME RADIO- NAVIGATION- SATELLITE RADIOLOCATION Amateur	
48-50	(Not allocated)		48-50	G, MG	RADIOLOCATION	RADIOLOCATION	

Table 7.5.6. Spectrum Allocations For 21.2 GHz to 275 GHz (Continued)

INTERNATIONAL			UNITED STATES				
Region 1 GHz	Region 2 GHz	Region 3 GHz	Band GHz	National Provisions	Government Allocation	Non-Government Allocation	Remarks
			1	2	3	4	5
50-51	FIXED-SATELLITE (Earth-to-Space)		50-51	G, NG	FIXED FIXED-SATELLITE (Earth-to-Space) MOBILE	FIXED FIXED-SATELLITE (Earth-to-Space) MOBILE	
51-52	EARTH EXPLORATION-SATELLITE SPACE RESEARCH		51-52	G, NG	EARTH EXPLORATION- SATELLITE SPACE RESEARCH	EARTH EXPLORATION- SATELLITE SPACE RESEARCH	
52-54.25	SPACE RESEARCH (Passive) 412J		52-54.25	G, NG 412J	SPACE RESEARCH SPACE RESEARCH (Passive) G45	SPACE RESEARCH SPACE RESEARCH (Passive)	
54.25-58.2	INTER-SATELLITE		54.25-58.2	G, NG	FIXED INTER-SATELLITE MOBILE	FIXED MOBILE except aeronautical mobile	
58.2-59	SPACE RESEARCH (Passive) 412J		58.2-59	G, NG 412J	SPACE RESEARCH (Passive) G45	SPACE RESEARCH (Passive)	
59-64	INTER-SATELLITE		59-64	G, NG	FIXED INTER-SATELLITE MOBILE	FIXED MOBILE except aeronautical mobile	
64-65	SPACE RESEARCH (Passive) 412J		64-65	G, NG 412J	SPACE RESEARCH (Passive) G45	SPACE RESEARCH (Passive)	
65-66	EARTH EXPLORATION-SATELLITE SPACE RESEARCH		65-66	G, NG	EARTH EXPLORATION- SATELLITE SPACE RESEARCH	EARTH EXPLORATION- SATELLITE SPACE RESEARCH	

Table 7.5.6. Spectrum Allocations For 21.2 GHz to 275 GHz (Continued)

INTERNATIONAL			UNITED STATES				
Region 1 GHz	Region 2 GHz	Region 3 GHz	Band GHz	National Provision 2	Government Allocation 3	Non-Government Allocation 4	Remarks 5
66-71		AERONAUTICAL MOBILE-SATELLITE MARITIME MOBILE-SATELLITE AERONAUTICAL RADIONAVIGATION- SATELLITE MARITIME RADIONAVIGATION-SATELLITE	66-71	G, NC	AERONAUTICAL MOBILE AERONAUTICAL MOBILE- SATELLITE MARITIME MOBILE MARITIME MOBILE- SATELLITE AERONAUTICAL RADIONAVIGATION AERONAUTICAL RADIONAVI- GATION- SATELLITE MARITIME RADIONAVIGATION MARITIME RADIONAVI- GATION- SATELLITE RADIOLOCATION	AERONAUTICAL MOBILE AERONAUTICAL MOBILE- SATELLITE MARITIME MOBILE MARITIME MOBILE- SATELLITE AERONAUTICAL RADIONAVIGATION AERONAUTICAL RADIONAVI- GATION- SATELLITE MARITIME RADIONAVIGATION MARITIME RADIONAVI- GATION- SATELLITE RADIOLOCATION	
71-84	(Not allocated)		71-76 76-84	G, NC G, NC	FIXED MOBILE	Amateur FIXED MOBILE	
84-86	BROADCASTING-SATELLITE		84-86	G, NC US211	FIXED MOBILE	FIXED BROADCASTING- SATELLITE MOBILE	

Table 7.5.6. Spectrum Allocations For 21.2 GHz to 275 GHz (Continued)

INTERNATIONAL			UNITED STATES				
Region 1 GHz	Region 2 GHz	Region 3 GHz	Band GHz	National Provisions 2	Government Allocation 3	Non-Government Allocation 4	Remarks 5
86-92	RADIO ASTRONOMY SPACE RESEARCH (Passive) 412.7		86-92	G, NC 412.7 US74	RADIO ASTRONOMY SPACE RESEARCH (Passive) G45	RADIO ASTRONOMY SPACE RESEARCH (Passive)	
92-95	FIXED-SATELLITE (Earth-to-space)		92-93	G, NC	FIXED FIXED-SATELLITE (Earth-to-space) MOBILE G107	FIXED MOBILE	
			93-95	G, NC	FIXED FIXED-SATELLITE (Earth-to-space) MOBILE	FIXED FIXED-SATELLITE (Earth-to-space) MOBILE	
95-101	AERONAUTICAL MOBILE-SATELLITE MARITIME MOBILE-SATELLITE AERONAUTICAL RADIONAVIGATION- SATELLITE MARITIME RADIONAVIGATION-SATELLITE		95-101	G, NC	AERONAUTICAL MOBILE AERONAUTICAL MOBILE- SATELLITE MARITIME MOBILE MARITIME MOBILE- SATELLITE AERONAUTICAL RADIONAVIGATION AERONAUTICAL RADIONAVI- GATION- SATELLITE MARITIME RADIONAVIGATION MARITIME RADIO- NAVIGATION- SATELLITE Radiolocation	AERONAUTICAL MOBILE AERONAUTICAL MOBILE- SATELLITE MARITIME MOBILE MARITIME MOBILE- SATELLITE AERONAUTICAL RADIONAVIGATION AERONAUTICAL RADIONAVI- GATION- SATELLITE MARITIME RADIONAVIGATION MARITIME RADIO- NAVIGATION- SATELLITE	

Table 7.5.6. Spectrum Allocations For 21.2 GHz to 275 GHz (Continued)

INTERNATIONAL			UNITED STATES				
Region 1 GHz	Region 2 GHz	Region 3 GHz	Band GHz	National Provisions	Government Allocation	Non-Government Allocation	Remarks
101-102	SPACE RESEARCH (Passive) 412J		101-102	G, NG 412J	SPACE RESEARCH (Passive) G45	SPACE RESEARCH (Passive)	
102-105	FIXED-SATELLITE (Space-to-Earth)		102-103	G, NG	FIXED FIXED-SATELLITE (Space-to-Earth) MOBILE G107	FIXED MOBILE	
			103-105	G, NG	FIXED FIXED-SATELLITE (Space-to-Earth) MOBILE	FIXED FIXED-SATELLITE (Space-to-Earth) MOBILE	
105-130	INTER-SATELLITE		105-110	G, NG	FIXED INTER-SATELLITE MOBILE	FIXED MOBILE except aeronautical mobile	
			110-117.5	G, NG	FIXED INTER-SATELLITE MOBILE	FIXED INTER-SATELLITE MOBILE except aeronautical mobile	
			117.5-122.5	G, NG	FIXED INTER-SATELLITE MOBILE	FIXED MOBILE except aeronautical mobile	
			122.5-130.0	G, NG US211	FIXED INTER-SATELLITE MOBILE	FIXED INTER-SATELLITE MOBILE except aeronautical mobile	

Table 7.5.6. Spectrum Allocations For 21.2 GHz to 275 GHz (Continued)

INTERNATIONAL			UNITED STATES				
Region 1 GHz	Region 2 GHz	Region 3 GHz	Band GHz	National Provisions	Government Allocation	Non-Government Allocation	Remarks
130-140	RADIO ASTRONOMY SPACE RESEARCH (Passive) 412J		130-140	G, NC 412J US74	RADIO ASTRONOMY SPACE RESEARCH (Passive) G45	RADIO ASTRONOMY SPACE RESEARCH (Passive)	5
140-142	FIXED-SATELLITE (Earth-to-space)		140-141	G, NC	FIXED FIXED-SATELLITE (Earth-to-space) MOBILE G107	FIXED MOBILE	
142-150	AERONAUTICAL MOBILE-SATELLITE MARITIME MOBILE-SATELLITE AERONAUTICAL RADIONAVIGATION- SATELLITE MARITIME RADIONAVIGATION-SATELLITE		141-142	G, NC	FIXED FIXED-SATELLITE (Earth-to-space) MOBILE	FIXED FIXED-SATELLITE (Earth-to-space) MOBILE	
			142-150	G, NC	AERONAUTICAL MOBILE AERONAUTICAL MOBILE- SATELLITE MARITIME MOBILE MARITIME MOBILE- SATELLITE AERONAUTICAL RADIONAVIGATION AERONAUTICAL RADIONAVI- GATION- SATELLITE MARITIME RADIONAVIGATION MARITIME RADIO- NAVIGATION- SATELLITE Radiolocation	AERONAUTICAL MOBILE AERONAUTICAL MOBILE- SATELLITE MARITIME MOBILE MARITIME MOBILE- SATELLITE AERONAUTICAL RADIONAVIGATION AERONAUTICAL RADIONAVI- GATION- SATELLITE MARITIME RADIONAVIGATION MARITIME RADIO- NAVIGATION- SATELLITE	

Table 7.5.6. Spectrum Allocations For 21.2 GHz to 275 GHz (Continued)

INTERNATIONAL			UNITED STATES				
Region 1 GHz	Region 2 GHz	Region 3 GHz	Band GHz	National Provisions 2	Government Allocation 3	Non-Government Allocation 4	Remarks 5
150-152			150-151	G, NG	FIXED FIXED-SATELLITE (Space-to-Earth) MOBILE G107	FIXED MOBILE	
			151-152	G, NG	FIXED FIXED-SATELLITE (Space-to-Earth) MOBILE	FIXED FIXED-SATELLITE (Space-to-Earth) MOBILE	
			152-165	G, NG	FIXED MOBILE RADIOLOCATION	FIXED MOBILE RADIOLOCATION	
			165-170	G, NG	FIXED MOBILE RADIOLOCATION	FIXED MOBILE RADIOLOCATION	
			170-175	G, NG	FIXED INTER-SATELLITE MOBILE	FIXED MOBILE except aeronautical mobile	
			175-182	G, NG	FIXED INTER-SATELLITE MOBILE	FIXED INTER-SATELLITE MOBILE except aeronautical mobile	
182-185			182-185	G, NG 412J	SPACE RESEARCH (Passive) G45	SPACE RESEARCH (Passive)	

Table 7.5.6. Spectrum Allocations For 21.2 GHz to 275 GHz (Continued)

INTERNATIONAL			UNITED STATES				
Region 1 GHz	Region 2 GHz	Region 3 GHz	Band GHz	National Provisions 2	Government Allocation 3	Non-Government Allocation 4	Remarks 5
185-190			185-189	G, NG	FIXED INTER-SATELLITE MOBILE	FIXED INTER-SATELLITE MOBILE except aeronautical mobile	
			189-190	G, NG	FIXED INTER-SATELLITE MOBILE	FIXED MOBILE except aeronautical mobile	
190-200			190-200	G, NG	AERONAUTICAL MOBILE AERONAUTICAL MOBILE- MOBILE- MOBILE- SATELLITE SATELLITE MARITIME MOBILE MARITIME MOBILE- SATELLITE AERONAUTICAL AERONAUTICAL RADIO NAVIGATION RADIO NAVIGATION RADIO NAVI- GATION- SATELLITE SATELLITE MARITIME RADIO NAVIGATION RADIO NAVI- GATION- SATELLITE SATELLITE	AERONAUTICAL MOBILE AERONAUTICAL MOBILE- MOBILE- SATELLITE SATELLITE MARITIME MOBILE MARITIME MOBILE- SATELLITE AERONAUTICAL RADIO NAVIGATION RADIO NAVIGATION RADIO NAVI- GATION- SATELLITE SATELLITE MARITIME MARITIME RADIO- NAVIGATION- SATELLITE	
200-220			200-220	G, NG	FIXED MOBILE	FIXED MOBILE	

(Not allocated)

Table 7.5.6. Spectrum Allocations For 21.2 GHz to 275 GHz (Continued)

INTERNATIONAL			UNITED STATES				
Region 1 GHz	Region 2 GHz	Region 3 GHz	Band GHz	National Provisions	Government Allocation	Non-Government Allocation	Remarks
265-275			265-275	G, NC	FIXED FIXED-SATELLITE MOBILE	FIXED FIXED-SATELLITE MOBILE	5
Above 275			275-300	G, NC	FIXED MOBILE	FIXED MOBILE	
			Above 300	G, NC	(Not allocated)	(Not allocated)	For use by experimental or amateur stations.

The procedure was to form a BPSK signal as the product of a square wave and a sinusoid:

$$f(t) = (\sin 2 \pi f_c t) \left[\sum_{n = 1, 3, 5}^{k_{\max}} \frac{1}{n} \sin n \pi f_d t \right]$$

where

f_c = carrier frequency (Hz)

f_d = data rate (b/s)

Note that in this expression the period of the square wave is twice the reciprocal of the data rate; this explains why the argument of the Fourier series terms contains " $n\pi$ " rather than " $n\pi 2$." The FFT of the (sampled) $f(t)$ function was performed and this yields an aliased line spectrum as shown in Figure 7.5.7-1, in which $f_d = 1$ Gb/s and $f_c = 1$ GHz is assumed. The aliasing would be reduced if f_c were higher; however, mixer bandwidth limitations constrain the maximum carrier frequency. Note that if a random data sequence had been used the shape of the spectrum would be $(\sin(kf)/kf)$, $k = \text{constant}$.

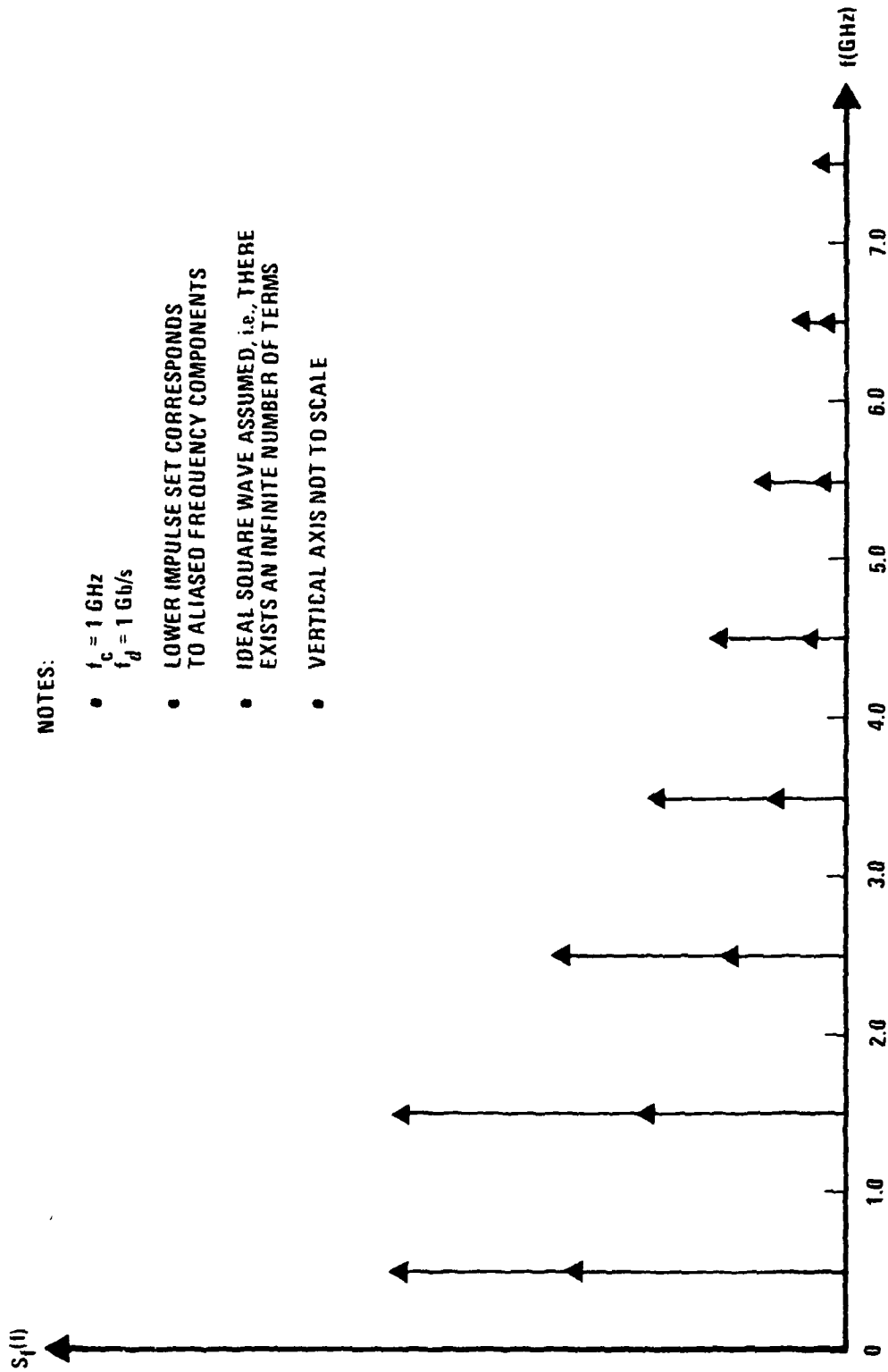
The calculations involved varying two parameters of the model: (1) the number of Fourier series terms representing the square wave and (2) the degree of bandlimiting of $S_f(f)$ (i.e., the bandwidth of the mixer output).

In the computer plots presented in Figures 7.5.7-1 through 7.5.7-10 the number of retained Fourier series terms may be ascertained from the value of k_{\max} as follows:

<u>k_{\max}</u>	<u>Number of Fourier Series Terms</u>
1	1
3	2
5	3
7	4

The number of retained terms in the Fourier series is a measure of the "goodness" or "squareness" of the square wave data. The parameter f_{cut} corresponds to the bandwidth of the mixer output and determines the number of sidelobes present in the mixer output.

In order to interpret these computer plots, refer to Figure 7.5.7-1 and locate f_{cut} on the abscissa, while keeping in mind that the number of terms in the unfiltered output spectrum depends upon the number of retained terms in the Fourier series for the data square wave. Figure 7.5.7-11 is a listing of the computer program used to generate the results in Figures 7.5.7-2 through 7.5.7-10.

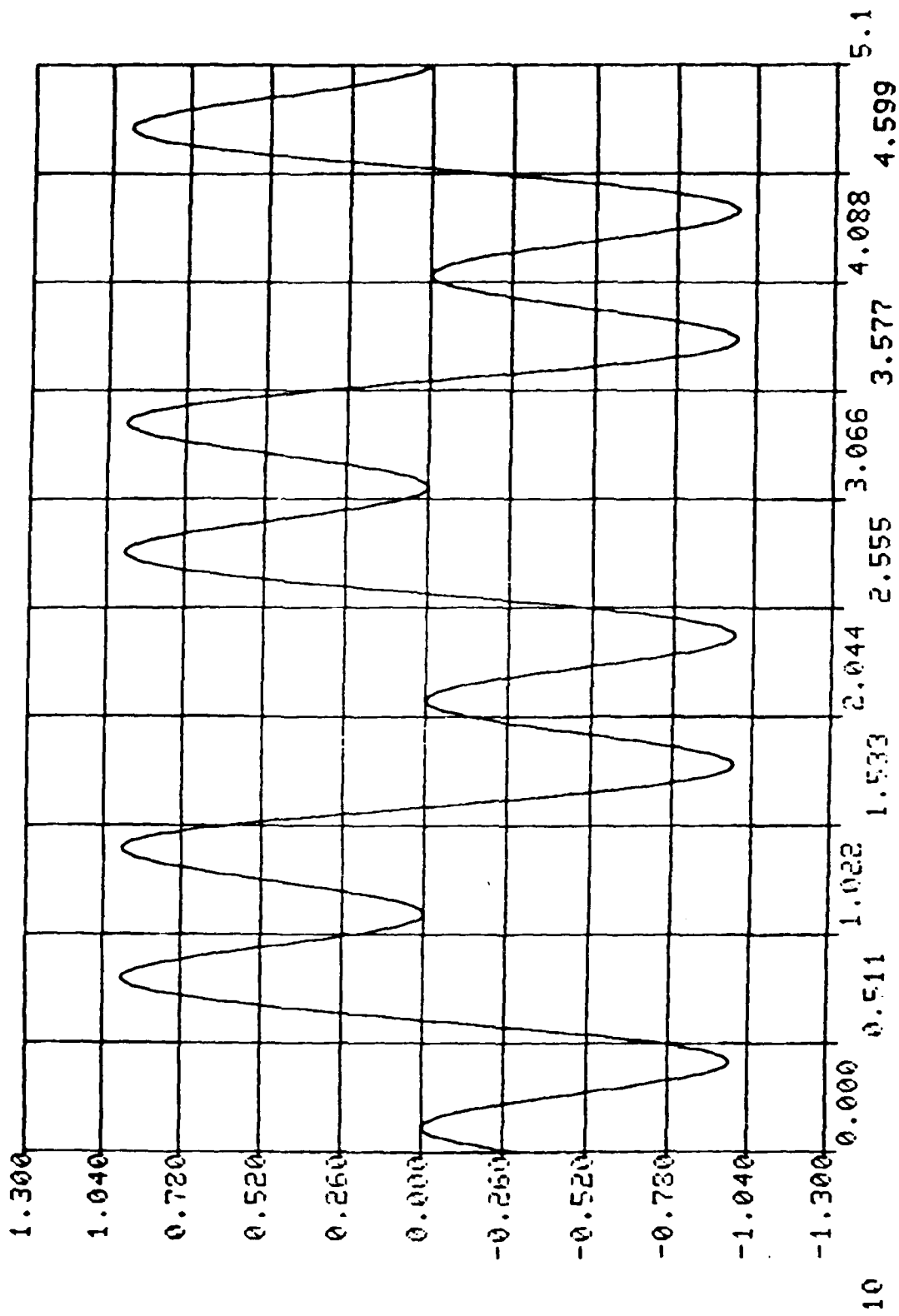


NOTES:

- $f_c = 1 \text{ GHz}$
 $f_d = 1 \text{ Gb/s}$
- LOWER IMPULSE SET CORRESPONDS TO ALIASED FREQUENCY COMPONENTS
- IDEAL SQUARE WAVE ASSUMED, i.e., THERE EXISTS AN INFINITE NUMBER OF TERMS
- VERTICAL AXIS NOT TO SCALE

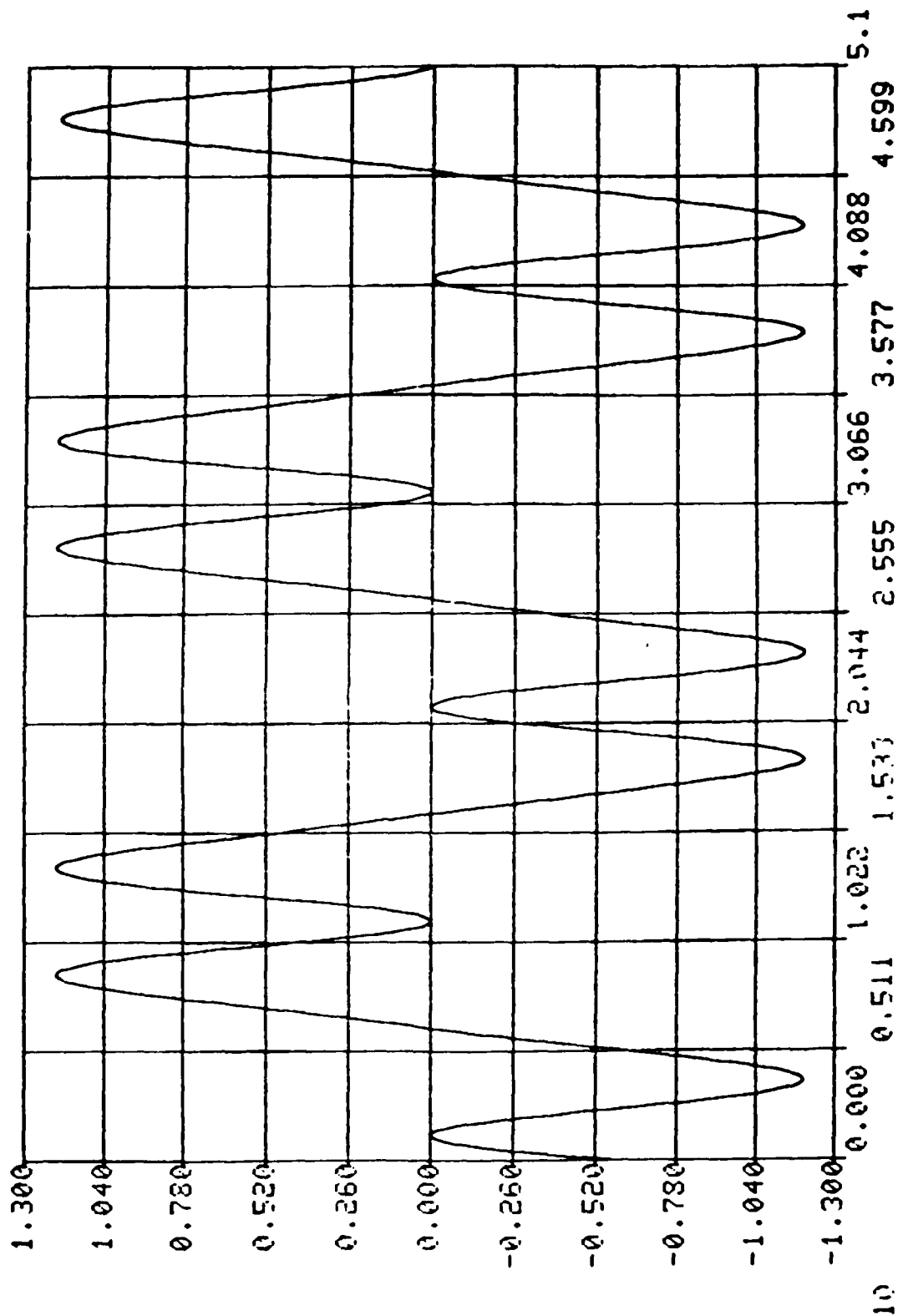
A90401-36

Figure 7.5.7-1. Aliased (One-Sided) Spectrum of a BPSK Signal With Square Wave Data Input



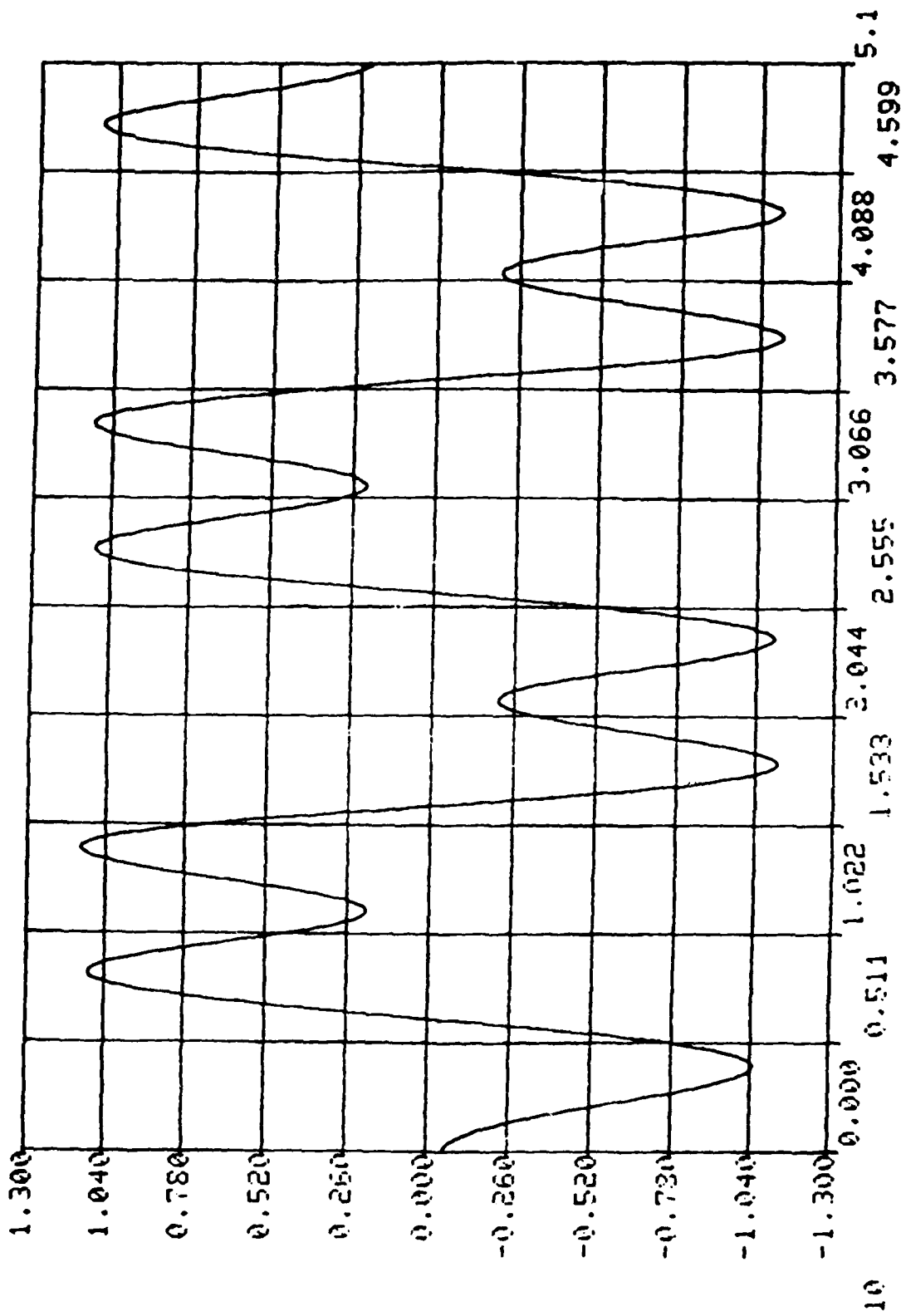
A90401-37

Figure 7.5.7-2. One Term Square Wave No Filtering



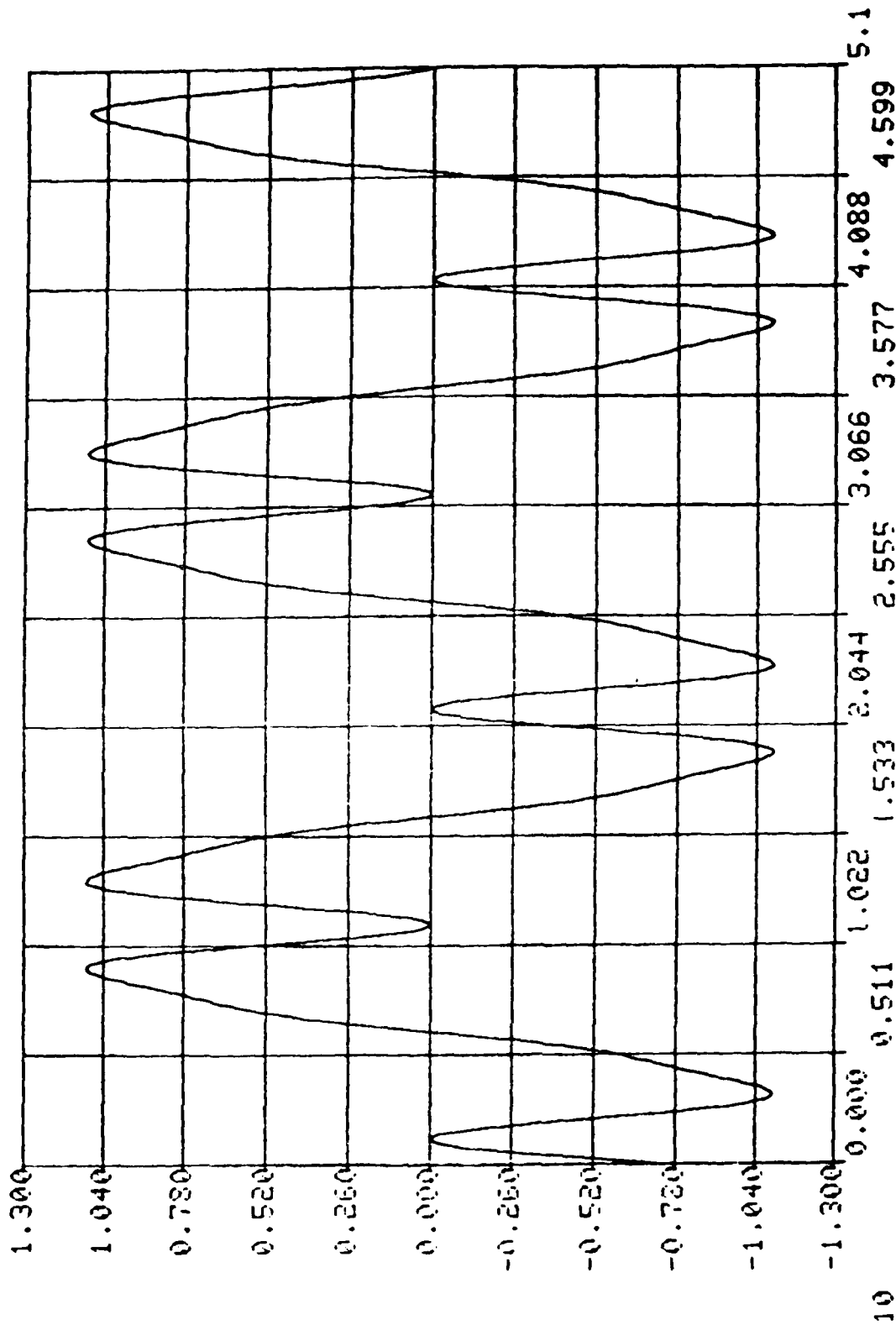
A90403-38

Figure 7.5.7-3. Two Term Square Wave No Filtering



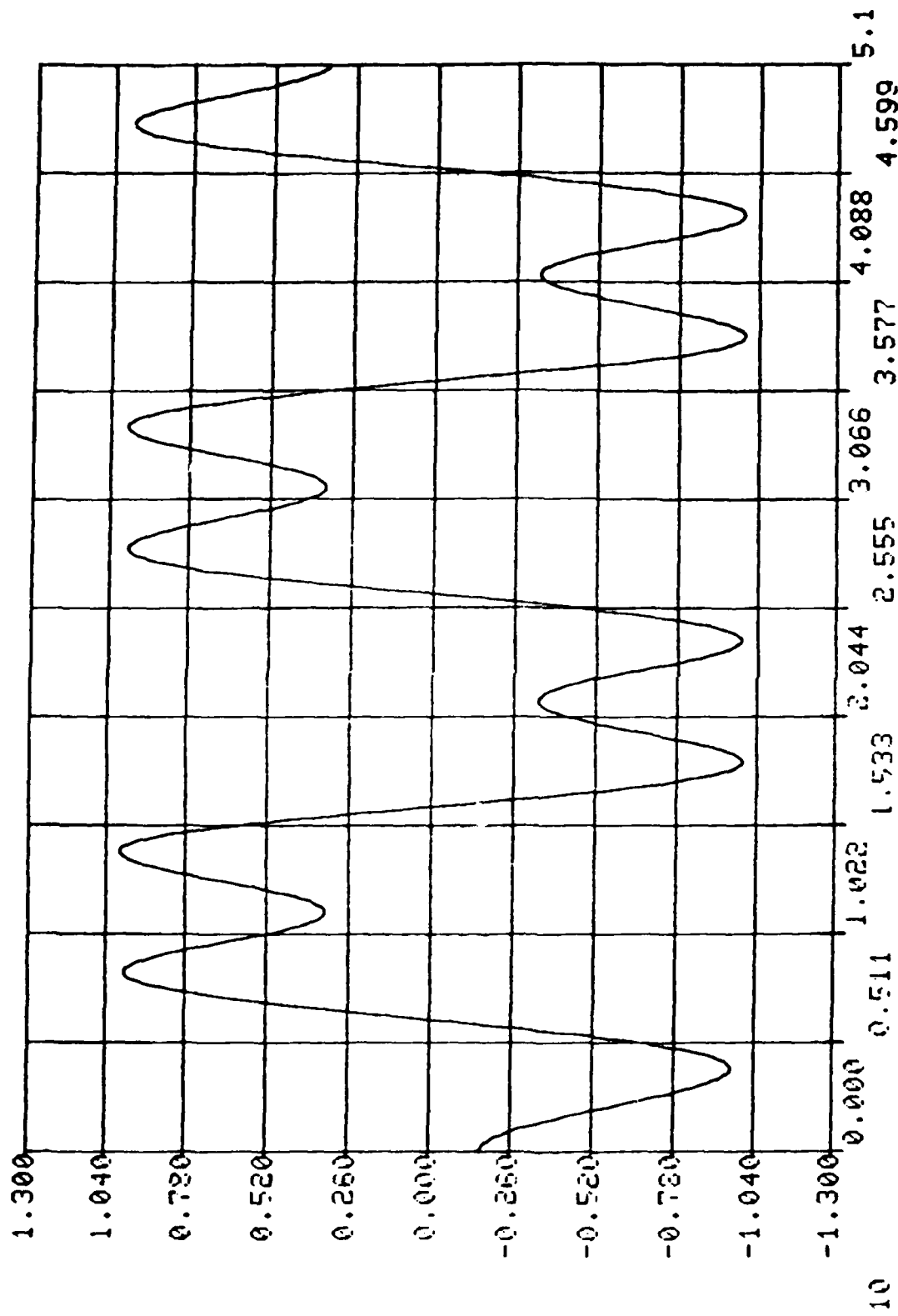
A90401-39

Figure 7.5.7-4. Two Term Square Wave $f_{cut} = 1.95$ GHz



A90401-40

Figure 7.5.7-5. Three Term Square Wave No Filtering



A90401-41

Figure 7.5.7-6. Three Term Square Wave $f_{cut} = 1.95$ GHz

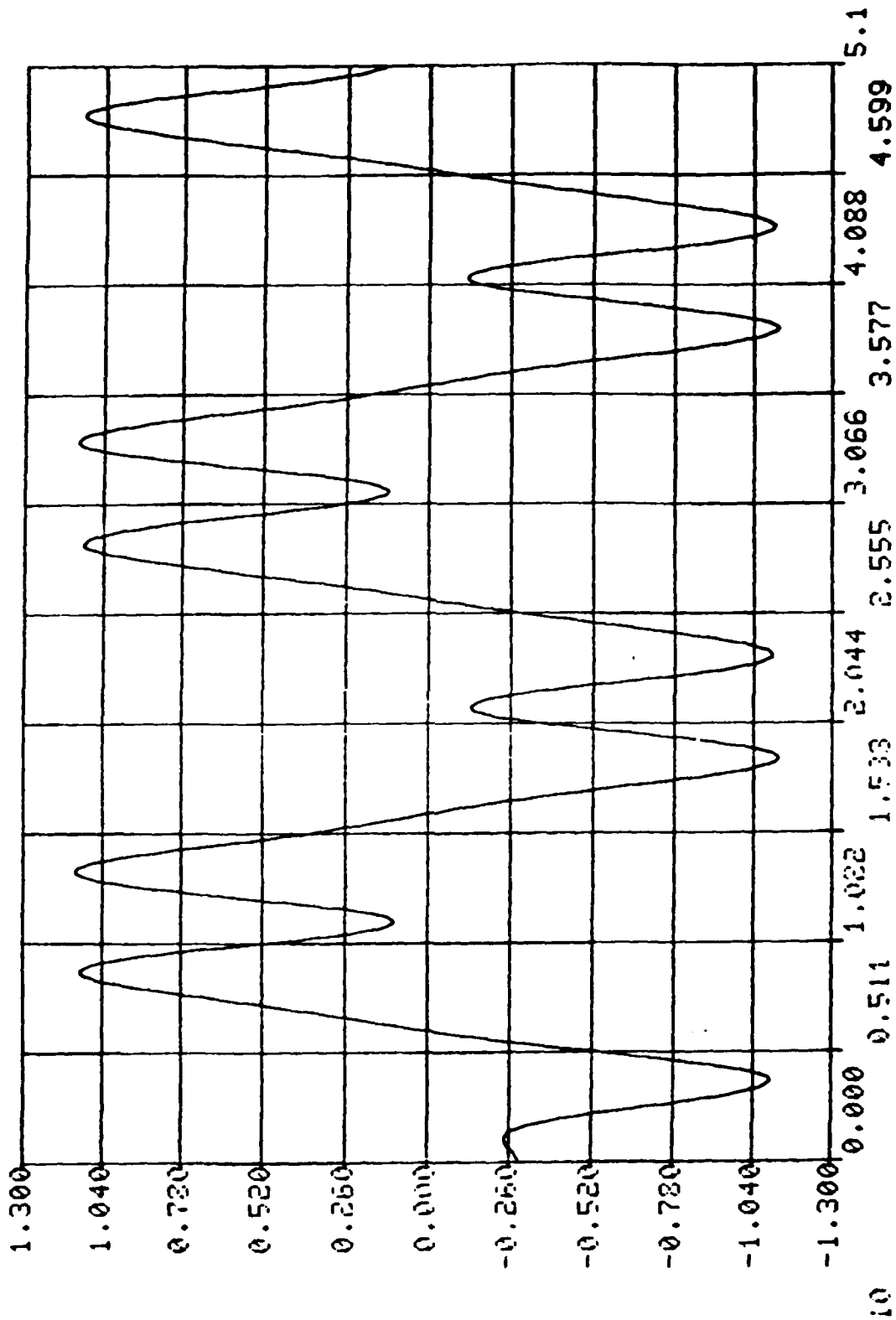
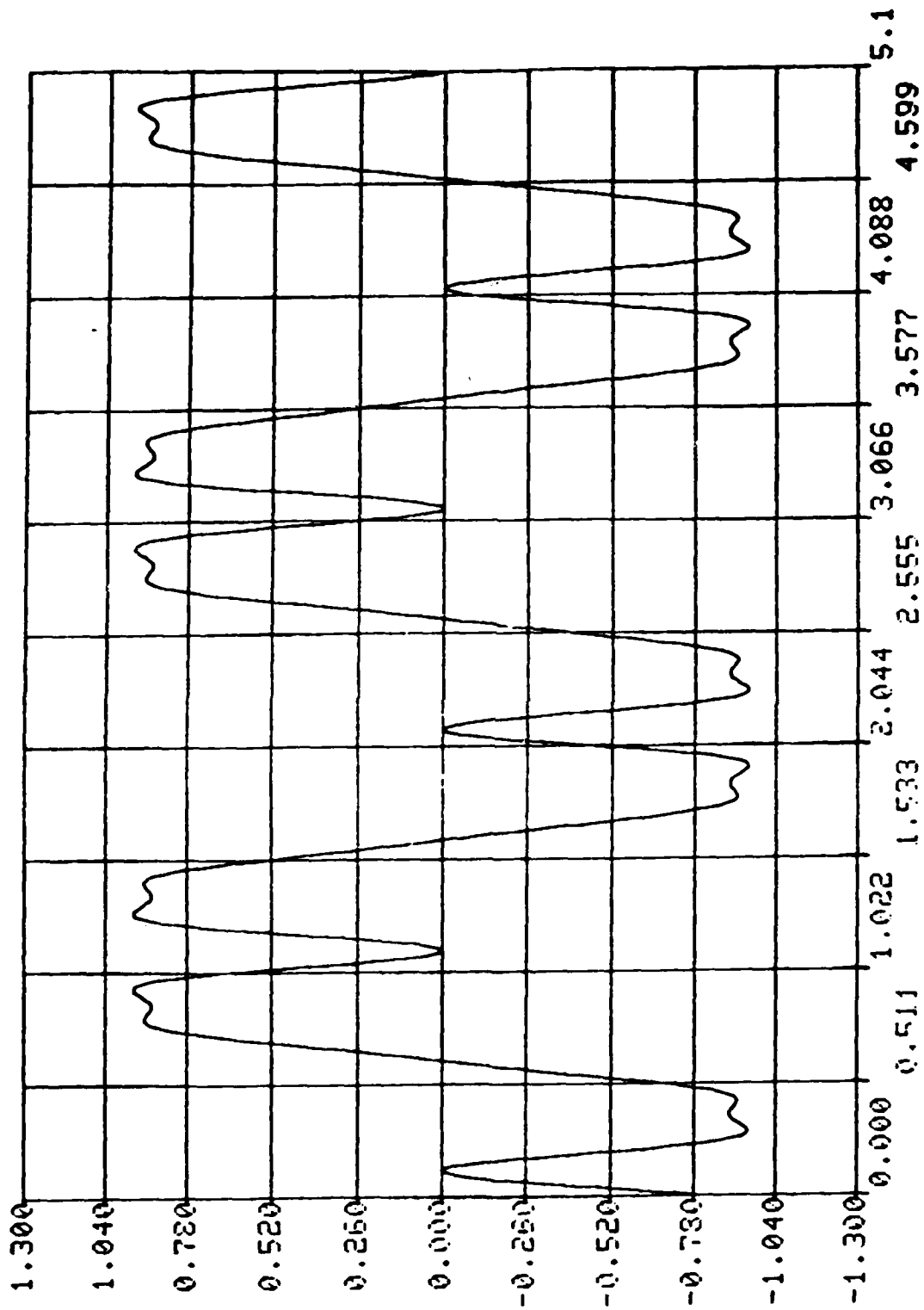


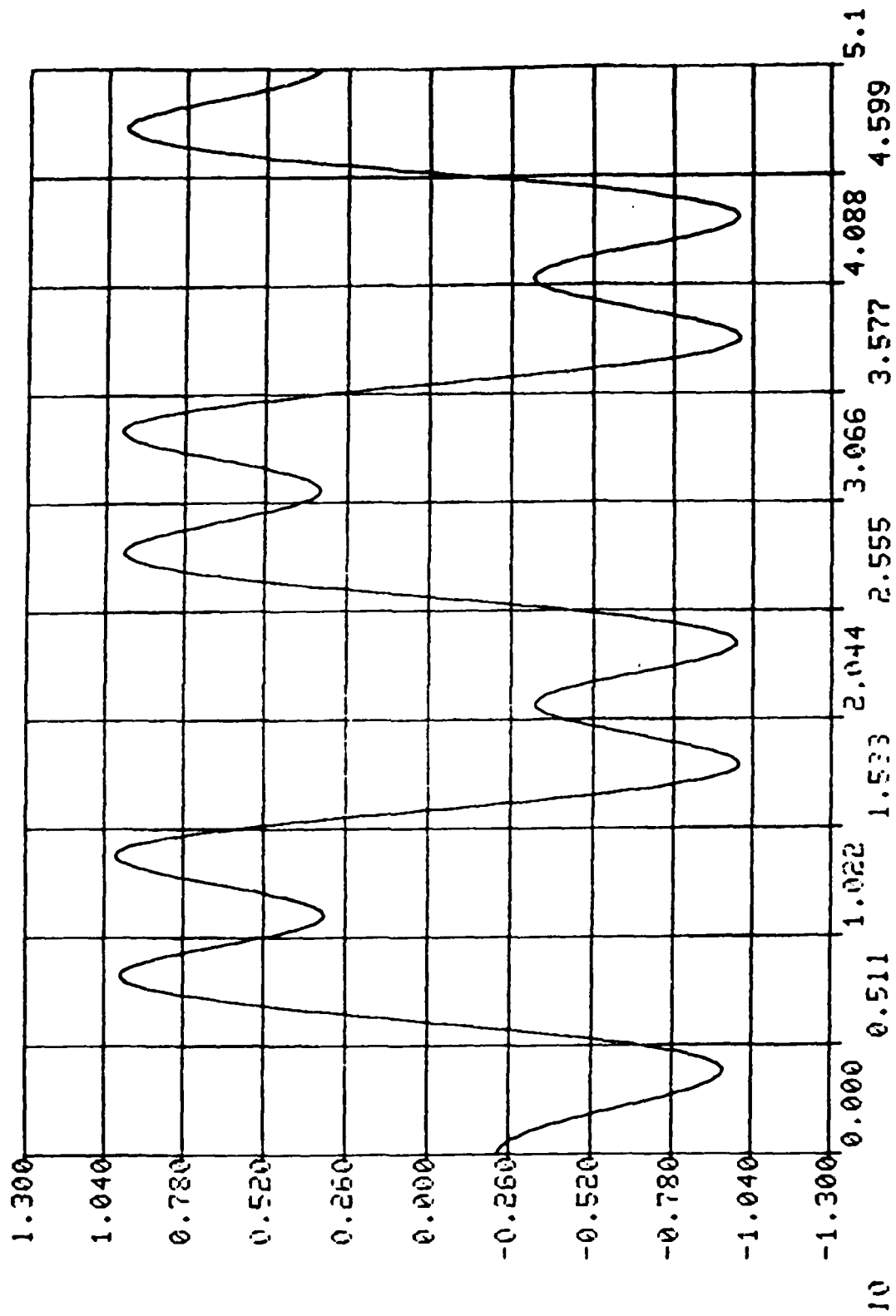
Figure 7.5.7-7. Three Term Square Wave $f_{cut} = 2.93$ GHz

A90401-42



A90401-43

Figure 7.5.7-8. Four Term Square Wave No Filtering



A90401-44

Figure 7.5.7-9. Four Term Square Wave $f_{cut} = 1.95$ GHz

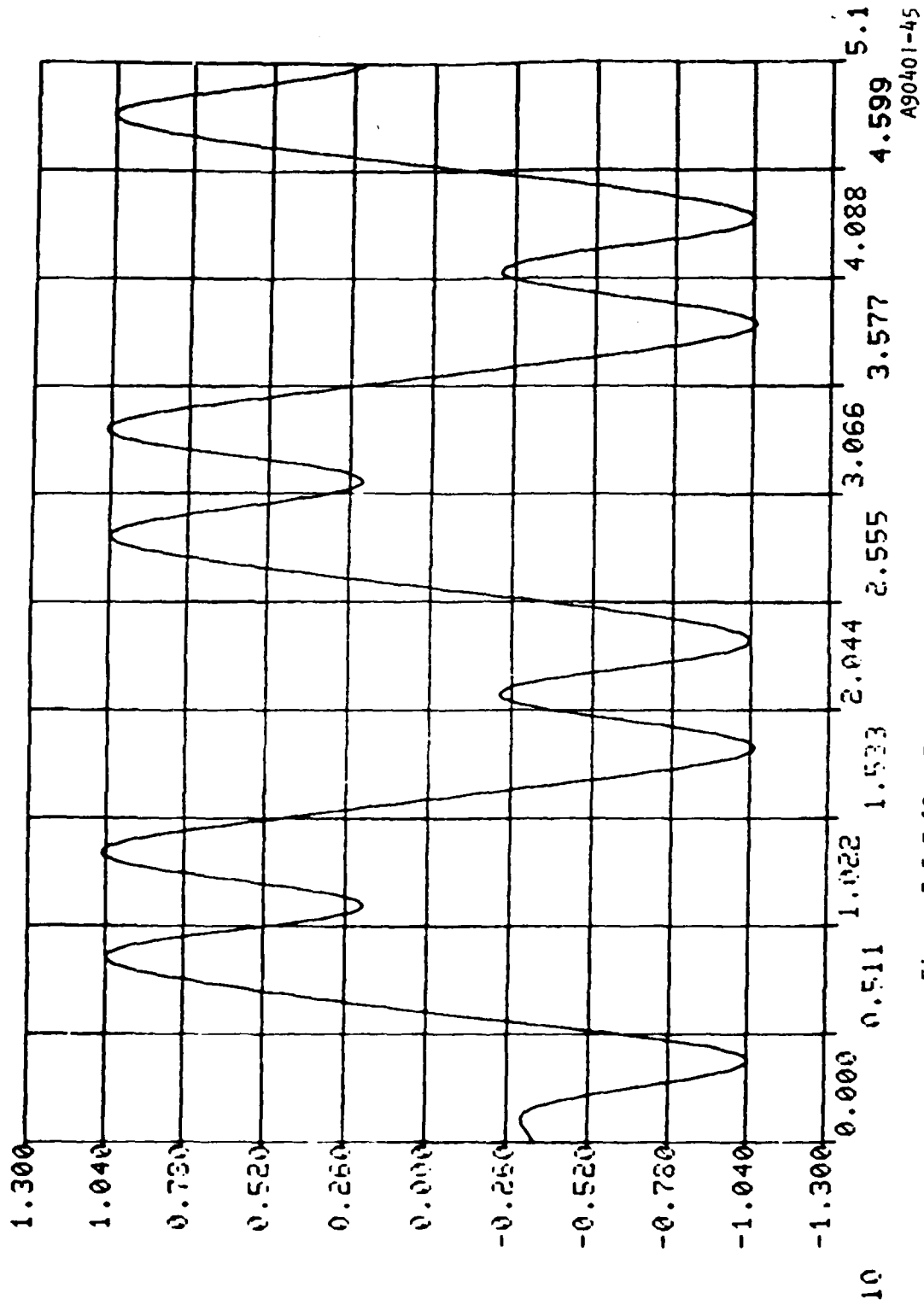


Figure 7.5.7-10. Four Term Square Wave $f_{cut} = 2.98$ GHz

```

    DIMENSION XX(1024),Y(1024),Z(1024)
    COMPLEX F(1024)
    NN=1024
    IC=0
3   CONTINUE
    FDATA=1.
    FCARR=1.
    DELTAT=0.1
    PI=3.1415927
    FN=0.
    READ(7,-) KMAX
    READ(7,-) NCUT
    DO 100 N=1,1024
    DO 200 K=1,KMAX,2
    X=4.*SIN(PI*K*(N-513)*DELTAT*FDATA)*SIN(2.*PI*FCARR*(N-513)*DELTAT
    Y)/(PI*FLOAT(K))
200  F=F+X
    F(N)=CMPLX(FN,0.)
    Y(N)=FN
100  FN=0.
    FLAG=-1.
    CALL FFT(F,10,1024,FLAG)
    NTOP=1024-NCUT
    DO 300 N=1,1024
    XX(N)=FLOAT(N-1)/(DELTAT*FLOAT(NN))
    IF ((N .GT. NCUT) .AND. (N .LE. (NTOP+1))) F(N)=CMPLX(Y(0),0)
    Z(N)=CABS(F(N))
300  CONTINUE
    CALL PLOTIT(1,512,XX(1),Z(1),0.,0.,0.,0.,0.,0.)
    FLAG=1.
    CALL FFT(F,10,1024,FLAG)
    DO 400 K=1,NN
    XX(K)=FLOAT(K-1)*DELTAT
    F(K)=F(K)/CMPLX(FLOAT(NN),0.)
    Z(K)=REAL(F(K))
400  CONTINUE
    CALL PLOTIT(1,512,XX(1),Y(1),0.,0.-1.3,1.3,0.,0.)
    CALL PLOTIT(1,512,XX(1),Z(1),0.,0.-1.3,1.3,0.,0.)
    IC=IC+1
    IF (IC .LT. 12) GO TO 3
    STOP
    END

```

SIZE 10559 24477

A90401-46

Figure 7.5.7-11. Computer Program Listing For Aliasing and Bandlimiting Effects Upon BPSK

The general trend in these computer plot figures show that bandlimiting the upper portion of the mixer output spectrum distorts the BPSK waveform. The quantity of interest is the *matched filter correlation* loss between the received waveform and the stored replica available at the receiver. While this correlation loss was not actually computed, it appears that the correlation loss due to bandlimiting distortion should not contribute an unacceptable degradation of system performance. The surprising result is that the distortion is not more severe than indicated in these figures.

7.6 Summary and Conclusions

In this section we examined link budget considerations and alternate routing techniques. In addition we surveyed AJ techniques and determined jamming effects at MMW frequencies. We examined the two components of total AJ protection for these techniques, viz., that due to spectrum spreading and the directivity of nonadaptive antennas. AJ protection obtained against main beam jammers via adaptive antenna arrays was treated in Section 6.0 and Appendix A and was not treated here. This section concluded with a brief treatment of various system considerations.

In view of the implementation limitations imposed by the relatively high data rates, viz., 1 Mb/s to 20 Mb/s, and 150 Mb/s, a QPSK direct sequence spread spectrum was selected as being most cost effective. Some details of the implementation of such a system were considered with emphasis upon the generation of very high PN chip rates via syncopation of PN generators.

Performance predictions in terms of total processing gain for this system at 8 GHz, and 38 GHz were presented assuming both 1 and 5 meter diameter dish antennas. These predictions assumed a CW jammer in order to lower-bound system performance for all jammer types since CW jammers are most effective against DS systems. Recall that the jam resistance or AJ capability of an AJ system is equal to the total processing gain in dB less the required E_b/N_0 in dB. The E_b/N_0 value as used in this expression is assumed to include any system (implementation) losses; also, the total processing gain is defined as the sum of the spread spectrum processing gain in dB and the nonadaptive antenna gain in dB.

The effects of atmospheric absorption and rain at MMW frequencies were described and their importance was illustrated by graphing net link gain at 38 GHz referenced to 8 GHz versus rainfall rate with link distance as a parameter. The implications of rain attenuation at MMW frequencies for jamming in the presence and absence of rain were briefly discussed.

The implications of the narrower beamwidths and higher gains of antennas used at MMW frequencies were discussed in terms of the concomitant lower probability of intercept and increased AJ protection. For the relatively small antenna diameters likely to be used, the antenna surface tolerance is not likely to be a problem.

The issue of coherence bandwidth of the MMW propagation medium was raised and the limitation on data rate due to coherence bandwidth was discussed. The results of MMW coherence bandwidth measurements were presented and interpreted. Finally, national and international spectrum allocations in the 21.2 GHz to 275 GHz band were presented.

Spread spectrum techniques are applicable at any radio frequency. The advantages of going from microwave frequencies to MMW frequencies are that wider channel bandwidths are available, there is less spectral congestion, and the increased antenna gain leads to LPI and higher AJ performance. The disadvantages are that atmospheric losses are somewhat

higher and rain losses are much higher than at microwave frequencies. For the most part, the devices and components needed to implement MMW systems are commercially available and the state-of-the-art of MMW technology should continue to rapidly advance.

For short to medium length links (<10 km) the MMW systems exhibit a net link gain in clear weather and light-to-moderate rainfall rate situations when compared to microwave systems. Although MMW systems exhibit a net loss in heavy rainfall rate conditions when compared to microwave systems, additional rain margin can ensure adequate availability for short or moderate length links.

8.0 HARDWARE ANALYSIS

The hardware analysis and design problems associated with high-capacity millimeter wave digital radio systems are presented in this section. It is interesting to note that the high data-rate millimeter wave digital radio for tactical applications, with AJ and LPI capabilities, allows a relatively large degree of freedom in hardware designs. Various AJ antennas, such as the adaptive null-steering array and sidelobe cancellor, and different spread spectrum modulation techniques, such as frequency-hopping (FH), pseudonoise (PN) spread spectrum and the FH-PN hybrid approach, are all considered to be feasible as a result of the hardware design effort. It is understandable that the more sophisticated modulation schemes require more effort and expensive electronic components. The rain attenuation in the millimeter wave frequency band demands a relatively large system margin, short hop-length, and increasing number of repeaters with short spacings in order to obtain a desired link availability. Therefore, due to many problems which are pertinent to millimeter-wave short-hop tactical systems, there is concern about the possibility of transmission capability being provided at a cost competitive to microwave links and with an adequate reliability.

To find a technique that permits transmission through a large number of regenerative (active) and/or passive repeaters with very low distortion and low hardware cost, a first choice that must be made in the design of digital systems is the most suitable modulation method. The choice is determined by the available bandwidth and the error rates obtained for given carrier/noise ratios. Both modulation techniques and error rate calculations are discussed later in this section providing a start point for the determination of major system parameters, fade margin, and repeater spacing.

The problem of efficient bandwidth utilization must be considered in parallel with hop-length calculations. When the modulation method has been selected, filters must be chosen that allow minimum passband distortion and limit the adjacent channel interference as well.

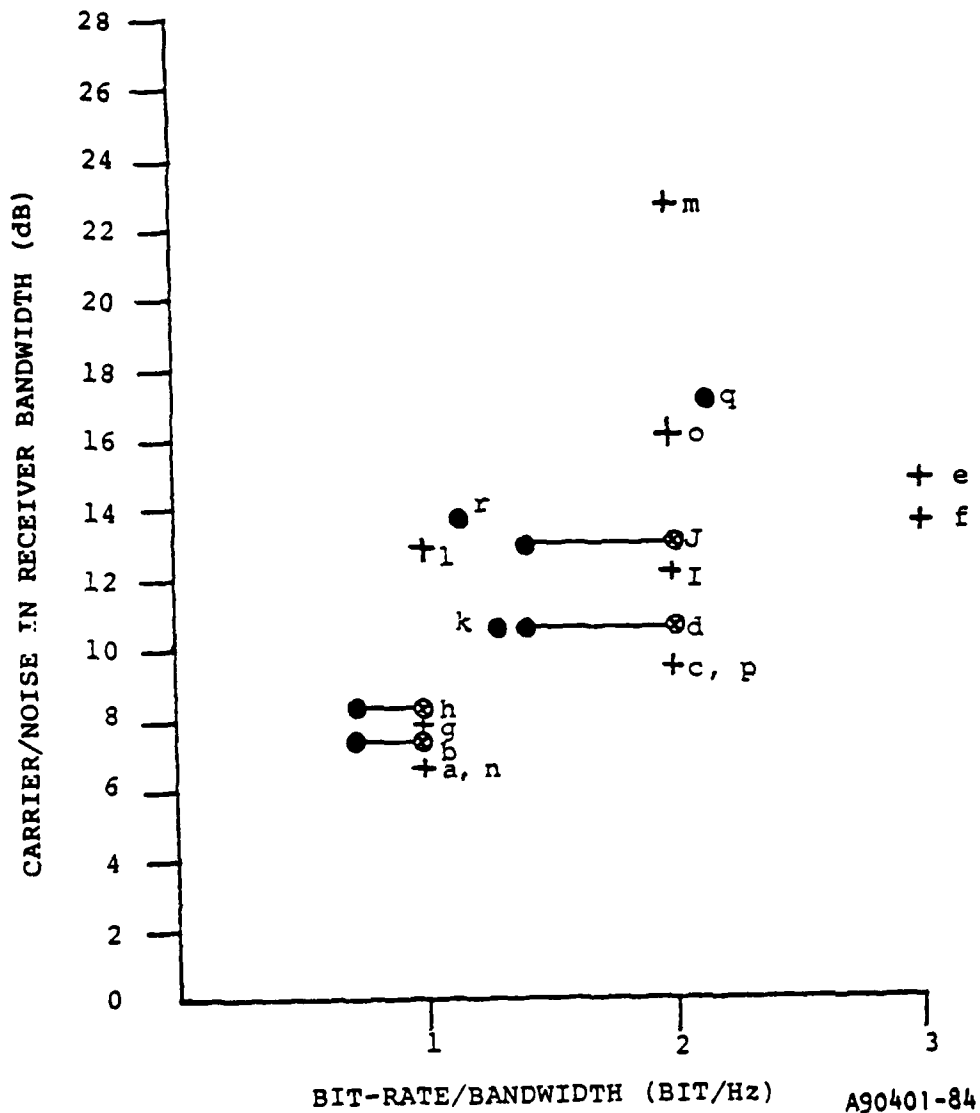
8.1 System Considerations

8.1.1 Modulation Method Consideration

It is well known that the two following major factors should be considered in the selection of the modulation scheme for a digital radio system:

- a. The BER achieved for a given received carrier/noise ratio.
- b. The bandwidth required for a given bit rate to be transmitted.

Comparative performance of several different modulation methods is illustrated in Figure 8.1.1. It is obvious that of these methods coherent phase shift keying (CPSK) modulation requires the lowest carrier/noise ratio of 1 bit/Hz.



- + IDEAL NOISE FILTER, NO INTERSYMBOL INTERFERENCE
- x PRACTICAL RECEIVER FILTERS, ADJACENT CHANNELS NOT CONSIDERED
- o PRACTICAL FILTERS, ADJACENT CHANNELS CONSIDERED
- a, b 2-PHASE CPSK
- c, d 4-PHASE CPSK
- e 8-PHASE CPSK
- f 8-STATE CAPM
- g, h 2-PHASE DCPSK
- i, j 4-PHASE DCPSK
- k 2-STATE FSK: OPTIMUM DEVIATION
- l 2-LEVEL AM FULL CARRIER,
- m 4-LEVEL AM COHERENT DETECTION
- n 2-LEVEL AM SUPPRESSED CARRIER,
- o 4-LEVEL AM COHERENT DETECTION
- p 2-LEVEL QAM
- q QPRS
- r BPRS

Figure 8.1.1. Comparative Performance of Different Modulation Methods for a BER of 10^{-3}

8-3

8.1.2 Calculation of Error Probabilities

For systems using coherent detection, the probability of symbol error in the presence of Gaussian noise rms level is calculated with reference to the decision boundaries between signal states. Assuming all signal states equally likely, then the average error probability will be:¹

$$\begin{aligned}
 P_e &= \frac{1}{n} \sum_{j=1}^n \left\{ 1 - \iint_{A_j} \frac{1}{2\pi\sigma^2} \exp \left\{ -\frac{|\underline{r} - \underline{S}_j|^2}{2\sigma^2} \right\} d\underline{r} \right\} \\
 &= 1 - \frac{1}{n} \sum_{j=1}^n \left\{ \iint_{A_j} \frac{1}{2\pi\sigma^2} \exp \left\{ -\frac{|\underline{r} - \underline{S}_j|^2}{2\sigma^2} \right\} d\underline{r} \right\} \quad (8.1.1)
 \end{aligned}$$

Where \underline{S}_j is the signal state enclosing an area A_j .

In the presence of intersymbol interference, the signal states are no longer single points and may be represented by:

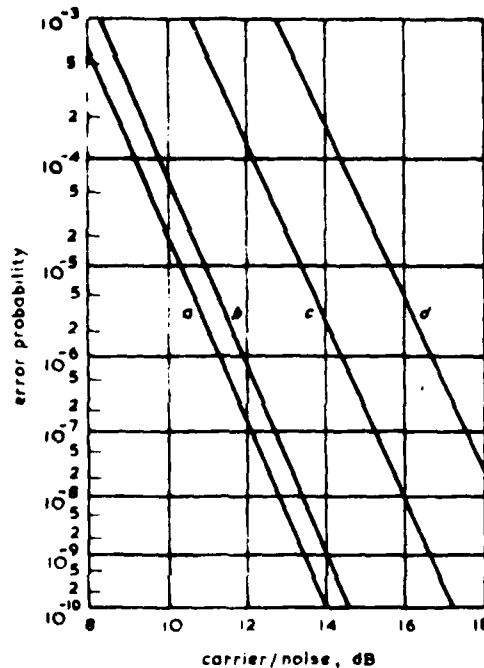
$$\underline{S}_j + \underline{Z}_j$$

Where \underline{Z}_j is a random vector describing the distortion introduced from the adjacent pulses. Then, the average error probability becomes:

$$P_e = 1 - \left\{ \sum_{j=1}^n \int p(z_j) \iint_{A_j} \frac{1}{2\pi\sigma^2} \exp \left\{ -\frac{|\underline{r} - \underline{S}_j - \underline{Z}_j|^2}{2\sigma^2} \right\} d\underline{r} d\underline{Z}_j \right\} \quad (8.1.2)$$

¹G.M. Thomas, M.Y. Weidner and S.H. Durrani "Digital Amplitude - Phase Keying With M-ary Alphabets," IEEE Trans on Com. 1974, pp. 168-180.

Using these techniques of calculation, Figure 8.1.2 exhibits curves of BER against C/N for 2- and 4- level CPSK and DCPSK (differential CPSK) which are often used in high data rate digital radio. The curves also display the characteristics of how the probability of errors decreases very rapidly as C/N increases. From Figure 8.1.2, it is also realizable that there is negligible distortion, regardless of the number of repeaters, if the C/N is maintained.



- a = 2-level CPSK
- b = 4-level CPSK
- c = 2-level DCPSK
- d = 4-level DCPSK

Figure 8.1.2. Error Probability Curves of 2- and 4-Level CPSK and DCPSK

8.1.3 Frequency Selection

8.1.3.1 Introduction

Although the frequency allocation for the millimeter wave spectrum i.e., from 30 to 300 GHz, is not yet defined, there is a tentative spectrum assignment between 30 to 90 GHz. As seen in Table 8.1.3.1, 36.0 to 38.6 GHz was allocated for government fixed/mobile services. By referring to previous sections where the problem of millimeter wave communication associated with atmospheric and rain attenuation has been treated, Figure 2.1.1 indicates that 36.0 to 38.6 GHz band falls within the "window" band where the water and oxygen attenuation are relatively low.

Table 8.1.3.1. Spectrum Allocations for Frequency Above 30 GHz

36.0-38.6 GHz	Government Fixed/Mobile Services
30.0-31.3 GHz	Nongovernment Fixed/Mobile Services
38.6-40.0 GHz	Nongovernment Fixed/Mobile Services
31.8-32.3 GHz	Space Research
34.2-35.2 GHz	Space Research
31.5-31.8 GHz	Fixed/Mobile Services
30.0-33.4 GHz	Radio Astronomy Services, Radio Navigation
88.0-90.0 GHz	Radio Astronomy Services

Another advantage in utilizing the 36.0 to 38.6 GHz band is that the radio frequency front-end hardware, e.g., LNA's, mixer, HPA, is readily available in this range and its fabrication is rapidly becoming a maturing technology.

8.1.3.2 System Bandwidth Consideration

A bit rate of 20 Mb/s or 100 Mb/s for the communication link is assumed. In order to enhance the system security, a PN spread technique is proposed. With the advent of the GaAs technology, gigabits logic integrated circuit techniques can be incorporated into the system design.

8.1.3.3 Determination of Intermediate Frequencies (IF)

The actual selection of intermediate frequencies will be a compromise between the requirement for spurious rejection and other requirements such as image rejection, IF rejection, bandwidth and industry standards. The choice between single and dual conversion stage will influence the IF selection.

8.1.3.3.1 1 GHz IF Bandwidth

The proposed operating frequency for the system is 36.0 to 38.6 GHz which will provide a number of combinations for non-overlapping receiving/transmitting frequencies. For example, the receiving frequency may be centered at 36.5 GHz and transmitting frequency may be centered at 37.5 GHz with 1 GHz operating bandwidth. The IF selection is rather straightforward in this case, although attention should be given to the image rejection and IF rejection problems.

8.1.3.3.2 2 GHz IF Bandwidth

In the case where the 2 GHz bandwidth is required, it is obvious that the transmit and receive frequencies will be the same or overlapped. Since the bandwidth is 2 GHz, the IF bandwidth should be chosen in a way such that it will not be more than an octave bandwidth. The reason is that it would result in imposing some impractical specifications on the IF equipment such as the gain flatness, phase linearity, intercept points' ... just to name a few. It would be rather an easy task to fabricate a 2 to 4 GHz amplifier; however, to operate an amplifier reasonably well between 100 MHz and 2100 MHz could be difficult.

8.1.3.3.3 Single or Dual Conversion

The single conversion has an inherent advantage of being simple and economical to build. Dual conversion does provide a more superior image and IF rejection. Moreover, fine tuning and automatic frequency control can be accomplished in the second oscillator, and the second IF can be selected for optimum bandpass filter and demodulation performance. The major disadvantage of dual conversion is the greatly increased probability of spurious signal generation. The dual conversion downconverter is more subject to the presence of spurious outputs than the single conversion equipment. This problem is even more severe when the local oscillators use either frequency multiplying or phase lock techniques and the basic frequency is around 100 MHz. A summary of comparison between single and dual conversion is tabulated in Table 8.1.3.3.3.

Table 8.1.3.3.3. Pros and Cons of Single and Dual Conversion Scheme for 36-38.6 GHz Band

Single Conversion	Dual Conversion
Bandpass filter required to achieve good image rejection	Good image rejection
Low probability for in-band spurs	High probability for in-band spurs
Conversion hardware include one LO and one mixer	Conversion hardware doubled
IF rejection fair	Better IF rejection

8.1.3.3.4 Inspection of Spurious-Free IF Bandpass Spectra

Figures 8.1.3.3.4-1 and 8.1.3.3.4-2 depict the frequency plan for the single and dual conversion schemes. The first and second (in the case of dual conversion) intermediate frequencies which produce few or no measurable spurious products within the desired IF bandwidth may be determined by mathematical analyses. This approach has a serious shortcoming: it yields only discrete solutions for discrete conditions; however, it does provide the system designers a general idea of any in-band spurs for the IF frequencies chosen.

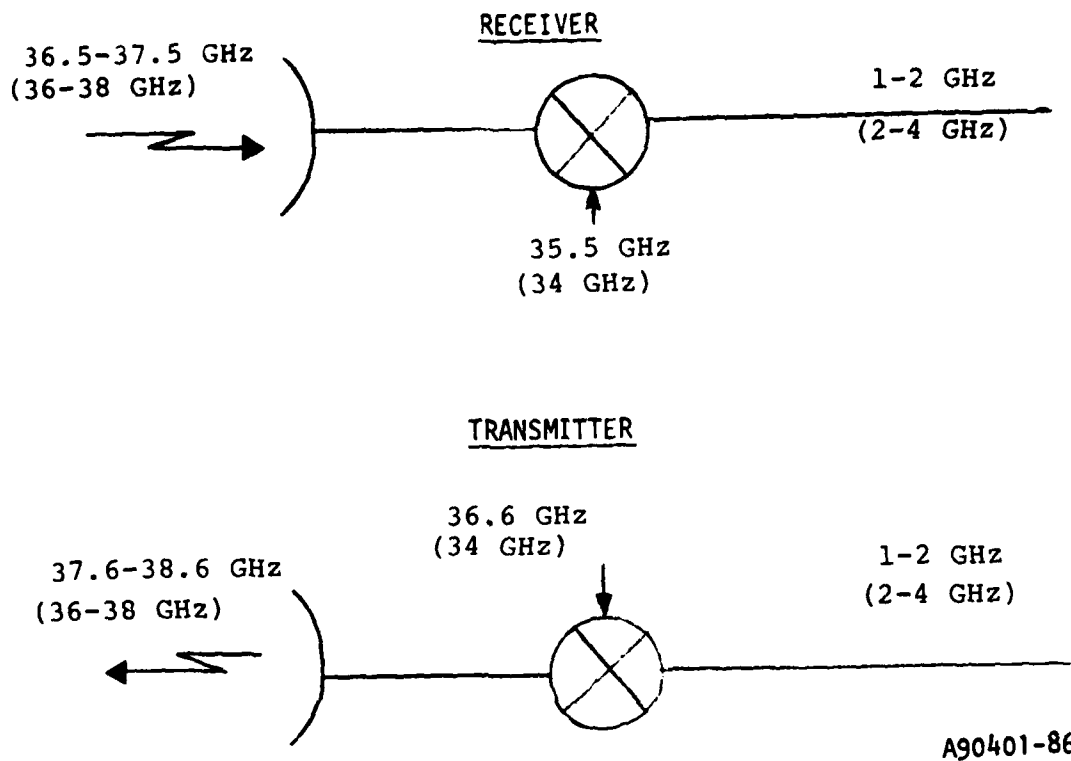
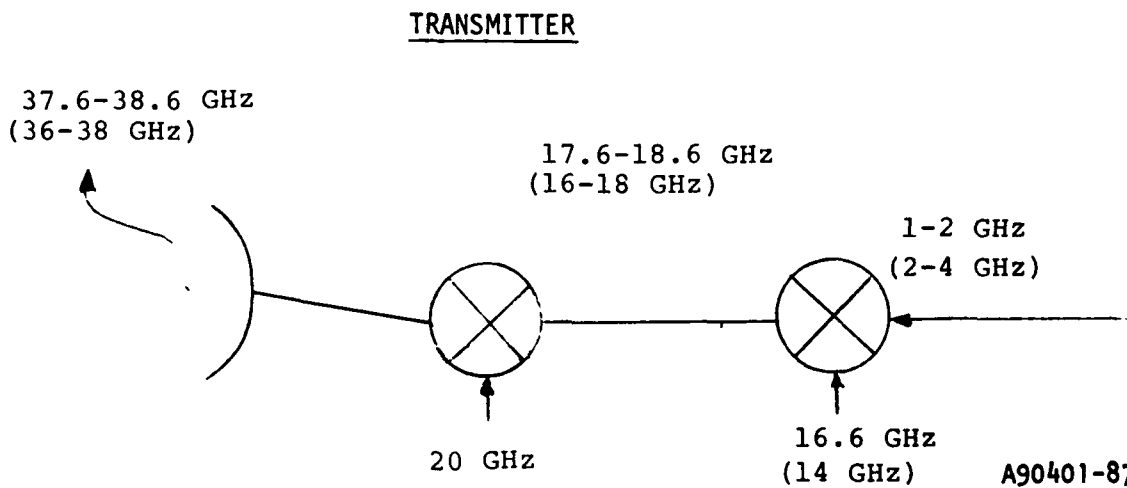
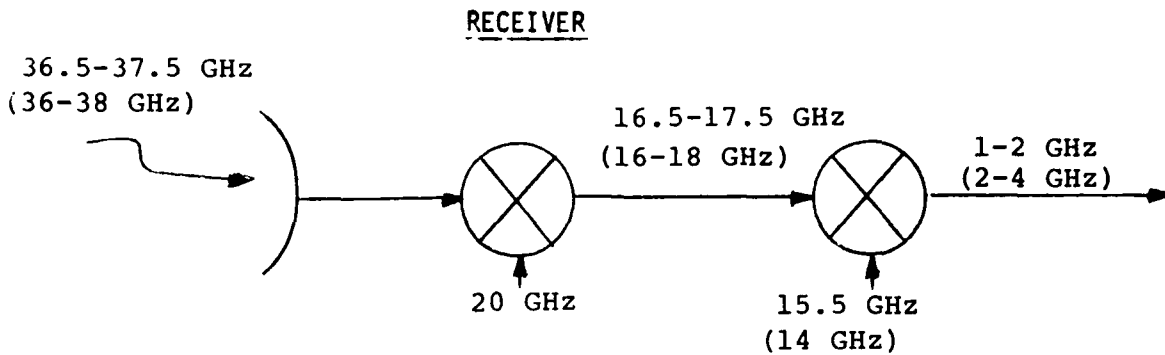


Figure 8.1.3.3.4-1. Single Conversion Frequency Plan
 IF BW = 1 GHz
 (IF BW = 2 GHz)



A90401-87

Figure 8.1.3.3.4-2. Dual Conversion Frequency Plan
 IF BW = 1 GHz
 (IF BW = 2 GHz)

8.1.3.3.5 In-Band Spurs Calculation

A computer program called "Spur Analysis" was used to compute the in-band spurs in a particular combination of local oscillator frequency (LO) and intermediate frequencies. Figures 8.1.3.3.5-1 through 8.1.3.3.5-3 show the printouts of the in-band spurs for the single and dual conversion, respectively.

SPUR=ABS (MF1-NF2) DISPLAY=M.N V1.0		SPUR=ABS (MF1-NF2) DISPLAY=M.N V1.0	
36.	=F1	36.5	=F1
38.	=F1	37.5	=F1
34.	=F2	35.5	=F2
34.	=F2	35.5	=F2
2.	=F3	1.	=F3
4.	=F3	2.	=F3
1.		1.	
2.		2.	
1.01	SPUR	1.01	SPUR
2.00	THRU	1.00	THRU
4.00		2.00	
3.		3.	
4.		4.	
5.		5.	
6.		6.	
7.		7.	
8.		8.	
9.		9.	
10.		10.	
11.		11.	
12.		12.	
13.		13.	
14.		14.	
15.		15.	
16.		16.	
17.		17.	
8.09	SPUR	18.	
2.00	THRU	19.	
18.00		20.	
18.		21.	
19.		22.	
9.10	SPUR	23.	
-2.00	ZERO		
16.00			
20.			
21.			
10.11	SPUR		
-6.00	ZERO		
14.00			
(A) 2 GHz Bandwidth		(B) 1 GHz Bandwidth	

Figure 8.1.3.3.5-1. Single Conversion In-Band Spur Calculator Printouts

SPUR=ABS (MF1-NF2) DISPLAY=M.N V1.0	SPUR=ABS (MF1-NF2) DISPLAY=M.N V1.0	SPUR=ABS (MF1-NF2) DISPLAY=M.N V1.0
36. =F1	19.	12.
38. =F1	7.12 SPUR	13.
20. =F2	12.00 THRU	6.07 SPUR
20. =F2	26.00	-2.00 ZERO
16. =F3		10.00
18. =F3	20.	
	21.	14.
1. =F1	16. =F1	15.
2. =F1	18. =F1	7.08 SPUR
1.01 SPUR	14. =F2	0.00 THRU
16.00 THRU	14. =F2	14.00
18.00	2. =F3	
	4. =F3	16.
3.		7.09 SPUR
4.	1.	0.00 THRU
5.	2.	14.00
6.	1.01 SPUR	
7.	2.00 THRU	17.
8.	4.00	8.09 SPUR
9.		2.00 THRU
10.	3.	18.00
11.	4.	
12.	5.	18.
13.	6.	8.10 SPUR
14.	7.	-4.00 ZERO
15.	3.04 SPUR	12.00
5.10 SPUR	2.00 THRU	
10.00 THRU	8.00	
20.00	8.	
	9.	
16.	4.05 SPUR	
6.10 SPUR	-2.00 ZERO	
16.00 THRU	6.00	
28.00		
	10.	
17.	11.	
18.	5.06 SPUR	
6.12 SPUR	-4.00 ZERO	
12.00 THRU	6.00	
24.00		

Figure 8.1.3.3.5-2. Double Conversion In-Band Spur Calculator Printout (1 GHz BW)

SPUR=ABS (MF1-NF2) DISPLAY=M.N V1.0		SPUR=ABS (MF1-NF2) DISPLAY=M.N V1.0	
36.5	=F1	16.5	=F1
37.5	=F1	17.5	=F1
20.	=F2	15.5	=F2
20.	=F2	15.5	=F2
16.5	=F3	1.	=F3
17.5	=F3	2.	=F3
1.		1.	
2.		2.	
1.01	SPUR	1.01	SPUR
16.50	THRU	1.00	THRU
17.50		2.00	
3.		3.	
4.		4.	
5.		5.	
6.		6.	
7.		7.	
8.		8.	
9.		9.	
10.		10.	
11.		11.	
12.		12.	
13.		13.	
14.		14.	
15.		15.	
5.10	SPUR	7.08	SPUR
12.50	THRU	1.50	THRU
17.50		8.50	
16.		16.	
17.		17.	
18.		8.09	SPUR
6.12	SPUR	-0.50	ZERO
15.00	THRU	7.50	
21.00		18.	
19.		19.	
7.12	SPUR	9.10	SPUR
15.50	THRU	-2.50	ZERO
22.50		6.50	
20.		20.	

Figure 8.1.3.3.5-3. Double Conversion In-Band Spur Calculator Printout (1 GHz BW)

In the printout,

F1 | RF Input Frequency Range
F1 |

F2 | LO Frequency
F2 |

F3 | IF Frequencies
F3 |

M - is the multiplier of the RF frequency

N - is the multiplier of the LO frequency

For example, in Figure 8.1.3.3.5-1, the single conversion case,

RF frequency is from 36 to 38 GHz

LO frequency is 34 GHz

IF frequency is 2 to 4 GHz

The seventeenth order spur is $M = 8$, $N = 9$, and the spur ranges from 2 to 18 GHz which covers the desired IF passband of 2 to 4 GHz.

Referring to the same printout, the nineteenth order spur zero implies that the spur range crosses zero frequency.

A summary of the in-band spur analysis is tabulated in Tables 8.1.3.3.5-1 and 8.1.3.3.5-2 for the 1 GHz and 2 GHz bandwidth single/dual conversion, respectively.

Table 8.1.3.3.5-1. Spur Analysis Summary (IF BW = 1 GHz)

Single Conversion	Dual Conversion					
	First IF In-band Spur			Second IF In-band Spur		
	M	N	Order	M	N	Order
No Spur Up To Twenty-Second Order	5	10	15	7	8	15
	6	12	18	8	9	17
	7	12	19	9	10	19

Table 8.1.3.3.5-2. Spur Analysis Summary (IF BW = 2 GHz)

Single Conversion			Dual Conversion					
			First IF In-band Spur			Second IF In-band Spur		
M	N	Order	M	N	Order	M	N	Order
8	9	17	5	10	15	3	4	7
9	10	19	6	10	16	4	5	9
			6	12	18	5	6	11
			7	12	19	6	7	13
						7	8	15
						7	9	16
						8	9	17
						8	10	18

8.1.3.4 Spurs Other Than IF In-Band's

8.1.3.4.1 Spurious Output Generation Mode

Spurious outputs can be generated in any nonlinearity in the downconverter or they can inadvertently be fed to the transmission path through the local oscillators. Although the nonlinearity in amplifiers and mixers, phase characteristics of the filters, and the spectral purity of signals from local oscillators affect the spurious output of the downconverter, only the mixers and the LO's will be discussed here since they are the major spur-related items.

Two types of interfering signals are possible in the downconverter, i.e., spurious response and spurious signal. Spurious response is meant to be those outputs involving the input RF carrier but which appear at the downconverter output other than the desired carrier. There are four major types of spurious responses; they are 1) undesired mixing products in the first mixer, 2) undesired spurious signal coming from the first LO which can mix with RF carrier to cause a spurious response, 3) undesired mixing product in the second mixer, and 4) undesired spurious signal coming from the second LO which can mix with the undesired carrier in the first IF stage to cause a spurious response. Spurious signals are those undesired output which can come from the local oscillators but do not involve the input RF carrier. The spurious signals come in the form of: 1) spurious outputs of the first LO which can be mixed down to cause a spurious output; 2) spurious outputs of the first LO which can appear at the first IF stage; 3) spurious outputs of the second LO which can be mixed down to cause a spurious output; and 4) spurious outputs of the second LO which can appear at the second IF stage.

8.1.4 Repeater Spacing

Under normal propagation conditions, the probability of error, as described in Section 8.1.2, is completely dependent upon the received C/N. However, especially for millimeter waves, the propagation condition changes with precipitation state which degrades C/N. This means that there is always a large degree of uncertainty in the digital radio system performance. The rain effects and system design procedure have been described in relative detail in Section 2.0. The fade margin is defined as follows for standard radio systems:

Fade Margin = Transmitter output power

- C/N (for given error rate)
- Receive noise factor
- Basic transmission loss
- Fixed and feed losses
- + Path antenna gain
- $10 \log_{10} (kT)$
- $10 \log_{10} (\text{symbol rate})$

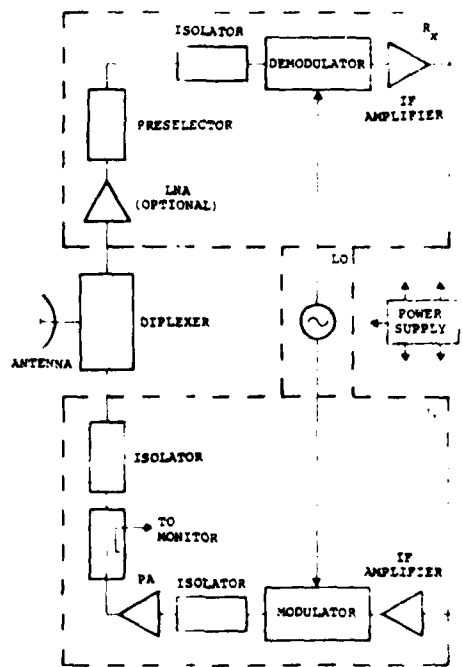
If a repeater (or repeaters) is utilized in the system design, then the term of "Path Antenna Gain" shall include the repeater (or repeaters) gain. Then the repeater spacing can be optimized according to geometrical, link architecture and jamming information. Multipath fades have an additional effect on system performance compared with rain fades, as briefly mentioned in Section 4.0, owing to their frequency-selective nature which can enhance interchannel interference. This affects frequency planning if millimeter wave/microwave diversity is used (See Section 4.0).

8.2 Nodal Terminal

8.2.1 Transmitter/Receiver Components Consideration

The block diagram of the millimeter wave radio transmitter and receiver is depicted as Figure 8.2.1-1. The transmitter consists of HPA, HPA driver, modulator, local oscillator (LO), filter, isolator, etc.; and the receiver includes low noise amplifier (LNA), demodulator, LO, filters, isolators, clock, etc. In order to minimize the physical size/weight, reduce the fabrication cost and improve system reliability, the following steps are recommended in the hardware design:

- Use microstrip configuration instead of rectangular metallic waveguide.
- Use MESFET or InP Gunn Diode LNA instead of bulky, expensive parametric amplifier.
- Use solid-state HPA instead of large size tubes (TWT, Klystron, etc.) and also simplify the HPA control and cooling systems.



A90401-91

Figure 8.2.1-1. Block Diagram of Millimeter Wave Transmitter/Receiver

Before the discussion of using solid-state devices for the transmitter and receiver (Tx/Rx) application, some emphasis has to be devoted to the local oscillator. The LO is the heart of the Tx/Rx. Compared with most analog systems, an advantage of digital systems, using baseband regeneration at every repeater, is that the local oscillator deviations are not transmitted from hop to hop. Taking this into consideration, together with the wider bandwidth of the high-capacity systems, a reduction in the stability of LO's of up to an order of magnitude can be tolerated. For the nonspread, high data-rate system, this relaxation allows use of free running cavity-stabilized (or resonator stabilized) oscillators using IMPATT diode and transferred-electrons devices (TED, also called Gunn diode). Oscillators implemented with these devices have excellent frequency stability, owing to their simple physical arrangement, small size, low power consumption, and

convenient output power at millimeter frequencies. The comparison of the different solid-state LO's is presented in Table 8.2.1-1. The GaAs IMPATT diode normally has less noise generation than the Si IMPATT diode. The disadvantage of the conventional cavity-controlled oscillator is its poor temperature stability. However, this shortcoming can be minimized using metallized low thermal expansion fused-quartz as cavity material. As illustrated in Table 8.2.1-2, the temperature stability of 3×10^{-7} parts $^{\circ}\text{C}$ can be obtained at 40 GHz.

Table 8.2.1-1. Comparison of Solid-State Millimeter Wave LO Active Devices

	IMPATT Diode	TED (Gunn Diode)	MESFET
Efficiency	2-8%	2-6%	25-30%
Noise	High	Low	Low
Bias	High Voltage	High Current	4-6 V 20-100 MA
Power Generation (Present, 40 GHz)	1 W	0.2 W	0.03 W
Pulling Figure	Medium	High	Low
Reliability	Fair	Good	Excellent
Cost	Relatively High	Relatively High	Relatively Low

Table 8.2.1-2. 40 GHz Glass Cavity-Controlled Source

TE ₀₁₁ Cavity Size	1 cm Diameter X 1 cm
Total Oscillator Size	1.2 cm Diameter X 3.5 cm
Frequency Stability	0.5 x 10 ⁻⁷ Parts/Minutes 1.0 x 10 ⁻⁷ Parts/Hour
Temperature Stability (Without Any Stabilization)	3 x 10 ⁻⁷ Parts/ $^{\circ}\text{C}$

Besides the high-Q cavity controlled fundamental oscillator (FO), other LO's such as phase-locked oscillators (PLO), injection-locked oscillator (ILO), and phase-locked and AFC oscillator (PLO + AFC) are all feasible for millimeter wave radio. The cost and other performance parameters are compared in Table 8.2.1-3.

Table 8.2.1-3. Comparison of Millimeter Wave Local Oscillators

	FO	PLO	ILO	PLO + AFC
Near Carrier PM or FM	Low	Depend on Loop Filter BW	High	Same as PLO
Frequency Stability	Good	Good/Excellent	Fair	Good/Excellent
Temperature Stability	Good	Good/Excellent	Good/Excellent	Good/Excellent
Cost	Low	High	High	High
Simplicity/Reliability	Excellent	Good	Good	Good
Switching Time	N/A	Fair	Fair	Good
Phase-Coherent Applications	N/A	Good	Fair	Good
Size/Weight	Relatively Small	Relatively Large	Relatively Large	Relatively Large
FO: Fundamental Oscillator		ILO: Injection-Locked Oscillator		
PLO: Phase-Locked Oscillator		AFC: Automatic Frequency Control		

For the spread-spectrum systems, a frequency synthesizer is required for LO interfacing with the code generator. The step-size and switching speed of the synthesizer are determined by data rate, spread bandwidth and hopping rate. Figure 8.2.1-2 is a typical millimeter wave frequency synthesizer.

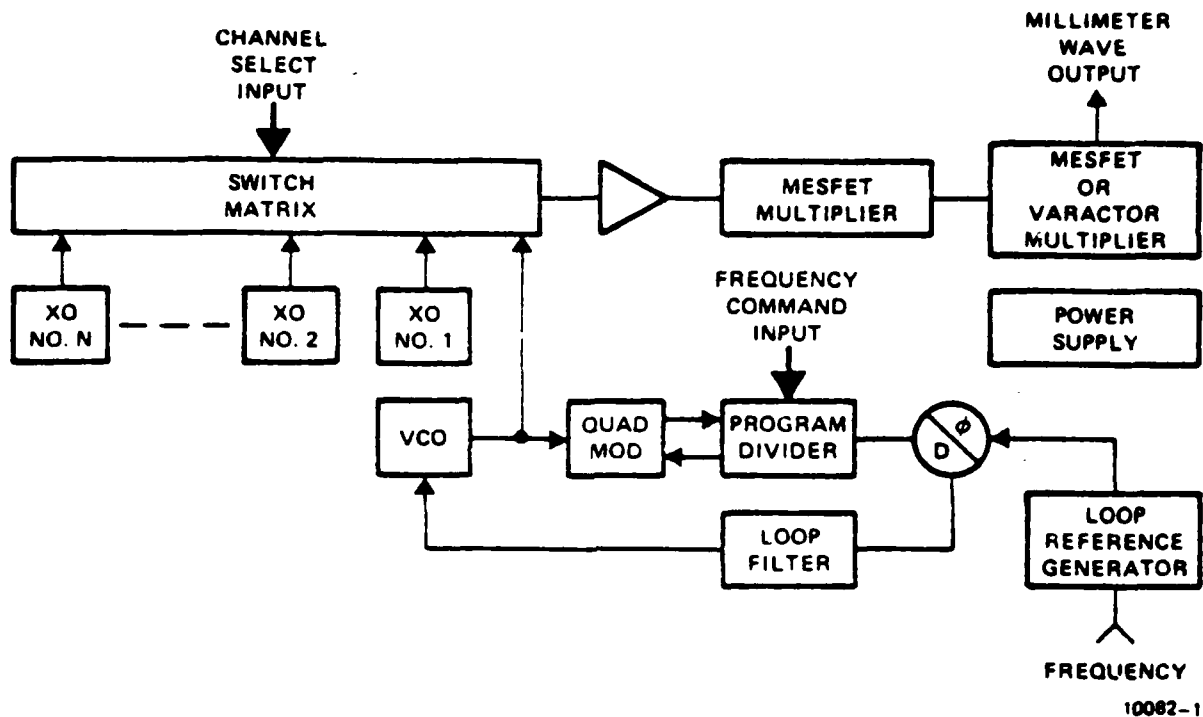


Figure 8.2.1-2. Wideband Millimeter Wave Frequency Hopping Synthesizer

Simple, cost-effective hybrid integration using microstrip-, suspended stripline or fin line eliminates the expensive machined metal waveguide and offers the designer flexibility and simplicity. Solid-state electronics enhances the advantages of hybrid techniques even further, in addition to providing the excellent operational reliability generally acknowledged as inherent in solid-state characteristics.

For the transmitter, HPA IMPATT diodes are excellent candidates (Gunn diodes for power below 200 mW). Over the past several years, significant progress in output power and efficiency has been achieved with IMPATT diodes. This progress has pushed the power output capability to the point where it is competitive with medium-power Traveling-Wave Tube Amplifiers (TWTA's). IMPATT diode amplifiers offer better RF performance than TWTA's with excellent reliability, in addition to weight and size savings. Both double-drift and modified Read-profile IMPATT diodes are popular for microwave and millimeter wave applications. The GaAs IMPATT diode is preferred today for operation in the vicinity of 20 GHz because of its relatively high efficiency and low-noise performance. Si devices still dominate the frequencies above 30 GHz. Figure 8.2.1-3 depicts the present power output trend of Si double-drift (DD) IMPATT diodes as a function of frequency. The dots indicate what power levels have actually been obtained. Table 8.2.1-4 illustrates several state-of-the-art devices and their packages, including their efficiencies and junction temperature (T_j) at Q-band frequencies (36-46 GHz). The power outputs of these devices are more than sufficient for tactical and urban digital radio transmitter applications, including their use of TWTA drivers. Higher power is attainable by using a resonant cavity, corporate or chain combiners. A 10 W amplifier at 40 GHz has been demonstrated in the laboratory, and Table 8.2.1-5 presents some significant millimeter-wave IMPATT-diode power amplifiers. Higher output power is realizable when 16 or 32 diodes are utilized; however, the thermal dissipation of packaging must be properly considered and designed.

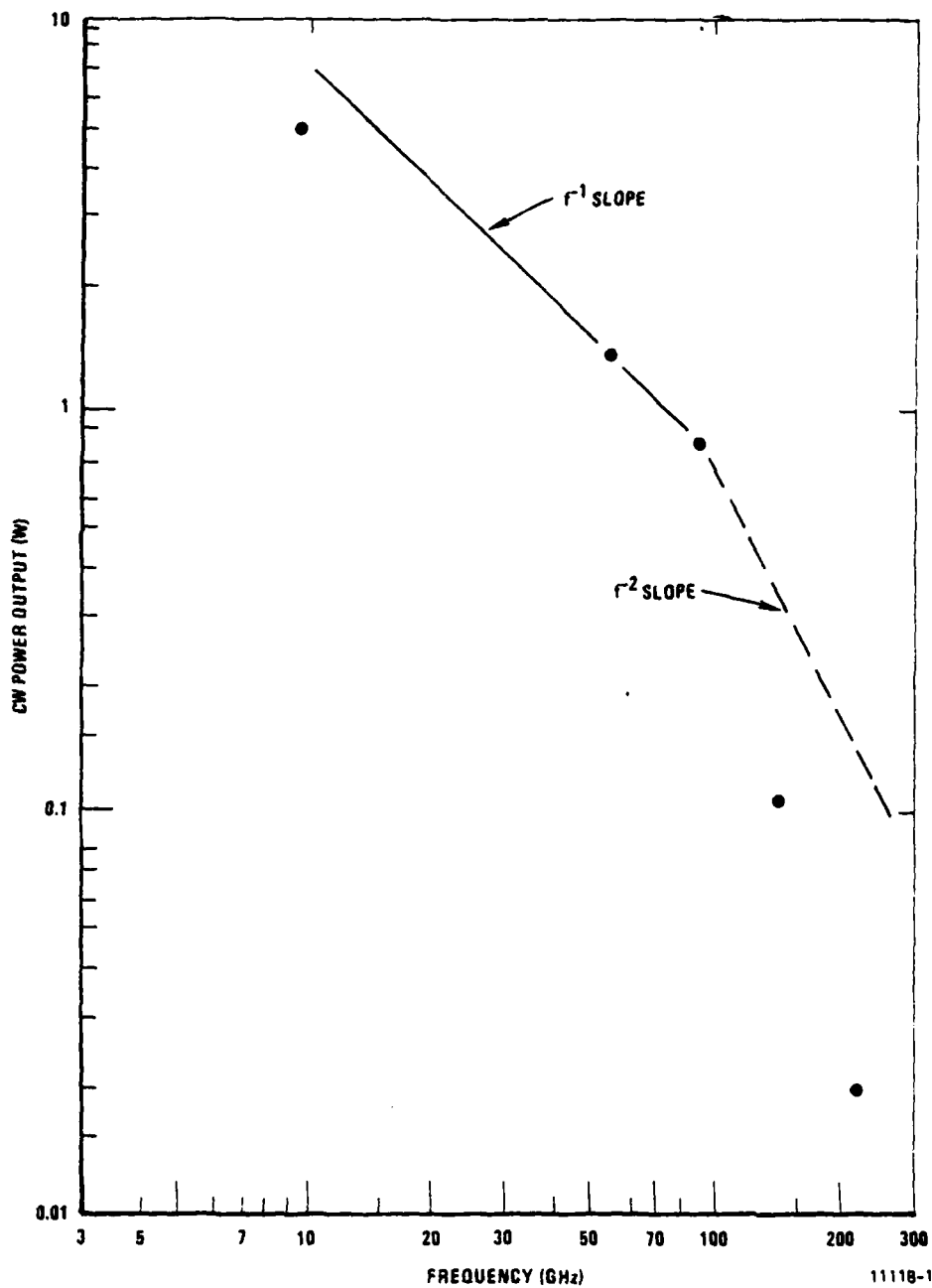


Figure 8.2.1-3. Power Output Versus Frequency of CW IMPATT Diode (April, 1979)

Table 8.2.1-4. High Power Q-Band IMPATT Diode

Mode	Configuration	Power (W)	Efficiency (%)	Estimated T_J ($^{\circ}$ C)	Package	Reference (Company Key Person/Date)
CW	Si, DD	1.52	12.9	250	Ceramic ring full ribbon	Hughes, T. Midford Dec., 1978
CW	Si, DD	2.26	10.6	440	Ceramic ring full ribbon	Hughes, T. Midford Dec., 1978
PULSE (2% 200 ns)	Si, SD	25		260	Ceramic ring full ribbon	Hughes, T. Midford Dec., 1978
CW	Si, DD	0.8	8	170	Ceramic ring full ribbon	NEC ND8N40W-IN
CW	GaAs, DD	1.5-1.9	14-18	-	Beam lead diode in ceramic package	Raytheon, 1979 Masse, Chu, et al

Table 8.2.1-5. MMW IMPATT Diode Amplifier Using Combining Technique

Company/Key Personnel	Type	Frequency (GHz)	BW (GHz)	Number of Diodes (Final Stage)	Power/Gain (W)/(DB)	Reference/Date
Hughes/Kuno	Reflection/Combine	60	6	6 (2-stages)	1/22	IEEE Trans on MTT 1976, p. 758
TRW/Raue	TM ₀₁₀	37.3	0.7	8	5/33	Seventh European M.C. paper SS3.2
TRW/Raue	TM ₀₁₀	60	2.3 1.2	6 6	1/15 1/20	AFAL-TR-78-170 report
Hughes/Weller	TM ₀₁₀	60	1.3	20	1/10	AFAL-TR-78-189 report

Receiver low noise amplifiers, low noise local oscillators and transmitter HPA drivers all require low noise devices. Both InP TED's and GaAs MESFET's are recommended for different millimeter wave frequency bands. Some performances of these devices are described as follows:

InP TED. Advanced GaAs transferred-electronic devices (TED's, or Gunn Diodes) have noise figures of 16 to 18 dB at the K-band frequency, much lower noise figures than Si IMPATT diodes. In the past several years, the InP TED has demonstrated characteristics of lower noise figures, higher operational frequency, greater efficiency and better power handling capability than the GaAs counterpart. In the 1979 Cornell Conference on Active Semiconductor Devices Circuits, Crowley of Varian Associates reported InP TED wideband noise amplifier yields of 7.8 dB noise figures at 35 GHz. Two-layer diodes yield 194 mW of power at 56.5 GHz with 4.7 percent efficiency, about twice the power derived from GaAs devices.

GaAs MESFET. With the advent of GaAs MESFET's in recent years, some impressive results of the 0.5- μm gate-length device have been achieved above 18 GHz. Using electron-beam lithography and liquid-phase epitaxy, Hughes has built prototype MESFET's to yield 11 dB gain at 19.8 GHz for wideband amplifier applications. Recently, low noise amplifiers have been constructed in many laboratories, using 0.5 μm gate devices as illustrated in Table 8.2.1-6. The 0.25 μm gate device may exhibit even better performance if the metal-to-semiconductor contact resistance and contour problems are resolved. Theoretically, optimal noise figures of 2.0 dB at 20 GHz, 2.8 dB at 30 GHz and 2.4 dB at 40 GHz are possible for 0.25 μm gate length and 0.065 μm gate width at room temperature.

Table 8.2.1-6. Above 20 GHz GaAs MESFET Amplifier

Frequency (GHz)	Gain (dB)	NF (dB)	Reference/Date
38	12	6-7 (predicted)	Hughes, August 1979, Midford, Kim, Schellenberg, etc.
27-35	4-11	5-7	Hughes, 1978, C.F. Krum, et al.
27	6	8	NTT, 1978, NEC 388 Tohyama and Mizuno
23	8	6	NTT, 1978 NEC, 388 Tohyama and Mizuno
20	8	5.0-5.5 (predicted)	Harris, 1979, HP 2201
20	5	5.0	RTC-LA Radio Technique Complelec, Paris

Besides the low noise advantage, the MESFET also has the characteristics of wide dynamic range and operational bandwidth and high efficiency. Low noise amplifiers, switches, modulators, limiters, oscillators, mixers, and frequency multipliers have been fabricated and demonstrated with remarkably high performances using MESFET's. The dual-gate, MESFET variable gain amplifier provides both amplification and limiting functions with more than 40 dB gain variation capability controlled by the second gate bias voltage. The wide dynamic range improves the system performance in adverse jamming environments. Instead of a multiplication loss, the single-gate^{1,2} or dual-gate MESFET³ frequency multiplier often

¹M.S. Gupta, et al, "Frequency Multiplication with High-Power Microwave Field-Effect Transistors," 1979 International Microwave Symposium Digest, pp. 498-500.

²J.J. Pan, "Wideband MESFET Frequency Multiplier," 1979 International Microwave Symposium Digest, pp. 307-308.

³P.T. Chen, et al, "Dual-Gate GaAs FET as a Frequency Multiplier at Ku-Band," 1978 International Microwave Symposium Digest, pp. 309-311.

provides gain even at low RF driving levels. It has been demonstrated that the dual-gate MESFET doubler produces 8 dB gain at 12 GHz, -2 dB at 20 GHz, with 0 dBm input signal.

Frequency synthesizers and phase-locked oscillators used in many advanced communications systems, especially frequency hopping systems, demand wideband and low noise frequency multipliers with high efficiency and low-driving power. Of course, the MESFET is a natural choice, and Figure 8.2.1-2 is included as an example.¹ Recently, it was found that the depletion-layer thickness and conductivity of GaAs MESFET's change proportionally to light intensity. This characteristic makes optical-controlled modulators, oscillators and high-speed switches realizable.²

The noise temperature and conversion loss in a mixer, detector sensitivity, conversion efficiencies in frequency multipliers, and the pump power necessary to fully pump the varactors in a parametric amplifier are all dependent on the quality of the 0 volt bias cutoff frequency of these devices. The GaAs Ta-Schottky-Barrier diode³ with double passivation of



and



¹J.J. Pan, "New Millimeter Wave Technology for Tactical Applications," 1979 International Conference on Communications, June 1978, Toronto, Canada.

²J.J. Pan, "Optical Tunable MESFET Microwave Source," 1978 Government Microcircuit Applications Conference Digest, pp. 105-107.

³J.A. Calviello, J.L. Wallace and P.R. Bie, "High Performance GaAs Beam-Lead Mixer Diodes for Millimeter Wave and Submillimeter Applications," Electronics Letters, 16 August 1979, pp. 509-510.

was recently developed, having a zero-bias junction capacitance near 10 fF,* and a zero-bias cutoff frequency as high as 5000 GHz. This zero-bias cutoff frequency is approximately eight times the value of a comparable nonmetallized device and promises higher power handling capability. By using this device, an image-enhanced mixer at 35 GHz with a conversion loss less than 2 dB and less than 5.2 dB SSB noise figure is realizable. A 94 GHz broadband fine-line mixer has already been tested with a conversion loss below 6 dB.¹

High data-rate tactical digital radios, high-speed satellite data links with on-board signal processing and many other millimeter wave communications applications require reliable, lightweight, low-cost and high-speed logic circuits including word and bit pattern generators, PN-code generators, frequency dividers, comparators, modulator/demodulators, A/D converters, and synthesizers for signal processing. The current development of monolithic GaAs gigabit logic using MESFET's, transferred electron logic devices (TELD), or a combination of these, will have a tremendous impact on future system signal-processing design, perhaps curbing the proliferation of diverse electronics on ships and aircraft. High electron mobility and low switching energy of GaAs IC's, six times faster than Si IC's, make them the preferred circuits for high-speed logic; GaAs TELD's are faster than FET's and probably operate beyond 20 Gb/s. The monolithic 8 Gb/s TELD A/D converter² and dc to 4.5 GHz GaAs MESFET frequency counter³ have already been developed and utilized. Integration of MESFET low noise amplifiers,

¹ J.A. Calviello, J.L. Wallace and P.R. Bie, "High Performance GaAs Beam-Lead Mixer Diodes for Millimeter Wave and Submillimeter Applications," Electronics Letters, 16 August 1979, pp. 509-511.

² B.G. Bosch, "Gigabit Electronics - A Review," Proc IEEE, March 1979, pp. 340-379.

³ J. J. Tujl, et al, "4 GHz Frequency Division with GaAs MESFET IC's," Proc. IEEE, Pap., 1977 IEEE Int. Solid-State Circuits Conf. pp. 198-199.

mixers and local oscillators onto a monolithic chip provides economic advantages, low noise, and simplicity for circuitry; and X-band low noise monolithic receiver front-ends have been developed by many companies. Currently, monolithic 10 to 10 GHz and 10 to 26.5 GHz MESFET amplifiers are being developed under U.S. Government contracts.

8.2.2 Modem General Description

The high rate data transmissions in this millimeter wave communications system are of sufficient importance that every effort should be employed to ensure data integrity. Spread spectrum modems incorporated into the system will offer an added measure of link reliability. These modems will help protect against unwanted signal detection, demodulation and interference.

8.2.2.1 Modem Design Goals

The modem designed must satisfy the primary communication requirements of the Alternate Route System. For analyses purposes, we assume three different data rates are of importance:

- Data Rate - 20 Mb/s
100 Mb/s
150 Mb/s
- RF Bandwidth - Dictated by transmitter/receiver/antenna characteristics - less than 2 GHz

The spread spectrum link must use the maximum available bandwidth to achieve the lowest probability of intercept (that is minimum signal power density), maximum jamming margin and process gain. The code clock generator is of primary concern if this criteria is to be met.

The present state-of-the-art suggests that digital code generators are limited to frequencies less than 1 GHz. For this system a 1 GHz code clock rate is the design goal. Also, a BPSK Modulator will be utilized for maximum bandwidth, since a QPSK modulator can be built using two BPSK modulators properly configured. A rule of thumb for Process Gain is:

$$G_p = \frac{BW_{RF}}{BW_{INFO}}$$

which yields the following results:

<u>Data Rate</u>	<u>Process Gain</u>
20 Mb/s	100 = 20 dB
100 Mb/s	20 = 13 dB
150 Mb/s	13.3 = 11.2 dB

This process gain is the improvement in the signal-to-noise ratio at the receiver baseband output over that of the receiver RF input.

There is still a more important design goal, that of jamming margin. This is a measure of the systems rejection to undesired signals while still maintaining an acceptable output signal to noise ratio. Jamming Margin can be approximated by Process Gain - System Losses - S/N Ratio Required. Given the system data rates the following is obtained:

<u>Data Rate</u>	<u>Jamming Margin</u>
20 Mb/s	9 dB
100 Mb/s	2 dB
150 Mb/s	0.2 dB

These numbers assume a 1 dB implementation loss and 10 dB S/N ratio as the minimum acceptable for the required BER.

As can be seen, except for the lowest data rate, these margins are quite low. However, these numbers are based on a 1 GHz chip rate and BPSK Modulation format. As advances are made in logic devices, this clock rate could be increased for improved AJ performance.

8.2.2.2 Modem Code Generator Guidelines

The intent of this modem design is to take advantage of the benefits of spread spectrum communication as they relate to this requirement. That is, low density signals, message privacy and interference rejection.

A low density signal is extremely important in a hostile environment when undesired signal interception is desired. Also, signal multiplexing is easier due to the low power densities.

Spread spectrum signals are inherently private due to the pseudonoise code generator. However, for effective spectrum spreading the code generator should be of the linear maximal type.¹ Also from a hardware design standpoint, this type of code generator is the easiest to configure, a necessity at the high rates involved. The maximal codes are the longest codes that can be generated given a fixed length shift system, the shift register being configured with linear (additive) feedback taps precisely connected to generate the appropriate code.

¹R.C. Dixon, "Spread Spectrum Systems," John Wiley and Sons, New York, 1976.

A number of benefits come about by the choice of a linear maximal code. The first is that the one/zero balance in the code sequence is well defined, i.e., the number of ones exceeds the number of zeros by one. This helps maintain good carrier suppression since the average modulator offset level is near zero. The offset over the code length is proportional to the inverse of the code length or $\frac{1}{(2^n-1)}$. The carrier, in a perfect modulator, is attenuated by $(2^n-1)^{-1}$. Given a 15-bit sequence as proposed for this system, 45 dB carrier suppression could be obtained. This is sufficient since it is well below the residual carrier leakage in a practical modulator.

To achieve maximum antijam performance, the one-zero distribution must be well behaved to prevent sync errors, caused by cross correlation with undesired signals. According to Freymodosson,¹ exactly: $2^{(n-(p+2))}$ runs of length P exist in a linear maximal code for both ones and zeros. White,² by virtue of computer analysis, showed this case to be the best overall for statistically independent distribution of bits.

Of course the code does repeat every 2^N-1 clock periods for a maximal linear code. The repetition rate for this system is:

$$\begin{aligned} \text{(BIT Period)} \quad (2^{15}-1) &= 1 \times 10^{-9} \times 32767 = 3.2767 \times 10^{-5} \text{ sec} \\ &\text{or } 30.5 \text{ kHz} \end{aligned}$$

In the frequency domain, this appears as spectral lines occurring at 30.5 kHz intervals over the spread bandwidth. From a probability of intercept standpoint, minimum spectral spacing makes the signal appear more noise-like. Given a 2 GHz operating bandwidth, the 30.5 kHz spacing should be sufficient.

¹R.C. Dixon, "Spread Spectrum Systems," John Wiley and Sons, New York, 1976.

²R.C. White, Jr., "Experiments with Digital Computer Simulation of Pseudo-Random Noise Generators," IEEE Trans Elect. Comp, June 1967.

A final point of attention is to the code effects on the synchronization circuitry. The linear code has a well defined autocorrelation function. The correlation of the code sequence with itself, shifted in time, always yields the relative value of 1 (assuming correlation is an XNOR function). When the sequence is aligned in time, the relative value becomes $2^N - 1$ or, in this case, 32767 or a 45 dB increase. The well defined nature of this code makes the design of the synchronization circuitry a manageable task. Also, the high degree of correlation makes receiver synchronization false alarm rates low while providing a high degree of rejection for undesired signals.

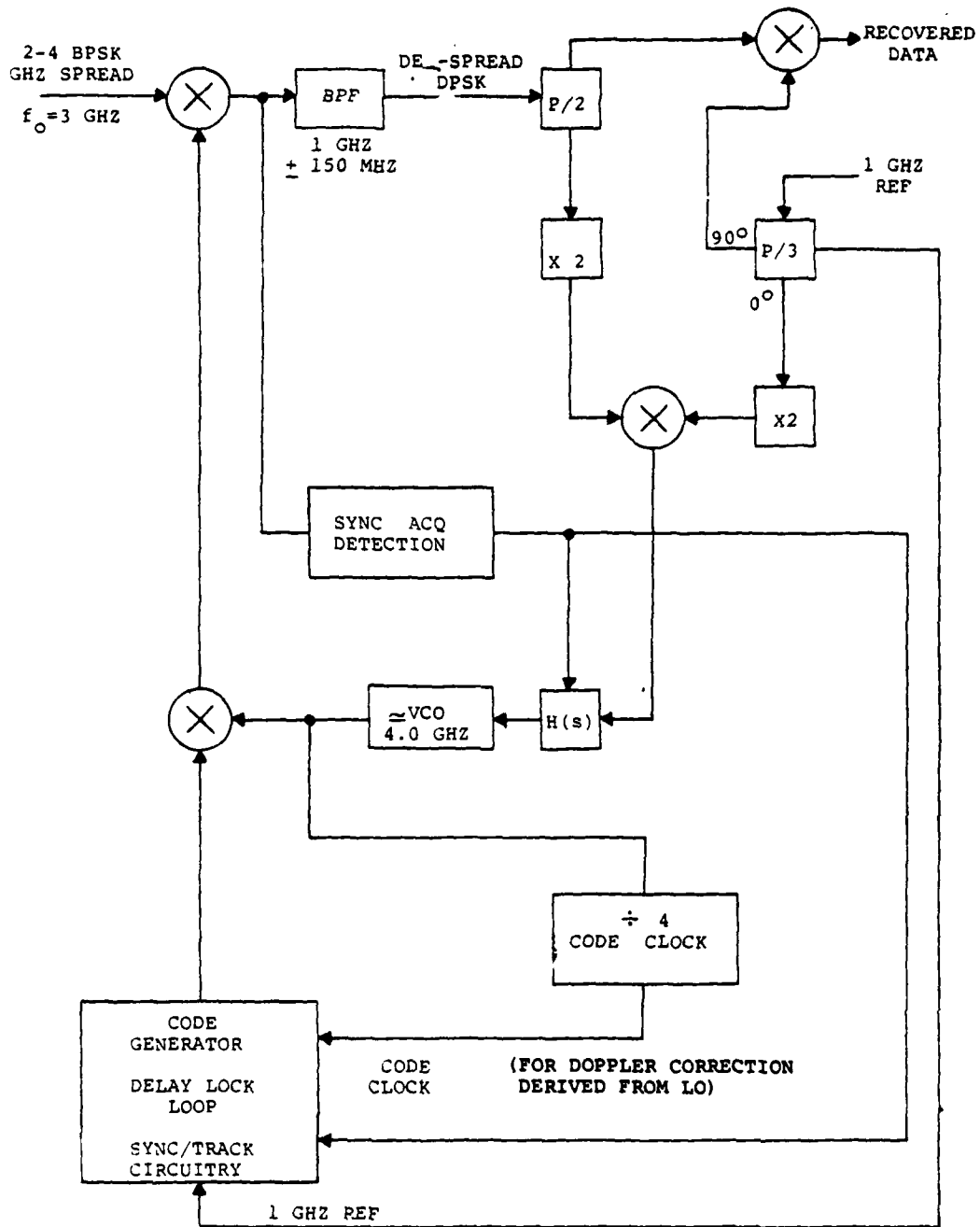
8.2.2.3 Modem Circuit Design

The modem block diagram is shown in Figures 8.2.2.3-1 and 8.2.2.3-2. Briefly, the diagram can be subdivided into six main areas of interest and is as follows:

1. Hetrodyne Correlator/Translator
2. Code Clock Acquisition
3. Sync Detect Circuitry
4. Code Clock Tracking
5. Doppler Correction
6. Data Recovery

Each area will be discussed independently including alternate approaches if possible. In each case these areas represent the conceptual design and should be interpreted as a starting place for the detailed electrical design.

The transmitter portion is relatively simple and functions identically to the Modem Local Oscillator. This is shown in Figure 8.2.2.3-2.



A90401-92

Figure 8.2.2.3-1. Modem Block Diagram Receive Section

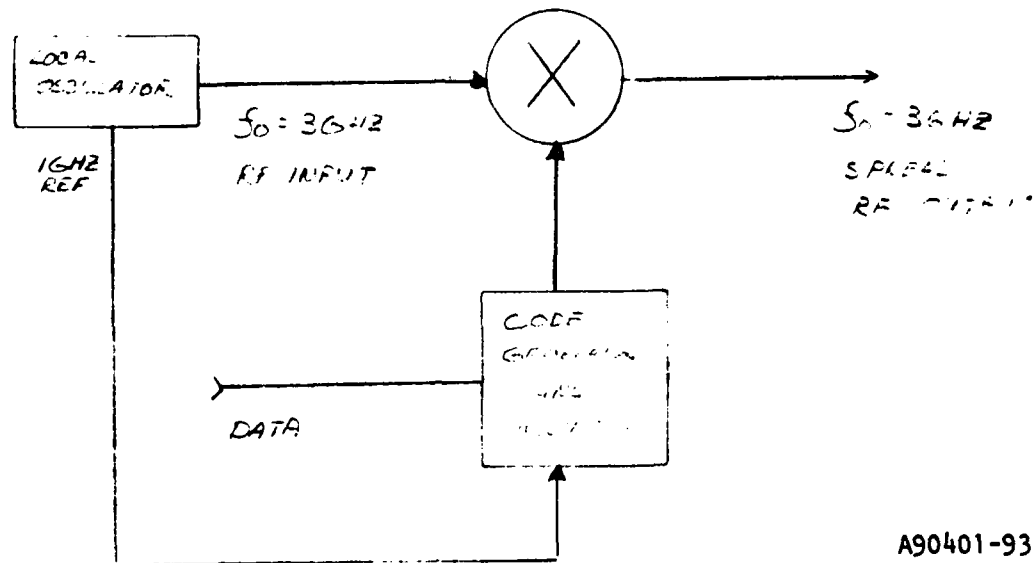


Figure 8.2.2.3-2. Modem Block Diagram Transmitter Section

Hetrodyne Correlator

The incoming signal from the downconverter is at a center frequency of 3 GHz. The correlation, or signal compression, is done at the front end of the modem to minimize spurious signals that may be generated due to high level interferers. Also, the task of amplification and gain control of the compressed or despread signal is easier than the wideband spread case. The output frequency of the correlator is 1 GHz or translated by 2 GHz. This is accomplished by modulating the local oscillator with the code clock and using this phase shift modulated LO for a low or high side injected down conversion and signal compression simultaneously.

The benefits of this technique include the reduction of direct feedthrough from a jamming signal and simplified receiver design due to the lower frequencies involved after the down conversion. In addition, the LO signal is identical to the transmitted signal except for the IF frequency offset. In some cases, this fact could be used for hardware reduction. The number one function of the correlator is to restrict the flow of any interfering signals in their original form, that is, to reject jammers. If a CW jammer passed through, it could fool the receiver into false acquisition, or a narrowband signal could appear as the despread data. With this technique, the CW or narrowband signals are spread by the DPSK modulated LO and are therefore reduced in interfering level. This, coupled with the elimination of direct feedthrough due to heterodyne correlation, makes this the most reliable approach.

The alternative approach is to use in-line correlation in which the LO is on exactly the same frequency as the incoming signal. This contributes to modem simplicity in that the BPSK modulated signal is on exactly the same frequency as the transmitted signal but rejection to direct feedthrough is limited to correlator isolation, since filtering is impossible.

Code Clock Acquisition

The sync acquisition and tracking circuitry is one of the most important subsystems in the modem since no communications can be exchanged until synchronization occurs. Due to the relatively simple and short code proposed, the initial design approach to code clock acquisition should be that of a sliding correlator. In this type of correlator the code sequence of the LO is moved ahead or behind in time until synchronization occurs. Because of the short code lengths, sync will occur quickly. The search rate, however, is limited to the post correlation bandwidth or the data bandwidth. Some mechanism of search rate control could be included to minimize synchronization times given the various data bandwidths.

Sync Detect Circuitry

The sync detect circuitry is perhaps the key to the successful operation of the acquisition circuitry. The burden of identifying proper synchronization while rejecting false starts due to jammers and noise is placed on this circuitry.

Initially, the modem is not in sync. The sliding correlator is moved ahead in time by operating the code clock at a rate slightly higher than the correct frequency. As the codes slide into sync, a coherent despread signal is passed by the IF, demodulated, and a signal detect circuit is initiated. The sliding correlator is usually frozen and one or more integrators and threshold detectors employed to check for valid synchronization. Multiple integrators of different bandwidths are useful to provide for noise immunity.

If the detection algorithm is properly designed, an acceptable false alarm rate can be achieved. Of course, the false alarm rate is a function of signal-to-noise ratios and therefore a function of the total system. Before the detailed circuit design of this type of circuit can be accomplished, a complete system profile must be available.

An alternative approach to the sync detect circuitry could be the use of a delay line matched filter. In this technique, a delay line is configured with taps at bit period intervals. These taps are then properly weighted and summed to represent a replica of a fixed code sequence. When the coded input signal input to the filter matches the preset code sequence, the output response of the filter is at a maximum. This technique will recognize one code and one code only, but it is an excellent way of starting the receiver code generator in proper sync with the transmitter. Figure 8.2.2.3-3 shows a typical tapped delay line matched filter suitable for initial sync acquisition.

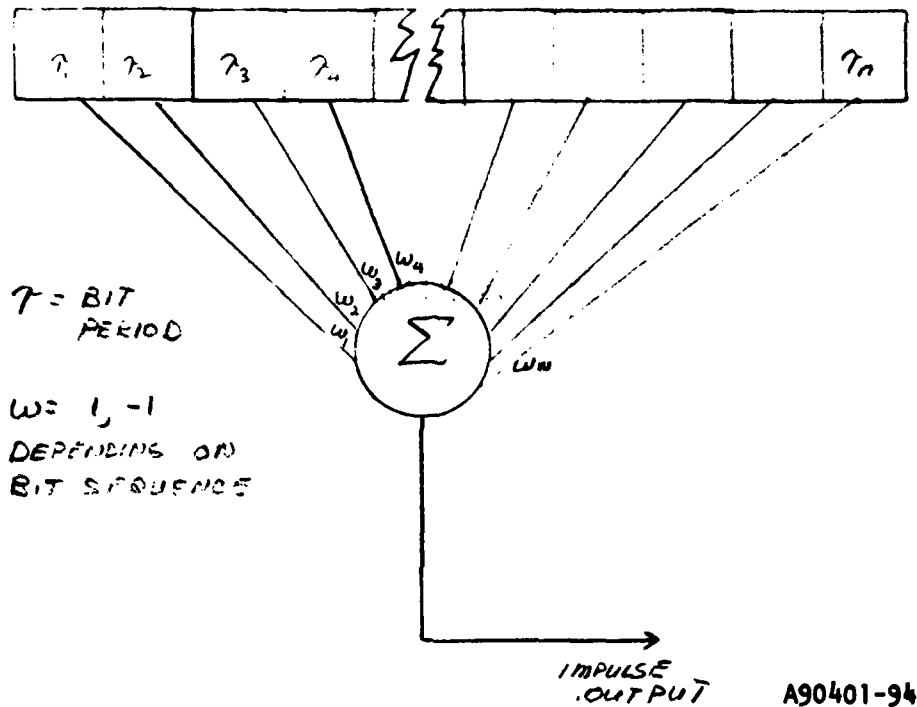


Figure 8.2.2.3-3. Tapped Delay Line Matched Filter

Code Clock Tracking

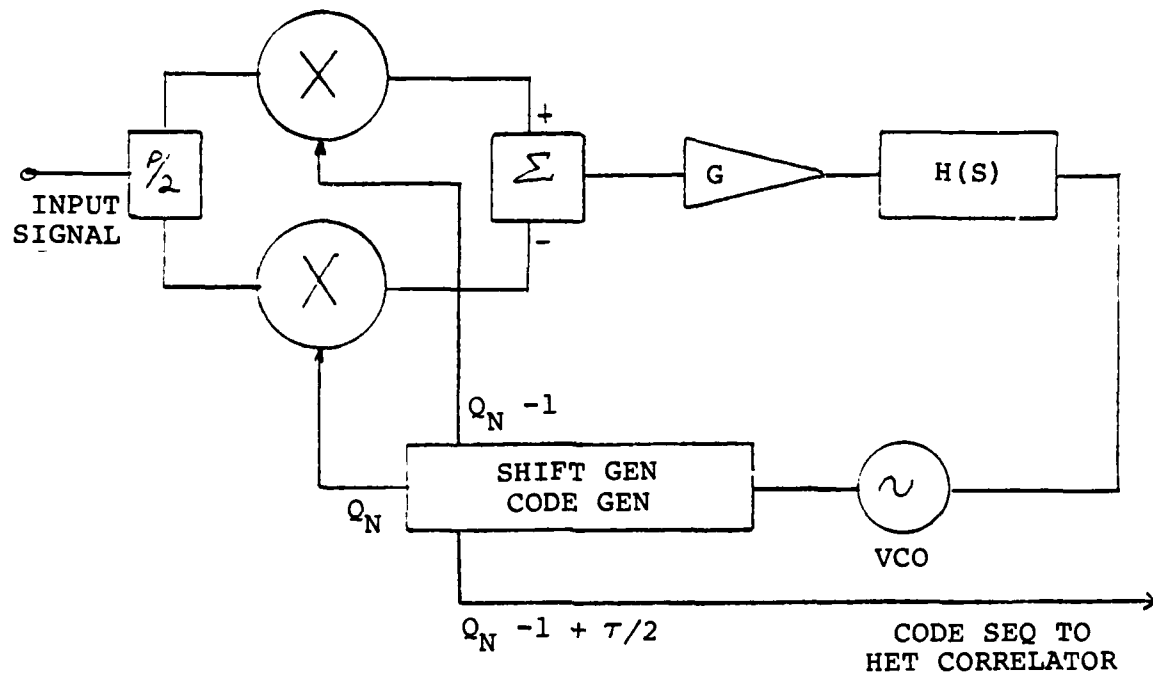
Once initial synchronization occurs, a method of code clock tracking must be devised. First, the limits of uncertainty must be examined to bound the tracking response. Errors due to frequency uncertainty, Doppler shifts, and code phase errors will exist in any real system.

The classic approach to code clock tracking is to implement a delay lock loop. Spilker¹ has discussed this approach in depth and it appears to be a low risk approach. Basically, two consecutive taps on the code generator are used to drive correlators in such a fashion as to derive a discriminator function, that is voltage versus code phase error, to control a voltage controlled oscillator that is used for the code clock. Figure 8.2.2.3-4 is a block diagram of this technique. Figure 8.2.2.3-5 is a modified version of the delay-lock-loop² that is modified to allow sequence inversion modulation. This modification allows tracking to take place even when the sequence is inverted by virtue of the imbedded data. The rectifiers change the correlator output polarities so that regardless of the output data the control voltage will be of the correct polarity for tracking. The remaining problem that exists is that the nonlinearity introduced by the rectification process requires that positive signal-to-noise ratios be present prior to rectification. This requires, in most spread systems, a data filter to reduce the bandwidth to yield a positive P_S/N_0 where P_S is the signal power. This requires careful consideration to avoid system conflicts.

An alternate approach is to utilize some method of coherent carrier tracking. As the block diagram suggests, the 1 GHz code clock can be derived from the 22 GHz local oscillator. Since both the RF carrier and the code clock are acted on identically by the transmitted path, frequency uncertainties cancelled by the LOW SIDE injected LO can be used directly by the code clock generator. Of course, this applies only if the transmitter generates the code clock in this manner. In this coherent carrier system the code clock is one half the local oscillator. Tracking the carrier will also track the code clock. While the initial synchronization problem is just as hard, this simple method of code clock tracking may be sufficient with a large reduction in cost.

¹J.J. Spilker, Jr., "Delay-Lock Tracking of Binary Signals," IEEE Trans. on Space Electronics and Telemetry, March 1963.

²Robert B. Ward, "Digital Communications on a Pseudonoise Tracking Link Using Sequence Inversion Modulation," IEEE Trans. on Communication Technology, February 1967.



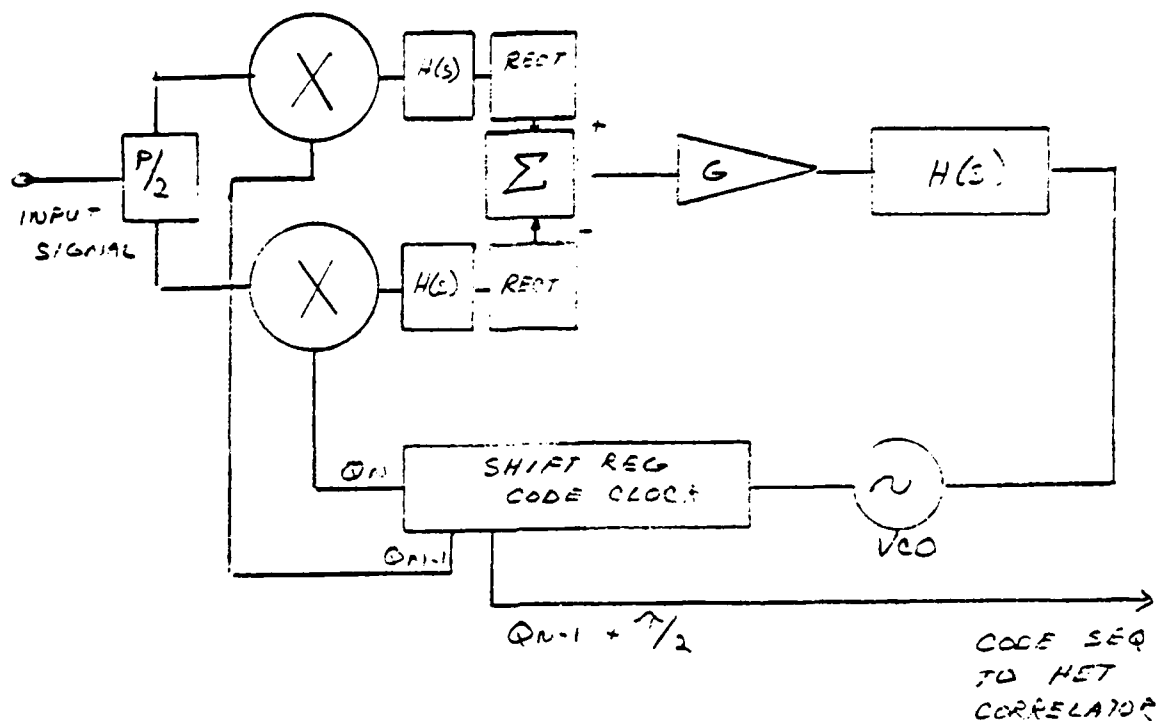
A90401-95

Figure 8.2.2.3-4. Basic Delay Lock Loop

Doppler Correction

Doppler shifts affect both the transmitted carrier and code clock rates. At present, the extent of doppler correction needed, if any, is not known. A study characterizing antenna movements due to the elements would bound this problem.

In any event, the mechanism for doppler correction is present in this modem conceptual design. The carrier tracking and code clock tracking loops must be designed to simply include this uncertainty. The carrier coherent approach again excels because doppler shifts on the carrier frequency and code clock frequency will be at the same rate and can be removed simultaneously by the carrier tracking loop.



A90401-96

Figure 8.2.2.3-5. Delay Lock Loop for Sequence Inversion Modulation

Data Recovery

The modem's primary function is to transmit and receive data. The entire preceding discussions all but neglected the final data output. This is because the majority of the problems that must be solved have to do with the signal compression and synchronization.

Once this takes place the recovered IF signal is only a BPSK signal containing the data. A classical Costas loop, which is used for the carrier tracking also provides the coherent carrier for data demodulation. The proper filter selection then must be made to minimize the implementation losses. This will probably be of the matched filter variety with switchable parameters optimized for the various data rates.

AD-A102 303

HARRIS CORP MELBOURNE FL GOVERNMENT COMMUNICATION SY--ETC F/G 17/2.1
MILLIMETER WAVE ALTERNATE ROUTE STUDY.(U)

APR 81 W C ADAMS; J J PAN; W C WHITEHEAD
RADC-TR-81-42

F30602-79-C-0055
NL

UNCLASSIFIED

4-5

AD

4112314



8.2.2.4 Spread Spectrum Modulation Format

Two wideband frequency generator techniques were considered for this system: BPSK and QPSK. Each has positive and negative attributes that must be weighed.

BPSK modulation with a 1 GHz chip rate will occupy greater than 2 GHz of bandwidth. This is advantageous to this requirement in terms of AJ performance. However, the transmitter/receiver/antenna hardware will be more difficult to implement. This is compounded by the fact that BPSK is unforgiving to nonlinearities placed in the transmission path.

QPSK occupies half the bandwidth, easing the transmitter/receiver/antenna requirements. It is also more tolerant to nonlinearities.

For this task, because of the wider bandwidth, BPSK seemed best if the R/T equipment can be implemented. Since a QPSK modulator can be configured from two BPSK modulators, it will be a low risk approach to initially try BPSK with QPSK as a reasonable alternative.

8.2.2.5 Detailed Circuit Design - Code Generator

All of the above discussions reference a chip rate of 1 GHz. Since the code generator is the initial building block for a spread spectrum system, it seemed proper to examine the available devices and design this key item.

The design guidelines were few, but do require the generator to be completely digital so that it may be integrated into an LSI package and that it be upwardly compatible with higher chip rates. The generated code will be linear, maximal if possible, and be of the maximum length consistent with the circuit topology delays. Circuit delays limit pulse width; i.e., high speed code generators can be generated by combinations of a basic high speed element.

The extremely high code rate of 1 GHz is very difficult to achieve if one shift register is to be used. It was decided to multiplex two 500 MHz code generators to yield the final 1 GHz rate.

These 500 MHz generators may be configured using off-the-shelf parts. Two Fairchild F100141 8-stage shift registers will be cascaded to achieve a 15-bit length. According to tables compiled by Dixon¹, a maximal linear sequence can be generated with one feedback tap for the 15-bit case. Only one feedback tap is allowed in this case so that lookahead techniques can be used to cancel the propagation delays and setup times of the devices. Figure 8.2.2.5-1 shows this configuration with the timing diagram computed to verify performance.

The remaining problem is to multiplex the two 500 Mb/s streams to a 1 GHz stream. The resultant syncopated generator will employ 500 MHz phase shifted clocks and some sort of multiplexer.

Des Brisay, Horwood and Lee² configured a data multiplexer using GasFET switches and a latch, also an FET, to reclock the data in the output. The significance of the latch is that by reclocking the data, edge jitter introduced by switch leakage is eliminated. Figure 8.2.2.5-2 outlines this approach.

An alternate method is to develop a high speed XOR gate to modulo-two add the 500 Mb/s data streams. Using dual gate FET's, Figure 8.2.2.5-3 outlines the approach. The FET's, when properly biased, will switch sufficiently fast and true. Modulo-Two addition can be obtained. This is important to preserve the linear qualities of the code sequence.

¹R.C. Dixon, "Spread Spectrum Techniques," John Wiley and Sons, New York, 1976.

²G.S. Des Brisay, Jr., D.F. Horwood, G.E. Lee, "Two GBPS QPSK Modem," 1979 IEEE MTT-S International Microwave Symposium, 1979.

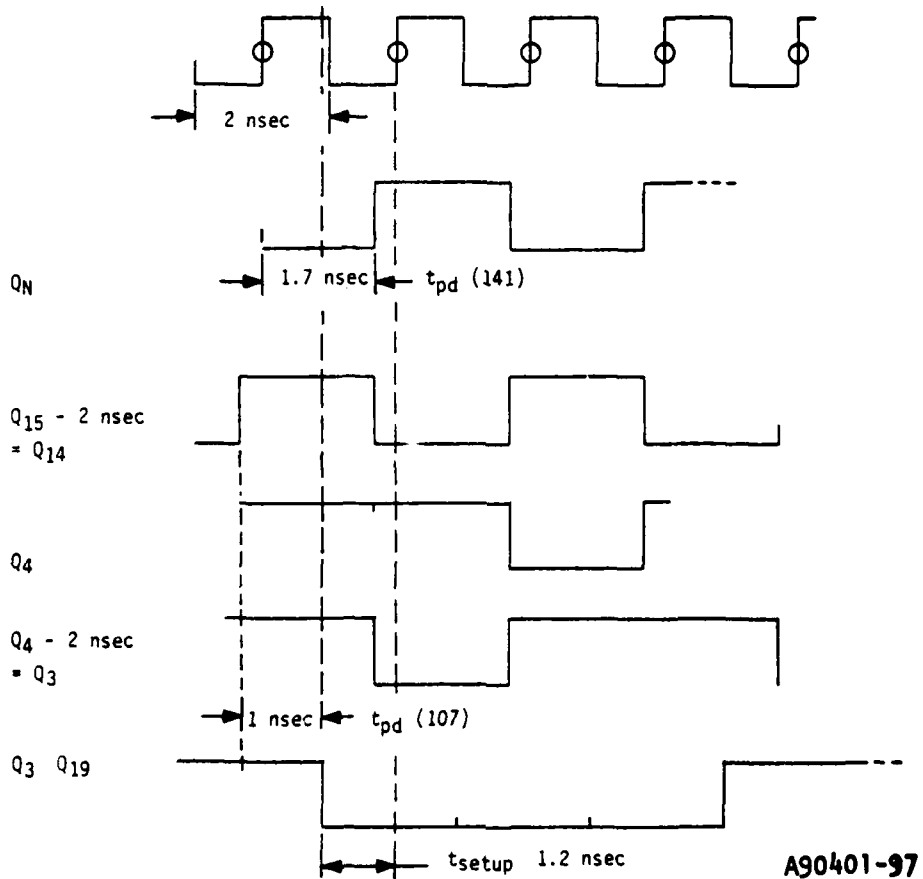
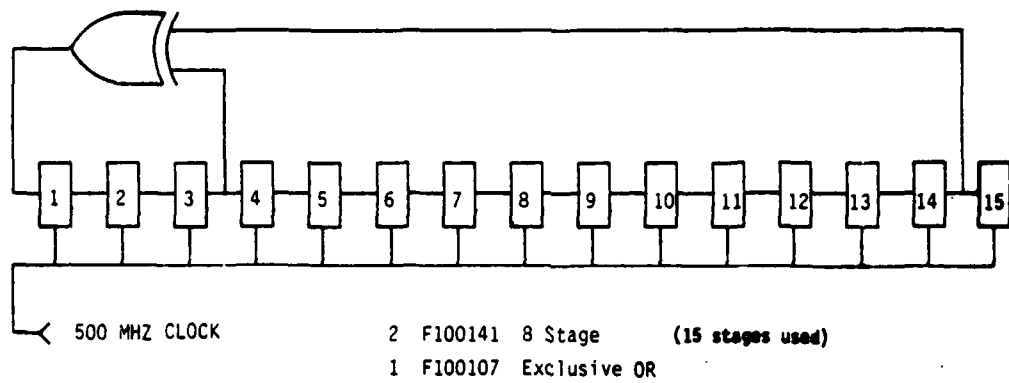


Figure 8.2.2.5-1. 500 MHz Code Generator

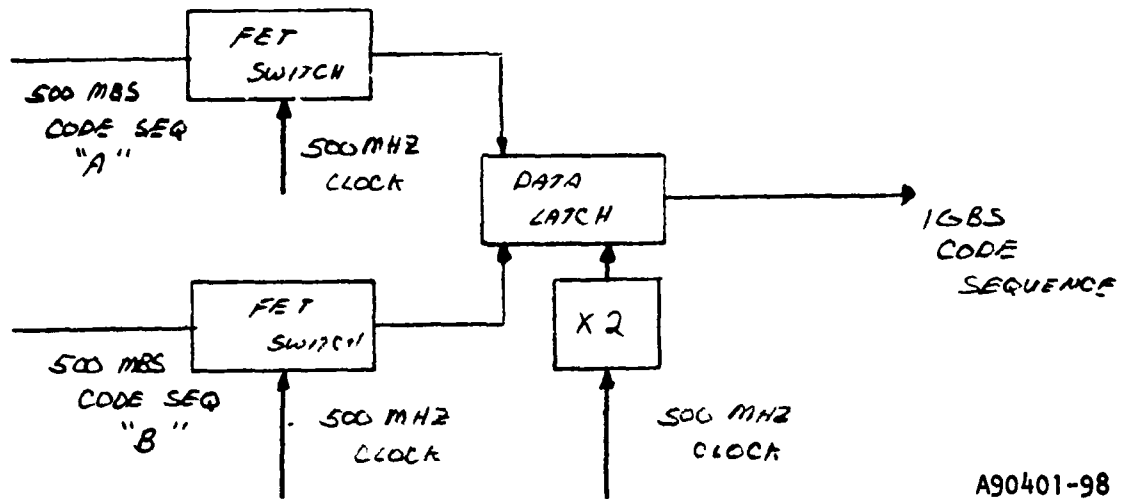


Figure 8.2.2.5-2. Code Sequence Multiplexer

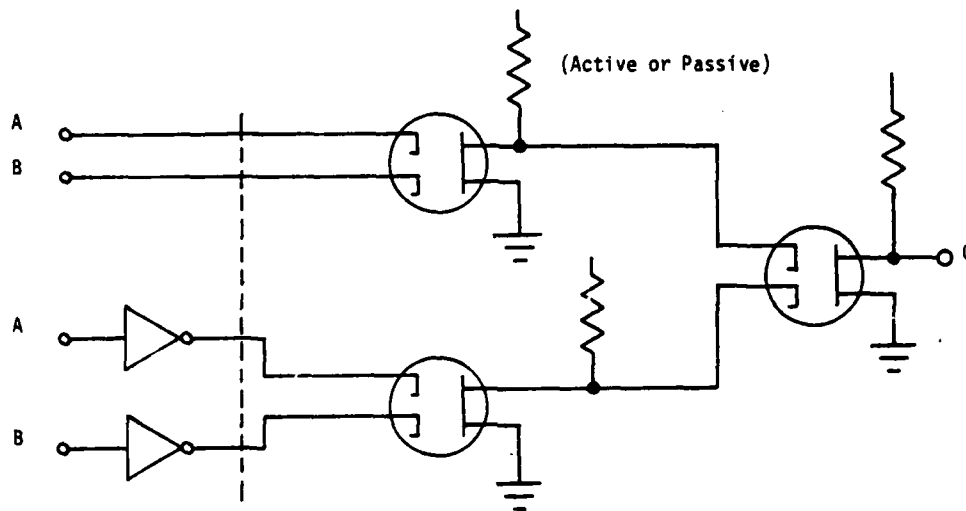
With ECL logic driving this circuit, complemented data is readily available. The symmetry of the circuit should help to minimize edge jitter, but if an appreciable amount should exist, it can be eliminated with a data latch as in the alternate approach.

8.2.3 Selection of Filters

Apart from the modulator and demodulators, the basic IF and RF components of a digital radio are generally similar to those of analog system, but the major difference takes place in the filter design. Even the requirement of interference below carrier of the digital filter is much less sensitive than the analog system filter (30 dB versus 70 dB); however, apart from the interference consideration, the digital filter must be designed to:

- a. Achieve a good balance between intersymbol interference and the receiver noise in the demodulator.
- b. Carry out multiplexing and demultiplexing RF channels.

Given two inputs A, B:



A	B	C
0	0	1
0	1	0
1	0	0
1	1	1

All FETS biased such that:

A	B	C
0	0	1
0	1	0
1	0	0
1	1	0

A90401-99

Figure 8.2.2.5-3. Digital Filter

In determining a suitable set of filters, an interactive process according to the following order may be taken:

- a. Channel passband amplitude and group delay.
- b. Additional channel shaping due to multiplexing and demultiplexing.
- c. Overall channel response which should have approximately Gaussian amplitude and flat group delay over symbol-rate bandwidth.
- d. Stopband attenuation and rejection of unwanted signals.

The details of filter design, optimization and the computer program can be found elsewhere, and shall not be discussed in this report.

8.2.4 Baseband Components

Digital baseband components in the transmitter receiver and repeater carry out the functions of timing extraction, threshold detection, coding, decoding, and, in some systems, supervisory control and equalization. A critical parameter in the design of the regenerator circuits is the number of transitions from 0 to 1 and vice versa in the data stream, this number determining the amount of timing information present. To ensure a sufficient number of transitions in the presence of long runs of ones and zeros, it is desirable to add either a known bit pattern to the incoming data or to code the data so that its digital sum variation is restricted. Since the aspects of baseband coding, decoding, and synchronization have been well developed in the past, this report will not give any further discussion.

8.2.5 Fiber-Optic Interconnection

Fiber-Optic (FO) communications provides many significant advantages over conventional coaxial cable systems. These advantages include wide bandwidth, transmission security, and minimum interference; however, fiber optics may lack the installation simplicity, survivability in subzero temperature environments, and economic viability for many local distribution networks. For militarily deployable tactical applications, either in battlefields or on bases, the transportability and deployment speed of the FO system sometimes precludes use of FO implementations.

A Hybrid Communications System, incorporating millimeter wave (MMW) Integrated Terminals and Fiber-Optic (FO) local distribution networks can offer the advantages of wideband operation, secure data transmission, and reduced costs. For many military tactical systems operating in hostile environments and commercial broadband links in both congested urban areas and remote rural communities, the hybrid approach also provides impressive advantages of system transportability, flexibility, installation and maintenance simplicity, and lower construction/hardware costs over the total FO system.

While the potential advantages of FO communications have been recognized for a long time, recent technological advancements in the fabrication of practical FO connectors, couplers, and switches have made a variety of commercial and military applications both feasible and attractive. Utilized in both point-to-point links and multiterminal data buses, the FO cable can transfer telephone, teletype, video, CATV, instrumentation data, facsimile, radar, imagery, computer and control information without EMI/EMP, cross-talk, or ground-loop problems. Particularly, with 32 to 105 Mb/picture rates, the fiber cable relays high-density imagery pictures with great fidelity. The distances of local distribution networks are ordinarily short, and conditions are favorable for utilization of off-the-shelf FO components, especially since the price has recently been greatly reduced.

Applications

Two applications are given to illustrate the use of FO's in the local distribution network. In the modern evolution of information handling techniques, use of more efficient, paperless automated business office systems will become common. Various office functions and processes such as facsimilies, copiers, dictation recorders, and so on, can be electronically processed, and their outputs transferred, stored and accessed. With appropriate design of FO computer-to-peripheral interconnects and the multiplexer/demultiplexer (M/D), the multiple asynchronous, full-duplex peripheral data lines are capable of transparently passing through a single pair of optical fibers. Figure 8.2.5 depicts a system block diagram of the Harris Model 4359, multichannel, full duplex, Fiber-Optic Concentrator for digital data transfer, used to link peripherals on separate floors of a building.

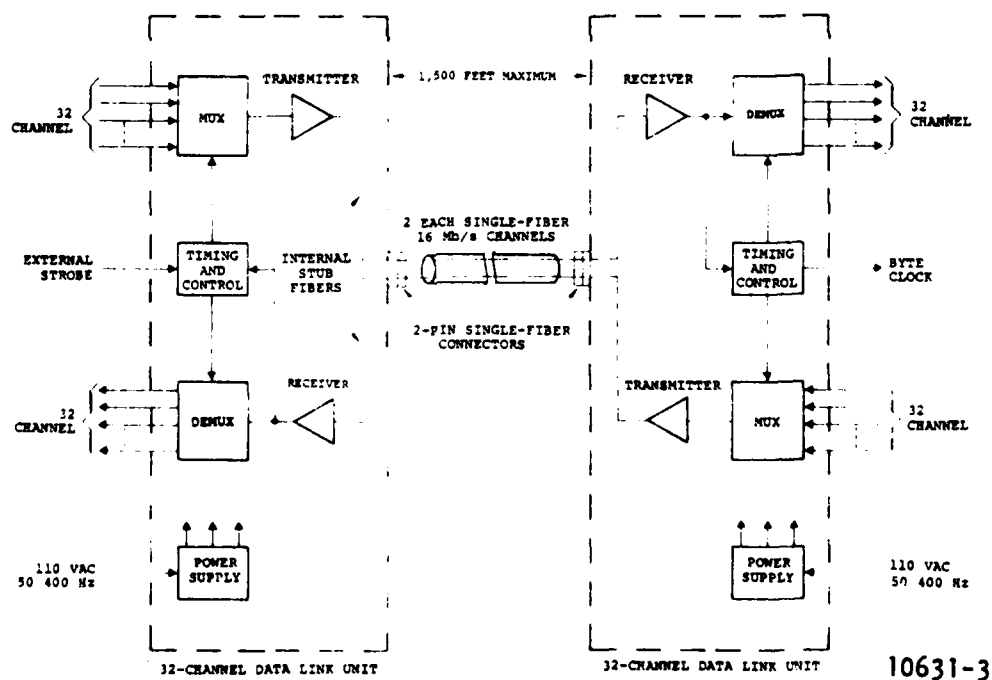


Figure 8.2.5. Block Diagram of Harris Model 4359
13-Channel Fiber-Optic Concentrator

Another, more pertinent application is a military tactical network node with communication elements in connective configuration. AJ MMW portable radios will link the intrabase information facility and FO links will interconnect the local distribution of telephones and digital data within the command post. A 13-Channel, 350 meters, FO system has been field demonstrated successfully to replace the conventional 26-twisted pair cable (CX-4566) system for analog telephone and DSVT transmission.

Cost-Effective Fiber-Optic Hardware.

Either multimode graded index or single mode fiber is recommended to transfer wideband, high frequency analog or high data-rate digital information from MMW converters to multiplexer/demultiplexer (M/D), depending on the IF frequency and its bandwidth. When the IF frequency operates above 300 MHz, and injection laser diode (ILD) is suggested as an optical source. Avalanche photo diodes (APD), PIN PD, and GaAs MESFET are all feasible for optical detection. The MESFET is especially preferred because of its high frequency response, low noise and low bias voltage.

Normally, the data-rate of the distribution network is relatively low between multiplexer/demultiplexer (M/D) and individual users. The inexpensive, medium-loss, step-index fiber cable, light-emitting diode, and PIN PD are candidates for use in this low-rate configuration. The relative large numerical aperture of the medium-loss fiber will couple more optical power into the fiber core to offset the extra attenuation.

Single-strand multimode fiber connectors with an insertion loss of 0.5 to 1.0 dB, are readily available from many vendors. Various "T" and "Star" couplers, bidirectional or unidirectional, have been measured in several laboratories to have losses ranging from 0.4 to 1.0 dB. Currently, fiber-optic switches are still mechanically limited. However, either integrated optics or acousto-optic switches will operate more efficiently in the future.

System Implementation Considerations

The performance of the system, either analog or digital, mainly depends on the total system signal-to-noise ratio (S/N), nonlinearity and transient behavior. The turn-on delay of injection laser diodes or light emitting diodes may also create intersymbol distortion, particularly for high-speed operation. This system nonlinearity generates harmonic, intermodulation and cross-modulation distortions which degrade the analog system even more severely than the digital system. By proper selection of components and circuit designs, the S/N will be optimized. Because the characteristics of emitter and detector are all adversely affected by temperature and cycling, some temperature compensation procedures are required in the design in order to keep the yearly outage time to a few minutes. During installation, it is advisable to decouple the stresses induced in the cable to improve reliability since the fiber lifetime is dependent on the amount of long term residual stress placed on the fibers.

The hybrid communications system, combining MMW Integrated Terminals and FO local distribution networks can offer the advantages of wideband operation, secure data transmission, and reduced costs. For many military tactical systems operating in hostile environments, and commercial broadband links in both congested urban areas and remote rural communities, the hybrid approach also provides impressive advantages of system transportability, flexibility, installation and maintenance simplicity, and lower construction/hardware costs over the full FO system.

8.2.6 Hardware Package Concept

MMW Integrated Terminal Concept

The conventional MMW terminals utilize transmission waveguides to interface the antenna to the transmitter/receiver. Extra unwanted waveguide losses degrade the transmitter EIRP and receiver S/N, sensitivity and dynamic range. Furthermore, transmission waveguide increases the terminal

cost. Both cost reductions and performance improvements will be realized if the solid-state Tx/Rx integrates directly with the antenna and links to the processing room (or users) through an FO cable. Wideband FO's can handle the secure communications using frequency hopping or direct sequence spread-spectrum, without difficulty.

Terminal Using Hybrid Circuits

The elimination of expensive machined-metal waveguides and related hardware from the system offers design flexibility and order of magnitude reductions in fabrication costs. A number of hybrid fabrication and integration techniques are becoming available, including microstrip, suspended stripline, image guide and fin line, all of which are expected to be used to meet specific needs having noncritical tolerances. Antennas, low noise amplifiers, local oscillators, mixers, filters, and switches can all be fabricated using integrated hybrid configurations on various substrates such as fused quartz, GaAs, and Duroid.

Package and Housing

Millimeter wave hardware assembly and housing dominate the system environmental performances for tactical application. Normally, aluminum is feasible as the package material because of light weight and ease of machining. To provide ease of soldering, freedom from oxidization, and to ensure overall connection integrity, the aluminum housing should be nickel flashed and then tin or gold plated. The module cavities (or compartments) of each microstrip component must be designed to prevent energy propagation in the waveguide mode. The package center wall may be chosen in the package design to function both as a mounting for the bias RFI decoupling and as an RF wall. The bias regulator and protective circuitry can be placed adjacent to the RF circuitry. Decoupling of individual components is assured through the use of distributive RF by-pass components or small RFI filters. Hermetic feedthrough is suggested for the connection to the external supply.

To ensure against electromagnetic interference, an RF lid is required. First, attached firmly with a number of screws. A second lid can then be used to provide hermetic seal. The hermetic lid is attached by using suitable epoxies; leak rates of better than 10^{-9} CC/sec are achievable.

To improve deployment speed and reduce cost, a foldable compact tripod mounted with proper height, instead of an antenna tower, is recommended for most millimeter wave small size transceivers and repeaters. A telescope attached beside the transceiver (or repeater) will provide better alignment accuracy and reduce the alignment time.

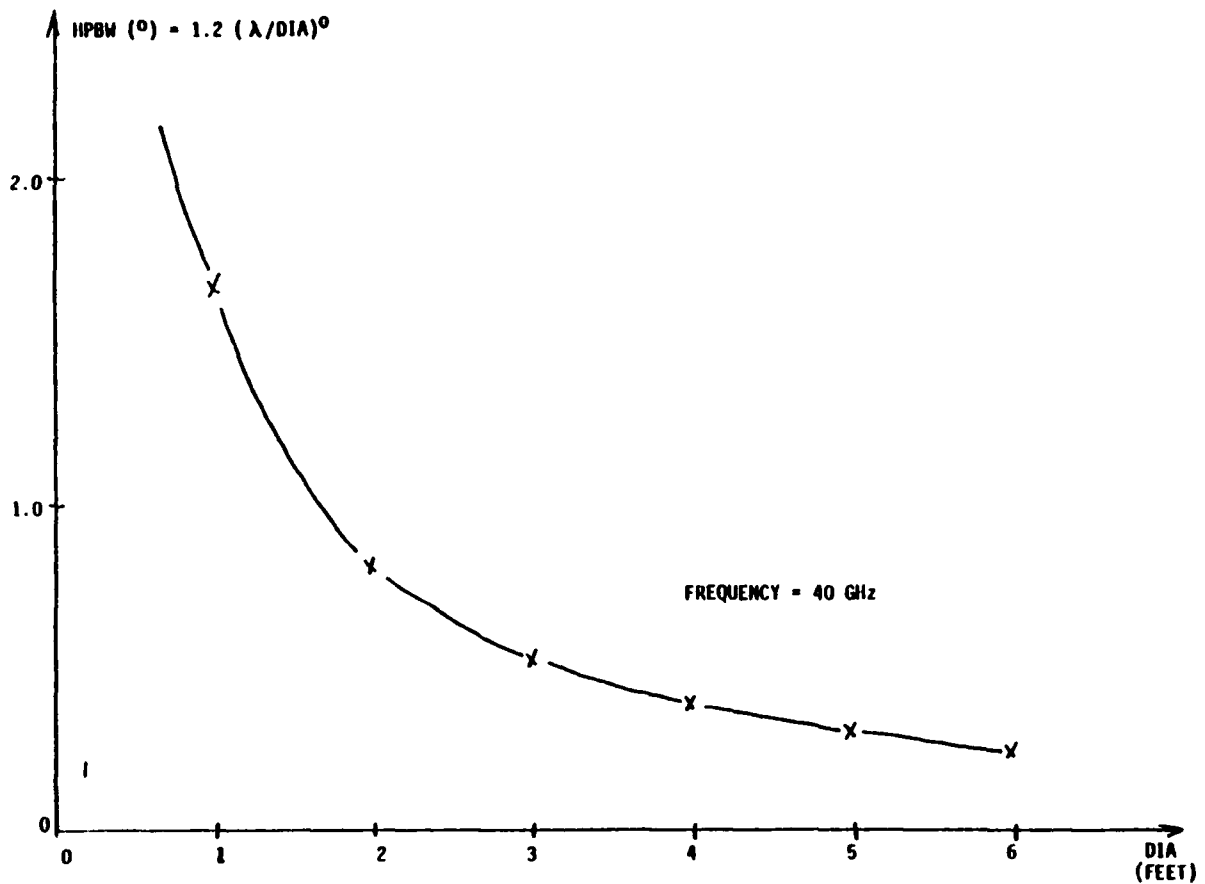
8.2.7 Nodal Terminal Antennas

There are two key issues connected with the nodal terminal antennas: 1) initial spatial acquisition of the transmitting antenna beam, i.e., initial alignment, and 2) maintenance of alignment in the face of wind gusts or vibrations. This will be discussed in terms of the relationship between antenna alignment and antenna mounting rigidity and the use of adaptive antenna techniques to maintain antenna alignment.

These issues are briefly discussed below.

Initial Antenna Alignment

The use of millimeter wave frequencies give rise to very narrow beamwidths even for small antenna apertures. This is illustrated in Figure 8.2.7-1 which shows how the half-power beamwidth (HPBW) of the main lobe decreases with increasing aperture size. For the application at hand, the HPBW will probably lie between 0.1 degrees and 1.0 degrees. While the narrow beamwidth is quite advantageous from a LPI and AJ point of view, it does make the tasks of initial antenna alignment and maintenance of alignment difficult.



A90401-47

Figure 8.2.7-1. Half-Power Beamwidth Versus Aperture Size

There are several techniques for initial alignment:

- a. Spoiled beam with sweep.
- b. Optical telescope rigidly mounted to antenna.
- c. Infrared ranging instruments.
- d. Unspoiled beam with CW carrier and AGC monitor in receiver.

The swept spoiled beam approach would use a mechanical displacement of the feedhorn to obtain a much broader beamwidth (lower gain results from this). This broad beam could then be spatially swept in azimuth and elevation until acquisition by the receiving terminal was acknowledged (via a HF radio link, perhaps). After peaking up on the spoiled beam (i.e., "fine" sweeping) the beam could then be despoiled and the sweep procedure repeated if necessary. Thus, this spatial acquisition technique is a two-step procedure in which coarse alignment is obtained with a spoiled beam and fine alignment is obtained with the unspoiled narrow beam. The disadvantage is that the coarse alignment procedure must operate with the lower antenna gain associated with the spoiled beam; in addition, the mechanical movement of the feedhorn could prove troublesome.

The optical telescope approach is simple and fast and requires that the optical boresight be co-aligned with the RF antenna boresight, preferably to within a small fraction of the HPBW of the antenna. If not, this approach would also require "fine" alignment via spatial sweep and a HF acknowledgement link from the receiving site.

Yet another approach involves the use of commercially available, compact, battery-operated infrared rangefinding instruments used for surveying. These instruments operate by emitting repetitive pulses of infrared light and determining the time delay between the emitted pulses and the received pulses that are returned from a three-cornered reflector located at a distant point. There are versions of this instrument that operate at distances of up to 20 miles. Although exact range is of no interest in initial alignment, these instruments could be used to find exact azimuth and elevation to the receiving antenna. This information could then be used to point the two antennas. The disadvantage is that a precise, calibrated method for pointing the antennas to a desired azimuth and elevation is required.

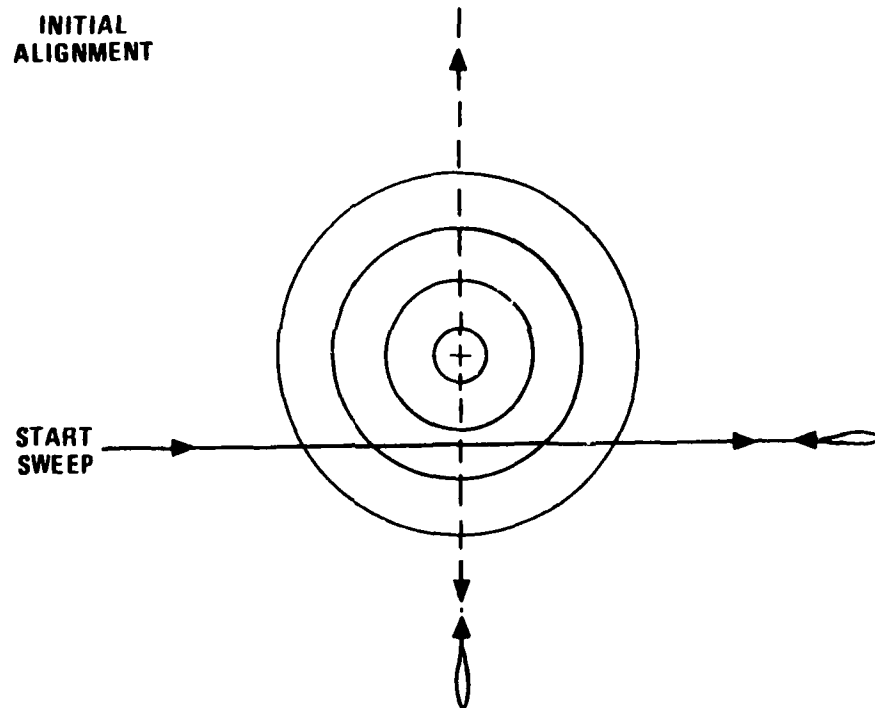
The fourth and perhaps most attractive technique for initial alignment utilizes an unspoiled beam and a spatial sweep procedure in conjunction with a CW carrier. Because of the very high data rates (< 20 Mb/s) required for normal operation, the SNR in a very narrow receiver bandwidth will be quite high. Thus, this method simply requires that the operator monitor the receiver AGC voltage level during spatial sweep with a very narrow IF filter in front of the AGC detector. If the very narrow IF filter is placed in front of the AGC detector and a CW carrier is received, then the receiver can detect the transmitted signal in the face of severely mispointed (i.e., many beamwidths) transmitting and receiving antennas. The procedure is to peak up the AGC voltage during azimuth sweep, then further peak AGC voltage during elevation sweep. This is shown in Figure 8.2.7-2 in which the concentric circles correspond to the sidelobe peaks of the antenna. This sweep procedure would be applied twice, first to the transmitting antenna, then to the receiving antenna. Normal data transmission is not affected since the narrow IF filter appears only in the AGC detector path, not in the signal flow path. This method is inexpensive since it requires only the addition of a single narrow IF filter and the alignment could be accomplished in a relatively short time.

Maintenance of Antenna Alignment

Once initial antenna alignment has been accomplished it must be maintained in the face of wind gusts and vibrations of the mounting structure. The most straightforward solution is to utilize a sufficiently rigid antenna support. Although this would not be too difficult for strategic, more or less permanent, communications links, it presents a significant problem in highly mobile, tactical communication situations. Several types of antenna support structures are listed below:

- a. Telescoping tubular mast.
- b. 3-faced light tubular frame sections.

- c. Telescoping conical mast.
- d. Concrete structures: poles, buildings.
- e. 4-faced heavy tubular frame sections.



- MONITOR RECEIVER AGC LEVEL DURING HORIZONTAL AND VERTICAL SWEEP
- SPATIAL SWEEP IMPLIES AN APPROPRIATE MECHANICAL STRUCTURE

A90401-48

Figure 8.2.7-2. Spatial Sweep Acquisition

Of these, the first three would probably require guy wires, whereas the latter two would not. The difficulty is that for the treetop level antenna supports required the first three supports listed above may not be sufficiently rigid even with an elaborate guying system. The latter two types of support are sufficiently rigid but are not nearly as transportable as the first three types of support. The adequacy of the first three types of support (with or without guy wires) can only be established with confidence through a field measurement program, which is beyond the scope of this study. On the other hand, it is felt that either tall, monolithic wooden/concrete poles or 4-faced heavy tubular frame sections would provide a sufficiently rigid antenna support.

An alternative to providing very rigid antenna support is to use an adaptive antenna technique in conjunction with a duplex link between antennas. Using a half-duplex link is not desirable since the transmitter/receiver role would have to be exchanged by each terminal at least hundreds of times per second in order to track out wind-induced oscillations in each antenna. The exchange protocol, the time-of-flight link delay, and the high data rates all combine to yield an intolerable data buffering requirement and an inordinately high overhead rate. Full duplex operation, on the other hand, may be a system requirement due to other considerations. If this is true and adaptive antennas are used, then the only remaining problem is ensuring that the weight control loop bandwidth is sufficiently high to track out wind-induced rapid mechanical oscillations. However, there is a potential problem in requiring an adaptive antenna control algorithm to perform two widely disparate tasks. On the one hand, the algorithm must steer a null onto a strong jammer with relatively slow dynamics; on the other hand, the main antenna lobe must track a considerably weaker desired signal with much faster dynamics (wind-induced oscillations). The eigenvalues associated with the jammer will be much larger than those associated with the weaker desired signal. This means that the adaptation to the desired signal will proceed much more slowly than the steering of nulls onto the jammer. Unfortunately, the desired signal dynamics are much higher than those of the jammer. Because of second order effects associated

with nonideal adaptive array elements and commonly used algorithms, instabilities are possible in this situation. This instability problem can be ameliorated somewhat by using a self-orthogonalizing adaptation algorithm in which the magnitudes of the difference between jammer eigenvalues and the desired signal eigenvalue are minimized. All told, there appears to be some risk in using antenna adaptation to maintain alignment while attempting to simultaneously null jammers. As a minimum, extensive computer simulation and algorithm development work should be performed prior to implementation. Until such additional simulation and development is performed, the most promising interim solution appears to be utilization of sufficiently rigid antenna support structures at the expense of easy transportability.

8.2.8 Link Quality Measurement at Nodal Terminals

One of the key requirements of a communications system based upon an alternate route architecture is the ability to quickly and accurately determine the quality of the various links terminating at a node without seriously degrading the normal operation of the communications system.

Three candidate approaches to link quality measurement were considered:

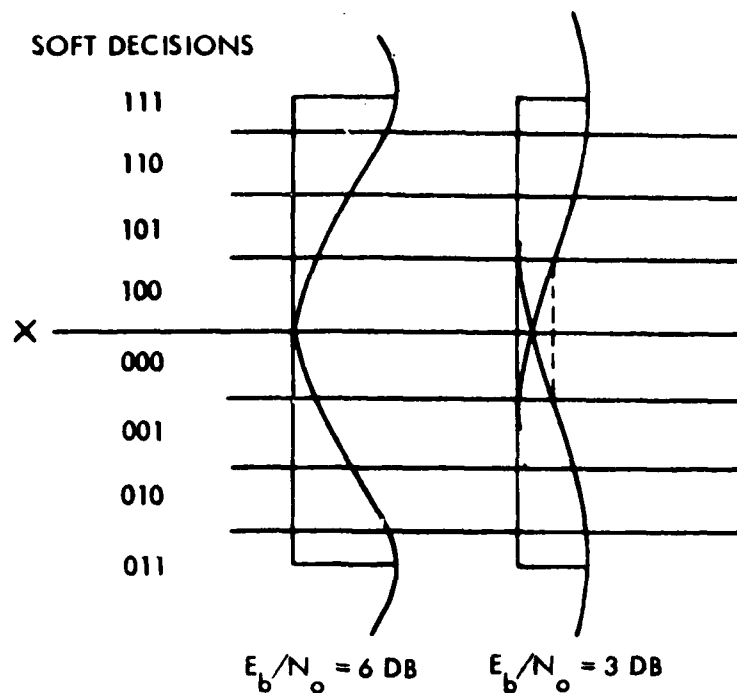
1. Monitor received power level (i.e., AGC level).
2. Measure PN sequence BER.
3. Estimate probability density function of (signal + noise + jammer).

The first of these approaches exhibits extreme simplicity but can be immediately ruled out since there is no way to distinguish jammer signals from desired signals.

The second approach is straightforward in that a direct measurement of link quality, i.e., BER, is obtained by transmitting a known PN sequence of bits over each link in question and counting bit errors in the received sequence. At the high data rates involved, a reliable estimate of link quality could be obtained in less than one second, with little impact upon communication overhead rate. A serious disadvantage of this approach is that normal data flow must be periodically disrupted in order to perform the BER measurement. This interruption of normal data flow implies that very large, high speed data buffers with appropriate control functions are required. Clearly, a more elegant approach is desirable.

The most desirable approach to link quality measurement is indirect in the sense that link BER is not measured directly. Instead, a parameter of the probability density function (pdf) of (signal + noise + jammer) is recursively estimated. This technique is characterized by rapid response, low complexity, and operation with random data. A detailed discussion follows.

Figure 8.2.8-1 shows the pdf of a BPSK signal plus thermal noise and jammer for two different signal levels. The vertical axis represents voltage (+ and -) and the horizontal axis represents probability density. Note that the pdf corresponding to the higher signal level ($E_b/N_0 = 6$ dB) is more sharply peaked about the means and hence permits accurate decisions a higher fraction of the time. Also shown in Figure 8.2.8-1 are the threshold levels corresponding to an eight level quantizer; the corresponding representation levels are labeled with a three-bit binary number. The most significant bit (MSB) is "1" for positive voltages and "0" for negative voltages. Thus, the magnitude of the baseband voltage is represented by the two right-most bits. The probability that these two right-most bits will assume the values 00, 01, 10, and 11 are a function of the ratio of the received signal level and the thermal noise-plus-jammer level, E_b/N_0 . This functional relationship is shown in Figure 8.2.8-2 and indicates that for high E_b/N_0 the 11 result occurs much more often than the others; this is a result of the peaking of the pdfs about the means.



A90401-49

Figure 8.2.8-1. Quantizer Output Probability

The information in Figure 8.2.8-2 can be used to estimate signal quality in terms of E_b/N_o ; the link BER can then be easily determined from the E_b/N_o versus BER performance curve associated with the link in question. This may be accomplished by forming a weighted sum of the logical outputs corresponding to the quantizer output states and recursively averaging this sum. A top-level block diagram of this operation is given in Figure 8.2.8-3. The steady-state accumulator value is reached when the accumulator value scaled by $1/\Delta$ is equal to the weighted sum of the logical outputs of the quantizer. Changing the value of $1/\Delta$ affects the rate at which the accumulator responds to changes in E_b/N_o . Note that the inputs

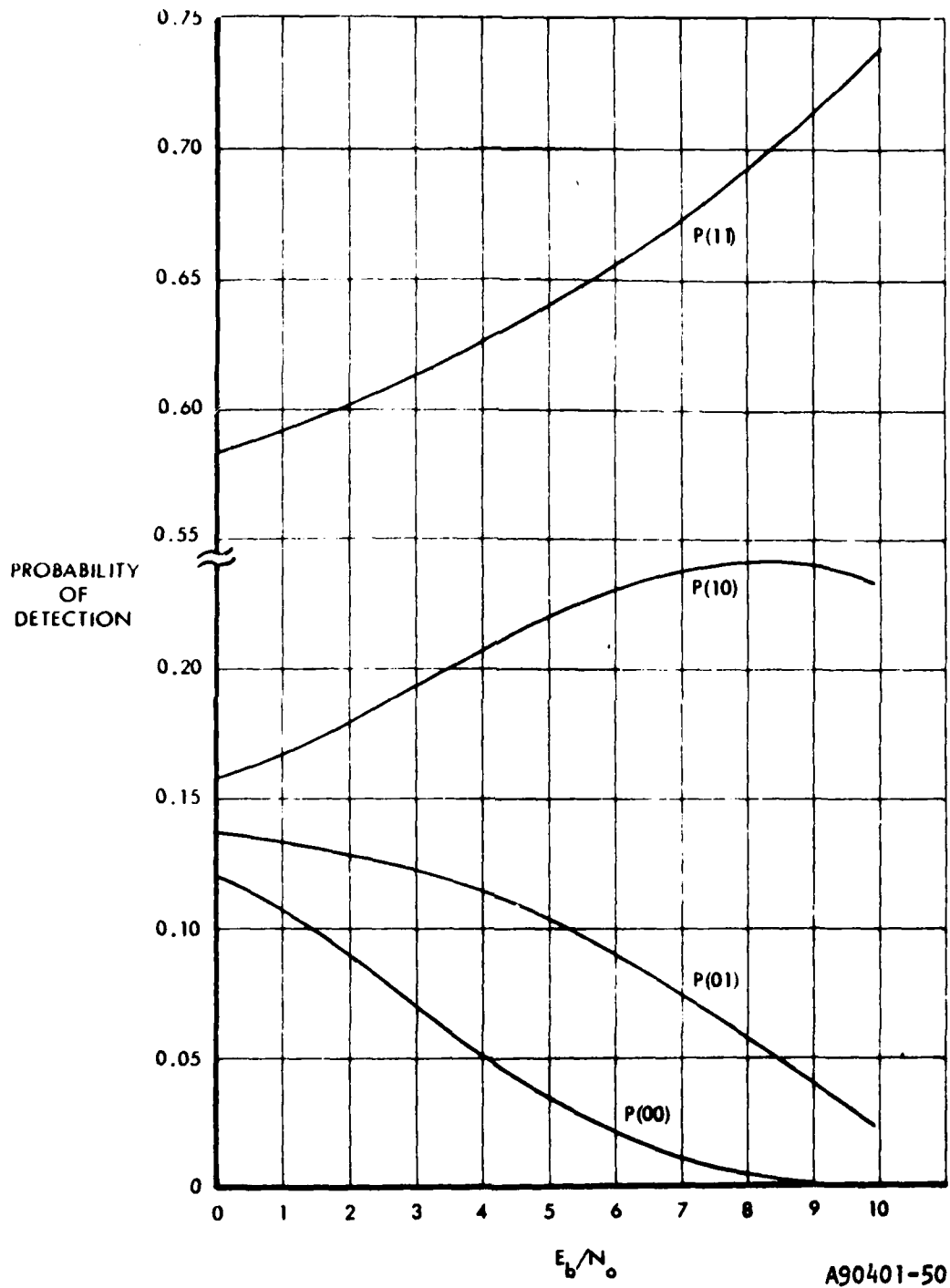


Figure 8.2.8-2. Quantizer Magnitude Detection Probabilities

to the weights of Figure 8.2.8-3 are not literally the binary numbers 00, 01, 10, and 11; rather the inputs labeled in this fashion are true or "1" if the corresponding quantizer states are activated for a particular sample. For example, the input labeled "11" has the value 1 (true), if either of the quantizer states "111" or "011" occurs at a particular sample time, and has the value 0 (false) otherwise.

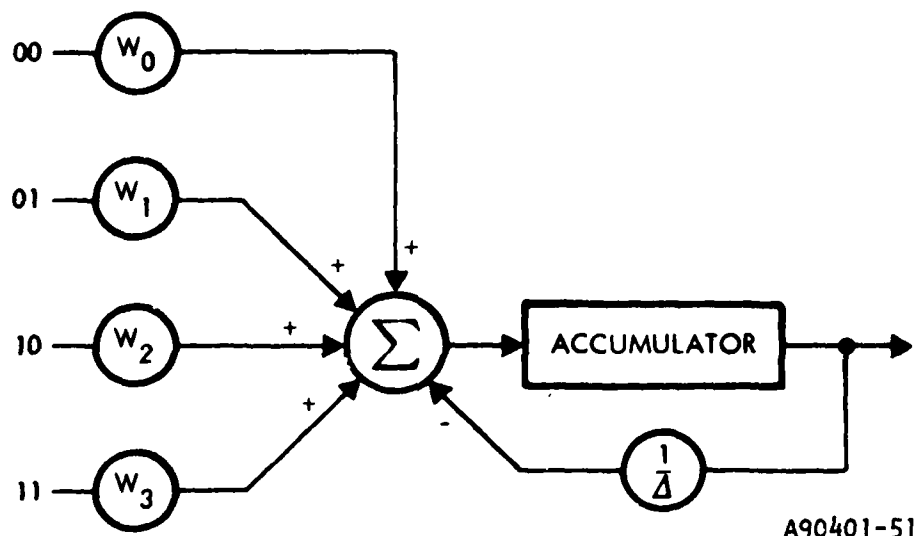


Figure 8.2.8-3. Quantizer Monitor

A more detailed diagram of a practical implementation for a single link quality monitor is shown in Figure 8.2.8-4. This implementation uses a 20-bit accumulator and a weighting programmable read-only memory (PROM). Extensive simulations and tests of this link quality circuit have been performed at Harris in conjunction with another program. These simulations were used to optimize the choice of weights and the results were used in a circuit that monitored link quality in an actual satellite link subject to fading caused by rain and other atmospheric phenomena.

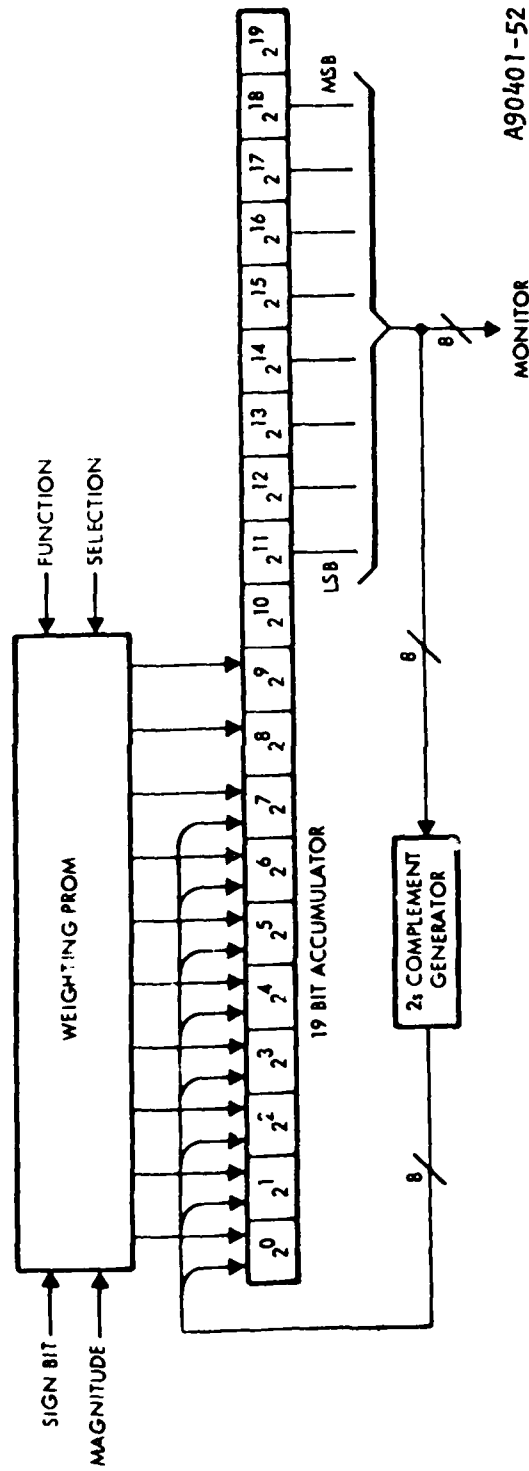


Figure 8.2.8-4. Practical Quality Monitor

The test results show that this approach to link quality monitoring is very effective. The precision to which link E_b/N_0 can be estimated is indicated in Figures 8.2.8-5 (2 sheets). In these figures the pdf of the accumulator values, based on 5000 samples/level, is shown for several E_b/N_0 values. It is noteworthy that even for low E_b/N_0 values the pdf's are still sharply peaked. Thus, knowledge of the accumulator values permits accurate determination of current link E_b/N_0 and, therefore, current link BER.

For the nodal terminal which has access to multiple links, one might consider an alternative to building a dedicated link quality monitor for each of the links. One approach is to utilize a microprocessor-based design which sequentially samples each of several link quantizer states, weights these states, and stores these weighted sums in separate accumulators after subtracting a scaled version of the previous content of the appropriate accumulator. In essence, this approach is the same as that of Figure 8.2.8-3 except that the weight inputs are multiplexed over several quantizers and several accumulators are used rather than one. Such a microprocessor-based design could also automatically determine the best link for communications (with some hysteresis so as not to switch links to obtain only small improvement) and provide all of the control functions and protocol required for automatic switchover among links.

8.3 Repeater Terminals

Both active and passive repeaters are feasible for millimeter wave tactical information relay. Nonregenerative and regenerative repeaters have been widely used in the microwave band for digital radio networks and are feasible for extension to the millimeter wave frequency. The block diagrams of these two active repeaters are illustrated in Figure 8.3-1 and Figure 8.3-2, respectively. The passive repeaters are merely the reflector antennas, in the shapes of flat mirrors, parabolic reflectors, or corner reflector. The reflector antenna is capable of redirecting the incident

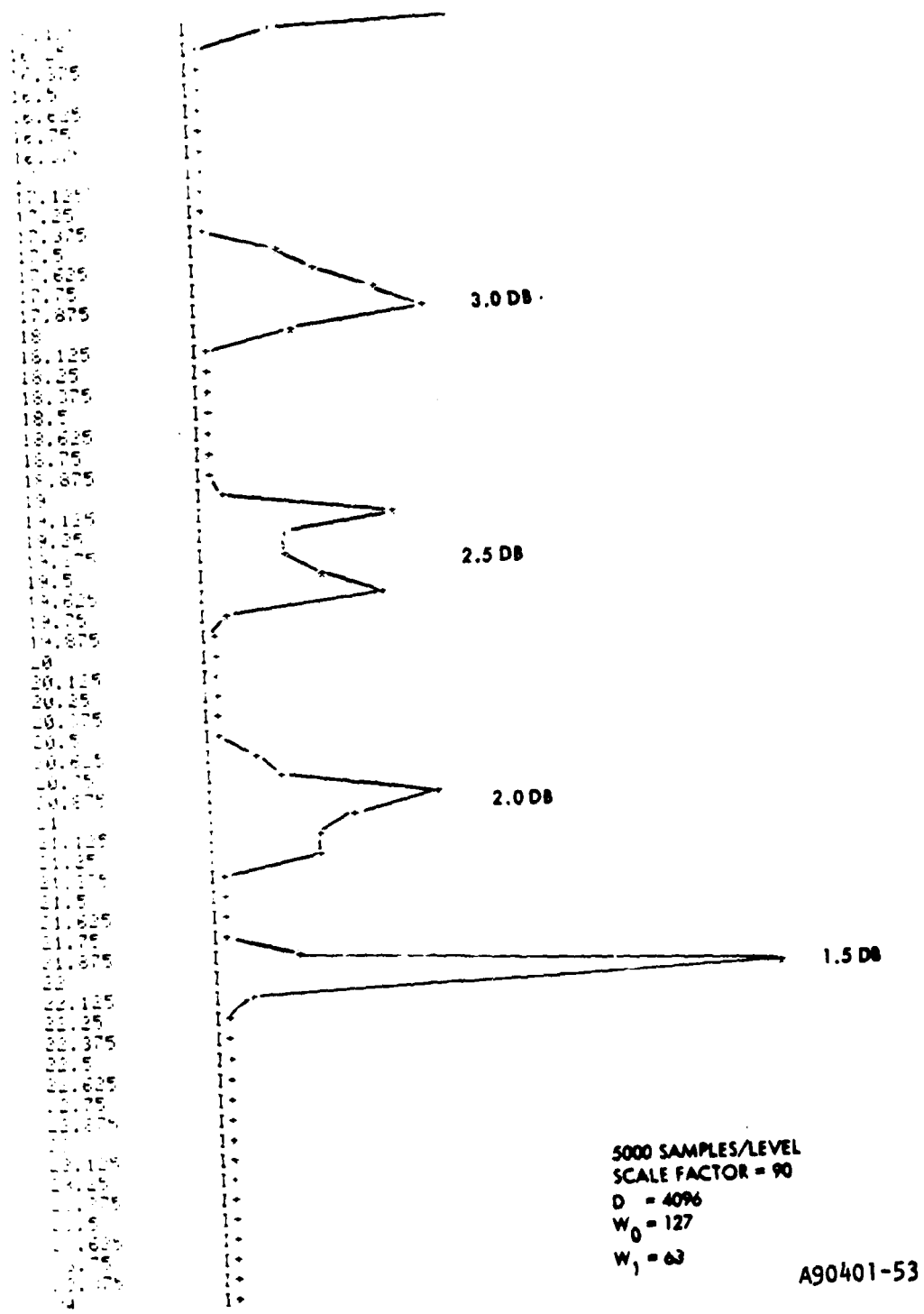


Figure 8.2.8-5. Accumulator Distribution (Sheet 1 of 2)

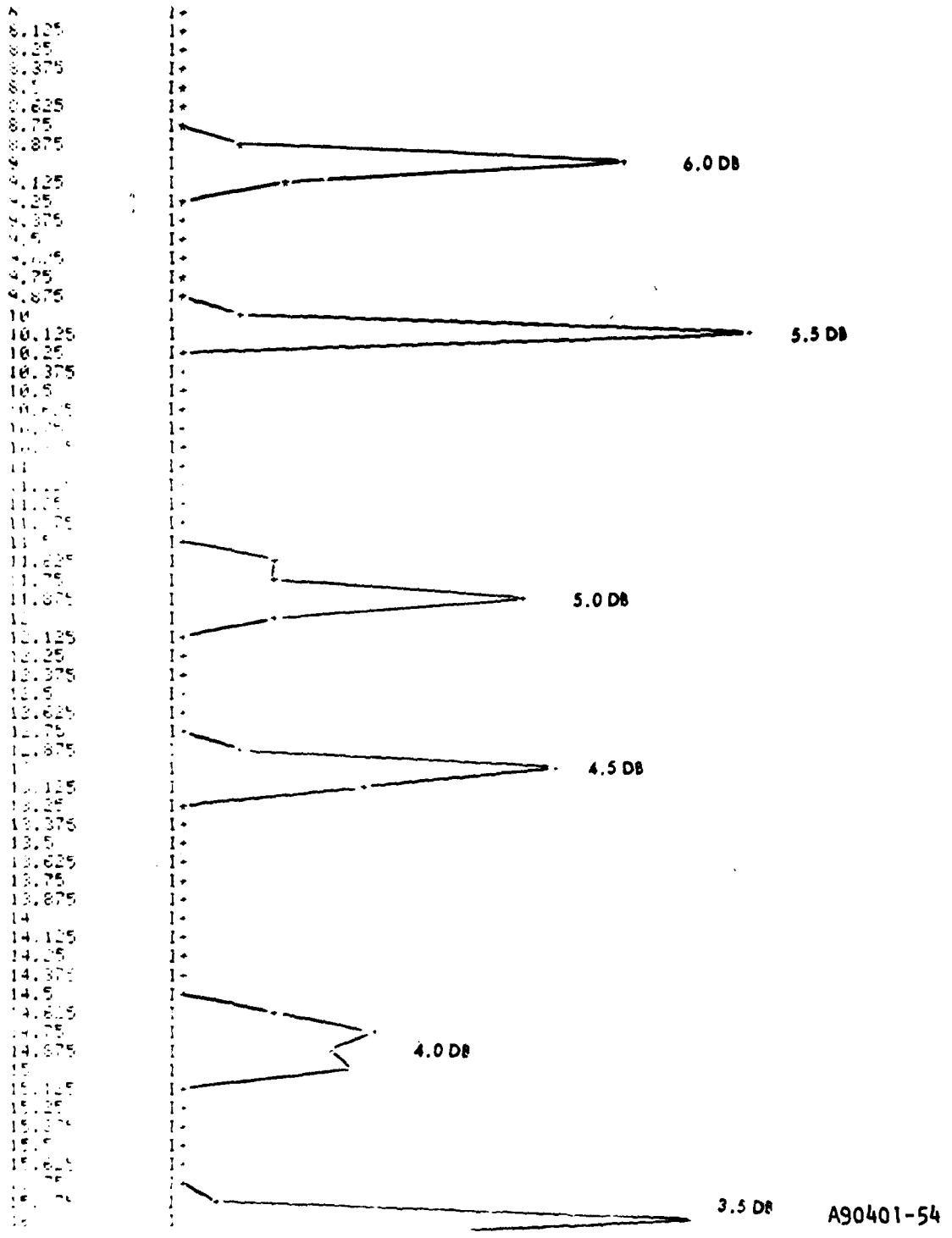
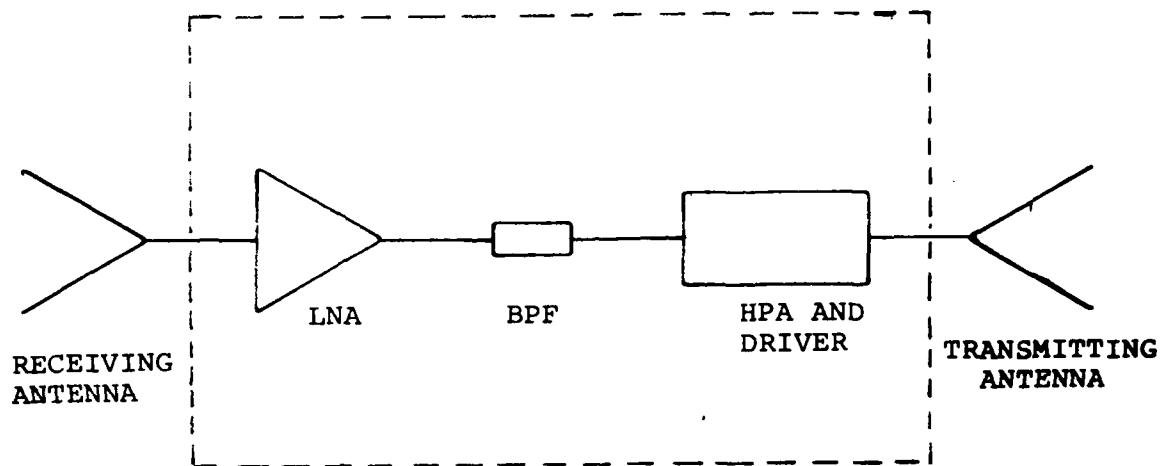


Figure 8.2.8-5. Accumulator Distribution (Sheet 2 of 2)

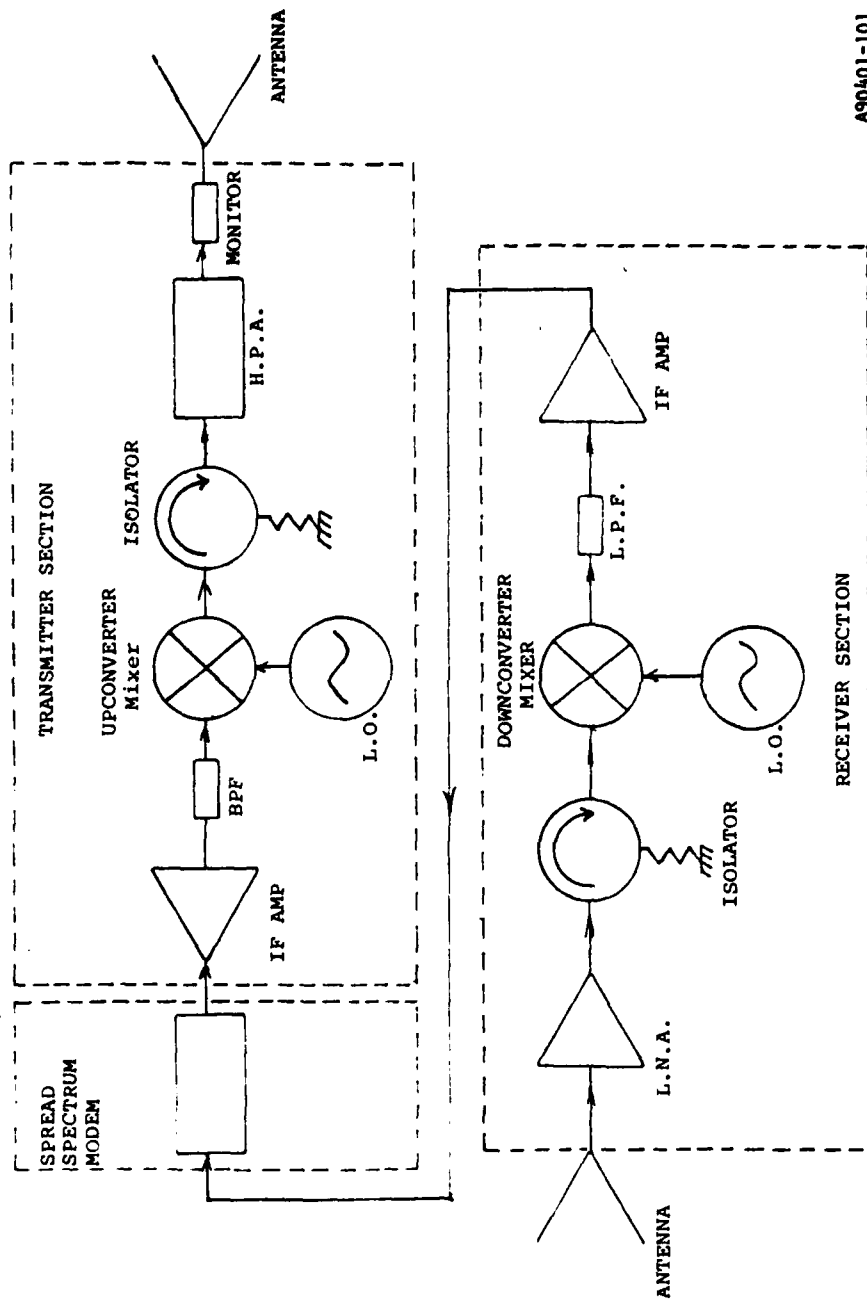
beam in a desired direction, in space focusing them with adjustable degrees of convergence and dropping channels in quasi-optical form. Combinations of several reflective mirrors, such as depicted in Figure 8.3-3, can redirect the millimeter wave beam in almost any direction in space, a feature which is required to circumvent obstacles.



A90401-100

Figure 8.3-1. Nonregenerative Repeater for Millimeter Wave Tactical Radio

Comparing the passive and active repeaters, each has its own merits, as shown in Table 8.3. From the cost viewpoint the passive antenna has considerable advantage, but it lacks transportability and mechanical vibration resistance.



A90401-101

Figure 8.3-2. Regenerative Repeater for Millimeter Wave Tactical Radio

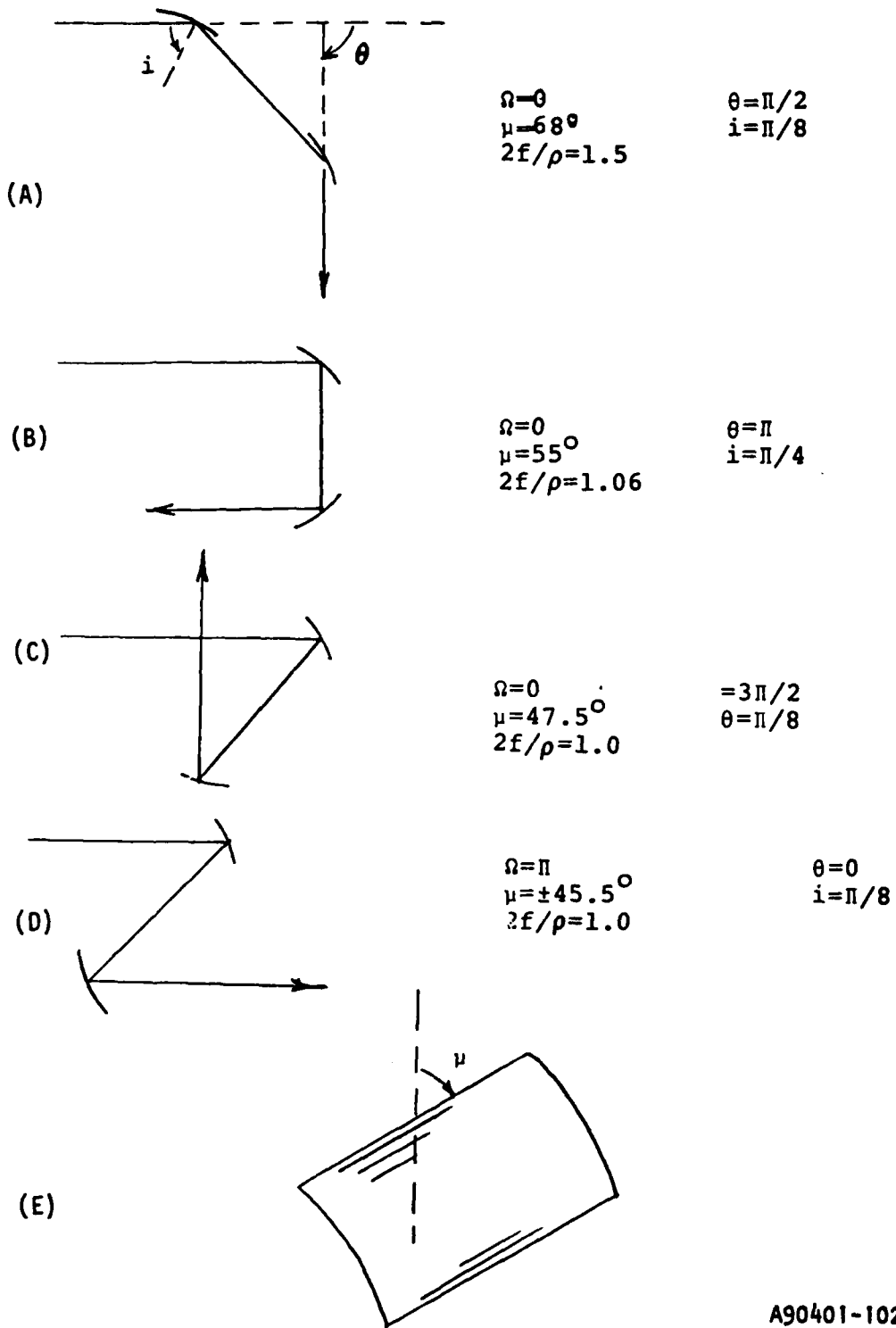


Figure 8.3-3. Illustration of Cylindrical Passive Reflection Mirrors

Table 8.3. Comparison of High Data-Rate Active and Passive Repeaters

	Active Repeater	Passive Repeater
Cost	Very high	Low
Reliability	Good	Excellent
Installation Simplicity	Good	Good
Transportability	Excellent	Fair
Retiming and Reshaping	Yes	No
Amplification Gain	Yes	No
Antenna Polarization Distortion	No	Possible
Dc Power Requirement	Yes	No
Maintenance Simplicity	Good	Excellent

8.3.1 Systems Considerations for Active and Passive Repeater Terminals

8.3.1.1 Introduction

Repeater terminals are defined, for the purposes of this discussion, as being terminals that are added to an existing, essentially tandem, network in order to provide an alternate route capability for the existing network. These repeater terminals may be either regenerative or nonregenerative. Regenerative repeaters demodulate, amplify, and remodulate the desired signal, whereas nonregenerative repeaters simply amplify the RF signal and the associated noise as well. Passive repeaters are quite simple by comparison and can consist of planar reflectors or perhaps back-to-back dish antennas connected by waveguide; there are no active devices associated with a passive repeater. Generally speaking, regenerative repeaters are quite expensive and complex; nonregenerative repeaters require no baseband electronics and are thus less expensive. Passive repeaters are quite

inexpensive and, most importantly, do not require a source of electrical power. The issue of available electric power could be crucial for repeater sites that are not easily accessible. Installing power lines or an extensive battery system at an active repeater site could be an expensive undertaking.

In order to obtain an alternate route capability at minimum cost, the added nodes and links must be inexpensive relative to the existing nodes and links. Utilizing passive reflectors at the added nodes is an attractive approach for minimizing the added node and link costs. The use of passive reflectors as nonregenerative repeaters at the added nodes is feasible only because the data need not be recovered, i.e., demodulated, at the added nodes. If we envision an alternate route network in which the existing nodes are manned, regenerative repeaters containing a full complement of receivers, transmitters, demodulators, modulators, switching equipment, and antennas, and the added nodes are simply unmanned passive reflectors, then the alternate routing capability can be achieved at very little additional cost relative to the original network of "existing" nodes.

Since the use of passive repeaters or reflectors promises to be a very cost effective way of augmenting an existing network to obtain an alternate route capability, the emphasis of the discussion that follows will be upon passive reflector repeaters. The active repeater problem is well understood and need not be treated at length, whereas passive reflectors are rarely used in practice at microwave frequencies, except in "near-field" "periscope-type" applications in which a small metal reflector is located at the top of a tower and the transmitter or receiver is located at the bottom of the same tower.

8.3.1.2 Near Field Versus Far Field Passive Reflector Considerations

The derivation of the equations that govern the performance of links containing one or more passive reflectors is based upon the assumption that the energy that arrives at each reflector is in the form of a plane wave rather than a spherical wave. This is the same as saying that the reflector lies in the "far field" of the radiating element. The point at which the far field ends and the near field begins is a function of not only the absolute distance to the radiating element (i.e., the RF source), but also the frequency of the wave and the spatial dimensions of the passive aperture under consideration. The transition between near field and far field for a given aperture size and frequency is commonly defined to be that source-to-aperture distance at which the spherical wave departs from being a plane wave by 1/16 of a wavelength at the edge of the aperture. This definition is clarified in Figure 8.3.1.2-1, which shows a side view of a plane wave and a spherical wave incident upon an aperture of dimension (or diameter) a . The analytical expression for the radius at which the near field begins may be obtained from the geometry of the figure. The result is:

$$r_{\text{near}} = \frac{\lambda}{32} + \frac{2a^2}{\lambda}$$

where λ = wavelength

and a = aperture dimension (diameter for round apertures)

The near field radius is plotted in Figure 8.3.1.2-2 versus aperture size with frequency as a parameter. This figure shows that situations involving passive reflectors in the near field could conceivably arise in practice. It turns out that under certain conditions the "efficiency" of a passive reflector in the near field can actually exceed 100 percent. In other words, the primary antenna-reflector combination can exhibit more net gain than the primary antenna alone. This is borne out by some results taken

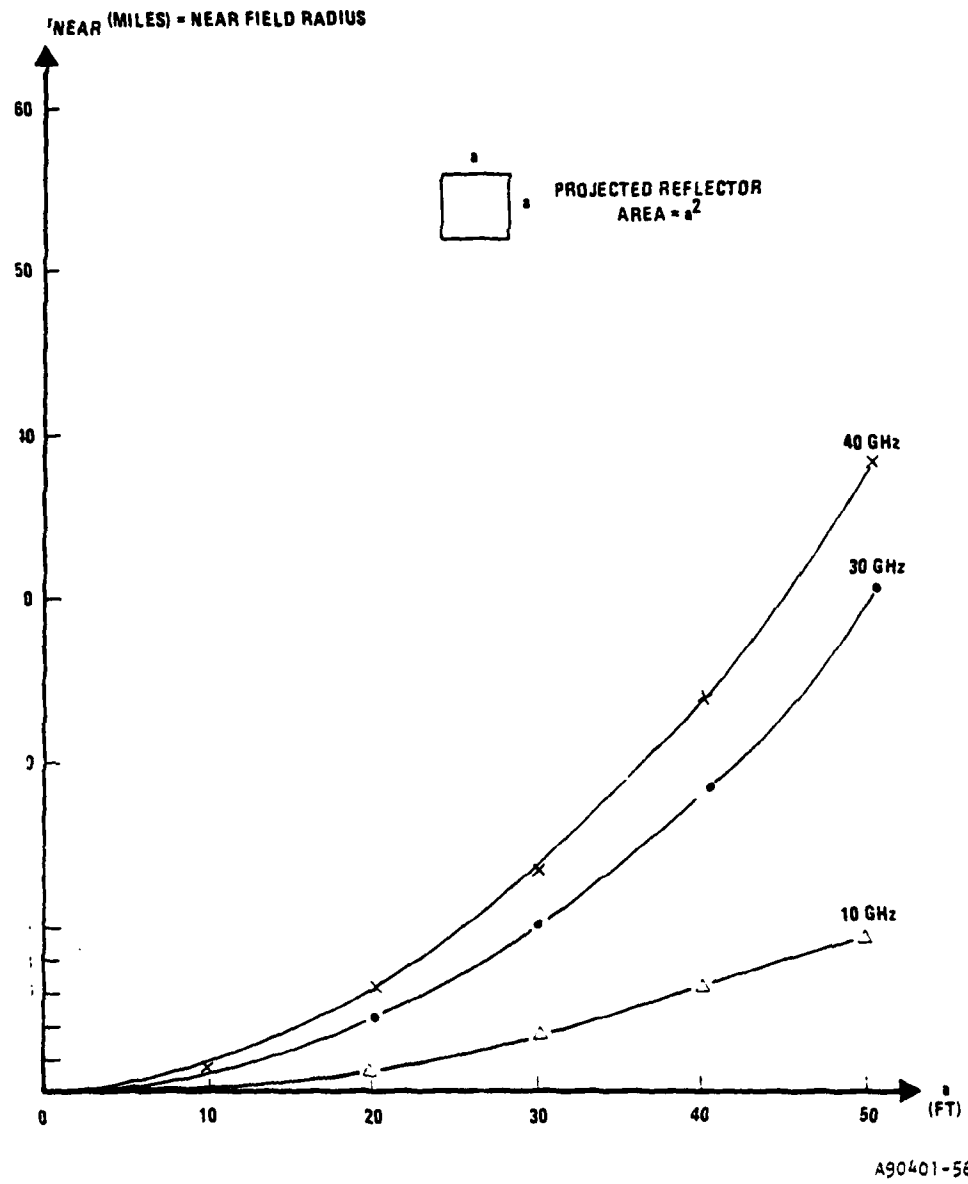


Figure 8.3.1.2-2. Near Field Radius Versus Aperture Size

from an excellent reference by Norton¹ regarding passive reflectors in the near field and far field. Figure 8.3.1.2-3 contains a figure from Norton's paper that shows that up to 6 dB gain can be obtained when using a passive reflector in the near field. Also shown in Figure 8.3.1.2-3 is an example that illustrates the use of the governing equations.

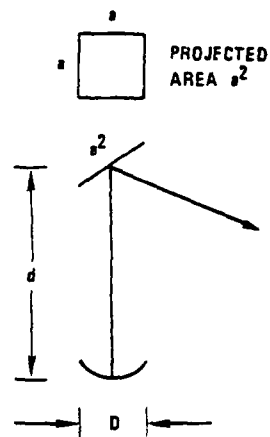
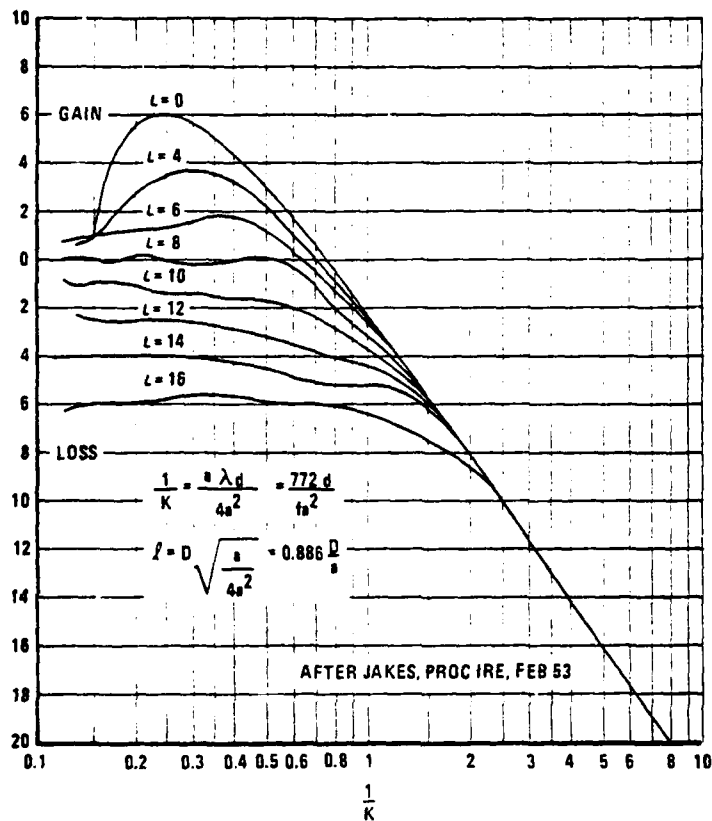
Another case in which a passive reflector is in the near field can arise when a double passive reflector is used in order to increase the projected area. Figure 8.3.1.2-4 shows how the maximum reflector spacing (for ≤ 1 dB loss) varies with frequency and reflector size.

In the remainder of this section we shall assume that reflectors are in the far field for purposes of discussion; this assumption represents the worst case and thus serves to bound the results.

8.3.1.3 Two-Hop Passive Repeater Configurations

Three two-hop passive repeater configurations are shown in Figure 8.3.1.3-1. The simple reflector of figure 8.3.1.3-1(A) suffers from the disadvantage that the effective area of the reflector is reduced from the geometric area by the factor $\cos \theta$. This loss can be appreciable for sufficiently large values of θ . This loss due to small projected reflector area can be greatly reduced by using the two-reflector arrangement shown in Figure 8.3.1.3-1(B). The two reflectors are co-located, i.e., mounted on the same tower, but are not so close so as to block the required views of the transmitter and receiver. The two reflector arrangement permits the alternate route path length ($r_1 + r_2 + \Delta r$) to be reasonably close to the primary path length r so that the additional space loss can be kept small. A disadvantage of the planar reflector approaches is that the reflected fields may exhibit interference patterns if the receiving aperture "sees" both the direct and reflected wave. A third alternative for a passive

¹M.L. Norton, "Microwave System Engineering Using Large Passive Reflectors," IRE Trans. Comm. Systems, Sept. 1962, pp. 304-311.



$$l = 0.866 \left(\frac{D}{a} \right) \quad \frac{1}{K} = \frac{0.772}{f_{\text{GHz}}} \left(\frac{d}{a^2} \right)$$

EXAMPLE: AT $f = 40 \text{ GHz}$ d IN FT, a^2 IN FT²

CHOOSE $D/a \leq 1 \Rightarrow l = 0.866$

CHOOSE $\frac{1}{K} < 0.5 = \frac{0.772}{40} \left(\frac{d}{a^2} \right) \Rightarrow d < 25.9 (a^2) \text{ FT}$

FROM THE FIGURE \Rightarrow "EFFICIENCY" IS $\geq 100\%$ FOR ANTENNA-REFLECTOR COMBINATION

FOR $D \leq a$ & $d < 25.9 (a^2)$

A90401-57

Figure 8.3.1.2-3. Near Field Passive Reflectors

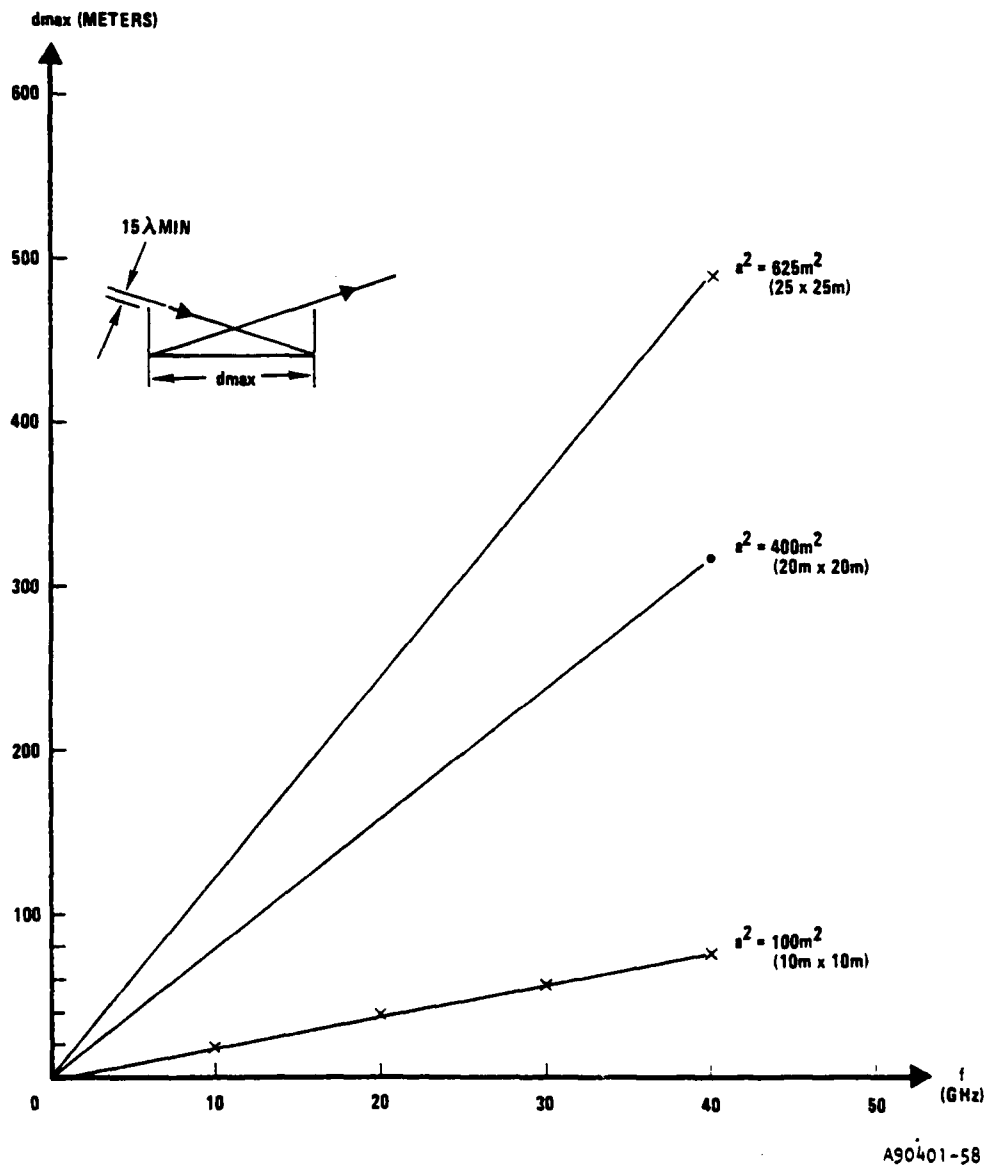
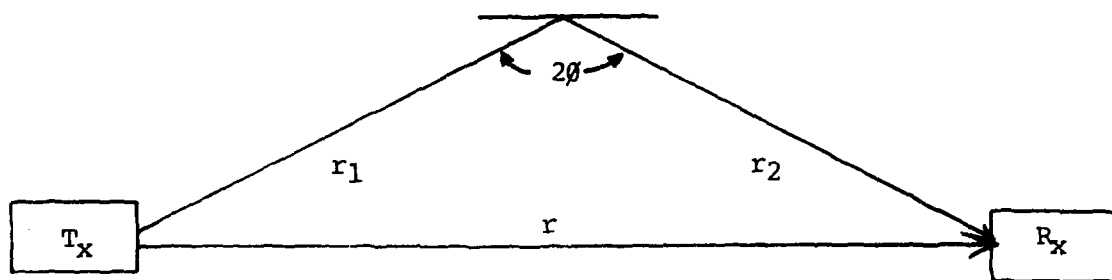


Figure 8.3.1.2-4. Maximum Spacing of Double Passive Reflectors for Loss <1 dB in Near Field

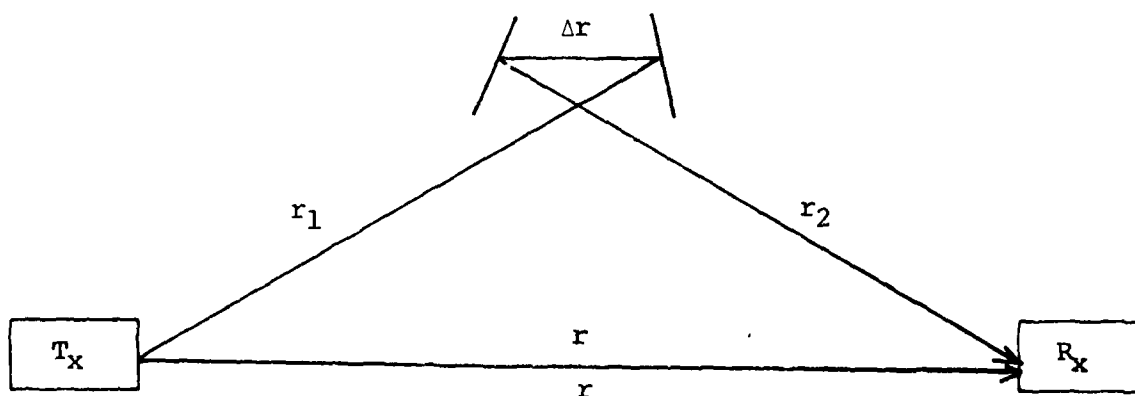
repeater is to use parabolic antennas rather than plane reflectors; this is shown in Figure 8.3.1.3-1(C). The parabolic dishes typically have efficiencies of about 60 percent and must be connected with a short length of waveguide but have the advantage that they can be pointed in any desired direction without suffering the projection loss of the single plane reflector approach and without being concerned about the potential blockage problem of the two-reflector approach.

The dish antenna approach of Figure 8.3.1.3-1 becomes particularly attractive for the more complex architectures of the types D, F and H discussed in Section 5.0 in which one node is associated with more than just two links. The four links entering an alternate node of a type D or H architecture must each be capable of being connected to any of the remaining three links. This could be accomplished using four antennas and a switch matrix, but this would require that the switch matrix be remotely commanded, either manually or automatically, in the event of disruptive jamming or rainfall. Although this remote switch commanding capability could be designed into a new system or added to an existing system at some expense, an attractive alternative is to simply trade an additional number of antennas at each added node for that additional complexity of a remote switch commanding capability. These two approaches for obtaining the required link connectivity are shown in Figure 8.3.1.3-2 along with the schematic representation of the required alternate node link configuration.

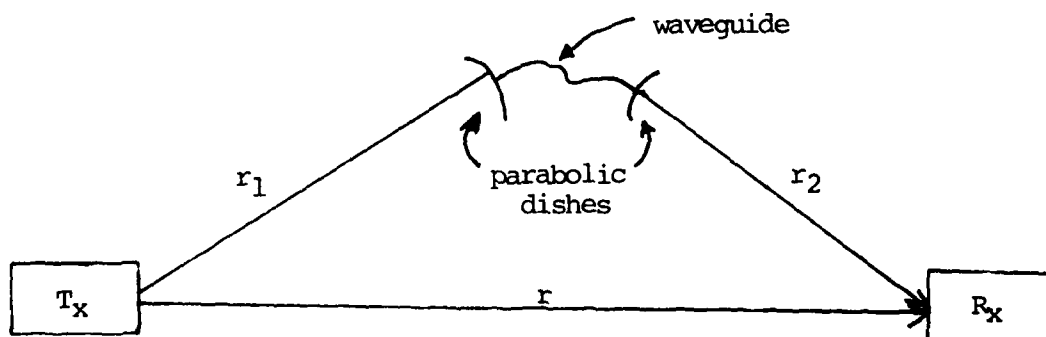
The ultimate decision as to whether the passive repeater approach of Figure 8.3.1.3-1 (A), (B), or (C) should be selected should be based upon detailed cost and performance tradeoffs. Likewise, whether the required link connectivity of the added nodes should be obtained using the remote switch commanding approach (with dishes) or the multiple antenna/link approach (Figure 8.3.1.3-2) should be decided after evaluating the cost/performance tradeoff.



(A)



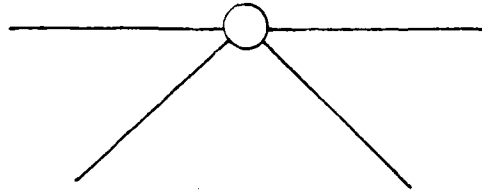
(B)



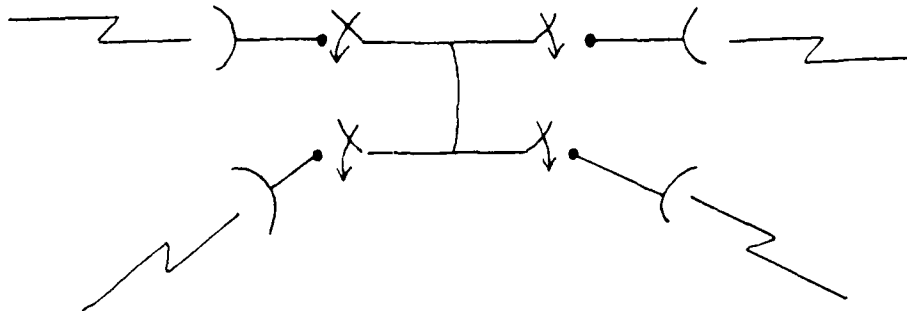
(C)

A90401-59

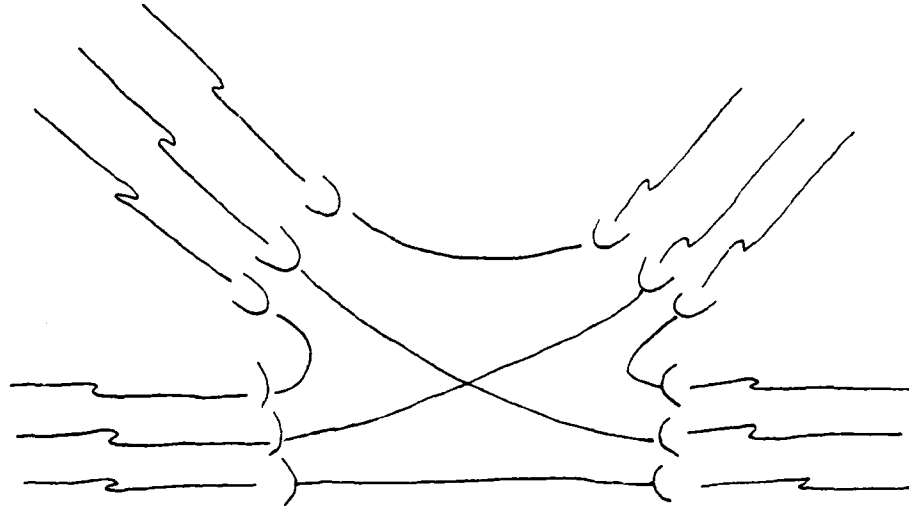
Figure 8.3.1.3-1. Three Passive Repeater Approaches



(A) POSSIBLE ALTERNATE LINK CONFIGURATION



(B) REMOTE SWITCH COMMANDING APPROACH



(C) MULTIPLE ANTENNAS PER LINK APPROACH WITH NO SWITCHING

A90401-60

Figure 8.3.1.3-2. Added Node Link Connectivity

Performance of Passive Repeater Links

In comparing the performance of alternate route links to primary route links we will find it convenient to use Figure 8.3.1.3-3 in which P and A represent the quantities power and antenna area, respectively. The subscripts T and R denote transmitted and received quantities, respectively, and the subscript D designates passive repeater, or deflector, parameters. The signal path along " r " will be called the primary route, and the signal path along route " r_1, r_2 " will be called the secondary route.

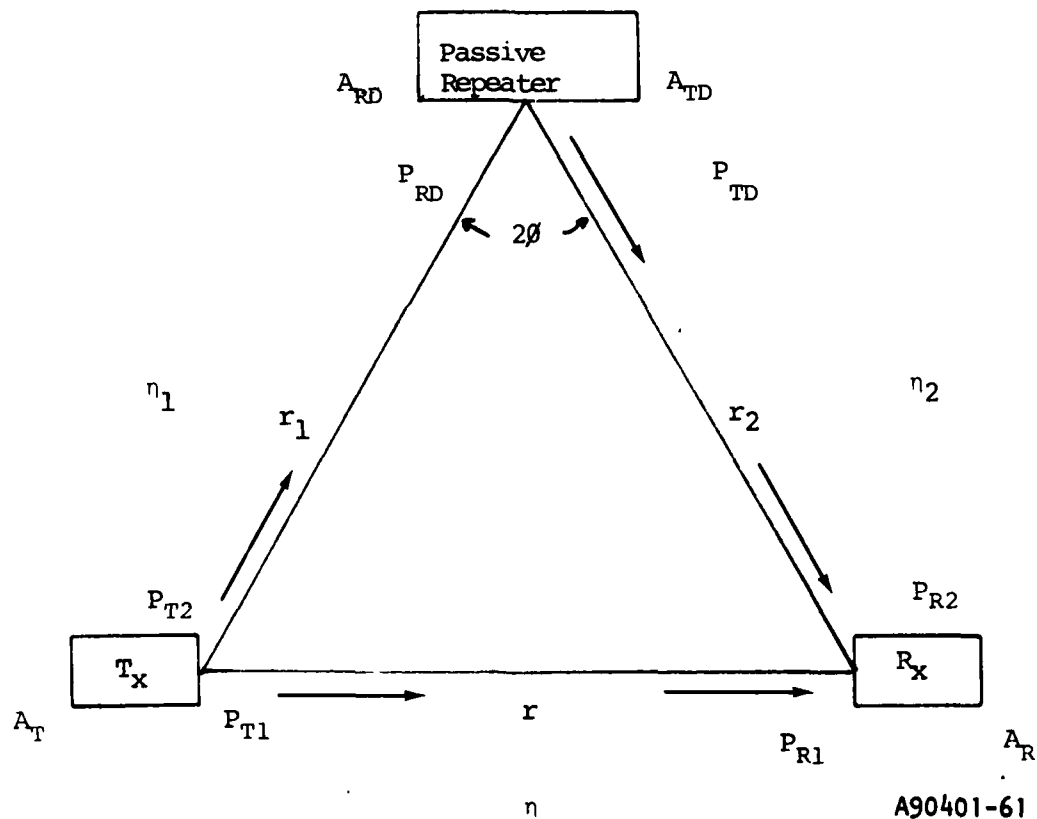


Figure 8.3.1.3-3. Signal Paths Geometry

Although we only treat the "existing node - repeater - existing node" case here, the extension of the analysis results to the "existing node - repeater - repeater - existing node" case is straightforward, and it will be discussed subsequently.

A useful performance metric for the alternate (secondary) path is its path loss relative to the primary route path loss, which we define as the alternate route efficiency η_A

$$\eta_A = \frac{P_{R2}/P_{T2}}{P_{R1}/P_{T1}} = \frac{\eta_1 \eta_2}{\eta} \quad (8.3.1.3-1)$$

where

$$\eta_1 = P_{RD}/P_{T2} \quad (8.3.1.3-2)$$

$$\eta_2 = P_{R2}/P_{TD} \quad (8.3.1.3-3)$$

$$\eta = P_{R1}/P_{T1} \quad (8.3.1.3-4)$$

and

$$P_{TD} = P_{RD} \text{ is assumed} \quad (8.3.1.3-5)$$

Substituting $P_R/P_T = \frac{A_R}{r^2} \frac{A_T}{\lambda^2}$ with appropriately modified subscripts we obtain

$$\eta_1 = \frac{A_{RD}}{r_1^2} \frac{A_T}{\lambda^2} \quad (8.3.1.3-7)$$

$$\eta_2 = \frac{A_R}{r_2^2} \frac{A_{TD}}{\lambda^2} \quad (8.3.1.3-8)$$

$$\eta = \frac{A_R A_T}{r^2 \lambda^2} \quad (8.3.1.3-9)$$

$$\eta_A = \frac{\left[\frac{A_{RD} A_T A_R A_{TD}}{r_1^2 r_2^2 \lambda^4} \right]}{\frac{A_R A_T}{r^2 \lambda^2}} = \frac{A_{RD} A_{TD} r^2}{r_1^2 r_2^2 \lambda^2} \quad (8.3.1.3-10)$$

Now substituting:¹

$$A = \frac{G \lambda^2}{4 \pi} \quad (8.3.1.3-11)$$

$$\eta_A = G_{RD} G_{TD} \frac{\lambda^4}{16 \pi^2} \frac{r^2}{r_1^2 r_2^2 \lambda^2} \quad (8.3.1.3-12)$$

$$\eta_A = \frac{G_{RD} G_{TD} \lambda^2 r^2}{16 \pi^2 r_1^2 r_2^2} \quad (8.3.1.3-13)$$

where

G_{RD} = Power gain of passive repeater receiver antenna

and

G_{TD} = Power gain of passive repeater transmitting antenna

¹Reference Data for Radio Engineers, 5th edition, 2nd printing March 1969, Howard Sams, Co., pp. 25-42.

If an amplifier is placed between the transmitting antenna and the receiving antenna, then the repeater is no longer passive and different rules govern the alternate route link performance. The active repeater case is fundamentally different from the passive repeater case in that the thermal noise of the repeater amplifier establishes a SNR_1 in the initial hop link; since the destination node also contains a receiver (i.e., amplifier), it is also characterized by a SNR_2 . The composite link is then characterized by the well-known expression:

$$SNR_{comp} = \frac{SNR_1 SNR_2}{1 + SNR_1 + SNR_2} \quad (8.3.1.3-14)$$

Differentiation of this expression with respect to r_1 or r_2 shows that SNR_{comp} is maximized when $r_1 = r_2$. Thus, the optimum placement of an active repeater is along the perpendicular bisector of the line joining the two nodes: the repeater should be equidistant from each node. This is in direct contrast to the result for passive repeater case as will be shown below.

Further insight into the behavior of the alternate route efficiency, η_A , for the passive repeater case may be obtained by using the cosine law to substitute for r_1 and r_2 :

$$r^2 = r_1^2 + r_2^2 - 2r_1r_2 \cos 2\phi \quad (8.3.1.3-15)$$

Define $\rho = r_1/r_2$

$$\text{Then } r^2 = \rho^2 r_2^2 + r_2^2 - 2 \rho r_2^2 \cos 2\phi \quad (8.3.1.3-16)$$

and solving for r_2 :

$$r_2^2 = \frac{r^2}{(1 + \rho^2) - 2\rho \cos 2\phi} \quad (8.3.1.3-17)$$

Similarly, solving for r_1 :

$$r_1^2 = \frac{r^2}{(1 + 1/\rho^2) - (2/\rho) \cos 2\phi} \quad (8.3.1.3-18)$$

and substituting (8.3.1.3-18) and (8.3.1.3-17) into (8.3.1.3-14) we obtain:

$$\eta_A = \left[\frac{G_{RD} G_{TD} \lambda^2}{16\pi^2 r^2} \right] \left[\left(\rho + \frac{1}{\rho} \right) - 2 \cos 2\phi \right]^2 \quad (8.3.1.3-19)$$

The link alternate route efficiency η_A may be maximized with respect to repeater geometry by finding the values of ρ and 2ϕ which simultaneously satisfy the following four equations:

$$\frac{\partial \eta_A}{\partial \phi} = \left(\rho + \frac{1}{\rho} \right) \sin 2\phi - \sin 4\phi = 0 \quad (8.3.1.3-20)$$

$$\frac{\partial^2 \eta_A}{\partial \phi^2} = \left(\rho + \frac{1}{\rho} \right) \cos 2\phi - 2 \cos (4\phi) > 0 \quad (8.3.1.3-21)$$

$$\frac{\partial \eta_A}{\partial \rho} = \left[\left(\rho + \frac{1}{\rho} \right) - 2 \cos 2\phi \right] \left[1 - \frac{1}{\rho} \right] = 0 \quad (8.3.1.3-22)$$

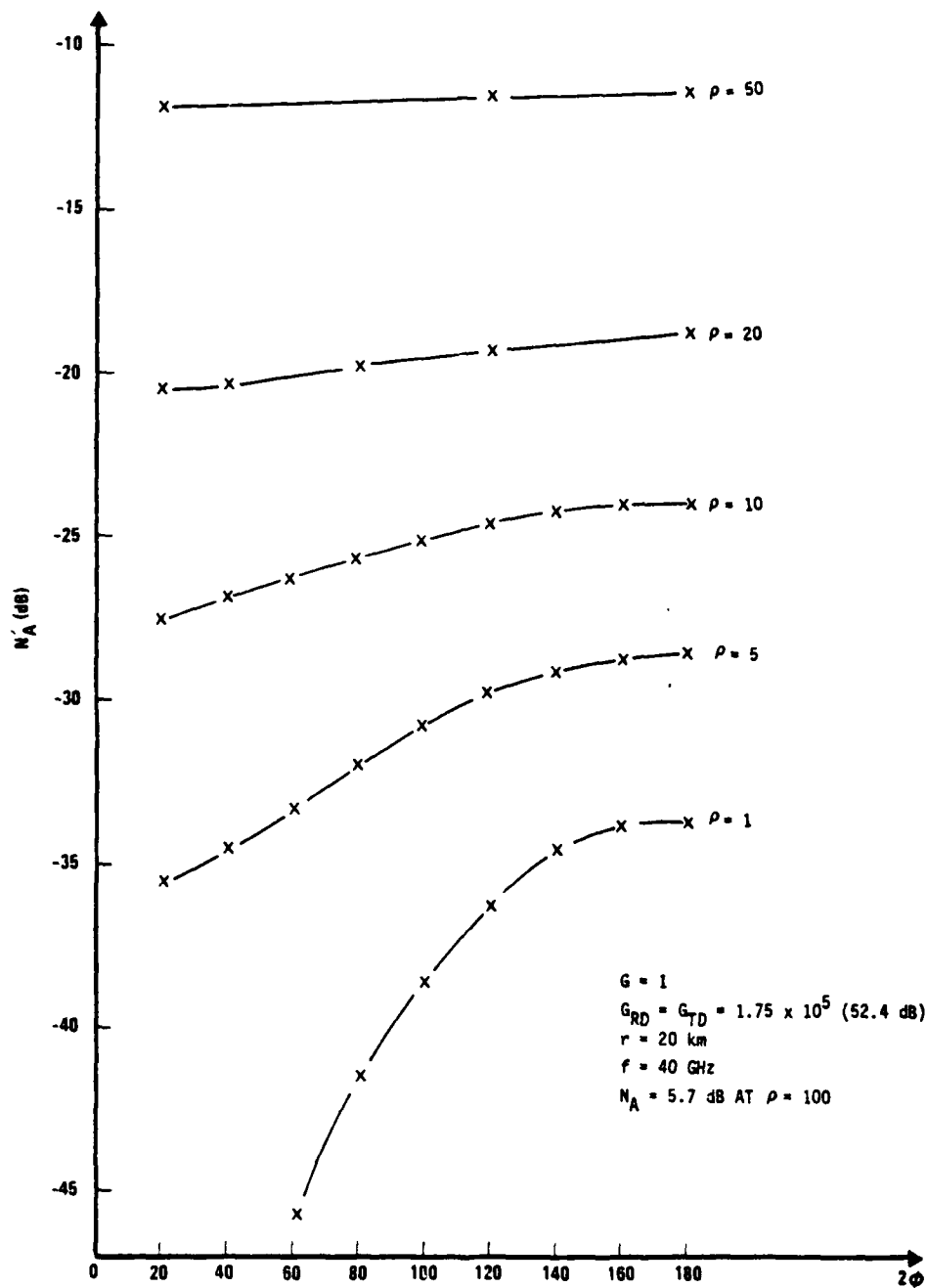
$$\frac{\partial^2 \eta_A}{\partial^2 \rho} = 1 + \frac{3}{\rho^4} - \frac{2}{\rho^3} (2 \cos 2\phi) > 0 \quad (8.3.1.3-23)$$

Unfortunately, the simultaneous solution of these four transcendental equations is not a trivial task. Although numerical and graphical procedures could be employed to arrive at the desired solution, it is perhaps more convenient to simply plot the behavior of η_A versus 2θ with ρ as a parameter. Figure 8.3.1.3-4 shows η_A versus 2θ with $\rho = r_1/r_2$ as a parameter.

Assuming that all the parameters within the first bracket of (8.3.1.3-19) are held fixed, it is clear that if $\rho \gg 1$ or $\rho \ll 1$ the value of η_A varies roughly as ρ^2 or ρ^{-2} , respectively, regardless of the value of θ . This suggests that the repeater should be placed as close as possible to one of the two existing nodes in order to minimize the attenuation along the alternate route. However, the repeater must not be placed so close to an existing node that the antijamming due to angular separation is lost.

Some reflection upon the results shown in Figure 8.3.1.3-4 shows that the optimum passive repeater placement is close to one existing node. The $\rho = 1$ curve in the figure corresponds to passive repeater locations that lie equidistant from both nodes; this represents the worst possible location for passive repeaters.

In the passive repeater approach the alternate route attenuation may be minimized by placing the repeater relatively close to one of the existing terminals; this corresponds to the $\rho \gg 1$ curves of Figure 8.3.1.3-4. The remaining link closure shortfall can be accommodated by increasing repeater antenna diameter or by yielding part or all of the link rain margin, or both. In order to help evaluate the feasibility of the passive repeater approach we treat three examples: $\rho = 10$, $\rho = 20$, and $\rho = 50$.

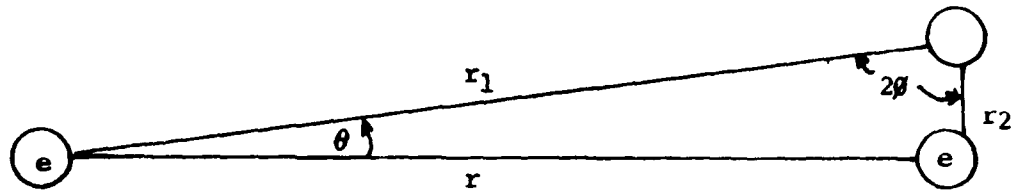


A90401-62

Figure 8.3.1.3-4. η_A Versus 2ϕ

For $\rho \gg 1$, the value of 2ϕ should always be chosen near 90 degrees in order to maximize the angle θ between the primary route and the alternate route. Under these conditions θ is given approximately by:

$$\theta = \tan^{-1} (\rho - 1)$$



$$\rho = r_1/r_2 \gg 1$$

A90401-63

Figure 8.3.1.3-5. Passive Repeater Geometry

For $\rho = 10$, $\rho = 20$, and $\rho = 50$, the values of θ are 5.71 degrees, 2.86 degrees and 1.15 degrees, respectively. We now ascertain the required antenna sizes at the repeater by entering the graph of Figure 8.3.1.3-4 at $2\phi = 90$ degrees and reading the link closure shortfall for $\rho = 10$, 20 and 50; these shortfalls are 25.5 dB, 19.7 dB, and 11.6 dB, respectively.

For the $\rho = 50$ case, the 11.6 dB shortfall can be accommodated with the 12 dB additional gain (6 dB each antenna) obtained by using 2 meter diameter antennas at the repeater. Since the 3 dB beamwidth for a 2 meter antenna at 40 GHz is 0.44 degrees and $\theta = 1.15$ degrees for $\rho = 50$, the alternate route is 2.6 beamwidths away from the primary route and thus retains angular discrimination against a primary route jammer.

For the $\rho = 20$ case, the 19.7 dB shortfall can be essentially accommodated with the 19.1 dB additional gain associated with using 3 meter antennas rather than 1 meter antennas at the repeater. For this $\rho = 20$ case the alternate route is 2.86 degrees/0.29 degrees = 10 beamwidths away from the primary route, and jammer angular discrimination is retained.

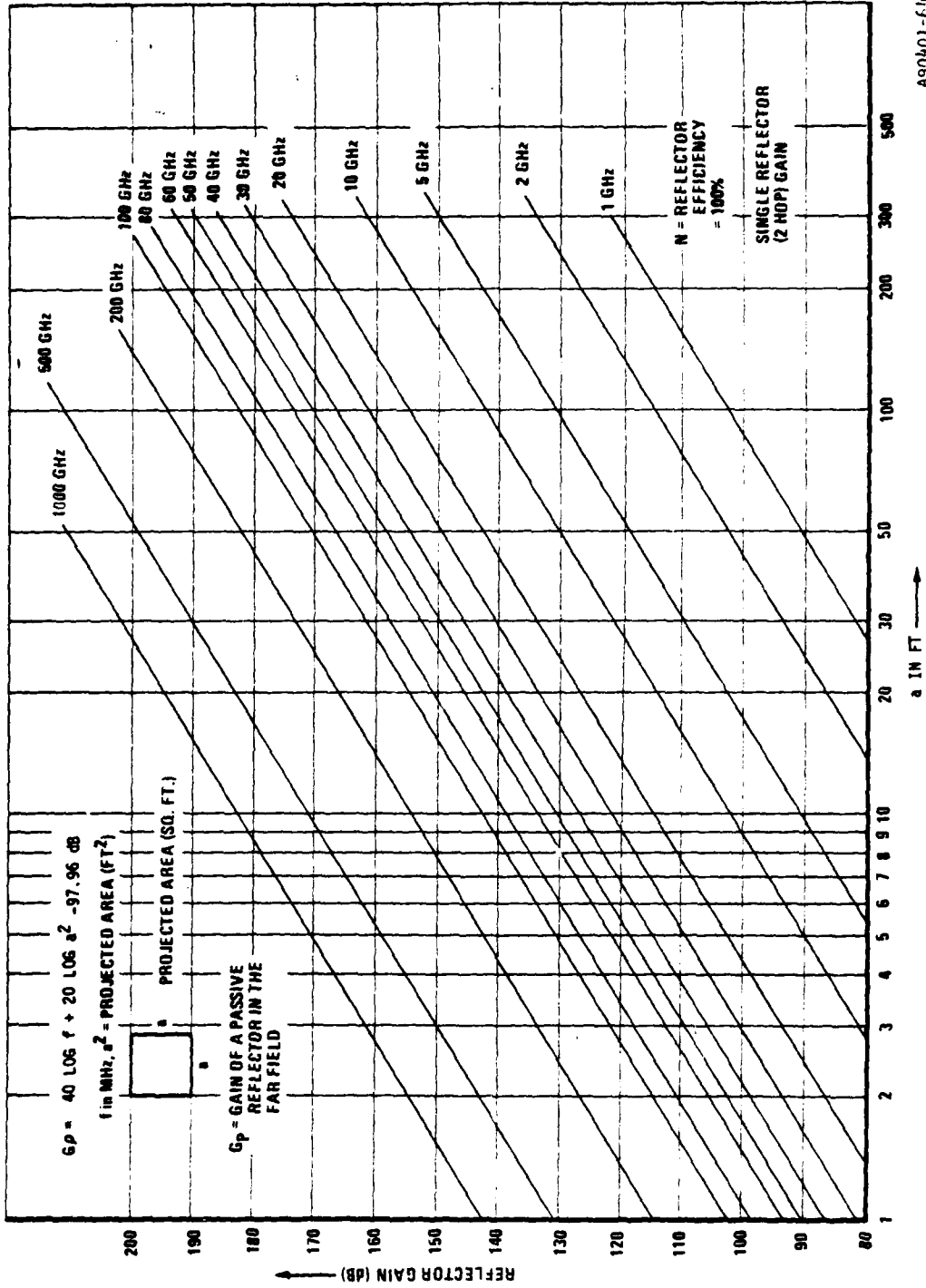
For the $\rho = 10$ case, the 25.5 dB link closure shortfall could be nearly met (within 1.5 dB) using 4 meter repeater antennas instead of 1 meter repeater antennas, for an incremental gain of 12 dB per antenna. The alternate route is 5.71 degrees/0.22 degrees = 26 beamwidths away from the primary route in this case, and the jammer angular discrimination is retained. If the 4 meter antennas are judged too expensive or unwieldy, smaller antennas can be used and some of the rain margin allocated to compensate the remaining shortfall. For example, using 2 meter antennas in the $\rho = 10$ case yields a 13.5 dB shortfall. Since millimeter wave links of reasonable length must have tens of dB's of rain margin for reasonable propagation availability, it is perhaps not unreasonable to reduce the rain margin of the alternate route significantly in order to reduce the cost of the alternate routes.

The planar reflector that serves as the passive repeater has a gain that is a function of projected aperture size a^2 and wavelength λ . In fact the reflector gain may be thought of as the product of the gains associated with a receiving aperture of size a^2 and a transmitting aperture of size a^2 , although the two apertures are physically the same aperture. The passive repeater gain may then be written as¹

$$G_p = 40 \log (f) + 20 \log (a^2) - 97.96 \text{ dB}$$

where f is in MHz and a is in feet. This equation is plotted in Figure 8.3.1.3-6. This result assumes 100 percent reflector efficiency; array imperfections such as surface roughness will slightly reduce the efficiency but not by an appreciable amount.

¹M.L. Norton, "Microwave System Engineering Using Large Planar Reflectors," IRE Trans. Comm. Syst., Sept. 1962, pp. 304-351.



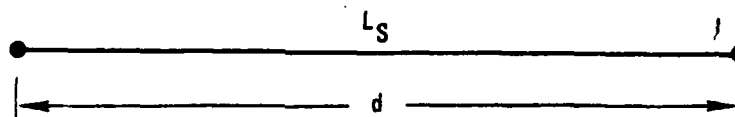
A90401-64

Figure 8.3.1.3-6. Single Reflector (Two-Hop) Gain

8.3.1.4 Three-Hop Passive Repeater Configurations

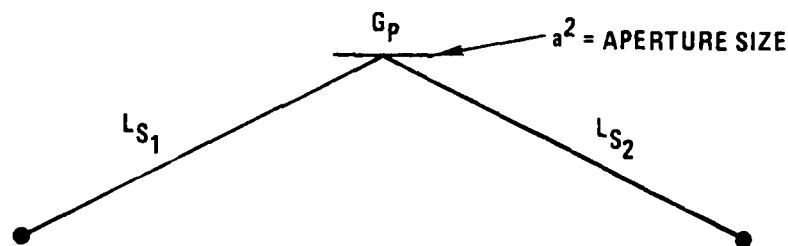
The equations governing the performance of a two-hop passive repeater system were derived in some detail in the previous section. The extension of these results to three-hop passive repeater systems is straightforward, and only the results will be presented here. It is interesting to summarize the behavior of total space loss between isotropic antennas for multihop systems using passive reflectors. In one-hop systems, i.e., those without any passive reflectors, the total space loss between isotropic antennas increases as the square of the frequency. For two-hop systems (one passive reflector), the total space loss between isotropic antennas is independent of frequency. For three-hop systems containing two passive reflectors, the total space loss between isotropic antennas actually decreases as the square of frequency. These relationships are summarized in Figure 8.3.1.4-1. Note that by using the equations for space loss L_s and passive reflector gain G_p , the total space loss for any number of hops may be easily obtained as the sum of the various losses (plus) and gains (minus) in a multihop system. Also note that although the frequency dependent term of multihop systems becomes more favorable with increasing number of hops, the constant term in the equation for total space loss increases very significantly with the number of hops. Choosing equal distances for each hop of the multihop system yields the largest space loss for passive repeaters. This fact was investigated in some detail for the two-hop case and is shown by an example in the three-hop case. Figure 8.3.1.4-2 is a plot of the loss versus frequency between two 30-foot, $\eta = 100$ percent, antennas for a one-hop system and for various three-hop systems. Note that the highest three-hop loss occurs when all three hops are of equal length, $d_1 = d_2 = d_3$. Also apparent from the figure is the dramatic decrease in loss when two of the hop lengths in the three-hop system are made very short. The dependence of loss upon reflector aperture size is also evident in the figure. Finally, it should be noted that the 30-foot dish size was arbitrarily chosen for the example; the same general behavior would be exhibited for the space loss between isotropic antennas, except that all

$$(a) L_{TOT} = L_S = 36.6 + 20 \text{ LOG } f_{\text{MHz}} + 20 \text{ LOG } \alpha_{\text{MILES}} \text{ [dB]}$$



$$(b) L_{TOT} = L_{S_1} - G_p + L_{S_2} = 170.9 + 20 \text{ LOG } d_{1\text{MILES}} + 20 \text{ LOG } d_{2\text{MILES}} - 20 \text{ LOG } a^2_{FT^2} \text{ [dB]}$$

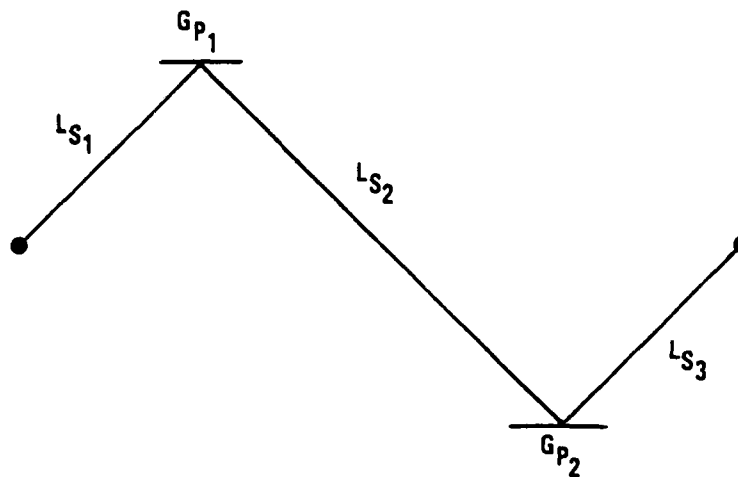
$$\text{WHERE } G_p = 40 \text{ LOG } f_{\text{MHz}} + 20 \text{ LOG } a^2_{FT^2} - 97.74 \text{ [dB]}$$



$$(c) L_{TOT} = L_{S_1} - G_{P_1} + L_{S_2} - G_{P_2} + L_{S_3}$$

$$= 305.15 + 20 \text{ LOG } d_1 + 20 \text{ LOG } d_2 + 20 \text{ LOG } d_3$$

$$- 20 \text{ LOG } a_1^2 - 20 \text{ LOG } a_2^2 - 20 \text{ LOG } f_{\text{MHz}} \text{ [dB]}$$



A90401-65

Figure 8.3.1.4-1. Space Loss for Multihop Systems

the curves would be shifted upward to reflect the higher terminal-to-terminal loss which includes the transmitting and receiving antenna gains. One further point regarding the figure is that the loss between two such terminals (no passive reflectors involved) can never be less than 0 dB; zero loss between terminals occurs when the receiving antenna aperture is large enough to collect all of the energy radiated by the transmitting antenna aperture. This would occur in a one-hop system when the transmitted beam is so narrow that its width at the receiving site does not exceed the aperture size of the receiving antenna.

The reference on page 8-79 to passive reflectors in the near field having "efficiency ≥ 100 percent" refers to the gain of a terminal antenna, passive reflector combination compared to the terminal antenna above. This is to be contrasted to the discussion above of terminal-to-terminal net loss, which can never be less than 0 dB (i.e., the receiving antenna can never collect more power than the transmitting antenna radiates).

In a practical situation we are interested in determining the additional link loss penalty for utilizing inexpensive passive reflector repeaters to achieve alternate route capability. Figure 8.3.1.4-3 shows the additional loss versus frequency of a three-hop (equal length hops) system with respect to a single hop system for a 100-mile link. Projected reflector aperture size is shown as a parameter. Since equal length hops is the worst case and practical links will be considerably shorter than 100 miles, these curves give pessimistic (i.e., large) results for the additional link loss incurred by going to a three-hop system.

8.3.2 Passive Repeater

Reflector antennas, such as flat mirror, paraboloid, dihedral corner reflector, trihedral corner reflectors, clusters of corner reflector, and Luneberg-lens reflector, as passive repeaters have been discussed elsewhere¹ and shall not be repeated.

¹Antenna Engineering Handbook, Ed. by H. Jasik; McGraw Hill, Chapter 13, Passive Reflector.

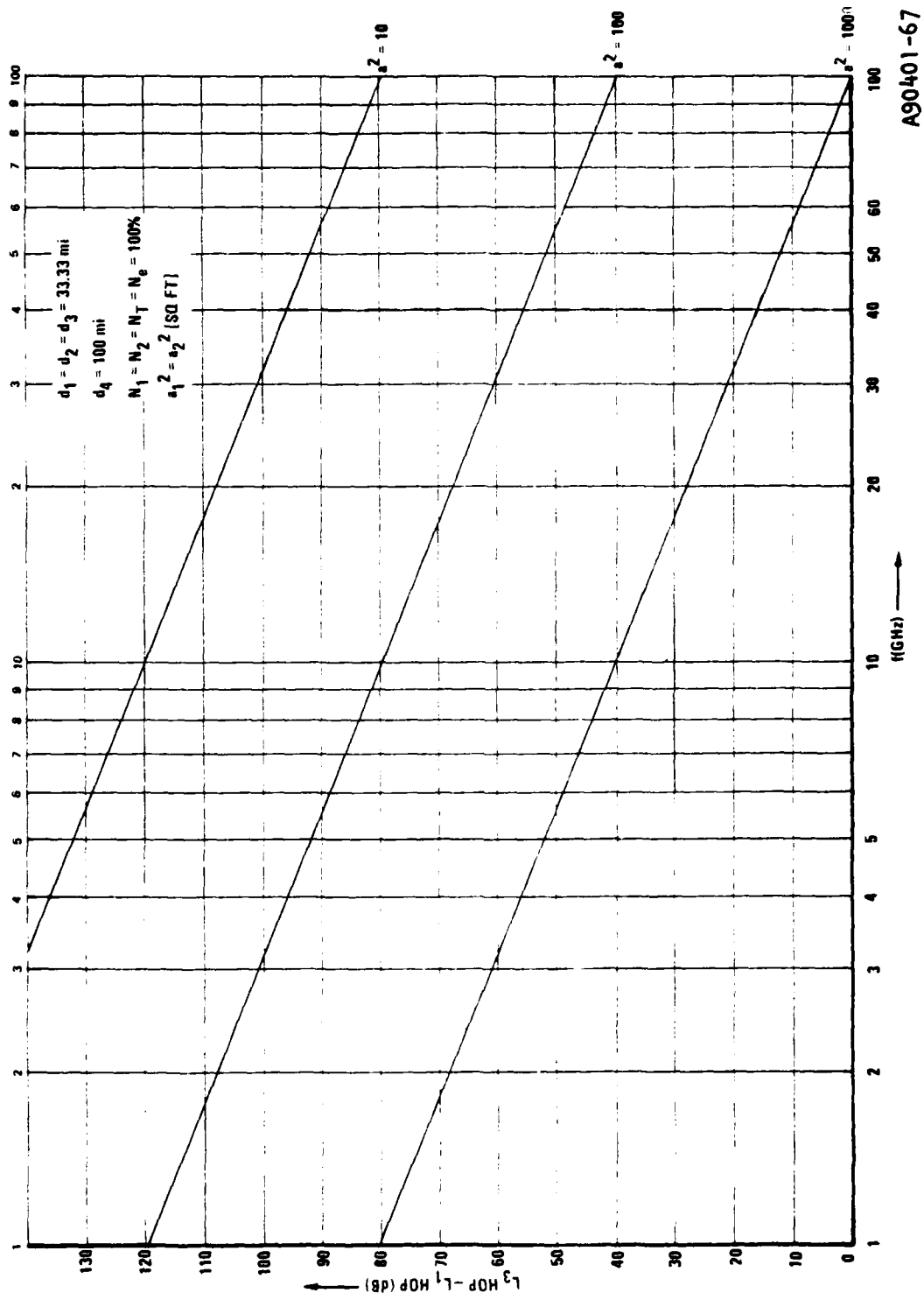


Figure 8.3.1.4-3. Loss Versus Frequency

For the envisioned application, a pair of cylindrical mirrors turns out to be more practical than any previously mentioned passive repeaters, because it is free of Fresnel reflection and redirect beams in almost any direction. Furthermore, the effective focal length of a pair of cylindrical mirrors can be changed, either by changing the mirror curvature through mechanical deformation, or by changing the mirror orientations. From a theoretical viewpoint, it is well known that under reflection on a cylindrical mirror, collimated ray manifolds coverage at distances

$$f = \left(\frac{\rho}{2} \right) \cos i \quad (8.3.1)$$

or

$$f^1 = \left(\frac{\rho}{2} \right) \cos i^{-1} \quad (8.3.2)$$

from the mirror vertex, depending on whether the incidence plane is perpendicular or parallel to the mirror generatrix. In equations (8.3.1) and (8.3.2), ρ denotes the mirror radius and i the incidence angle.

A combination of two cylindrical mirrors whose generatrices make an angle of 90 degrees to one another therefore provides sharp focusing of incident ray pencils, provided their radii ρ_1, ρ_2 are such that

$$\left(\frac{\rho_1}{2} \right) \cos i = \left(\frac{\rho_2}{2} \right) (\cos i)^{-1} \quad (8.3.3)$$

There are reasons, however, to choose more complicated orientations of the two mirrors than the one just described, and to let the mirror generatrices make angles close to 45 degrees with respect to the incident planes. In such an arrangement, better use is made of the available mirror area, and the deformation of the mirrors is minimized. Furthermore, the effective focal length of the system can be adjusted by changing the mirror orientation. The calculation of the system focal length is most easily made

by considering the change in path-length resulting from the mirror curvature and adding the contributions of the two mirrors. Examples of design values are given in Figure 8.3-3 for beam deflection angles θ of 90 degrees, 180 degrees, 270 degrees and 0 degrees. In Figure 8.3-3 the angle Ω refers to the twist of path. (Only two cases: $\Omega = 0$ degrees and 180 degrees are presented.) The angle μ denotes the angle that the mirror generatrices make with the incidence plane. The two mirrors are assumed to have the same radius of curvature ρ .

8.3.3 Repeater Modem

The active repeater will include transmitter/receiver equipment but it may be of little benefit to regenerate the data. This would require sync acquisition, despreading the signal, data demodulation, and finally, remodulation and transmission. The modem described in Paragraph 8.2.2 could be used for this function but would require adjustment when the data rates are changed.

A "passive" modem, a receiver/transmitter combination may be all that is required to satisfy the present requirement.

8.3.4 Receiver

Refer to Figure 8.3-2; the receiver section of the regenerative repeater mainly consists of low noise amplifier, isolator, downconverter, and various stages of IF amplifier and filters. Normally, for wideband operation, the IF signal is then fed through a low pass filter with time delay equalizer to avoid the distortion of the waveform. The equalizer, which operates at the IF of 2 GHz, is basically a meander line if microstrip transmission line is utilized. The equalizer is designed to provide a delay characteristic which is the compliment of that introduced by the dispersion.

The wideband low noise amplifier used in the millimeter wave range can be a reflection-type transfer electron device (TED), known as a Gunn diode amplifier. Lately, the low noise InP TED became a reality at frequencies up to 60 GHz and the amplifiers with 12 dB noise figure are possible. Each amplifier stage is comprised of a TED, a bandpass matching network, and a ferrite circulator. The key component of the amplifier is the high performance circulator which may limit the amplifier bandwidth and gain. For high performance, the microstrip circulator may be fabricated by using 10-mils thick ferrite substrate with a 5000-Gauss saturated magnet. The matching networks used in the negative-resistance amplifiers are designed to present a reflection coefficient with constant amplitude from the circulator over the frequency range of interest. They are passive, ideally lossless, and must be designed from the standpoint of amplifier stability. The power gain can be computed from the TED impedance at operation point, since microstrip is a low-Q transmission line and wideband operation is much more feasible than with waveguide. For tactical applications, the TED LNA must be temperature stabilized over a wide temperature range. Therefore, a bias stabilization network has to be used in each stage to minimize TED bias fluctuation and maintain gain amplitude and its flatness.

The local oscillator of the repeater is similar as that previously described in Paragraph 8.2.

A balanced mixer is recommended for the downconverter because it rejects the even order harmonics and provides low noise figure. Figure 8.3.4 is a balanced mixer designed at 37 GHz (center frequency) in which the signal is fed to the mixer through the waveguide to microstrip transition. The LO and RF signals are applied to the two series-mounted beamlead GaAs Schottky barrier diodes through a 3-dB branch directional coupler. High directivity and balance of the coupler are required to ensure the good performance of the mixer. A pair of stubs for impedance matching are placed between the diodes and the directional coupler. The RF choke circuits consist of two RF quarter-wavelength lines, each of which is connected to

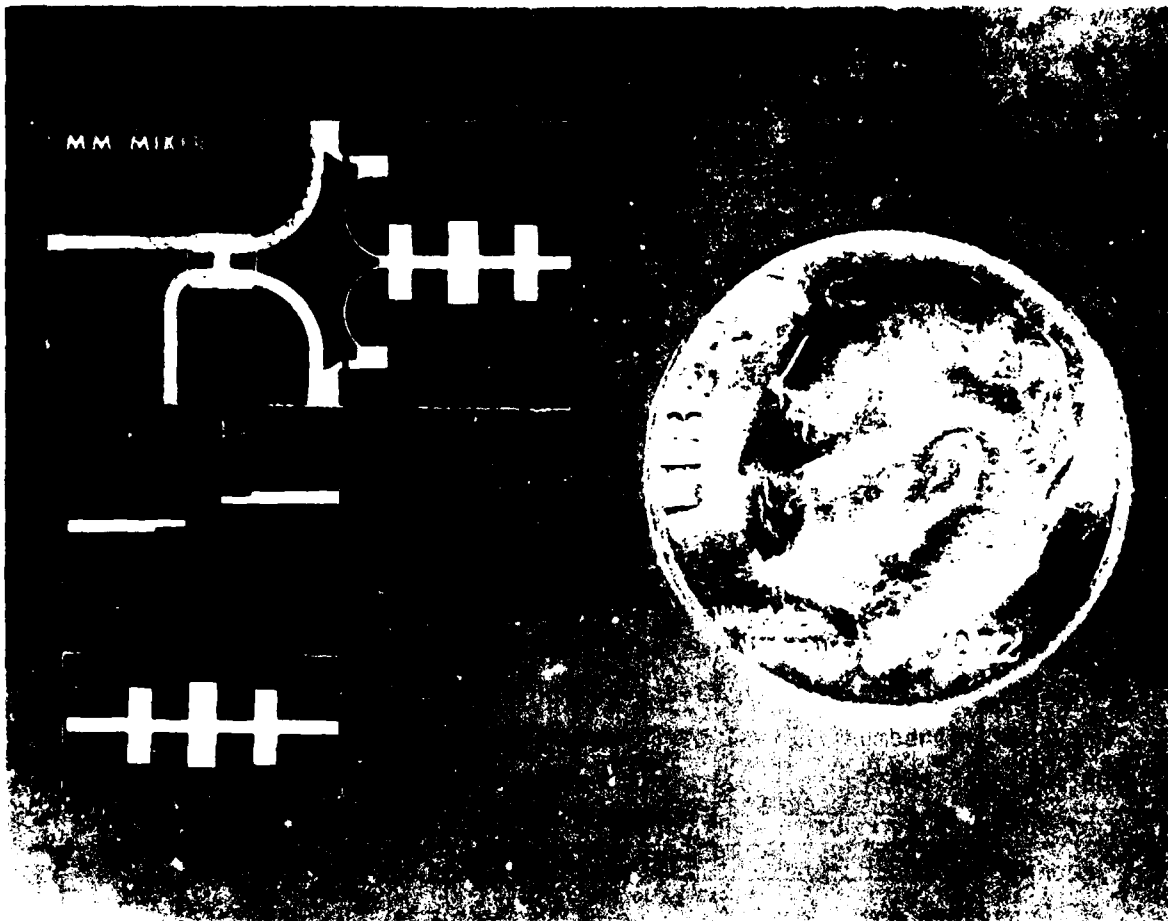


Figure 8.3.4. Microstrip Q-band Mixer, Bandpass Filter and Low Pass Filter Using 10 Mil's Thick Fused Quartz Substrates

both a microwave planar circuit and a plate capacitance for the IF return. The circuits, thereby, provide a high impedance at RF and a short circuit at the IF at the RF ends of the diodes. The IF outputs from the two diodes are connected via short sections of high impedance lines to their combination point at the input to the low pass filter. The RF short circuits, consisting of two $\lambda/4$ open circuited lines, connected in shunt behind the mixer diodes, provide the diodes with low impedance RF ground. This distance between diode and low pass filters is $\lambda/2$ at RF.

8.3.5 Transmitter

For 1 to 20 km tactical radio links, a transmitter power of 1 watt is sufficient for most systems. Relatively low noise TED's are ideal for the high power amplifier (HPA) driver and then followed by IMPATT diode HPA. Such an arrangement can reduce the total noise figure of the HPA considerably. The design of the TED HPA driver is similar to the LNA described in Paragraph 8.3.4. Unlike the small signal LNA, the large signal effects of HPA will generate harmonic distortion and amplitude-to-phase modulation conversion. Harmonic generation is generally not a problem for the millimeter wave HPA. However, the amplitude-to-phase may degrade the system performance, particularly for PSK modulation.

Currently, the commercially available Si double drift IMPATT diode has 0.5 W power capability, with 8 percent efficiency at 40 GHz and an 0.2 W, 6-7 percent efficiency at 60 GHz. Without further diode power capability improvement, it is required to either use power combining techniques or use multichip operation to boost the power output. Various combining techniques have been examined during this study. The multidiode resonant approach using a TM_{010} mode resonator provides design simplicity, but relative narrow bandwidth due to the high Q characteristics of the resonator. Contrastly, the nonresonant approach using a 3 dB directional coupler can offer wide bandwidth operation. Either an edge coupler or branch coupler is practical for the microstrip HPA application.

Besides the conventional combining technique, attractiveness of the push-pull configuration for IMPATT diode amplifier design is worth describing in this report. Methods of serializing or paralleling a number of IMPATT diodes for the purpose of increasing power have been reported at microwave frequency. Parallel connected diodes, besides reducing the overall thermal resistance, reduce the impedance level of the devices. The maximum achievable power capability still rolls off in $1/f^2$ fashion. Series connected diodes raise the impedance level. However, the series connection usually introduces serious parasitic problems, such as the large mounting inductance between the two diodes. The new push-pull circuit takes advantage of the merits of both methods.

In this push-pull circuit the two diodes with opposite polarities are in RF series connection, yet maintain the dc and thermal paths in parallel. Kawamoto and Liu¹ reported on an anti-parallel pair of avalanche diodes which are located a half wavelength apart and opposite in polarity. In their circuit, the two diodes also allow for push-pull operation but the circuit principle is entirely different.

In their circuit the two diodes are essentially in parallel while in the present circuit the two diodes are in series. In contrast to their anti-parallel name, the present push-pull diodes should be called an anti-series pair.

Figure 8.3.5(A) shows a basic push-pull configuration. A pair of diodes are dc biased in parallel but function as a series pair in the RF circuit shown in the figure. Each diode is biased at I_0 , V_0 as the quiescent point and experiences the same RF current " i_0 ". The polarity of the RF current is the same as the dc bias current in one diode but opposite in the other diode. Thus, the RF current pushes one diode to a high current state, $I_0 + i_0$. In this push-pull circuit, the overall impedance of the

¹H. Kawamoto and S.G. Liu, "Anti-Parallel Pair of High Efficiency Avalanche Diodes," Proc. IEEE, March 1971, pp. 427-428.

device is the arithmetic sum of each individual diode. For two identical diodes connected in push-pull, the overall impedance and the power handling capability should be doubled. For the overall device impedance level equal to that of a single diode, individual diodes in the push-pull circuit can have twice the junction area and thus raise the overall device power handling capability by a factor of four. Here we assume that there is no serious current crowding effect occurring when the junction area is doubled.

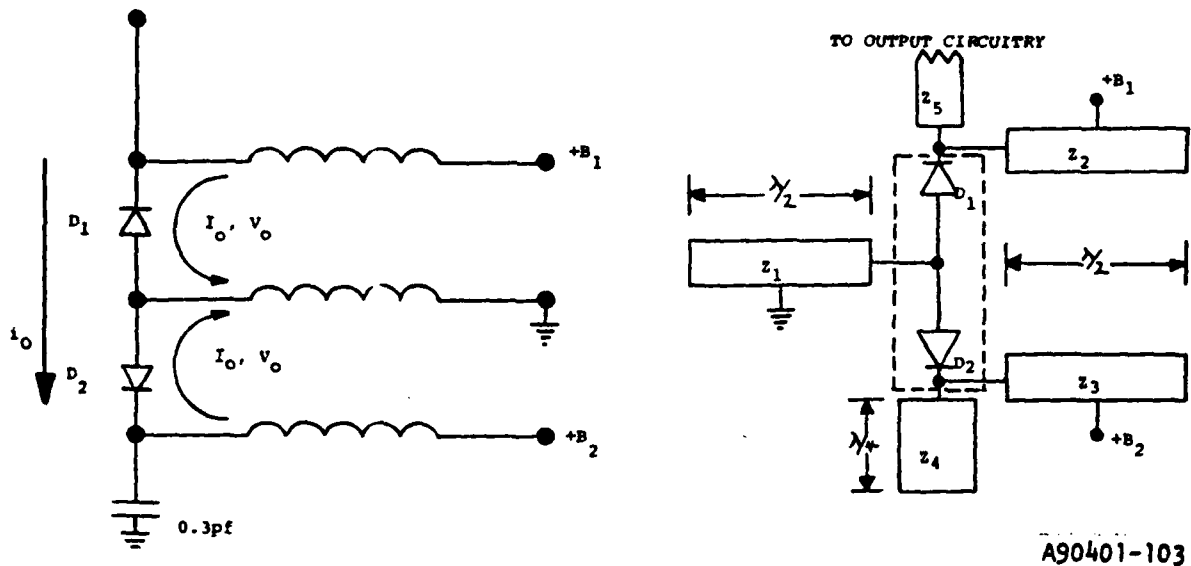
Figure 8.3.5(B) shows a circuit realization of the push-pull configuration. Half wavelength open circuited stubs with impedances Z_1 , Z_2 , and Z_3 are used for bias isolations. A quarter wavelength open circuited stub of impedance Z_4 provides an RF ground while maintaining dc isolation. In this circuit, each diode can be individually biased. This individual bias controllability offers the flexibility of minor adjustments in matching diode characteristics as well as operating points. If the individual biasing is not required, then the two diodes can also be biased together by a common dc source. With this new anti-parallel approach and two 0.5 W IMPATT diodes, a 0.8 W amplifier becomes realizable.

8.4 Millimeter Wave Frequency - Channel Arrangements

Main sources of interference in a digital radio system come from:

- a. Adjacent channel.
- b. Cross polarization.
- c. Local transmitter and receiver.

where the cross polarization interference only apply to the dual polarization antenna system.

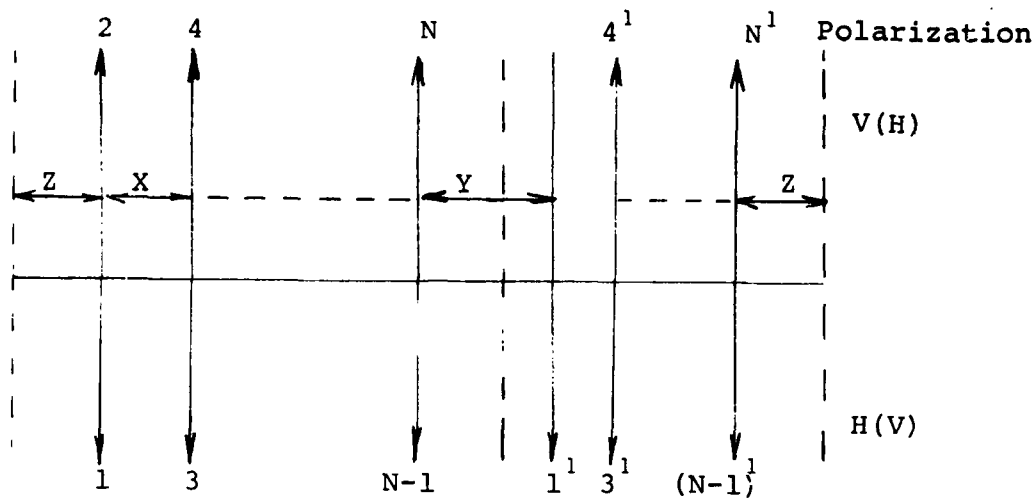


(A) CIRCUIT CONFIGURATIONS

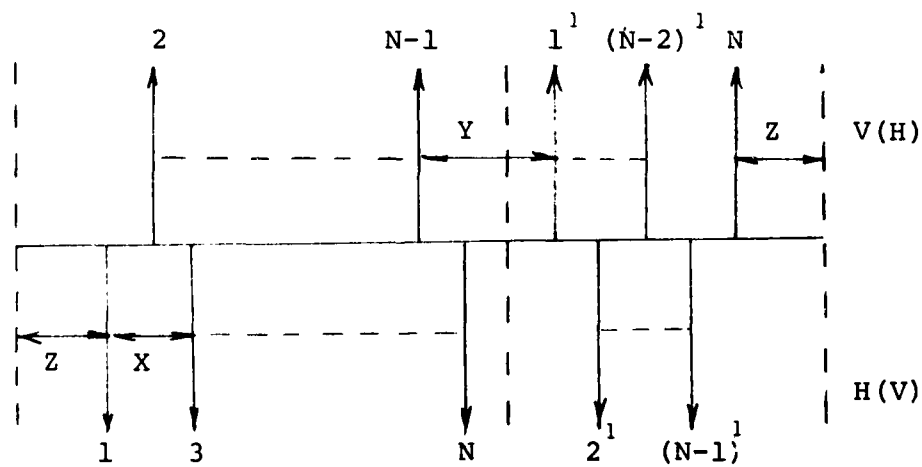
(B) CIRCUIT REALIZED ON MICROSTRIP

Figure 8.3.5. Push-Pull IMPATT Diode Amplifier

Figure 8.4 illustrates two possible RF channel configurations. Figure 8.4(A) shows a cochannel cross-polar arrangement and Figure 8.4(B) depicts an interleaved cross-polar arrangement. In the cochannel arrangement, RF channels of the same frequency but of opposite polarization are used, sometimes allowing an extra RF channel relative to the interleaved case. Obviously, employing the same frequency channels would be unacceptable if the cross-polarization discrimination is not sufficiently high to allow a satisfactory carrier/noise ratio to be achieved even before other degradations have been introduced. For millimeter wave frequencies, the rain effects often introduce cross polarization degradation; the system designer must provide reasonably high cross polarization discrimination margins in order to preserve the expected link availability. The computation of these cross polarizations is given in Section 2.0.



(A) COCHANNEL CROSS-POLAR ARRANGEMENT



(B) INTERLEAVED CROSS-POLAR ARRANGEMENT

Figure 8.4. Millimeter Wave RF - Channel Arrangements

Using an interleaved arrangement would typically provide a further 6 dB extra protection per RF channel owing to filter attenuations. This would give an increase of cross-polar noise protection of 3 dB when two adjacent channels of both higher and lower frequencies are present.

Referring to Figure 8.4, in the practical system one must evaluate the overall frequency considering the following factors:

- a. Adjacent - channel separation X.
- b. Local transmitter/receiver separation Y.
- c. Spacing of outmost channels from the band edge Z.

The protection against interchannel interference and selection of X can be achieved by proper filter design (cross polarization channels can also be taken into account by adding the appropriate cross pole discrimination value).

To reduce transmitter/receiver interference, additional isolation due to other components must be added to the protection afforded by filtering. Normally, a circulator between transmitter and receiver can provide 20 to 16 dB extra isolation in Ka and Q-Band. Locational separation of transmitter and receiver, an expensive arrangement, may offer excellent isolation better than 60 dB. The tradeoff of cost and performance of this approach is not justified in many tactical systems. The isolation between transmitter and receiver is often required to be 70-110 dB, depending on the dynamic range and the sensitivity of the receiver and the transmitter power level. If RF filters are used in the receiver channel, the determination of Y has to consider the performance of the filters, such as center frequency, bandwidth, the shape factor of the filter skirt, etc.

The spacing Z of channels from the band edges is determined by the allowable radiation outside the band of interest. No definite rules are given on the radiation outside the band; however, normally, the following criteria are suggested:

- a. Power spectral density at the band edge should be 20 dB below maximum value.
- b. Total power radiated outside the band should be 30 dB below the transmitter power.

These criteria lead to values of Z about 0.9.

Considering the previously outlined parameters, a complete frequency plan can be worked out and the transmitted bit rate on each carrier versus total band capacity can be calculated.

9.0 RECOMMENDATIONS

Sections 2.0 through 8.0 of this study report contain salient conclusions of their associated study tasks. However, there are additional recommendations for work efforts that we believe should be initiated to ensure that terrestrial MMW systems can be realized. Three recommended efforts are described.

- a. Wideband fiber-optic interface electronics.
- b. Millimeter wave adaptive array feed design.
- c. Low cost wideband millimeter wave VCO development.

9.1 Wideband Fiber-Optic Interface Electronics for Integrated Millimeter Wave Terminals

Statement of the Problem:

The proposed task addresses the design, fabrication, integration and testing of a wideband, reliable, fiber-optic/electronic interface subsystem for the millimeter wave integrated terminal.

The conventional millimeter wave terminal utilizes transmission waveguides and rotary joints to interface the antenna (or antenna tower) to the transmitter/receiver. The extra unwanted transmission losses associated with the conventional approach (at millimeter wave) degrade the transmitter EIRP and receiver S/N, sensitivity and dynamic range; and tend to increase the terminal cost. The integrated terminal concept, which integrates the upconverter and downconverter directly with the antenna, will alleviate or eliminate these shortcomings.

The link between the converters and the modem can be either fiber-optic cable or coaxial cable. However, coaxial cable operating at 1 GHz bandwidth or above is bulky in size and weight, and is expensive. Large size degrades the flexibility and transportability of the coaxial cable link; also, the coaxial cable is susceptible to EMP/EMI due to nuclear burst and other interferences. Fiber-optic cable does not have such disadvantages. The fiber-optic link between the integrated antenna/converters and the operation room will provide the following attractive advantages.

- a. Complete electrical ground isolation is achieved. The isolation eliminates ground loops that plague systems with long-distance remote antenna and provides high-voltage (lightning) isolation.
- b. Provides transmission security without steel conduit; therefore, reducing installation cost.
- c. Eliminates crosstalk.
- d. Eliminates short-circuit loading, ringing, and spark/fire hazards.
- e. Provides extremely flat bandwidth over the desired signal range.
- f. The low-loss, no gain, fiber-optic link requires a low dynamic range, and lower cost demodulator, in the terminal system design.

- g. Gain in the low-noise amplifier (LNA)/downconverter combination is reduced; therefore, reducing potential compression and isolation problems associated with high-gain front ends.
- h. The fiber-optic link can also serve the terminal local distribution network.

Solution Approach:

Six principal steps are included in the recommended approach to solving the stated problem.

1. Select and procure the proper injection laser diode (ILD) and photodetector with 1 GHz operational bandwidths.
2. Select proper fiber-optic cable.
3. Perform computer-aided design of 5 MHz to 1,005 MHz (1 GHz operational bandwidth) ILD transmitter and MESFET receiver. 1 GHz bandwidth complies with a 1 Gb/s data rate. Currently, 1 GHz bandwidth can be optimized up to C-band (e.g., 4 to 5 GHz).
4. Investigate a method to eliminate laser diode hazard in case of mishandling.
5. Fabricate and test a breadboard 1 GHz BW ILD transmitter and fiber-optic receiver.
6. Test integrated terminal concept with other components installed.

9.2 Millimeter Wave Adaptive Array Feed Design

Statement of the Problem:

The benefits of adaptive array null steering are well known, particularly for sidelobe canceller applications when the primary antenna is a reflector with substantial gain (such as would be desirable for a millimeter wave communication link). However, as discussed in Section 6.0 and Appendix A, there are numerous deficiencies in the sidelobe canceller approach. Some of these are as follows:

- a. Auxiliary Elements Required. In addition to the reflector feed elements, additional antenna elements, usually located around the periphery of the main reflector, are required to provide independent information for aid in jammer nulling. This is physically cumbersome and substantial loss is anticipated (compared with the method described later) in waveguide runs from the elements to the array combiner.
- b. Narrowband. Because of substantial differences in path lengths for signals entering through the main antenna and those entering through the auxiliary elements and the fact that these path differences are functions of the angle of arrival of the interference, the conventional sidelobe canceller is limited to providing good performance only for very narrowband signals.
- c. Minimal Main Lobe Cancellation. Due to the fact that the auxiliary elements have reduced gain and relatively large noise contributions, nulling of interferers which move into the main beam of the antenna becomes very difficult or impossible. Furthermore, even when only sidelobe nulling is being accomplished, the system noise figure is generally degraded by the noise contribution from the relatively small auxiliary antennas.

- d. Signal-to-Noise Ratio Maximization. Algorithms designed to be used with the sidelobe canceller approach are incapable of providing S/N ratio maximization. This in itself precludes nulling of jammers entering the mainbeam (unless signal and jamming can be distinguished) and also can prevent the use of pseudo-monopulse antenna steering techniques when jamming is present.
- e. Expensive. The conventional sidelobe canceller physical implementations usually require what is essentially a receiver in each of the auxiliary antenna inputs as well as in the main antenna signal pathway.

Solution Approach:

Harris has been taking a new approach to this problem which substantially alleviates the above mentioned problems. Basically this approach consists of a reflector antenna having a multi-element feed (for example, 5 elements) such as might conventionally be used for pseudomonopulse antenna pointing. In this approach, the element inputs are summed with variable weight coefficients rather than in a fixed combining network. A single conventional receiver is used; however, the intermediate frequency output of this receiver is available for sampling by a micro-computer based adaptive array processor. By means of a systematic perturbation of the weights in the feed element RF combining circuitry, the processor can obtain the necessary information for maximization of the desired signal-to-noise and interference ratio. This approach has the following advantages:

- a. No Auxiliary Elements. All of the necessary RF inputs for interference cancellation and retention of mainbeam gain are available from the main reflector feed elements. The mechanical inconvenience of mounting auxiliary elements is avoided.

- b. Wideband Nulling Capability. Because the relative time delay to the several feed elements is essentially the same, very wideband interference nulling (or deeper narrowband nulling) is possible (2 and 3 orders of magnitude wider bandwidths than with the sidelobe canceller approach).
- c. True S/N Ratio Maximization. This approach is capable of optimally maximizing desired signal-to-interference ratio even when the interferer enters the mainlobe of the antenna. Although it is true that the achievable performance degrades as the jammer approaches the DOA of the signal, as must be the case, optimum solutions for the given situation will be obtained.
- d. Low Cost/High Performance. Because most of the elements of the conventional communications system are preserved, this adaptive null steering approach adds only a relatively small cost increment to the basic system cost. The additional required elements are a variable weight (rather than fixed weight) combining network and a microcomputer with its associated receiver interface. Achievable performance is superior to that of the conventional sidelobe canceller.

Harris has been studying this reflector feed null steering concept for almost a year on internal research and development programs. Computer programs which calculate expected performance for given feed designs and desired signal and interference angles of arrival have been developed as well as hardware suitable for use in X-band; specifically, a very low loss RF weight has been designed and will be used soon in an experimental verification of the approach.

Much of the capability developed during the IR&D effort would be applied to the millimeter wave adaptive reflector feed design study in the following areas:

- a. Feed Design. A reflector feed specifically meeting the requirements of the millimeter wave communications link would be designed. This design would take into account the jammer threat expected as well as desired signal gain.
- b. Simulations/Performance Predictions. Attractive antenna feed candidates would be examined using the simulation computer programs with the result being curves of expected performance of the design against various jammer threats.
- c. Millimeter Wave Weight Design. A critical component in the reflector feed null steering concept is the RF weighting device used in the feed combining networks. This weight must have the capability of low loss and low dispersion. A low loss high performance millimeter wave weighting device would be designed using the approach taken earlier in the design and construction of the X-band weight for the IR&D program. The result of this effort would be a design which could be realized in hardware.

9.3 Low Cost Wideband Millimeter Wave VCO Development

Statement of the Problem:

Military millimeter wave communications systems with AJ capability require a wideband phase-locked local oscillator (PLL0) and frequency synthesizer for spread spectrum or frequency hopping. The low noise voltage controlled oscillator (VCO) is the key component of the PLL0.

Commercially available waveguide VCO units have many disadvantages such as high cost, high noise, narrowband tuning range and lack of production simplicity. In contrast, a VCO fabricated in a microstrip configuration will alleviate all of these shortcomings.

Conventionally, the IMPATT diode and transferred electronic device (TED, or Gunn diode) are utilized to fabricate the millimeter wave VCO. These diodes either require high bias current or high bias voltage. However, the low noise GaAs MESFET often has a cutoff frequency over 70 GHz and has the capability to oscillate above 38 GHz, with low phase noise and good pulling figure. The varactor is normally used as a tuning element. It is well-known that the varactor-tuned VCO has problems of post tuning drift, poor tuning linearity, high cost, and thermal instability. Lately, it has been found that a low-cost light-emitting diode (LED) can serve as the tuning element without these disadvantages which the varactor possesses.

Solution Approach:

The following design approaches can be used in the 38 GHz VCO development.

- a. Investigate and select a viable active device. The potential devices for the millimeter wave oscillator are IMPATT diodes, Gunn diodes and GaAs MESFET's.
- b. Evaluate the tradeoffs between the microstrip and waveguide design.
- c. Compare the VCO performance with optical tuning and varactor tuning.

- d. Use computer-aided design for circuit performance optimization.
- e. Fabricate and characterize a breadboard VCO in the vicinity of 38 GHz with a minimum tuning bandwidth of 1 GHz.

APPENDIX A

MILIMETER WAVE ALTERNATE ROUTE LINK ENGINEERING

AND

ADAPTIVE ARRAY PROCESSING TO PROVIDE ANTIJAM PROTECTION

1.0 INTRODUCTION

It was shown in Section 6.0 that using multifeedhorn parabolic dish antennas is a practical method of achieving high performance, narrow beam adaptive antenna operation using only a small number (≤ 5) of feedhorns and associated weights. This technique was shown to be more advantageous than the sidelobe canceller technique.

The purpose of this appendix is two-fold: 1) the link model and jammer threat model is first developed and discussed in some detail 2) the performance and complexity of the sidelobe canceller adaptive array techniques is compared to that of a multielement phased array adaptive antenna technique. As might be expected, an excessively large number of phased array elements and associated weights is required at millimeter wave frequencies in order to obtain the small beamwidth and large AJ protection that is desired. The conclusion is that using multifeedhorn dish antennas is more cost effective than either sidelobe cancellers or very large multielement phased array techniques in implementing an adaptive array.

In order to appreciate and evaluate the nature of the AJ protection provided by adaptive antenna arrays, it is essential to understand and assess the jamming threat to the desired link. In general, one needs to know such features as: type of jammer, number of jammers, power of jammers, location of jammers (e.g., angular separation from the main antenna beam in the desired communication link), and the mobility of the jammers.

Of secondary importance, one must clearly understand the scenario model of the desired communication link. That is, system parameters such as link separation distance, antenna heights, operating frequency, multipath due to atmospheric and terrain effects, as well as rainfall and atmospheric absorption are important when link availability must be determined.

Therefore, a transmission loss model [1, 2] which depends on the parameters described above is first utilized to provide estimates of multipath fading over the link. This value, when used with other practical system design parameters leads to the formulation of a reasonable set of system link allocations.

Next, a jamming threat model is developed which describes the type, range, number, power, and location of the jammers and which is assumed to constitute the potential threat. Constant signal-to-jammer (SJR) contours may then be constructed over the region of the desired link.

After the threat model is assessed and utilized in conjunction with the link multipath model, one can observe the effect produced by introducing the AJ processing gain afforded by adaptive antenna multielement arrays. Knowledge of the potential threat scenario enables one to place nulls in the antenna pattern at those angular separations (from the main beam) where the jammers are located. This is the significant objective: compute the processing gain as a function of jammer angular separation from the main antenna beam in the desired link.

Numerical results are offered which depict typical adaptive array antenna patterns. Curves of processing gain versus jammer angular distance from boresite are also presented. Utilizing the processing gain along with other system parameter values in a link budget enables one to assess whether link closure may be achieved in the presence of jamming.

A summary and conclusions are offered following the main development of this appendix.

2.0 LINK AND JAMMER THREAT MODEL

2.1 Link Model

The geometry of the MWAR system link (in the absence of a jamming environment) consists of a transmitting antenna on a tower at a height of h_{Te} , a receiving antenna on a tower at a height of h_{Re} , separated by a distance R of irregular terrain. The distance R represents the separation distance between the desired link terminals. The parameters h_{Te} and h_{Re} give the effective heights of the transmitter and receiver antennas, respectively.

The transmission loss model used in this study is the computer method developed by Longley and Rice [1]. The model produces values for multipath fading due to atmospheric and terrain effects for a specified link (or propagation) availability (e.g., values not to be exceeded for 99 percent of all hours of the year). The MWAR communication environment is especially suited to the objectives, assumptions, and limitations of this model since, in general, it must be assumed that the overall system may operate with a large degree of time and location variability.

Many input parameters are utilized to produce values for the total transmission loss over the link. This typically involves the selection of a suitable terrain model and an average value for the atmospheric refractivity at the station site. Effects of ground clutter (e.g., foliage effects) are also empirically included in the model. The effects of atmospheric and precipitation absorption are additive propagation losses which are not treated by the model. Predicted values of transmission loss may then be computed as a function of such parameters as the ground separation between any two terminals in the scenario, the heights of the terminals above average terrain, the transmission frequency, and the required time availability (fraction of all hours of the year when the link must operate in the system environment).

The required input parameters to the transmission loss model are:

- Atmospheric refractivity near the surface at the terminal sites
- RMS deviation of the intervening terrain
- Terminal separation distance
- Effective heights of the transmitter and receiver antenna above average terrain
- Operating frequency
- Ground constants (dielectric permittivity and conductivity)
- Link availability

Long-term variability, with respect to some computed median value of attenuation over the link, usually results from gradual changes in average atmospheric refraction, in the degree of atmospheric stratification, or in the intensity of atmospheric turbulence. In the prediction model, estimates of time variability about the long-term median attenuation value are primarily based on measurements. For example, hourly median values of transmission loss recorded for long periods of time over a particular path may show wide variations, especially in areas where marked seasonal changes occur in the atmospheric refractivity near the surface and in the refractive index gradient. In the model, long-term variability about the median attenuation value may be estimated in terms of a standard deviation and a standard normal deviate. Such a technique leads to an estimate of propagation availability.

At a frequency in the millimeter wave bands, radio absorption may seriously affect the communication links. This absorption is due primarily to rainfall, but some also results from propagation through atmospheric gases such as oxygen and water vapor.

Rainfall attenuation may be estimated by first referring to Figure 2.1. [1, 2] which illustrates the path average rainfall rate versus the effective rainbearing distance and propagation availability for a continental temperate climate (e.g., typical of the Federal Republic of Germany, where the MWAR link may be located) with a total annual rainfall of 1m. (For ground-to-ground low elevation angle LOS links, the effective rainbearing distance is approximately equal to the actual terminal separation distance if rainfall is observed over the entire link.) Knowledge of the link distance then enables one to find the path average rainfall rate which is exceeded for a certain percentage of all hours of the year. This rainfall rate, R_R , may then be used in the following expression to compute the attenuation loss (per km), $A_R(f)$, due to rainfall:

$$A_R(f) = K(f) R_R^{\alpha(f)} \text{ dB/km} \quad (2.1.1)$$

where $K(f)$ and $\alpha(f)$ are empirical adjustments to account for frequency.

Atmospheric transmission loss due primarily to oxygen and water vapor absorption is not as significant as that produced by rainfall. The computed value for this absorption will change little as a function of time for a given link separation distance.

2.2 Jammer Threat Model

A typical geometry of the MWAR jammer threat problem consists of either a Ground-Based Jammer or an Airborne Jammer transmitting jamming signals toward the transmitting or receiving antennas or both.

PATH AVERAGE RAINFALL RATE, \bar{R}_R , VERSUS EFFECTIVE RAINBEARING DISTANCE, r_{ER}
 (TOTAL ANNUAL RAINFALL, 100 CM)

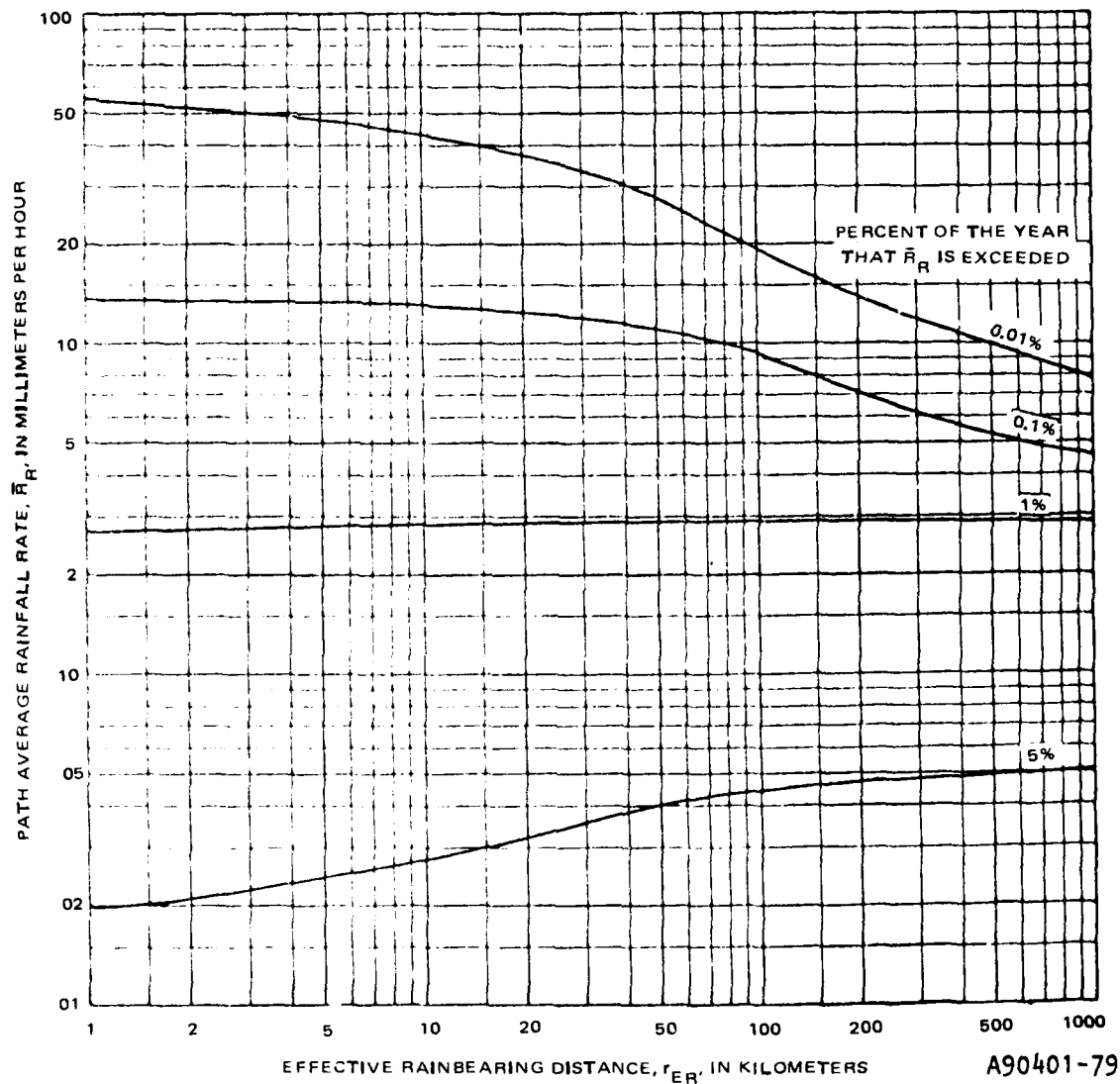


Figure 2.1. Path Average Rainfall Rate, \bar{R}_R , Versus
 Effective Rainbearing Distance, r_{ER} [1,2]

In the modeling effort, we consider one dedicated jammer which will attempt to disrupt the desired link. A line-of-sight (LOS) jammer is assumed at all times, and it may be ground-based or airborne. The jammer range is restricted to be less than 120 km. A continuous wave (CW) jammer is also assumed.

The dedicated jammer may be located anywhere in the plane (or a projection into the plane) containing the terminals of the desired link. That is, the angular separation of the jammer with respect to the main beam of the antenna may assume any value. For simplicity, it will be assumed that the jammer effective radiated power (ERP)-to-jammer range ratio will be constant. This scaling property allows investigation of high power jammers at long ranges and low power jammers at short ranges from the terminal site.

In order to properly evaluate and assess the vulnerability of the MWAR LOS links of jamming, it is generally desirable to construct contours of constant signal-to-jammer (S/J) ratio on a topographical map of the region where the link is to be located.

Effective jamming may be achieved when the S/J ratio ranges from 5 dB to 15 dB, depending on the communication link equipment. A ratio $S/J = 10$ dB is assumed here as sufficient to effectively jam a link. Since the ratio S/J at the communication receiver input can be computed as a function of jammer range and angle with respect to the main beam, constant S/J contours may be constructed (e.g., required jammer range versus jammer angle off boresite to produce a value $S/J = 10$ dB). Thus, it is useful to derive the jammer range from the communication receiver, R_j , as a function of the angular separation between the jammer and the main beam. This derivation is presented next.

The analytical development begins by first noting that for a linearly polarized, plane electromagnetic wave, the effective area of a transmitting or receiving antenna, A_{EFF} , is defined as:

$$A_{EFF} = \frac{P_R}{P_0} \quad (2.2.1)$$

where P_R is the available power at the output terminals of the receiving antenna, and P_0 is the power flow per unit area of the incident field at the receiving antenna.

Consider first a link consisting of an isotropic transmitting antenna and a receiving antenna with effective area A_R . Since a hypothetical isotropic antenna has the same radiation intensity in all directions, the power flow per unit area at a distance R from the transmitter is:

$$P_0 = \frac{P_T}{4\pi R^2} \quad (2.2.2)$$

where P_T is the power delivered to the transmitting antenna at its input terminals, and R is the distance between antennas.

Assuming a plane wave front at the receiving antenna, the space loss is given by:

$$\frac{P_R}{P_T} = \frac{A_R}{4\pi R^2} \quad (2.2.3)$$

If the isotropic transmitting antenna is replaced by an antenna having effective area A_T , the received power will be increased by the ratio A_T/A_I , and the expression for space loss becomes

$$\frac{P_R}{P_T} = \frac{A_R A_T}{4 \pi A_I R^2} \quad (2.2.4)$$

where A_I is the effective area of an isotropic antenna.

It can be shown that the effective area of an ideal isotropic antenna (no heat loss) is given by:

$$A_I = \lambda^2 / 4 \pi \quad (2.2.5)$$

so that substitution of (2.2.5) into (2.2.4) produces

$$\frac{P_R}{P_T} = \frac{A_R A_T}{(\lambda R)^2} \quad (2.2.6)$$

Using (2.2.5) in (2.2.6) ($A_I = A_R = A_T$), the path attenuation between isotropic antennas is given by

$$\left(\frac{P_R}{P_T} \right)_I = \left(\frac{\lambda}{4 \pi R} \right)^2 \quad (2.2.7)$$

so that if directive antennas are used in place of isotropic antennas, the transmission equation becomes

$$\frac{P_R}{P_T} = G_T G_R \left(\frac{P_R}{P_T} \right)_I = G_T G_R \left(\frac{\lambda}{4 \pi R} \right)^2 \quad (2.2.8)$$

where G_T and G_R are power gains due to the directivity of the transmitting and receiving antennas, respectively. This is the basic transmission equation involving frequency, range, and antenna gains.

Using the relationship between operating frequency, f , wavelength, λ , and the velocity of light in free space, c

$$c = f \lambda \quad (2.2.9)$$

produces for the received power in (2.2.8):

$$P_R = \left(\frac{c}{4\pi f} \right)^2 \frac{P_T G_T G_R}{R^2} \quad (2.2.10)$$

Thus, the power at the input to the receiver, S , from the link transmitter is given by

$$S = \left(\frac{c}{4\pi f} \right)^2 \frac{P_{TS} G_{TS} G_{RS}}{R^2} \quad (2.2.11)$$

where P_{TS} is the link transmitter power, G_{TS} and G_{RS} are the gains of the transmitter and receiver antennas, and R is the terminal separation distance. The received power from the jammer becomes

$$J = \left(\frac{c}{4\pi f} \right)^2 \frac{P_{TJ} G_{TJ} G_{RJ}(\phi)}{R_J^2(\phi)} \quad (2.2.12)$$

where now P_{TJ} is the jammer transmitter power, G_{TJ} and $G_{RJ}(\phi)$ are the jammer transmitter gain and the receiver gain in the direction of the jammer. If the signal and jammer frequencies and transmission bandwidths are equal, then S/J becomes, using (2.2.11) and (2.2.12),

$$\frac{S}{J} = \left(\frac{P_{TS} G_{TS}}{P_{TJ} G_{TJ}} \right) \cdot \left(\frac{G_{RS}}{G_{RJ}(\phi)} \right) \cdot \left[\frac{R_J(\phi)}{R} \right]^2 \quad (2.2.13)$$

Solving for $R_J(\phi)$ in (2.2.13) gives

$$R_J(\phi) = R \left[(S/J) \left(\frac{P_{TJ} G_{TJ}}{P_{TS} G_{TS}} \right) \cdot \frac{G_{RJ}(\phi)}{G_{RS}} \right]^{1/2} \quad (2.2.14)$$

The gain factor $G_{RJ}(\phi)$ is covered in the next section which discusses adaptive array techniques (see Paragraph 3.0, Adaptive Array Model).

The range to the jammer (2.2.14) is computed and plotted for the threat using constant $S/J = 10$ dB contours. This is performed in the section which discusses numerical results (see Paragraph 4.0, Numerical Results).

3.0 ADAPTIVE ARRAY MODEL

3.1 Background

Steering a null of the antenna pattern in the direction of a received jamming signal is, in effect, a technique of signal acquisition. Like spread spectrum, or other techniques, such a process results in an AJ protection by providing processing gain. Adaptive array processing is used mainly for Electronic Counter Counter-Measures (ECCM) and can provide high levels for AJ protection without utilization of additional frequency spectrum. Very high levels of protection are possible when adaptive array processing is utilized in conjunction with other processing techniques. Adaptive arrays are compatible with many existing systems and can be provided as additional capability without major modifications.

Research in the area of adaptive antennas has centered about the development of large, high performance, multiple-beam electronically steerable adaptive phased array antenna systems. These systems incorporate null-steering capabilities for command and control systems and sidelobe cancellation techniques for radar applications and small antenna arrays.

Large adaptive phased arrays utilize null-steering techniques such as random search and sampled matrix inversion and may be under the control of a high speed computer. Analog null-steering techniques using some form of the Least Mean Square (LMS) algorithm are employed by some small arrays. Various types of performance measures required for adaptive antenna system optimization have been developed. These include power minimization, signal-to-noise ratio (SNR) maximization, and the use of signal identifiers. For ECCM purposes, the use of an adaptive antenna system requires a careful investigation of a variety of technical as well as scenario-dependent parameters.

3.2 Operation

An adaptive null-steering array automatically establishes pattern nulls in the directions from which jamming signals are received. This is achieved by means of internal feedback control. A reference signal from the receiver is utilized for correlation signal processing. Any signals not contained in the reference signal will appear as noise at the array output. These signals are used to generate an error signal to control complex weighting functions which are then used to minimize the error signal.

In order for the nulling array to operate properly, the following conditions are required:

- The difference(s) between the angles of arrival of the desired and jamming signal(s) are sufficiently large.
- The temporal structures of the desired and jamming signals are sufficiently dissimilar.
- The reference signal adequately resembles the desired signal component of the composite signal incident on the array.

3.3 Analytical Development

3.3.1 Linear Null-Steering Arrays

The effectiveness of the adaptive null-steering array is dependent on many variables such as bandwidth of the array, number of antenna elements, and the geometry of the jammer location relative to the antenna main beam. An important consideration is the angular resolution which may be obtained between a signal and a jammer. For the case of zero bandwidth, the performance of optimal arrays has been worked out analytically. For large J/S ratios, the signal-to-total noise ratio is given by [3]

$$\frac{S}{N} = M \frac{S}{\sigma^2} \left[1 - P(\phi_S - \phi_J) \right] \quad (3.3.1.1)$$

where $\frac{S}{N}$ = output signal-to-total noise ratio

M = number of antenna elements for a phased array

S/σ^2 = signal-to-noise ratio at an input to one channel of an adaptive processor

$P(\phi)$ = antenna power pattern of the array as a function of ϕ , the angle measured from the axis of the array

ϕ_S = polar angle of the signal, measured from the axis of the linear array

ϕ_J = polar angle of the jammer, measured from the axis of the linear array

In (3.3.1.1), the factor $M (S/\sigma^2)$ gives the output signal-to-noise of an M-element linearly phased array pointed toward the desired signal, S, in the absence of jamming. The equation relates the best obtainable S/N, without jamming, to the S/N with jamming via a pattern factor. This factor is simply unity minus the ordinary pattern factor of a linearly phased array, evaluated at the difference angle between signal and jammer.

For a linear, equally spaced array, the pattern of the array is

$$P(\phi) = \left[\frac{\sin (M \pi x (\phi))}{M \sin (\pi x (\phi))} \right]^2 \quad (3.3.1.2)$$

where $x(\phi) = \frac{2d}{\lambda} \cos \phi$

and M = number of elements

d/λ = element spacing in wavelengths

ϕ = angle from the axis of the array

When the pattern is a function of the difference between the signal and jammer angle, we have

$$P(\phi_s = \phi_j) = \left[\frac{\sin (M \pi (x_s - x_j))}{M \sin (\pi (x_s - x_j))} \right]^2 \quad (3.3.1.3)$$

where $x_s = \frac{2d}{\lambda} \cos \phi_s$

$x_j = \frac{2d}{\lambda} \cos \phi_j$

If the jammer and signal are very close to each other, $\sin \pi(x_s - x_j) \approx \pi(x_s - x_j)$, so that (3.3.1.3) may be approximated as

$$P(\phi_s = \phi_j) = \left[\frac{\sin(M\pi(x_s - x_j))}{M\pi(x_s - x_j)} \right]^2 \quad (3.3.1.4)$$

The argument $M(x_s - x_j)$ is useful physically in that it is the number of local beamwidths of separation between the jammer and signal.

Normalization of the scan angle in terms of beamwidths is also useful when considering the dispersion of the array over signals of finite bandwidth.

Normalization of S/N to the maximum S/N ($S/N|_{MAX} = M(S/\sigma^2)$) after substitution into (3.3.1.4), yields

the S/N loss, L:

$$L = 1 - \left[\frac{\sin(M\pi(x_s - x_j))}{M\pi(x_s - x_j)} \right]^2 \quad (3.3.1.5)$$

Calculation of (3.3.1.5) reveals that a trade-off could be made for S/N loss versus the minimum allowable angular separation between signal and jammer.

An array having finite bandwidth, however, has an equivalent finite angular beamwidth. If a signal and close-by jammer have a large bandwidth, their equivalent angular beamwidths could overlap, making it impossible with phase and amplitude weights to null the jamming, without also reducing the signal.

A linear array is assumed here as a first-order approximation to the complexity of the null-steering array. The linear array is assumed to consist of many square radiating elements spaced by one-half wavelength. The number of required elements, M , is approximately given by

$$M = G_{REQ} / \pi \quad (3.3.1.6)$$

where G_{REQ} is the required gain in the main lobe of the array.

3.3.2 Discussion of Sidelobe Cancellation Employing Paraboloid Reflectors

Phase cancelling elements attached to a paraboloid reflector are utilized to place nulls inside the main beam of the antenna for the purpose of suppressing an unwanted jammer.

In order to consider sidelobe cancellation, it is instructive to consider the practical paraboloid reflector antenna. When an illumination (efficiency) factor of 50 percent is assumed, the gain of this antenna is given by

$$G = 0.5 \left(\frac{\pi D}{\lambda} \right)^2 \quad (3.3.2.1)$$

where d is the aperture diameter of the antenna, and λ is the signal wavelength. For a circular aperture having uniform illumination, the pattern factor in the azimuth plane (ϕ) parallel to the earth plane may be derived as

$$P(\phi) = \left[\frac{2J_1(\beta a \cos \phi)}{\beta a \cos \phi} \sin \phi \right]^2 \quad (3.3.2.2)$$

where $\beta = 2\pi/\lambda = \text{free-space wavenumber}$

$a = \text{radius of the circular aperture}$

$J_1(x) = \text{first-order Bessel function}$

With practical antennas that radiate from a circular aperture, it is difficult to obtain a uniform illumination. Moreover, such a uniform illumination may not even be acceptable for some applications, since according to (3.3.2.2), the sidelobe level is rather high. Consequently, many paraboloid reflectors, for example, are deliberately designed with an amplitude taper. Fortunately, in a circular aperture, aperture distributions of quite a general form can be integrated. In particular, if the aperture distribution can be approximated by a finite number of terms from an infinite series, then the field has a form which can be integrated. The result for the pattern factor, therefore, contains n-th order Bessel functions.

Typical computed patterns for antennas employing sidelobe cancellation techniques are illustrated and described in a later section. (See Paragraph 4.0, Numerical Results.)

3.3.3 Adaptive Array Processing Gain

Processing gain derived from utilization of adaptive array techniques, in general, has two components: passive gain and active gain.

Passive processing gain is that component which is the difference (expressed in dB) between the level of the main lobe of the antenna beam with, e.g., some of the sidelobe levels where the jammer is attempting to penetrate. This processing gain, of course, depends on jammer angle with respect to boresite and results without employing null-steering or sidelobe cancellation techniques. Knowledge of system parameters (such as size of the antenna and operating frequency) are necessary to determine passive processing gain when the jammer angle is known or can be estimated.

The other component, active processing gain, gives the additional protection when null-steering or sidelobe cancellation is utilized to combat jamming. It is additive to the passive component just discussed (and any other AJ processing gain component). For a dish employing one sidelobe canceller element, an expression has been derived for the active processing gain, G_{PA} [4]:

$$G_{PA} = 10 \log_{10} \left[1 - \frac{\sin(\pi B_s t_p)}{\pi B_s t_p} \right] \text{ dB} \quad (3.3.3.1)$$

where B_s = antenna system bandwidth

t_p = propagation time delay across the aperture

The processing gain components afforded by adaptive array techniques are illustrated in the next section as a function of antenna system bandwidth, transit time across the aperture, and jammer angle with respect to boresite.

4.0 NUMERICAL RESULTS

In this section, some important numerical results are derived using the analytical development presented in earlier sections of this report. The transmission loss due to atmospheric and terrain-induced multipath is first computed using the Longley and Rice prediction method. Rainfall and atmospheric attenuation are then evaluated. In an effort to assess the potential jammer threat, constant contours of S/J are next presented using the range equation given by (2.2.14). Theoretical patterns are then illustrated for the M-element linear array (an approximation for the null-steering adaptive array) and the uniformly illuminated circular aperture antenna (without amplitude tapering or sidelobe cancellers). The passive and active components of processing gain are then computed as a function of jammer angle off boresite, antenna system bandwidth, and the

propagation, or transit, time of the jammer signal across the circular aperture. These components of processing gain are then considered together with processing gain obtained using spread spectrum techniques in order to ascertain the overall processing gain that is obtainable over the link. Finally, some recommendations and comments are offered regarding a choice for an adaptive array processing system.

4.1 Link Transmission Loss Due to Multipath

The following input parameters are used to derive a transmission loss value due to multipath over the MWAR system link:

- Atmospheric refractivity = 313 N-units
- RMS deviation of terrain = 6m
- Terminal separation distance = 30 km
- Actual antenna heights = 5m
- Effective antenna heights = 10m
- Operating frequency = 38 GHz
- Surface conductivity = 0.005 siemens/m
- Surface dielectric permittivity = 15
- Link availability for communication link = 99 percent
- Climate = continental temperate

Using the Longley and Rice prediction method, transmission loss due to atmospheric and terrain-induced multipath is found to be 49.2 dB. This value is not exceeded for 99 percent of all hours of the year over the desired communication link.

4.2 Rainfall and Atmospheric Attenuation

Transmission loss due to rainfall absorption may be computed using (2.1.1). For a continental temperate climate having a total annual rainfall of 1m (typical in the Federal Republic of Germany), the path average rainfall rate, R_R , which is not exceeded for 99 percent of all hours of the year (over the desired link) is approximately

$$R_R = 2.88 \text{ mm/hr}$$

At a frequency of 38 GHz, the coefficients $K = 0.3816$ and $\alpha = 0.9093$ are substituted into (2.1.1). Thus, the rainfall attenuation over the desired communication link, when the terminal separation distance is 30 km, is computed to be 30 dB.

Atmospheric absorption loss, due to resonance lines of oxygen and water vapor, is computed to be 1 dB over the 30 km link, using curves illustrated in [2].

4.3 Contours of Constant Signal-To-Jammer (S/J) Ratio

Here, contours are developed for a constant signal-to-jammer (S/J) ratio on a typical topographical map using the range equation (2.2.14). Recall that (2.2.14) gives the jammer range as a function of the jammer angle relative to the main beam of the site antenna. The effective-radiated-power (ERP) of the link transmitter is known ($P_T G_{TS}$ in (2.2.14)), and the ERP value of the jammer ($P_{TJ} G_{TJ}$) is hypothesized or assumed. The gain of the communication receiver antenna along with the

AD-A102 303

HARRIS CORP MELBOURNE FL GOVERNMENT COMMUNICATION SY--ETC F/6 17/2.1
MILLIMETER WAVE ALTERNATE ROUTE STUDY.(U)

APR 81 W C ADAMS, J J PAN, W C WHITEHEAD

F30602-79-C-0055

RAOC-TR-81-42

NL

UNCLASSIFIED

b1-5

4/23/82



END
DATE
FILMED
8-81
DTIC

jammer angle of arrival are known parameters. $S/J = 10$ dB is assumed, as values lower than this usually result in rapid bit-error rate (BER) degradation over, e.g., QPSK data links, and thus, link failure.

In (2.2.14), we select the signal-to-jammer ratio, S/J , communication transmitter ERP, $P_{TS} G_{TS}$, and the communication receiver antenna gain, G_{RS} , to be fixed values:

- $S/J = 10$ dB
- $P_{TS} G_{TS} = 43$ dBW
- $G_{RS} = 43$ dB

Low and high ERP jammers ($P_{TJ} G_{TJ}$) are studied in two distinct cases:

- $P_{TJ} G_{TJ} = 43$ dBW (low ERP)
- $P_{TJ} G_{TJ} = 54$ dBW (high ERP)

Figure 4.3 illustrates contours using the range equation for the low and high ERP jammers. From these curves, information can be obtained as to whether the jammer represents a potential problem to the desired link.

4.4 Computed Adaptive Array Antenna Patterns

Using (3.3.1.6) as an approximate expression for the total number of elements in a linear array, M , necessary to produce $G_{REQ} = 43$ dB, we see that $M = 6400$. These elements could be arranged in an 80×80 square matrix. We may then compute the pattern factor per axis using $M = 80$ in (3.3.1.2). The product of the two axis pattern factors yields the composite pattern. The pattern factor (3.3.1.2) is illustrated in Figure 4.4-1 for half-wavelength spacing ($d/\lambda = 0.5$) of the elements, and is useful for

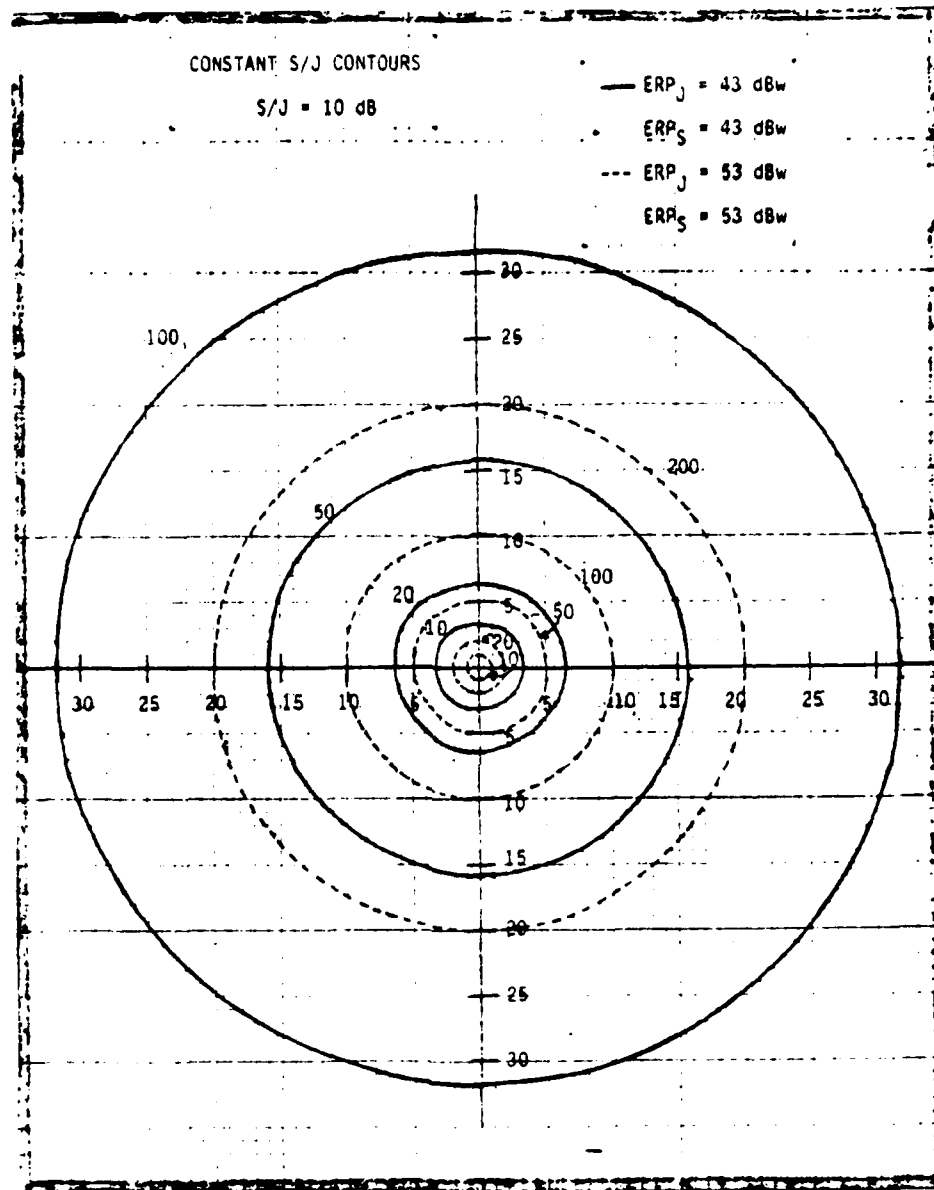


Figure 4.3. Constant S/J Contours for $S/J = 10 \text{ dB}$. Horizontal and vertical axis numerals indicate terminal separation distance in the desired link. Given this distance, numerals on the circles indicate maximum jammer range in which communication may be disrupted. (Example: $R = 16 \text{ km}$, $ERP_S = ERP = 43 \text{ dBw}$, which gives 50 km as the maximum jammer distance required to successfully disrupt the link.)

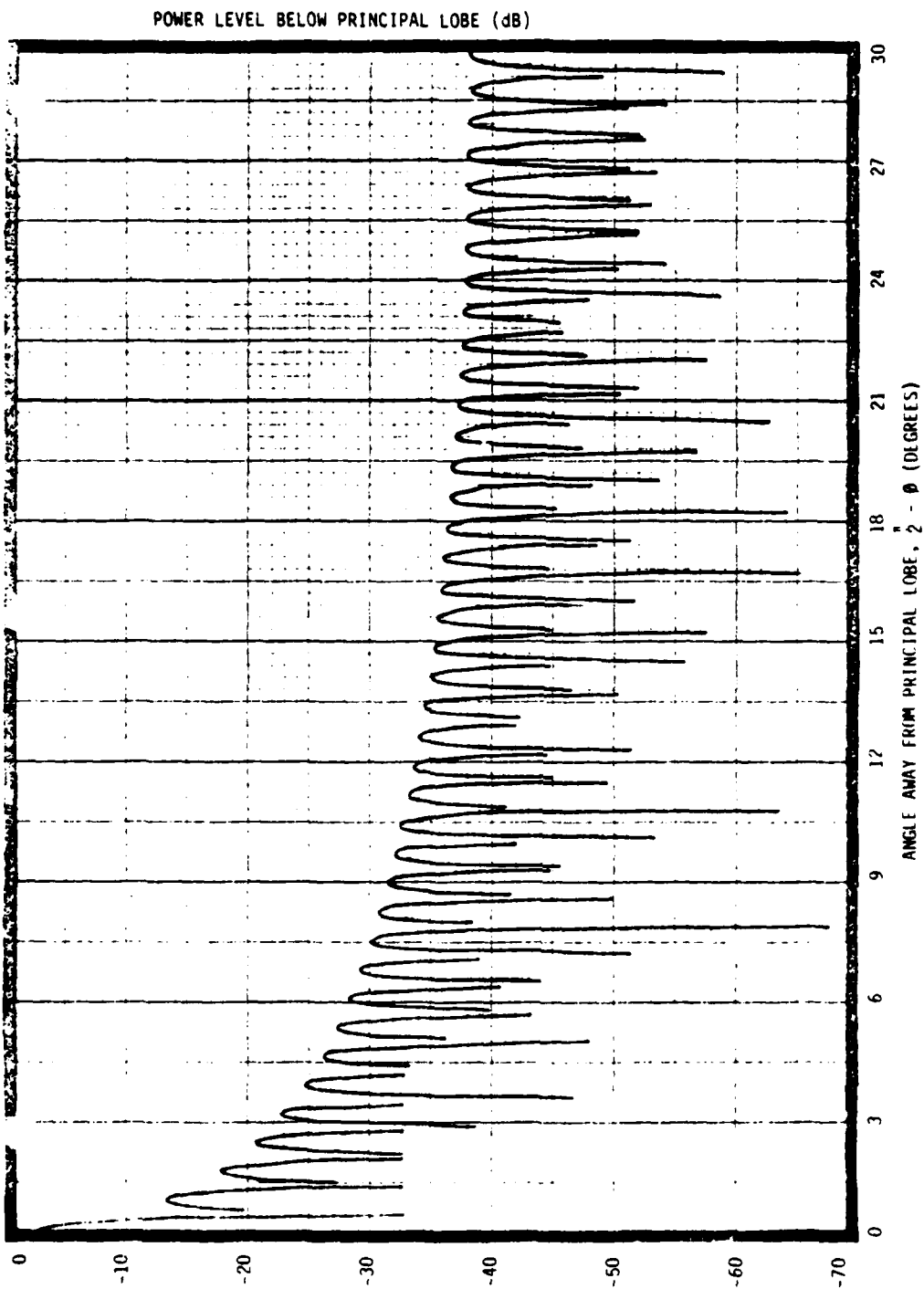


Figure 4.4-1. Pattern Factor, $P(\phi)$, for an 80-Element Linear Array (used as a first-approximation to a main beam null-steering adaptive array). $d/\lambda = 0.5$. Resolution to 0.1 degree.

approximately locating the nulls in the pattern. However, the sidelobe amplitude levels appear to be higher than what physically occurs in a practical null-steering array; hence, these levels are not useful when computing passive processing gain needed for AJ protection when using null-steering arrays.

The theoretical pattern for a uniformly illuminated circular aperture is given by (3.3.2.2). Using this equation with $\beta a = 200$, the result is illustrated in Figure 4.4-2; this corresponds to approximately a 0.5m diameter dish antenna operating at 38 GHz. As for the linear array discussed above, the sidelobe levels for this pattern are higher than what really occurs for a practical circular aperture antenna employing sidelobe canceller elements. As discussed previously, sidelobe cancellers are designed with an amplitude taper to lower the sidelobe levels. However, the location of the nulls, as illustrated in Figure 4.4-2, is fairly representative of physical reality.

4.5 System Processing Gain

4.5.1 Adaptive Array Processing Gain

4.5.1.1 Passive Processing Gain

This component of processing gain is found from knowledge of the theoretical or measured pattern function which depends on the jammer angle with respect to the main beam. Since the passive processing gain does not result from the actual employment of null-steering or sidelobe cancelling, it is immediately computed as the difference between the antenna gain along the axis of the principal lobe (directivity) and the gain at some arbitrary jammer angle away from boresite. Passive AJ protection may be large if, for example, the jammer signal should lie in a sharp null of the receiver antenna pattern, even before adaptive array techniques are implemented. Figure 4.5.1.1 illustrates the passive processing gain (in dB) obtained when

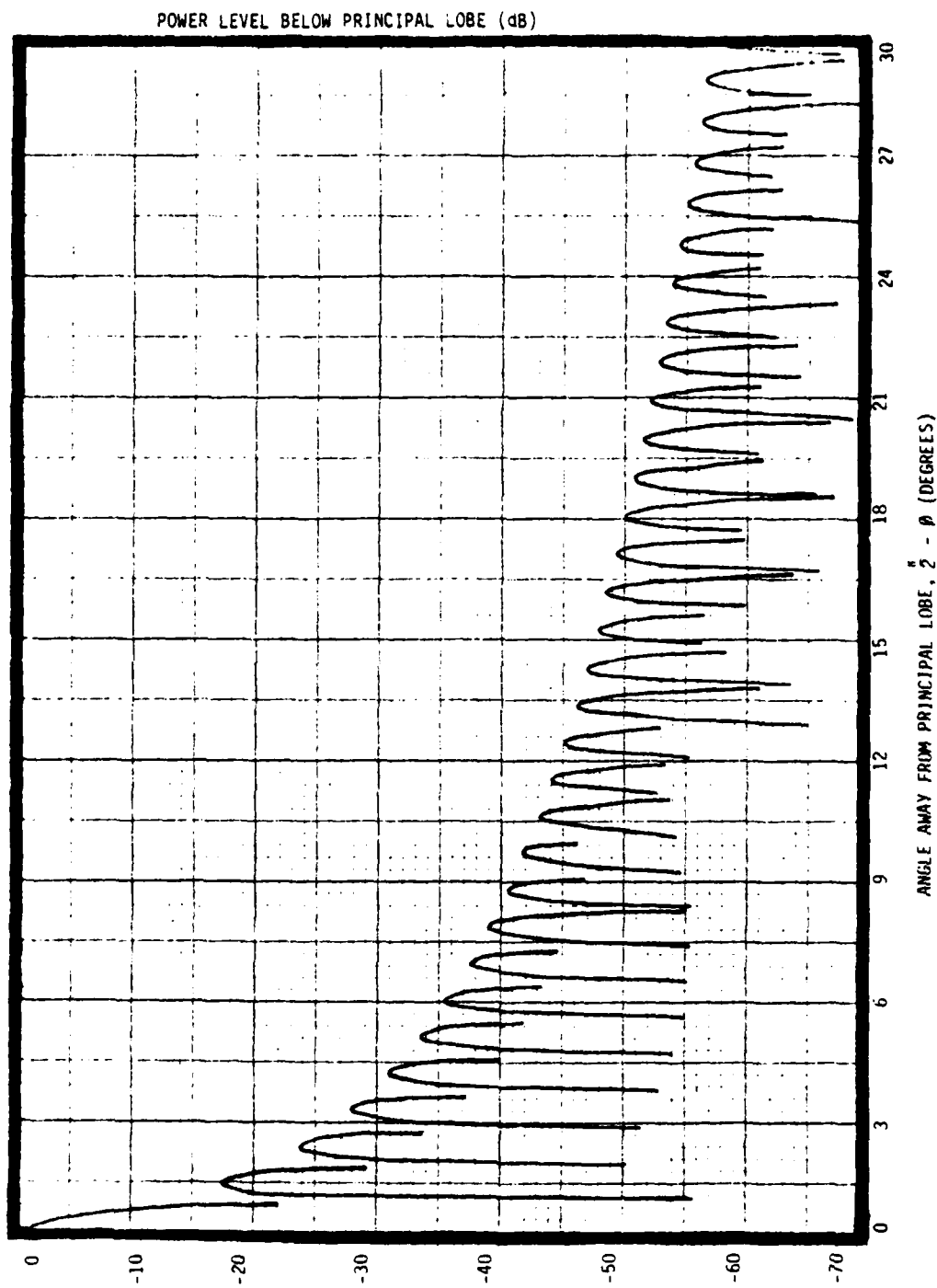


Figure 4.4-2. Pattern Factor, $P(\phi)$, for a Uniformly Illuminated Circular Aperture $\beta a = 200$. Resolution to 0.1 degree.

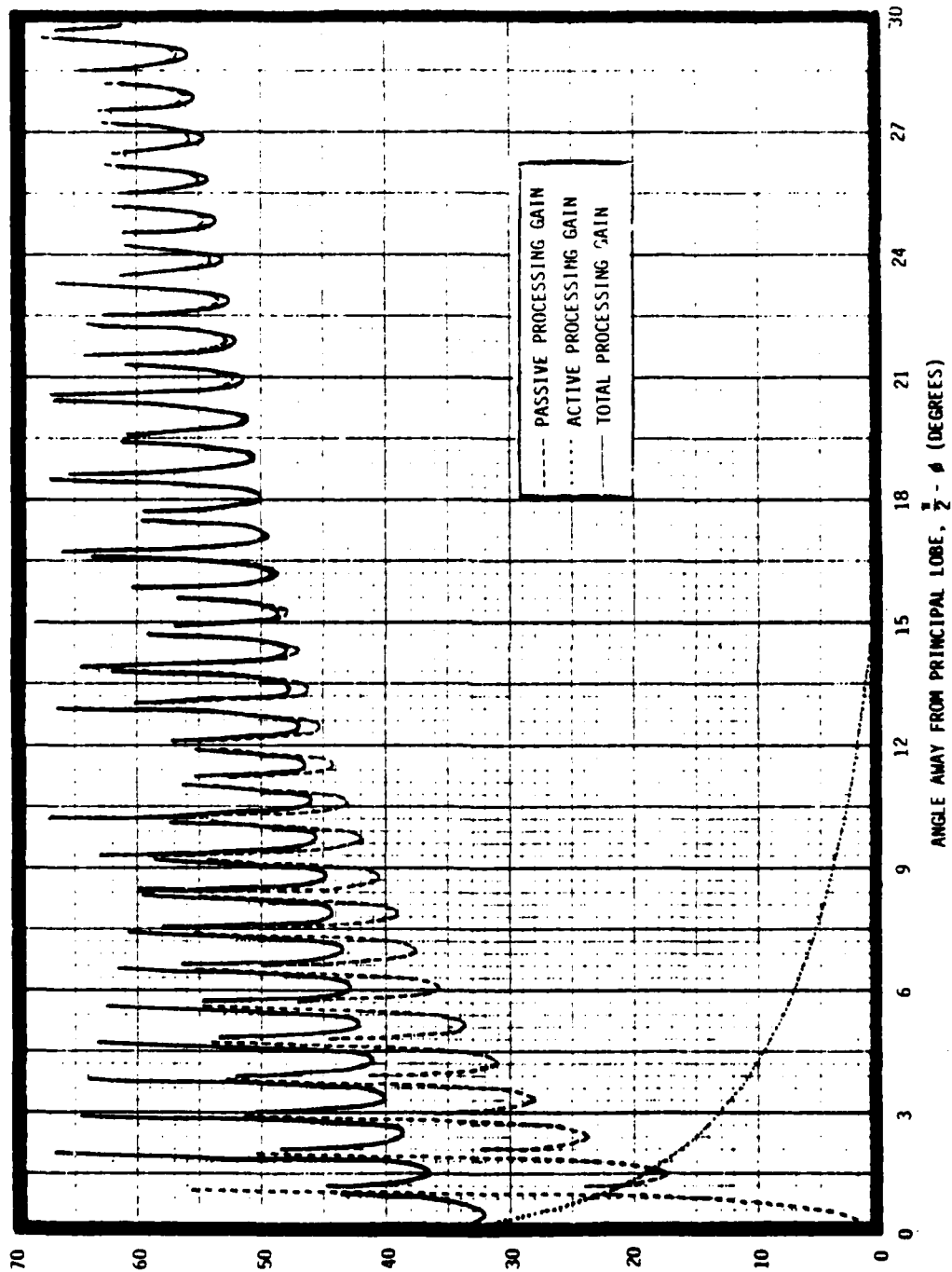


Figure 4.5.1.1. Passive, Active, and Total Processing Gains Obtained Using a Uniformly Illuminated Circular Aperture With One Side-lobe Cancelling Element $\beta a = 200$. Resolution.

utilizing the theoretical paraboloid reflector exhibiting uniform illumination characteristics. This processing gain is computed as a function of ϕ , the angle of the jammer with respect to the plane of the circular aperture.

4.5.1.2 Active Processing Gain

The active processing gain component is computed by utilizing (3.3.3.1) for the pattern cited above. An antenna system bandwidth, B_s , of 2 GHz is used to correspond to the largest bandwidth in the system (the PN chip rate is assumed to be 1 G chip/s; B_s is taken to be twice the chip rate bandwidth). The maximum value of the propagation time of the signal across the paraboloid reflector, $t_p(\max)$, is determined approximately by dividing the diameter of the dish (0.5m is used) by the velocity of light in free space. This value of t_p is used when the jammer signal is received at a right angle (along the axis of the array or in the plane of the aperture) to the desired signal and is denoted $t_{p(\max)}$. $t_{p(\max)}$ may then be multiplied by $\cos \phi$, in general, to obtain the transit time as a function of the jammer angle. The active processing gain is shown as a dotted line as a function of ϕ in Figure 4.5.1.1.

4.5.1.3 Total Array Processing Gain

The total adaptive array processing gain is found as the algebraic sum of the active and passive processing gains. The result corresponding to the uniformly illuminated circular aperture with one sidelobe canceller element is illustrated in Figure 4.5.1.1.

4.5.2 Spread Spectrum Processing Gain

Processing gain obtained from spread spectrum techniques using a direct sequence (DS) QPSK system is determined approximately by computing the ratio of the PN chip rate, R_c , to the transmission bit rate, R_b . For $R_c = 1$ G chip/s, processing gains of 30, 17, and 8.2 dB have been computed when $R_b = 1, 20,$ and 150 Mb/s, respectively.

4.5.3 Total System Processing Gain

The total system processing gain is found as the algebraic sum of the adaptive array and spread spectrum processing gains. Using Figure 4.5.1.1 for the adaptive antenna processing gain and the results for the gain afforded by spread spectrum techniques, we may immediately compute that sum.

4.6 Recommendations

Based on the preceding numerical results and some intuitive observation, it appears that usage of an adaptive null steering multielement array is neither feasible nor cost-effective for the MWAR concept. Using the linear array model as a first approximation illustrates that 6400 antenna elements (arranged, perhaps, in an 80 x 80 square matrix) would be required to achieve the desired 43 dB directivity in the main lobe. Also, if the jammer should intercept close to the axis of the main beam, a simple phasor analysis reveals that when one attempts to cancel the jammer signal, most of the desired communication signal is also lost in the process. Thus, alternate routing (transmission to other sites) would perhaps be necessary when the jammer is within the angle subtended by the principal lobe if a multielement phased array is used.

Outside the principal lobe, however, a sidelobe cancelling technique is somewhat useful since it is relatively easy to implement and is more cost-effective than the multielement phased array since only a few equally-spaced elements would be required on the circular aperture. Such an adaptive antenna utilizing sidelobe cancellers affords a reasonable amount of active processing gain against one or more dedicated jammers.

However, as shown in Section 6.0 of the final report, a multifeedhorn dish technique is the best approach for implementing an adaptive antenna.

5.0 SUMMARY AND CONCLUSIONS

The major objective of this appendix was to investigate processing gain afforded by multielement array adaptive antennas; this processing gain provides protection for the MWAR communication link against one or more dedicated jammers in a threat environment.

In order to understand quantitatively the significance of adaptive antenna processing gain, it was necessary to understand and assess the communication link model and the potential jammer threat. Derivation of a set of link allocations (not presented here) based on the link model and jammer scenario led to the necessity of having additional system margin in the form of adaptive antenna processing gain.

Numerical results pertaining to transmission multipath loss, rainfall and atmospheric absorption, contours of constant signal-to-jammer ratio, curves of adaptive array patterns, and system processing gain were derived to more clearly assess and evaluate the MWAR system performance.

Paraboloid reflectors employing sidelobe elements are useful for jammer signals outside of the principal lobe. Adaptive multielement array null-steering antennas are not recommended because, based on the linear array first approximation, a very large number of elements would be required to achieve the desired 43 dB directivity for a 0.5m diameter paraboloid reflector having 50 percent efficiency. The multifeedhorn parabolic reflector technique is the recommended adaptive antenna approach in view of its high performance and low cost, as shown in Section 6.0 of the final report.

APPENDIX REFERENCES

- [1] P.L. Rice, et al., "Transmission Loss Predictions for Tropospheric Communication Circuits," NBS Technical Note 101, ITSA, revised January 1967.
- [2] J.W. Reid, Jr., "A Tropospheric Propagation Model for Ground/Ground Low Elevation Angle LOS Systems," Harris Electronic Systems Division Technical Report, 9331-77-001, May 1977.
- [3] "Adaptive Processing for Antenna Array," Final Report, RADC-TR-72-174, July 1972.
- [4] C.A. Chuang, "Spatial Frequency Dispersion of a Sidelobe Canceller," Harris Electronic Systems Division Memo ACDL-TM-013, 20 January 1978.



MISSION
of
Rome Air Development Center

RADC plans and executes research, development, test and selected acquisition programs in support of Command, Control Communications and Intelligence (C³I) activities. Technical and engineering support within areas of technical competence is provided to ESD Program Offices (POs) and other ESD elements. The principal technical mission areas are communications, electromagnetic guidance and control, surveillance of ground and aerospace objects, intelligence data collection and handling, information system technology, ionospheric propagation, solid state sciences, microwave physics and electronic reliability, maintainability and compatibility.

DATE
FILMED
— 8